INTRODUCTION TO
GRAVITY EXPLORATION METHOD

First Edition

Hamid N. Alsadi
Former expert in Geophysics at Oil exploration Company, Iraq.

Ezzadin N. Baban
Professor in Geophysics at Department of Geology, University of Sulaimani.

Sulaimaniyah, Kurdistan Region, Iraq, 2014

II

Content

Chapter 9

Chapter 10

Chapter 11
GRAVITY EXPLORATION RECENT DEVELOPMENTS

VIII

Chapter 12

CASE HISTORY OF GRAVITY SURVEYS

PREFACE

This book is written mainly for university students taking a course on gravity as one of the methods used in geophysical exploration. It is designed to be an introductory text book that deals with the basic concepts underlying the application of the Earth gravitational field in the exploration of the subsurface geological changes and in prospecting of petroleum and other mineral deposits.

As it is familiar with the exploration geophysicists, this subject is fully dealt with in many original authentic internationally-known text books. In this publication, no new subjects were added to those found in the other standard books which are well known in the geophysical library. In fact these and other related scientific papers and research reports formed the solid references for the present work. There is, however, a difference in the design and presentation approach. The essential publications, used as references, are listed at the end of the book. The main feature of this work is being concise and logically sequenced. The objective was to present the subject in a simple and clear way avoiding excessive descriptions and unnecessary lengthy comments. For this reason the text was provided with numerous illustration figures for extra clarification.

The book consists of twelve chapters. The first five chapters cover the theoretical aspect of the subject including the gravitational attraction, shape of the planet Earth and nature of the gravity variations, which forms the basis for the exploration capability of the method. The following five chapters deal with measuring instruments, field surveying techniques, data processing, concept of the gravity anomaly and interpretation. A closely associated with gravity anomaly is the phenomenon of isostasy. This was presented in chapter 10. Some modern aspects of the method were covered in chapter 11 and in the last chapter 12 actual gravity field-surveys were reviewed. The first case history is an actual field survey conducted by one of the authors (Hamid Alsadi) in the south-west England in 1965-1966 and the others (by Zuhair Al-Sheikh and Ezzadin N. Baban) were carried out in Iraqi territories. These are included here to serve the purpose of showing how a real gravity surveying is carried out in practice under actual field and processing environments.

As always in any publication material, there is always a room for improvement if extra time and effort has been allocated. From personal experience this is an endless process. However, this book is no exception to this rule. With feed-backs from future users of the book it is hoped to make the improvement changes needed that will be incorporated in future editions.

Hamid N. Alsadi and Ezzadin N. Baban,
23 Jan. 2013

ACKNOWLEDGMENT

Chapter 1

INTRODUCTION

2.1. General Review

The basic concept underlying gravity surveying is the variation of the Earth gravitational field caused by lateral variation of subsurface rock-densities. In other words, a given rock body whose density is different from its surrounding medium (i.e. geological anomaly) produces a corresponding disturbance (gravity anomaly) in the Earth gravity-filed. The form and amplitude of the created anomaly depend on the subsurface geological anomaly such as a salt dome, granite intrusion, buried valley, folded or faulted beds. The gravity anomaly depends also upon large scale or regional structures such as regional dipping strata, sedimentary basins, geosynclines and mountain roots

Gravity surveying involves measurements of the changes in gravitational acceleration at a grid of points over a given area. The observation-data are then subjected to a series of corrections and mathematical analyses in order to reduce them to gravity values measured relative to a defined datum-plane, normally taken at the mean sea level. These corrections ensure that the produced gravity anomaly is that caused by the sub sea-level geological anomaly with all other effects removed.

In the last stage of the survey, the obtained gravity anomaly is subjected to further analysis with the aim of determination of the causing subsurface geological anomaly. This gravity-to-geology process (interpretation) forms the ultimate objective of any gravity-survey project.

2.2.   Historical Review

The historical development of gravity exploration may be summarized as follows:

Late 16th and early 17th centuries:

Galileo Galilei (1564-1642) discovered, in about 1590, that objects of different masses fall to Earth surface at same constant acceleration. Johannes kepler (1571-1630) derived three laws (Kepler Laws) which describe the motions of planets in the solar system. These laws were later used by the English physicist, Sir Isaac Newton (1642-1727), in formulating the universal law of gravitation, giving the mathematical expression ($F=Gm_1m_2/r^2$) for the force of attraction, F (gravitational force) that exists between any two masses, m_1 and m_2 which are located at r distance apart. The law was published in 1687.

18th century:

A pioneering work was done by the French scientist Pierre Bouguer (1698-1758), who had led an expedition in (1735-45) organized by the French Academy of Sciences to conduct gravitational studies and other investigations concerning the shape of the Earth. He derived the relationships connecting gravity variation with elevation and latitude. The Bouguer gravity anomaly is named after his name.

19th century:

The main development that took place then was the introduction in 1817, by the English physicist, Henry Kater (1777-1835), of the compound pendulum known now by his name, Kater pendulum which was used in gravity measurements during the following century. Also the Hungarian physicist, Roland von Eotvos (1848-1919), completed the torsion balance in 1890 with which the spatial derivative of the gravity changes can be measured.

First half of the 20th century:

The first application of the torsion balance was made in gravity surveying over an ice sheet of a lake in 1901 and the first torsion-balance survey for oil

exploration (in California and Texas) was conducted in 1922. The portable pendulum began to be used in the early 1920s. It (the pendulum) was used by F. A. Vening Meinesz in 1923 in gravity measurements on board of submarine to study the gravity variations over some oceanic areas.

Gravimeters were introduced and utilized in the search for oil and minerals. In 1932, the gravimeter (stable type) was introduced as an exploration tool, and in 1939, the LaCoste gravimeter (zero-length spring) appeared. In 1948, the Worden and Atlas gravimeters, as improved portable instruments, became in common use for gravity field-measurements.

Second half of the 20th century:

During the second half of the twentieth century, the gravity techniques have, like other branches of science and technology, witnessed appreciable advances. During the period 1940-1960, the techniques of mathematical computation of gravity anomalies of simple geometrical shapes were developed. In the few years around 1960, George Woollard (1908-1978) used Pendulum measurements to establish a world-wide network of gravity base-stations. The digital computers introduced in the 1960's have facilitated gravity data processing and interpretation capabilities. In particular, digital filtering by Fourier Transform, model analysis and inversion techniques were applied in the analysis and interpretation of gravity data.

In this period, gravimeters have been adopted to measurements in boreholes, on sea-floors, on moving ships, and on aircrafts (La Fehr, 1980). Satellite orbital paths furnished valuable knowledge on the detailed shape of the Earth (Kahn, 1983).

The Recent Developments

The main recent development that occurred in the gravity exploration method was the practical application of the airborne gravity as an effective exploration tool (Elieff, 2003; Hwang, et al, 2007; Alberts, 2009).

Satellite radar-based positioning technique, computer hardware, and software systems and all other modern supporting technologies (based principally on modern digital electronics) have collectively contributed to the recent developments of the gravity method.

2.3.   The Earth Shape

1.3.1 The Ellipsoid

The past geodetic and geophysical investigations coupled with the more recent satellite data led to the conclusion that the Earth is approximately ellipsoidal rather than being perfectly spherical. The model which is now adopted for the Earth shape, is an ellipsoid of revolution whose surface is taken to be the mean sea-level surface of the Earth. This model is called the reference or normal ellipsoid. It is sometimes called the reference spheroid (Fig. 1-1).
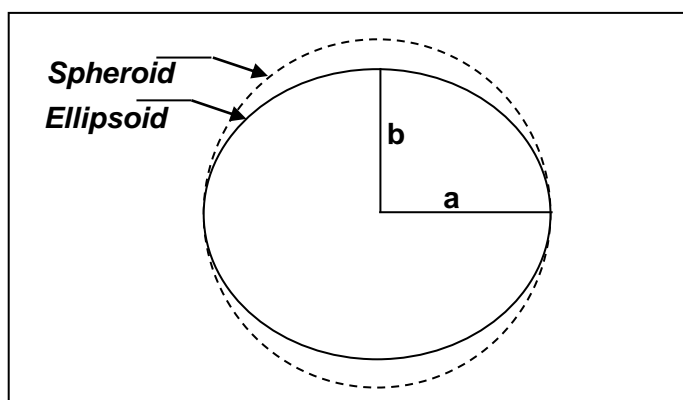
Fig. 1-1 The ellipsoidal model of the Earth

In 1930, dimensions of the agreed-upon normal ellipsoid were adopted by an organization called the International Union of Geodesy and Geophysics (IUGG). By 1967, the numerical constants of the ellipsoidal model were updated to the now- accepted values which are:

The equatorial radius (a)   = 6378.160 km

The polar radius (b)   = 6356.775 km

The difference (a-b)   = 21.385 km

The flattening factor (a-b)/a   = 1/298.25

The angular Rotation Speed (ω)   = 7.292 * 10^{-5} radian/sec

1.3.2 The Geoid

In order to have a reference datum level to which measurements can be related, a physical surface for the Planet Earth was defined. This surface is taken to be the average sea-level over the oceans and over the sea-water if it were extended in canals cut through the continents. This global surface is commonly referred to as the geoid. The geoid surface is horizontal (i.e. perpendicular to plumb line) at all its points (Fig. 1-2).
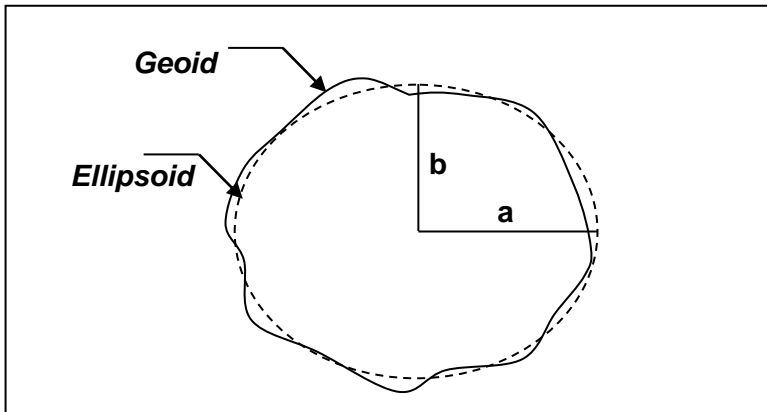
Fig. 1-2 The geoid with its undulations is defined by the mean sea-level.
The dotted line represents the Earth reference ellipsoid.

In general, the geoid surface does not coincide with that of the normal ellipsoid. In fact, the deviation between the two surfaces can be as large as 100 meters. The reason for this discrepancy is that the geoid suffers from certain surface deformations (geoid undulation) caused by small-scale and large-scale density anomalies in the Earth crust.

A small-scale localized excess-mass anomaly would warp the geoid upward. Under large-scale continental blocks, the geoid surface is warped upwards due to rock material existing above it, and it is warped downwards over the oceans because of the lower density of the water.

The geoid with its natural undulations presents a model closer to the actual Earth than any other suggested models. It differs from the ellipsoid model which is based upon a simplified theoretical Earth in which density is allowed to vary vertically (with depth) but not laterally (Fig. 1-3).
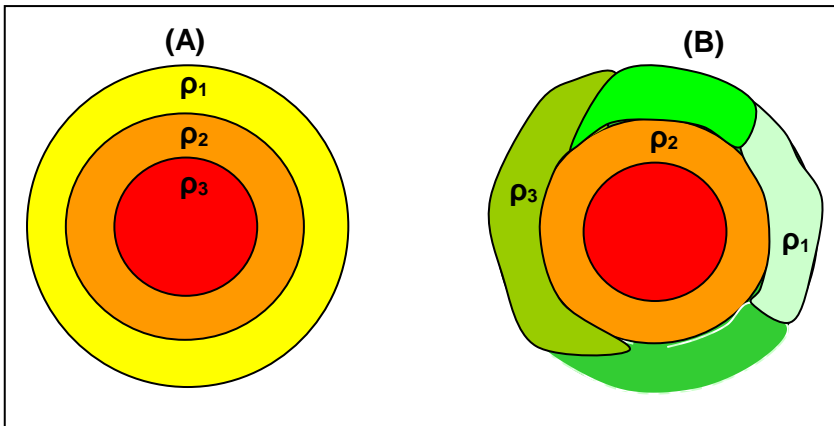
Fig. 1-3 Density distribution in the two models, the ellipsoid (A) and the geoid
(B) that are developed for the Earth.

According to the geopotential concept, the undisturbed ocean surface is an equipotential surface. This means that the geoid surface has, by definition, the same gravitational potential as the mean ocean surface

The geoid surface is used as a reference (datum level) for local geodetic and geophysical survey measurements. However, large-scale global measurements (such as astronomical surveying) are made relative to the reference ellipsoid.

Chapter 2

THE EARTH GRAVITATIONAL FIELD

One of the principal potential fields existing in nature is the Earth gravitational field. Within this field, a force of attraction occurs between any two masses existing in universe. The basic physics has furnished mathematical laws that govern the behavior of all the scalar and vector quantities associated with this phenomenon. In this chapter, we shall present simple explanatory notes for the scalar gravitational potential and for the gravitational vectors; force, acceleration and gradients.

2.1.   The Universal Law of Gravitation

Isaac Newton (1643-1727) formulated the universal law of gravitation which evaluates the attraction force $\mathbf{F}$ that exists between two particles of masses $\mathbf{m_1}$ and $\mathbf{m_2}$ located at distance $\mathbf{r}$ apart (Fig. 2-1):

$$\mathbf{F = G\ m_1 . m_2 / r^2}$$
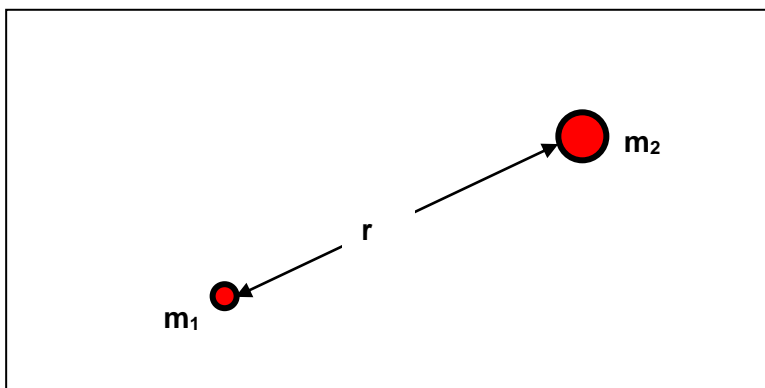
Fig. 2-1 Attraction force (F) between two masses; m1 and m2 at distance r apart.

The constant G, called the Universal Gravitational Constant, was experimentally determined and found to be of the value:

$$G = 6.673 \times 10^{-8} \text{ (cm}^3\text{.gm}^{-1}\text{.sec}^{-2}\text{)}$$

or,

$$G = 6.673 \times 10^{-11} \text{ (m}^3\text{.kg}^{-1}\text{.sec}^{-2}\text{)}$$

2.2.   The Gravitational Acceleration

Newton's second law of motion states that any body of mass (m) under the effect of force (F) moves with acceleration (a) where:

$$F = ma$$

Now, in the case of two particle-masses (m_1 and m_2), suppose one of them (mass m_2, say) is free to move, then this mass (m_2), which is under the influence of the attraction force due to the pull of the stationary mass m_1, will move towards m_1 with acceleration a_1.

By combining these two laws, equations 3-1 and 3-2 for the two-mass system, the following relationship is readily obtained:

$$a_1 = Gm_1 / r^2$$

Likewise, if m_1 is the mass that is free to move, then it will move towards the mass m_2 with acceleration a_2.

The acceleration **a** is directly proportional to the causing mass **m** and inversely proportional to the square of the distance **r**. Thus, the vector quantity **a**, which is the acceleration imposed, by a mass **m,** on a number of masses (**m_1, m_2, …**) located at the same distance from **m,** will be the same regardless of their individual masses (Fig. 2-2).
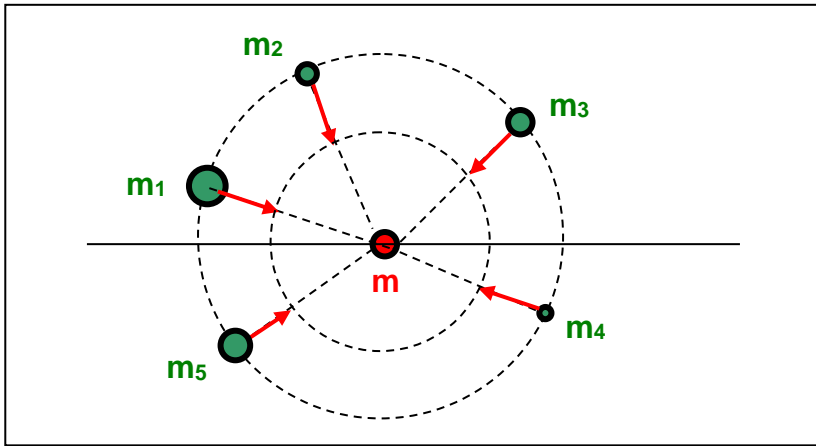
Fig. 2-2 Acceleration vectors (a) indicated by red arrows are due to the attraction force imposed by the mass (m) upon masses (m_1, m_2,… , m_5) which are at equal distances from the causing mass (m). Vectors (a_1, a_2, …) are of equal magnitudes regardless of the magnitude of these attracted masses.

2.3.   Gravity Computations of Large Bodies

Equation 3-3 expresses the relationship between a particle-mass (infinitesimal body) and the acceleration created at a point located at a defined distance from it. A particle of mass Δm would create an acceleration Δg at an observation point at r distance away is given by:

$$\Delta g = G \, \Delta m / r^2$$

In gravity surveying work, two modifications need to be introduced. The first is that the acceleration measured or computed is the vertical component, and the second modification is that the gravity source is a finite body-mass and not an infinitesimal particle. This is necessary since, in practice, all survey activities are concerning large mass-bodies buried at certain depths below ground surface.

The approach (Fig. 2-3) for the computation of the vertical component of acceleration (g_z) for a mass-body of finite size is by considering the body as being consisting of a large number of particles and then computing the vector sum of the contributions (Δg_z) of the constituent particles. For the nth particle (Δm_n) of a body buried at depth below the surface, the vertical component of its acceleration (Δg_n) at the observation point (P, Fig. 2-3) is given by:

$$\Delta g_n = (G \, \Delta m_n / r_n^2) \cos \theta_n$$
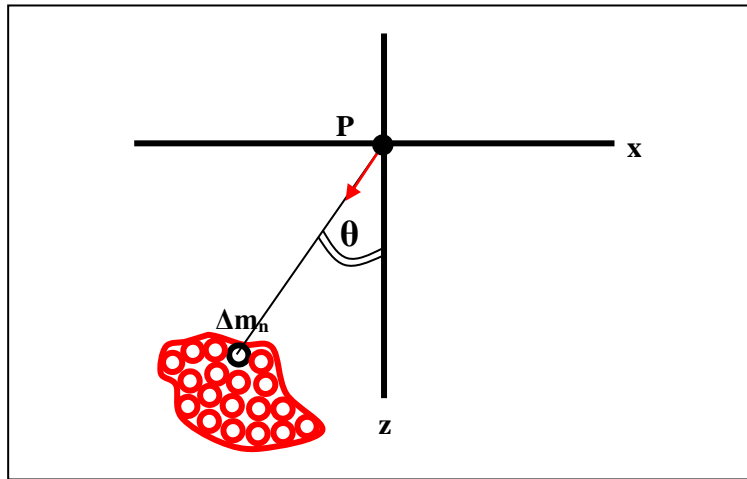
Fig. 2-3 The approach for computing the vertical component of acceleration caused by a mass-body of a finite size. Two-dimensional body (lamina) is used here to clarify the concept.

The net vertical component of acceleration (g_z) due to the whole body is obtained by summing the effects of the individual particles of the body, that is the sum $\Sigma \, \Delta g_n$, where:

$$g_z \; = \; G \; \Sigma \; (\; \Delta m_n / r_n^2) \; \cos \theta_n$$

Using Cartesian coordinate system for a three dimensional body of constant density (ρ), this equation may be re-expressed by the integral form:

$$g_z \; = \; G \; \rho \; \iiint z \; (x^2 + y^2 + z^2)^{-3/2} \; dx \; dy \; dz$$

It should be noted here that the term gravity is used in the geophysical literature to mean gravitational acceleration.

2.4. The Acceleration Unit

Normally the acceleration is measured by units having (in the cgs system) the dimensions of cm/sec^2 . This is called the gal after the Italian physicist Galileo. This unit is too large for practical survey measurements and thus the

milligal is normally used. The units that are in common use in gravity exploration work are:

1 gal = 1 centimeter /sec ^{2}

1 milligal = (1/1000) gal

1 microgal = (1/1000 000) gal

Another acceleration unit, the International Standard (SI) gravity unit (g.u.), is also used. One g.u. is equal to 1 micrometer/sec ^{2} . Hence,

1 g.u. = 1 micrometer/sec ^{2}

1 milligal = 10 g.u.

2.5.   Gravity Gradients

In general, the gradient of a natural field, such as gravity, is defined as the spatial rate of change of that field. In gravity surveying work, the gradient is defined as the rate of change of vertical component of gravity with respect to horizontal distance. On a gravity data-set shown as a contour map, the gradient at a point is measured in the direction of maximum slope. The common unit used for gradients is the Eotvos unit which is defined to be 10^{-6} milligal per centimeter of horizontal distance [Dobrin, 1960, page 179].

The gravity gradient (which is a vector quantity) is represented on a gravity contour map by an arrow of length which is proportional to its magnitude, pointing in the direction of the maximum rate of change of gravity (Fig. 2-4).

Sometimes this is referred to as the horizontal gradient to differentiate it from the vertical gradient which is defined as the rate of change of gravity with respect to displacement in the vertical direction. Mathematically we can define the terms as follows:

Horizontal Gradient :   d g / d x   ,   d g / d y

Vertical Gradient :   d g / d z
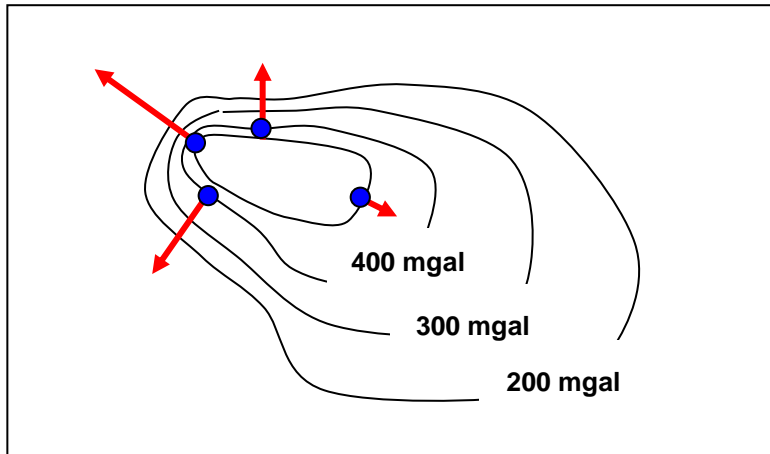
Fig. 2-4 Vector representation of the gravity gradient. Length of the arrow is proportional to the magnitude of the gradient at the point of measurement.

2.6.   Gravitational Field Intensity and Potential

In and around the Earth there exist a number of natural fields, such as the magnetic, electric, and gravitational fields. Any of these fields is defined as space in which the effect of force-source can be experienced. There are two main parameters associated with the field. These are the field intensity (field strength) and the field potential. Both of these parameters have measurable values at every point in the space where the field exists.

It is to be noted here that the geophysical techniques applied in oil and mineral explorations which utilize such natural fields (e.g. gravity, magnetic or electric) are sometimes referred to as potential methods because they are all having potential fields.

For the gravitational field, the field intensity at a given point is defined as the force (or acceleration, g) a unit mass experiences when positioned at that point. It is a vector quantity in the direction of the source of the field.

The second parameter is the potential of the gravity field (U). The gravitational potential at a given point is defined as the work spent in moving a unit mass from infinity to that point. Unlike the intensity, the potential is a scalar quantity.

By definition, the potential (U) at a point located at distance (r) from the centre of the Earth (of mass M) is given by U(r) where,

$$U(r) \ = \ G \, M \int (1/r^2) dr$$

That is:

$$U(r) \ = \ - \, G \, M \, / r$$

Conversely, differentiating the function **U(r)** with respect to the distance (r) gives the gravitational force (F), that is

$$F = dU/dr$$

Or:

$$F \ = \ G \, M \, / r^2$$

This is the mathematical relationship between the two parameters, the scalar (U) and the vector (F). It shows that the gravity force (F) or the acceleration (g) at a point is proportional to the gradient of the potential (U) of the gravitational field at that point.

The concept of potential can be used in gravity computations instead of the gravity force or acceleration. The gravitational potential U(r) has the units of cm^2 / sec^2.

2.7.   Concept of the Equipotential Surface

The equipotential surface is defined as the surface existing within a potential field on which the potential function U(r) is constant. This implies that there is no force component acting long that surface. This also means that the force at any point of the surface is always perpendicular to the equipotential surface at that point.

Over a part of the Earth surface where the subsurface medium is homogeneous, the gravitational equipotential surface of the gravity field will have a curvature which is equal to that of the earth surface which locally appears as horizontal to an observant. For the case of an anomalous mass existing below surface, the equipotential surface shall warp in such a way as it becomes perpendicular to the gravity direction (plumb line direction) at each of its points (Fig 2-5). The warping is upward for a mass of surplus density and downward for a deficient density.
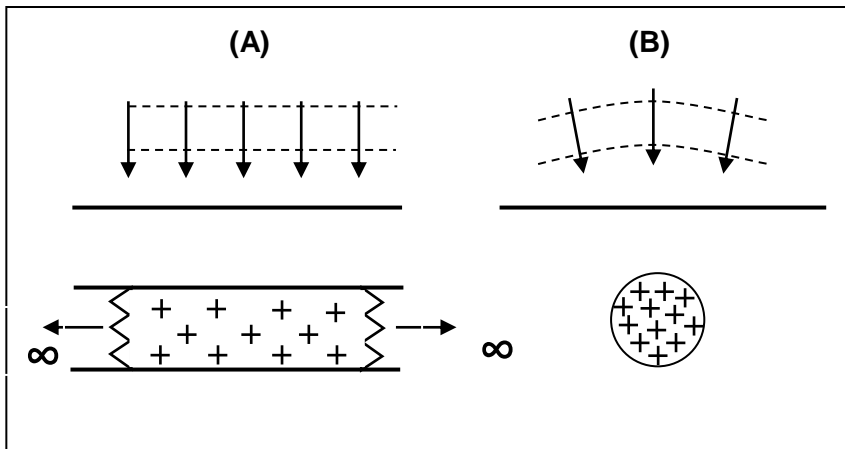
Fig. 2-5 Effect of density variation on the generated equipotential surfaces;
(A) Case of no lateral density changes, (B) Case of an anomalous, surplus-
density body

The ocean surface (geoid surface) is in fact an equipotential surface. It is
horizontal surface in the sense that it is perpendicular to the plumb lines at all
points of the ocean surface.

2.8. The Earth Gravity Variations

As a matter of fact, the Earth gravitational field in space is not constant, but
varies from one point to another. There are several factors that bring about
gravity changes on and above the Earth surface. At an observation point, the
measured gravity force (or acceleration) represents the vector sum of the various
gravity components generated from different sources.

If the Earth were stationary, homogeneous and perfectly spherical in shape,
then the intensity of its gravitational field would have been of constant value
over its entire surface. In reality, however, the earth is not homogeneous and it is
neither stationary nor perfectly spherical. The earth is an ellipsoid of revolution
rotating about its polar axis. These two factors, in addition to the inhomogeneous
nature of the Earth crust, are the main causes for disturbing the uniformity of the
gravitational field.

The rotating flattened earth causes the gravity value to change according to
latitude position. Beside this uniform global variation of the earth gravity there is
another type of variations of local origins. The main cause for the local
(anomalous) gravity changes is the existence of lateral density variations found

in the crust of the Earth. In fact, all local deviations in the Earth crust from the uniform ellipsoidal-model would disturb the uniformity of the Earth gravitational field. These detailed gravity changes that are of localized nature (caused by the existence of anomalous geologic bodies) form the basis for oil and mineral exploration by gravity surveying.

As shown in the following flowchart (Fig. 2-6), the Earth gravity-variations may be subdivided into two main types. The first type is the global (general) variation which is attributed to both rotation and flattening features of the earth. This is expressed by a mathematical formula that describes what is called the Normal Gravity of the Earth. Superimposed on this global type of variations, is the local (detailed) variation caused by the geological and topographic conditions prevailing in the neighborhood of any observation point used for the measurement.
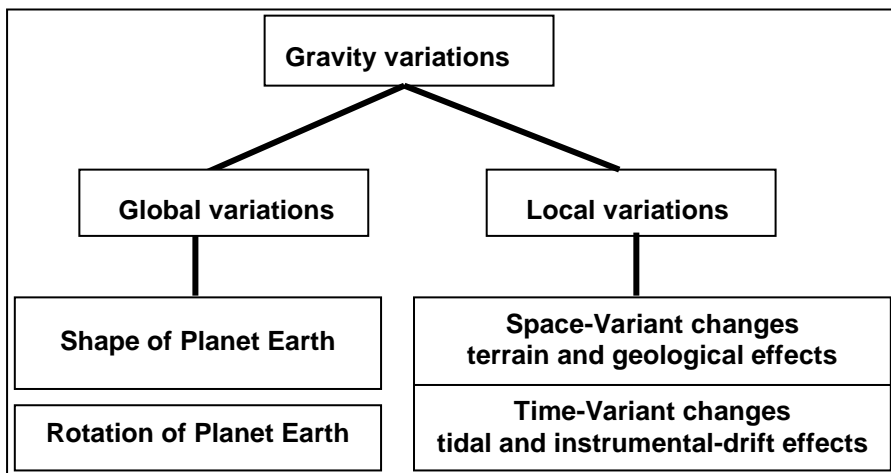
Fig. 2-6 Flowchart showing the two types of the Earth gravity variations; the global and the local types of variations.

Chapter 3

THE GLOBAL GRAVITY VARIATIONS

The earth is an ellipsoid of revolution rotating about its polar axis. These two factors (ellipsoidal shape and rotation) disturb the uniformity of the global gravitational field. Part of the effect is due to the Earth shape (shape effect) and the other part is due to its rotation (rotation effect).

3.1. The Shape Effect

As we have presented in a previous discussion, the gravitational acceleration (g), measured on the surface of a static homogeneous spherical Earth of mass M, density ρ, and radius R, is given by:

$$g = G M / R^2 \quad = 4\pi\ G\ R^3\rho/3R^2$$

Hence,

$$g = 4\pi\ G\ R\ \rho/3$$

In this case, since R and ρ are constant, g will be constant all over the Earth surface or over any other concentric spherical surface (Fig. 3-1).
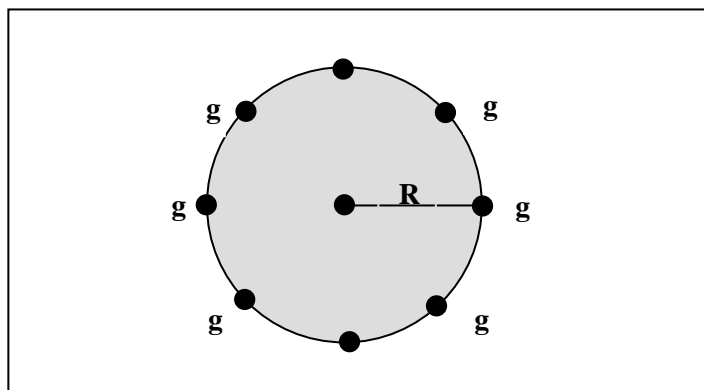
Fig. 3-1 Gravity field of a homogeneous spherical model of the Earth

In reality, the Earth is not a sphere but an ellipsoid of revolution with its polar radius shorter than the equatorial radius by 21 km. In this case, the distances of the surface-points vary from location to location and hence the gravity value changes accordingly (Fig. 3-2).
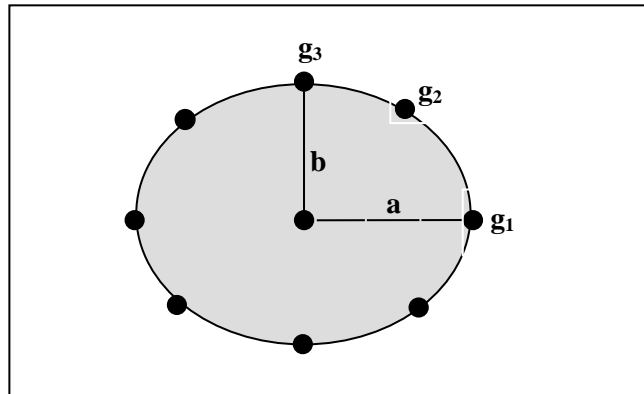
Fig. 3-2 Gravity field of a homogeneous ellipsoidal model of the Earth.

The ellipsoidal shape of the Earth has the effect of increasing gravity as the observation point gets nearer to the poles. In fact, the gravity value, measured at any point on the mean sea level surface, is always higher than that measured at the mean sea level surface at the equator. It reaches its maximum value at the polar points (Fig. 3-3).
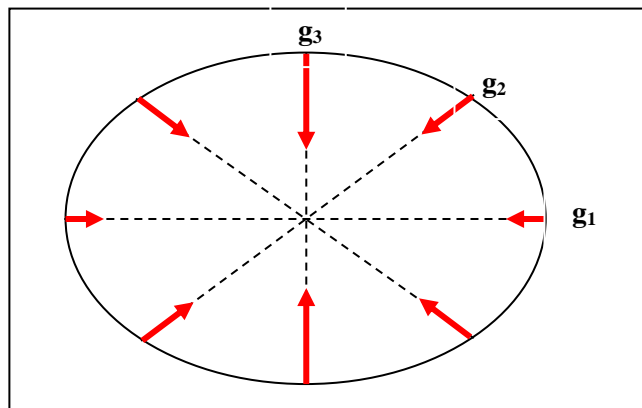
Fig. 3-3 Variation of the gravity vector (red arrows) over the Earth surface due to its ellipsoidal shape. Length of arrow is proportional to gravity magnitude.

3.2.   The Rotation Effect

A body on the surface of a rotating Earth experiences a centrifugal force that acts in opposite direction to the gravitational attraction force. Because the Earth is rotating about its polar axis, the developed centrifugal force attains its maximum value at the equator where the rotation radius attains its maximum length, r_{max} (Fig. 3-4).
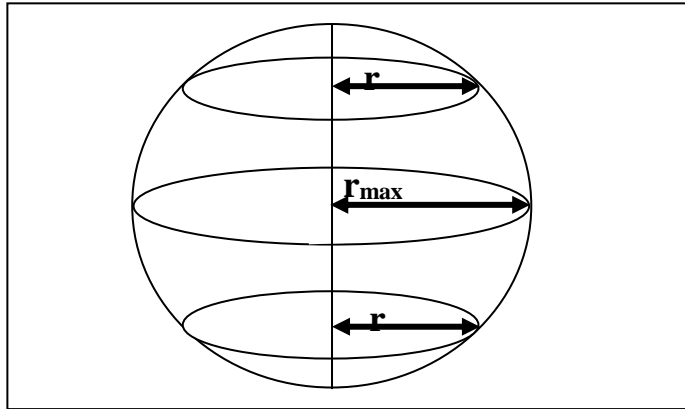
Fig. 3-4 Change of the rotation radius (r) with the location on the Earth surface.

The magnitude of the centrifugal acceleration of a body rotating at an angular speed (ω) is equal to ($\omega^2 r$), where r is the rotation radius. Thus, the gravity-vector contributed due to rotation is maximum at the equator decreasing gradually towards the poles (Fig. 3-5). It reaches zero-value at the polar points. The reason for the change is that the rotation radius becomes less as the rotation plane of a point at the earth surface gets nearer to the poles.

Development of the centrifugal force and the manner of its variation seem to give the logical explanation for the cause of the flattening phenomenon of the Earth. Accordingly, the flattening process is therefore, expected to continue with time bringing further flattening in the future.

3.3.   The Combined Effect

Because the Earth is ellipsoidal and rotating about its shorter (polar) axis, its actual gravity is made up of the two vectors; the gravitational attraction directed towards the Earth centre and the opposing centrifugal force in the direction perpendicular to the polar axis (Fig. 3-6).
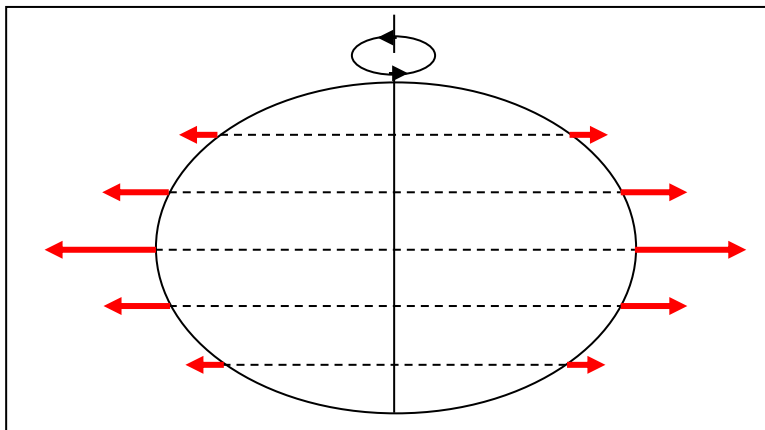
Fig. 3-5 Variation of the gravity-vector over the Earth surface due to Earth rotation.
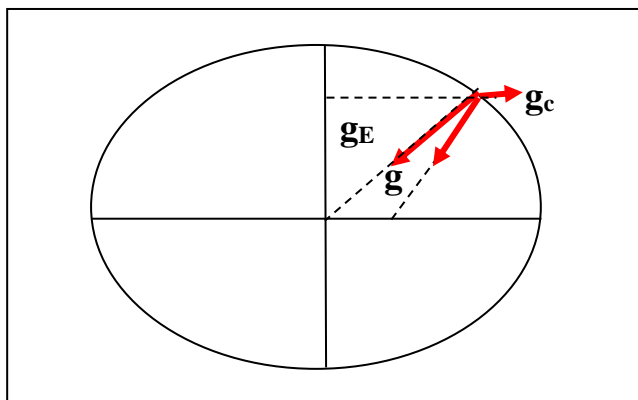
Fig. 3-6 Resultant gravity (g) of the two components; Earth-mass gravity (g_E) and centrifugal acceleration (g_c).

The measured acceleration vector at each point on the Earth surface is the resultant (i.e. combined effect) of two components acting at that point. These are the gravitational attraction of the Earth-mass and the centrifugal force due to the Earth-rotation.

The gravity has its maximum value at the Equator and its minimum value at the polar points. In fact, the observed gravity value at the poles exceeds that at the equator by about 5200 mgal. This difference is found to be about half the value expected from shape considerations only. The reduction is interpreted to be caused by the subsurface mass in the equatorial bulge which creates an extra gravity component that increases the equatorial value, giving the difference of 5180 (i.e. about 5200) mgal.

It is worth noting that the net gravitational vector does not point to the centre of the Earth except at the pole and at the equator. This is because at the pole, there is only the mass effect (rotation effect is zero) and at the equator where the two effects are collinear but in exactly opposite directions.

3.4.   Normal Gravity

As it is mentioned above, the Earth reference-surface for gravity computations is defined to be the surface of the ellipsoid which coincides with the mean sea level. This is called the reference ellipsoid or the normal ellipsoid, and the gravitational field determined over this surface is given the term *Normal Gravity*.

The Normal Gravity (g_N) is expressed as a mathematical function of latitude (Φ), that is $g_N(\Phi)$. It describes the global gravity variation which is attributed to both of flattening and rotation of the Earth.

The first normal-ellipsoid model was defined in 1930 by the International Union of Geodesy and Geophysics (IUGG). Based on the constants of this model together with the measured gravity value at the equator, the first theoretical formula for the Normal Gravity, $g_N(\Phi)$, was formulated (see Nettleton, 1976, p17). The measurements involved in the computations were adjusted to the pendulum measurements made at the German city Potsdam in 1906. This formula is normally referred to as the International Gravity Formula (IGF).

In 1963, the Society of Exploration Geophysicists (SEG) published the results of a global gravity measurements by G.P. Woollard. The publication includes the gravity values that were obtained from pendulum and gravimeter measurements made at the worldwide network of observation stations, (now called the International Gravity Standardization Net, 1971, IGSN71).

In about the year of 1965, accuracy of gravity measurements has largely improved, attaining a tenth of the milligal. After this time, more accurate measurements made by gravimeter and falling-mass methods revealed that the Potsdam-based value is 14-mgal too high. In view of this finding the data published by SEG in 1963 had to be corrected by subtracting 14 mgal.

In 1967, more accurate satellite data and more advanced measurement technology led to revision by the IUGG of the normal ellipsoid model of the Earth. The refined Normal Gravity formula based on this revised ellipsoid was determined. This formula, which replaced the IGF, is called the 1967-Geodetic Reference System (GRS67) formula and is expressed by:

$$g_N (\Phi) = 978.031846 \,(1 + 0.005278895 \sin^2 \Phi + 0.000023462 \sin^4 \Phi)$$

In 1980, the normal ellipsoid was subjected to further refinements. The produced changes were too small to be of practical significance. Thus the GRS67 formula stayed adequate for work in gravity exploration (Fig. 3-7).
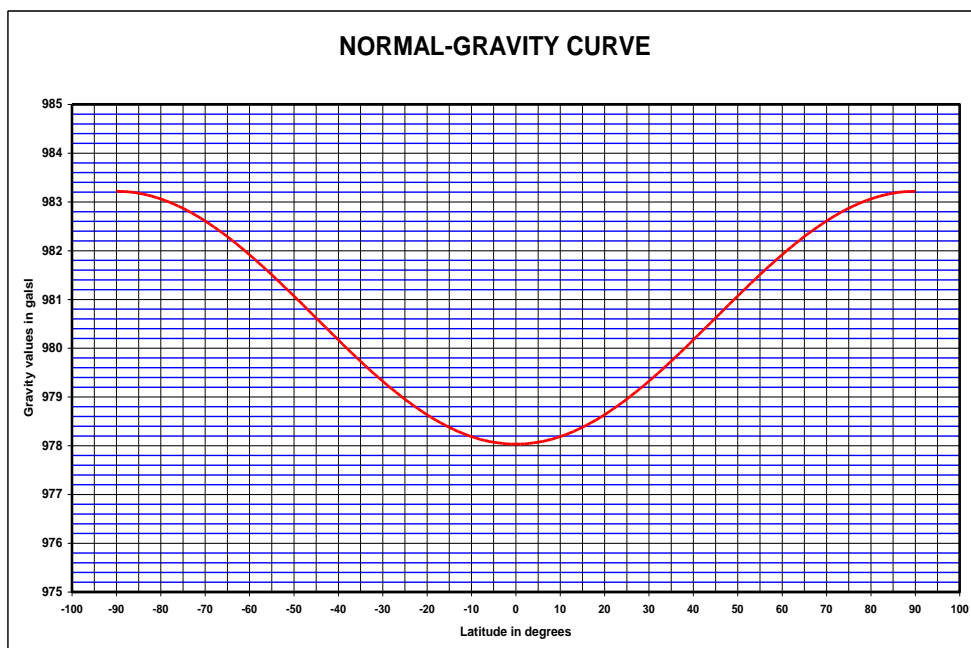
Fig. 3-7 Plot of the Normal Gravity function (GRS67 formula), gravity in gals against latitude in degrees, covering the latitude range of 0 to 90 degrees.

The Normal Gravity function, $g_N (\Phi)$, expressed by the GRS67 formula shows that the gravity value increases as the observation point approaches the polar points. In fact, it attains a minimum value of 978.0318 gals at the equator and a maximum value of 983.2178 at the polar points. This means that the polar value exceeds that of the equator by 5186 milligals.

To summarize; the Normal Gravity of the Earth, expressed by the GRS 67 formula, expresses the large-scale global gravity variations on the mean sea level surface of the rotating and flattened ellipsoidal Earth. Construction of the formula is based on actual gravity measurements made at observation-points distributed throughout the world. Special interpolation techniques were applied in the computations assuming the earth to be of uniform lateral-density ellipsoid.

Chapter 4

THE LOCAL GRAVITY VARIATIONS

As it is mentioned, the rotating flattened Earth causes the gravity value to change uniformly over the surface of the normal ellipsoid. The changes are expressed by the Normal Gravity function g_N (Φ). Another type of variations which are of localized nature is superimposed on this uniform global variation of the Earth gravity. The principal cause for the local gravity-changes (at sea-level) is the existence of lateral-density variations found in the crust of the Earth.

These detailed gravity changes (gravity anomalies) that are caused by local geological changes form the basis for oil and mineral exploration by gravity surveying.

Here below the main factors which are of local nature, that affect gravity.

4.1. Elevation Effect

According to the universal law of gravitation, the Earth gravity decreases with the increase of the distance between the center of the Earth and the observation point. Thus, at an observation point P (Fig. 4-1), of elevation (h), that is at height h above sea level, the gravity will reduce by Δg where :

$$\Delta g = g_0 - GM / (R+h)^2 = g_0 - g_0\,[R^2 / (R + h)^2$$

$$\Delta g = g_0\,\{ 1 - [R^2 / (R + h)^2] \} = g_0\,\{2hR + h^2\} / (R +h)^2$$

Hence,

$$\Delta g = 2g_0\,h/R\,, \quad \text{since } h<< R$$

The same result for $\Delta \mathbf{g}$ can be obtained from differentiating the equation of the gravitational universal law ($g_0 = GM/R^2$) with respect to R.

$$dg_0 / dR = - 2\,GM / R^3 = - 2g_0 / R$$
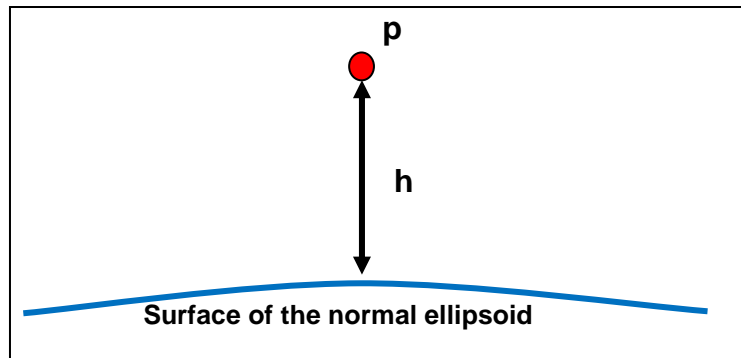
Fig. 4-1 Elevation effect: Decrease of gravity with the increase of elevation (h) of the observation point (P) above the surface of the normal ellipsoid.

Hence, for a finite increment **h** in **R**, and neglecting the minus sign:

$$\Delta g = 2g_0 \, h \, / \, R$$

It is noted here that Δg is dependant only on the Earth gravity (g_0), considering that the Earth radius (6370 km) being practically constant. From the Normal Gravity formula, g_0 is 983.2178 gal at the equator and 978.0318 at the poles. These figures give:

$\Delta g = 0.309$ mgal per meter of elevation at the equator

$\Delta g = 0.307$ mgal per meter of elevation at the poles

Giving:

$\Delta g = 0.308$ mgal per meter of elevation as an average

$\Delta g = 0.31$ mgal per meter of elevation as an average

For practical application in gravity normal work the rate of 0.31 mgal per meter of elevation change is considered adequate.

4.2.   Excess-Mass Effect

If the observation point is located on land surface which is rising by **h** meters above sea level, the rock mass existing between observation point and sea level has its own contribution to the gravity value measured at that point. For computation purposes, the rock layer above sea level is approximated by an infinite horizontal slab of thickness (**h**), tangent to the normal ellipsoid which is the sea surface.

The gravity effect due to the excess-mass present above the sea level is computed by assuming an infinite horizontal slab of rock-material, of thickness (**h**), mean density (**ρ**), and of infinite extent (Fig. 4-2). The gravity effect of such a slab is given by (see derivation in chapter-8):

$$\Delta g = 2\,\pi\,G\,\rho\,h$$

This means that the gravity contribution of an infinite slab of material (density, ρ) is given by $\Delta g = 0.0419\,\rho$ mgal per meter
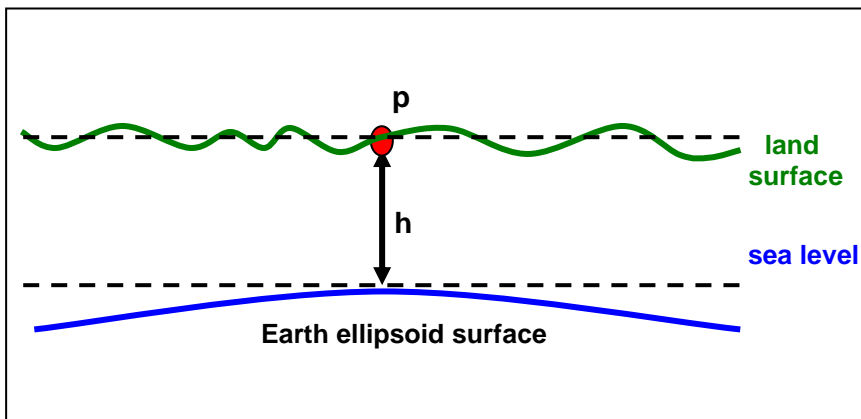
Fig. 4-2 Excess mass effect; increase of gravity at observation point (P) due to an infinite horizontal rock-slab is considered to be tangent to the surface of the normal ellipsoid.

This model is used in the adjustment process, which reduces the measured gravity at an observation point to what it would be if it located at the surface of the normal ellipsoid (sea-level).

4.3.   The Topographic Effect

In actual gravity surveys, observation points are not located on surface of ideal horizontal slabs but on surfaces of irregular topography. This means that the ideal slab has holes, valleys and hills. A rising hill in the neighborhood of an observation point will reduce the gravity at the observation point. The same effect (gravity reduction) is introduced by a hole or a valley since in this case the contribution is to increase gravity value as the observation point had not the infill of these holes been removed (Fig. 4-3).
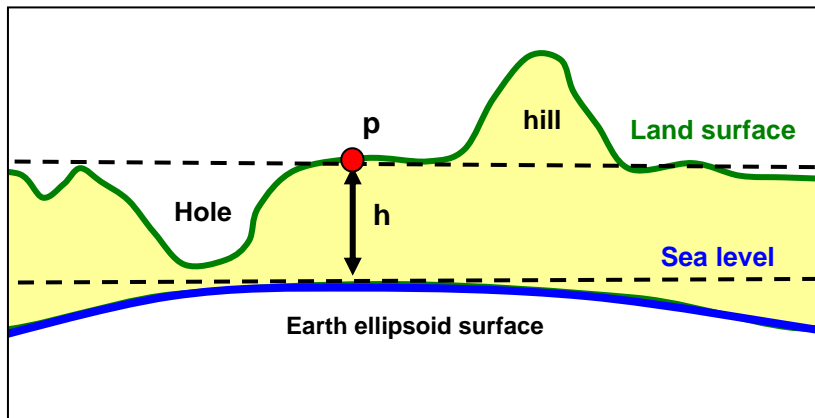
Fig. 4-3 Topographic effect; decreases of gravity due to topographic irregularities (hills and valleys) are defined with respect to the top-surface of the horizontal rock- slab that is tangent to the normal ellipsoid.

4.4.   Geological Effects

The main purpose of a gravity survey is to look for a subsurface geological anomaly. Such an anomaly that affects gravity value at an observation point may be a massive mineral body or a folded or faulted geological formation. As far as gravity variation is concerned, a geological change that can create a gravity anomaly is lateral density changes. In other words, gravity changes measured at or reduced to a horizontal plane (usually taken at the sea-level) reflect density contrasts among different geologic features that exist below the surface of the normal ellipsoid, which is the sea-level.

A density contrast between the anomalous body and the surrounding medium will cause a corresponding gravity anomaly. The created anomaly is a gravity increase (relatively positive) for a density-surplus and gravity decrease (relatively negative) for density deficiency. Thus for example a buried heavy

ore-body would create a positive gravity anomaly, whereas a buried salt dome of relatively low density would give a negative anomaly (Fig. 4-4).
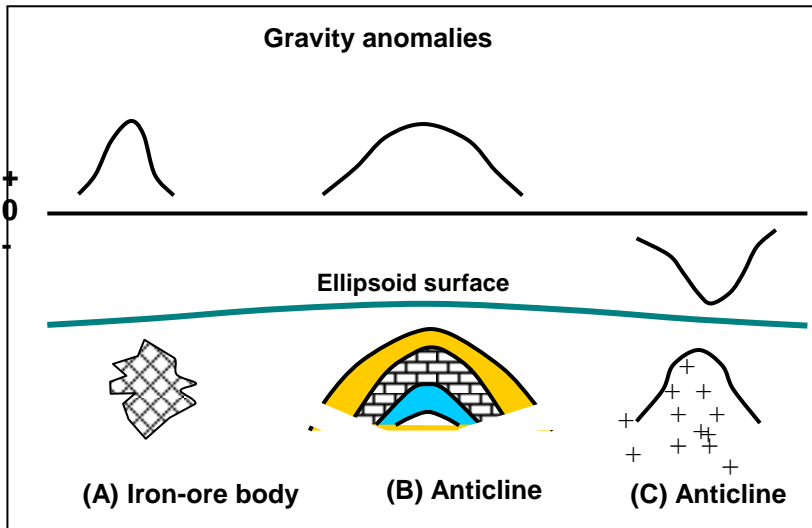
Fig. 4-4 Geological effect; decrease or increase of gravity (profile) of a geological anomalous-mass existing beneath the surface of the normal ellipsoid.

From computations at a number of points on a surface located above the anomalous body, one can construct gravity-profiles over selected straight lines (at a group of co-linear points). The so-obtained profile will show the variation of the gravity effect due to that body along the selected line. The three-dimensional variation may be shown as a contour map.

The gravity anomaly created by a buried geological body can be analytically computed if it is in the form of a defined geometrical shape as it is explained in chapter 9

4.5.   Time-Variant Changes

Both of the sun and the moon exert attraction on the Earth. Because of its near distance to Earth in comparison to that of the sun, the moon gravitational attraction on earth surface is larger than that due to the sun. The combined gravity effect due to sun and moon (which is periodic in nature) is called the tidal gravity effect. Tidal variations are normally within few tenths of milligal, and period of about 12 hours. It is considered to be of the same value if

measurements are made at sites which are less than a few hundred kilometers apart.

There is another type of time variant changes influencing gravity measurements which is due to the change with time of the scale factor of the measuring instrument. This effect (called the instrumental drift) is strictly speaking not a change in the gravity field, but it is always there and incorporated with the measured values. The instrumental drift caused as result of mechanical changes of the gravimeter levers and springs is continuous with time. Various measures are usually taken by manufacturers to minimize the effect but nevertheless it is taken into consideration in survey work.

Measurements of the time-variant changes in gravity normally include both the tidal effect and the instrumental drift combined together. The combined effect of the tidal and instrumental drift can be determined by repeated observations at the same site. These changes may be shown by a curve (gravimeter-reading against time) from which one can sort out the cyclic tidal variations from the non-cyclic instrumental drift (Fig. 4-5).
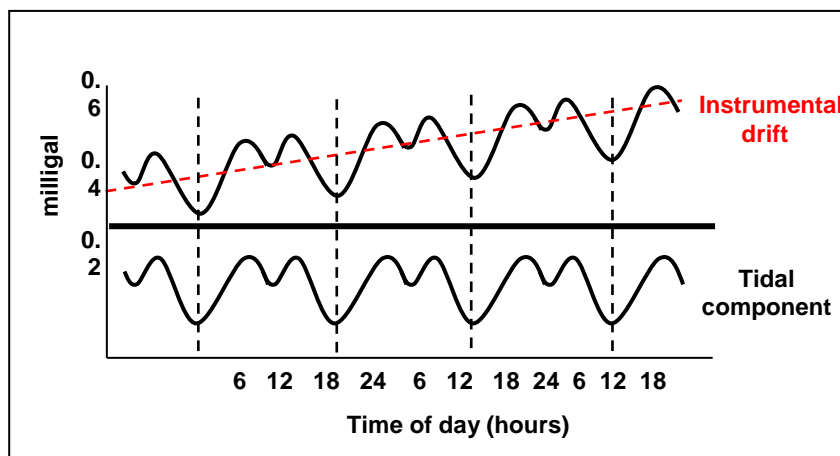
Fig. 4-5 Time-variant gravity variation. The cyclic (tidal) component superimposed on the none-cyclic instrumental drift (the dotted line). The lower curve represents the time-variant gravity variation (tidal component) with instrument drift removed.

Chapter 5

GRAVITY MEASUREMENTS

5.1. Features of Gravity Measuring Instruments

The Earth gravitational acceleration (g) and its changes are measured by specially designed gravitymeters, or gravimeters as they are normally called. Some of these instruments are designed to measure the absolute value of gravity, while others are designed to suit relative gravity measurements. In geophysical surveying work, measurements are mainly concerned with relative gravity determinations. This involves measuring gravity differences between two locations or between two different times at the same location. Measuring differences can be used to determine the absolute gravity by measuring the difference in gravity between an observation point and a base-station at which the absolute gravity is precisely known.

The measured gravity value (**g**) or gravity-difference (**Δg**) are normally expressed in milligal units or in SI gravity units (g.u.). Since the Earth gravity (**g**) measured at sea-level is nearly equal to one killogal (10^3 cm.sec^{-2}), one milligal is estimated to be about one-millionth (10^{-6}) of **g**.

Gravity changes, for which a gravity-measuring instrument is required to detect, are normally found in the range of a few milligals to few tens of milligals. Small-scale geological anomalies, such as deep structures or small subsurface cavities, may give rise to gravity anomalies that are as small as 0.1 milligal or even smaller. This means that a gravimeter is required to detect such small gravity changes in **g,** which are in the order of a few parts in 10^7. Thus, an accuracy of 0.1 mgal in measuring **g** would represent an accuracy of one part in ten millions. This is equivalent to measuring a 100-km distance with an accuracy of one centimeter.

Modern measurement techniques, such as the free-fall method, have attained an accuracy of 0.01 milligal which can detect changes in the Earth gravity with accuracy of 1 in 10^8. Any gravity-measuring instrument should, therefore, be designed in such a way as to be capable in measuring gravity with this kind of accuracy. In addition to being highly accurate, the measuring instrument is required to be portable, stable, and fast to operate. For any gravity-measuring

instrument, these features are necessary in order to be a practical tool in conducting an exploration gravity survey.

5.2.   Methods of Measuring Gravity

There are four main methods which may be used in measuring gravity. These are: Free-falling Mass, Swinging Pendulum, Spring Stretching, and Vibrating Fiber.

5.2.1 Free-falling

A mass falling from a rest position of height (h) will cover the distance h during time lapse (t) according to the equation:

$$h = (1 / 2) \, g \, t^2$$

Although the physical principle of this method is simple, it is difficult in practice to attain the kind of accuracy required. Thus, for a one meter fall, the distance (h) and time (t) must be accurate within 10^{-5} cm and 10^{-8} sec respectively. By the use of laser-interference devices, time and distance of falling mass can be determined with this kind of accuracy. However, achieving this standard of accuracy has not become available until after 1960 when laser and the associated electronic technology were introduced.

The instrument design, based on the falling-mass principle, consists of two corner-cube prisms and a laser-light source. The interference of reflected laser-light beams is used to measure the time covered by the falling prism in covering the pre-defined height (Fig. 5-1).

In practice, this instrument is not easy to operate as a portable instrument. It is more suited for use in geophysical observatories where gravity is required to be measured with an accuracy of 0.1 mgal or better.

The measurement-techniques based on use of falling mass instruments were introduced during the 1960s. These measurements have contributed in providing accurate gravity values at base stations of the world-wide network.
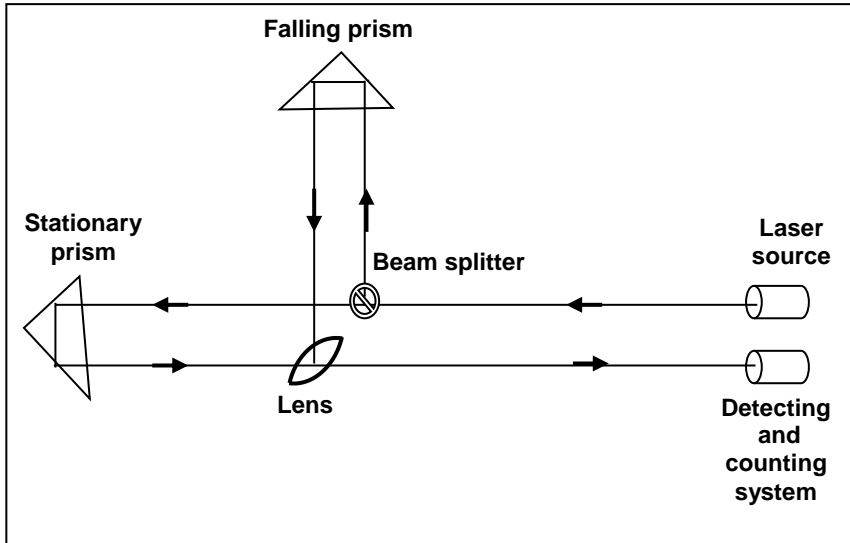
Fig. 5-1 Sketch layout of the falling-prism instrument for measuring gravity

5.2.2 Swinging Pendulum

A pendulum is defined as an instrument consisting of a freely-swinging mass which is suspended from a fixed point (Fig. 5-2). The pendulum swinging period (τ) is the function of the pendulum constants and the earth gravity (g). For the well-known simple pendulum, swinging with small amplitude, the period (T) is given by the function:

$$\tau = 2\pi\sqrt{L/g}$$

where **L** is the length of the string (considered to be weightless) which connects a point mass to a suspension point.

In general, $\boldsymbol{\tau}$ is given by:

$$\tau = 2\pi\sqrt{I/mgh}$$

$$\tau^2 = k/g \ ,$$

Where I is the moment of inertia about the suspension point, and h is the distance from the suspension point to the center of pendulum mass (m).
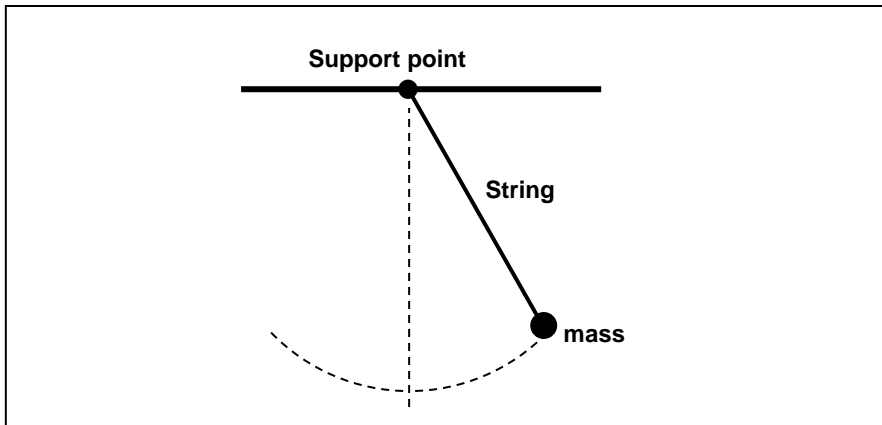
Fig. 5-2 The simple pendulum consisting of a mass attached to the end of a string.

This formula expresses the relation between g and the pendulum constant (k),

$$k = 4\pi^2\, l\, /\, mh$$

It is to be noted here that for the simple weightless string, shown above, the constant **k** will be equal to $4\pi^2 L$.

Hence g can be readily computed from the relation:

$$g = k\, /\, \tau^2$$

This is simple computation, but the main problem is in designing a pendulum that can measure **g** within the precision of 0.1 mgal. However the pendulum proved to serve well in accurate measurement of differences rather than absolute values of gravity. Thus, assuming **k** stays unchanged when the pendulum is moved from position-1 to position-2, we can write:

$$g_1\, \tau_1^{\,2} = g_2\, \tau_2^{\,2}$$

and

$$g_2 = g_1\, (\tau_1\, /\, \tau_2\,)^2$$

Thus from these two measurements we can find the gravity difference, **Δg** (= g_2-g_1). Assuming that **k** keeps unchanged, g_2 and g_1 would have the same amount of error and they cancel out in the subtraction process giving accurate value for **Δg**, at an accuracy that can reach a level of better than 0.1 mgal .

A standard portable pendulum, the Gulf Pendulum (Fig. 5-3), was used in geophysical exploration during the 1930s. It consists of glass bar with wedge-shaped supports on either side resting on glass plates which were attached to a heavy frame. The swinging mass is attached to a wedge which is resting on a stationary platform. The pendulum is encased in a vacuum chamber which is thermostatically controlled to maintain stable temperature.
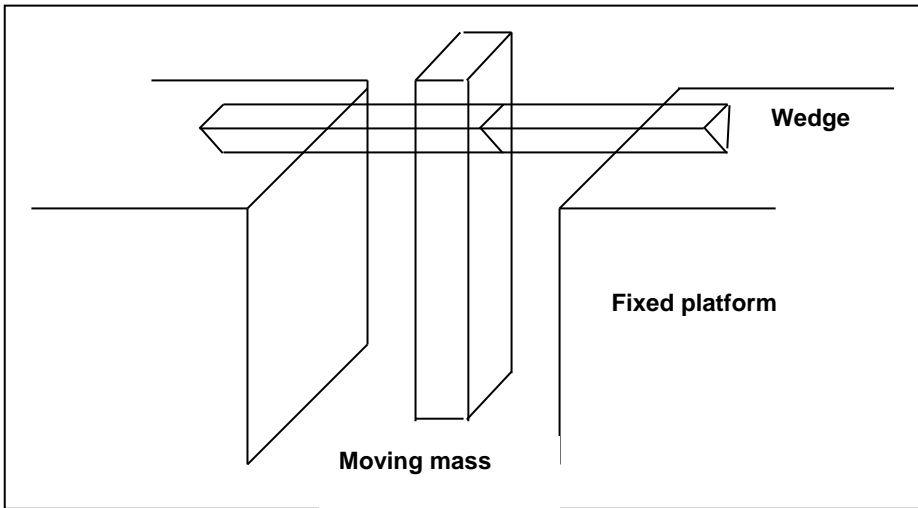
Fig. 5-3 Sketch showing the structure of the Gulf pendulum.

The Gulf Pendulum was used by G. P. Woolard (1908-1978) and his group in establishing the world-wide network of gravity base-stations during the years around 1960.

5.2.3 Spring Gravimeter

Unlike the falling weight and pendulum instruments gravimeters are designed to measure gravity differences rather than absolute gravity values. In principle, a gravimeter is a refined version of the spring balance. The extension of the spring depends on the pulling force. As it is shown in Fig. 5-4, the gravitational force (**mg**) is balanced by the spring upward force (**kx**). That is:

$$mg = kx$$
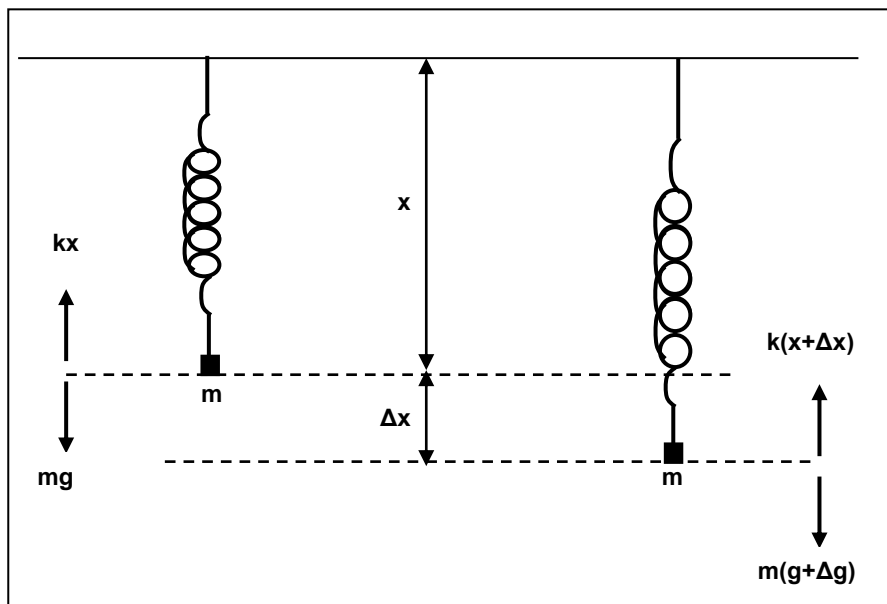
Fig. 5-4 Principles of the spring balance

This means that any change in gravity (Δ**g**) produces a corresponding change (Δ**x**) in the spring length. Since:

$$m \ \Delta g = k \ \Delta x$$

and

$$\Delta x / \Delta g = m/k$$

It should be noted here that the spring balance differs from the beam balance in that it determines weight (force) and not mass. That is why the spring balance is used for gravity changes whereas beam balance is unable to detect such changes.

In a gravimeter, a mass is attached at the end of a spring and when gravity increases the spring is stretched by a proportional amount. Thus from direct measurement of the change in the spring length (Δ**x**) the gravity change (Δ**g**) is determined from Δ**g = k Δx/m**.

A gravimeter is required to detect gravity changes of 0.1 mgal (one in ten millions of the earth gravity). The spring of a gravimeter is about 30 cm-long, which means that it is required to measure length change in the order of 0.03 microns (3×10^{-6} cm). For this reason, gravimeters employ magnification processes based on either optical, electrical or mechanical techniques.

It is worth noting that this type of a spring system (similar to a seismometer) has a natural period (τ), when it is freely vibrating in vertical direction. τ is given by:

$$\tau \ = \ 2\,\pi\ \sqrt{\ m/k}$$

Using the equation $(\Delta x \,/\, \Delta g \ = \ m/k\ )$,

 we get:

$$\Delta x/\,\Delta g \ = \ (\tau\,/\,2\,\pi)^2$$

This means that, the system sensitivity ($\Delta x/\Delta g$), which is proportional to τ^2, can be increased by choosing the system-parameters in such a way as to get larger natural period (τ). That is getting greater change in the spring length for a given gravity change.

All gravimeters are sensitive to changes in temperature, pressure and to earth seismic tremors, and all these effects are taken into consideration in the construction-design.

According to their construction-designs, gravimeters are divided into stable and unstable types:

5.2.3.1 The Stable Type of Gravimeters

A case of stable equilibrium is represented by a body that tends to return to its rest position if it were slightly displaced. The unstable equilibrium case, on the other hand, is the case where the body tends to move farther away from its original rest position.

In the stable type of gravimeters, the spring used is of stiffness (**k**) which is as low as possible to give highest possible sensitivity while at the same time it is strong enough that can support the suspended mass (**m**). Examples of stable gravimeters are *Hartley* and *Gulf gravimeters*.

The ***Hartley gravimeter*** is one of the simplest examples of the stable type of gravimeters. The vertical motion of the mass is magnified about 50,000 times by a system of mechanical and optical levers. It is the first gravity instrument that used the principle of the null method by which the displacement is measured through adjustment of an auxiliary spring (Fig. 5-5).
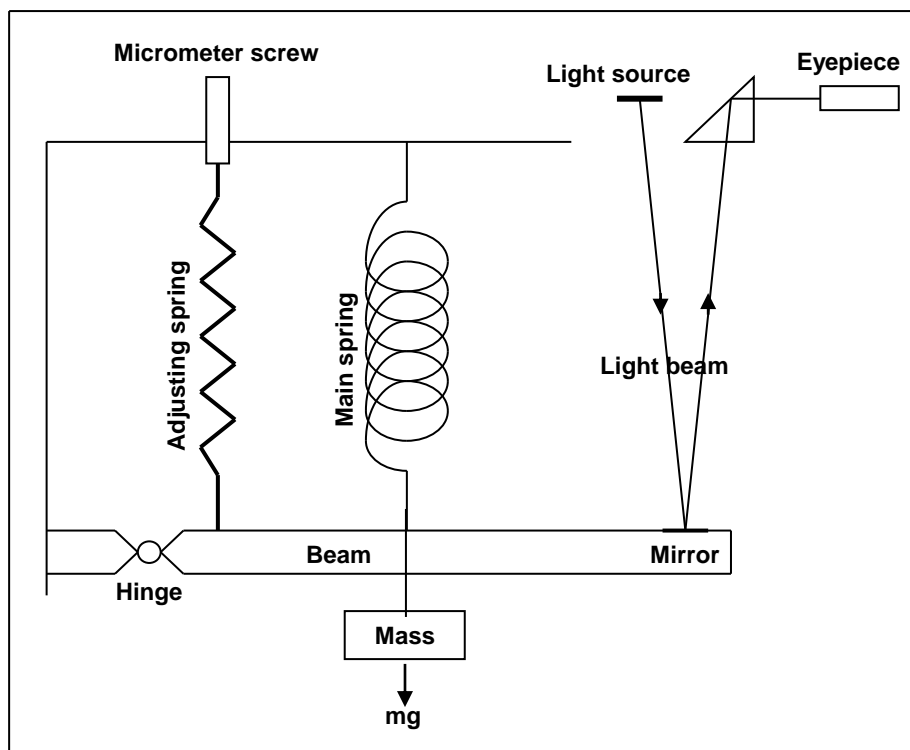
Fig. 5-5 Schematic representation of the Hartley gravimeter

The accuracy of this gravimeter is only about one milligal which is not sufficient for normal gravity exploration work.

The *Gulf gravimeter* consists of a mass attached to the lower end of a helical spring which is made in the form of a helix with the flat surfaces always parallel to the spring axis (Fig. 5-6).

When the gravity increases the spring is rotating as well as increasing in length. In the Gulf gravimeter, the rotation is magnified by a system of mirrors giving an accuracy of 0.02 mgal.
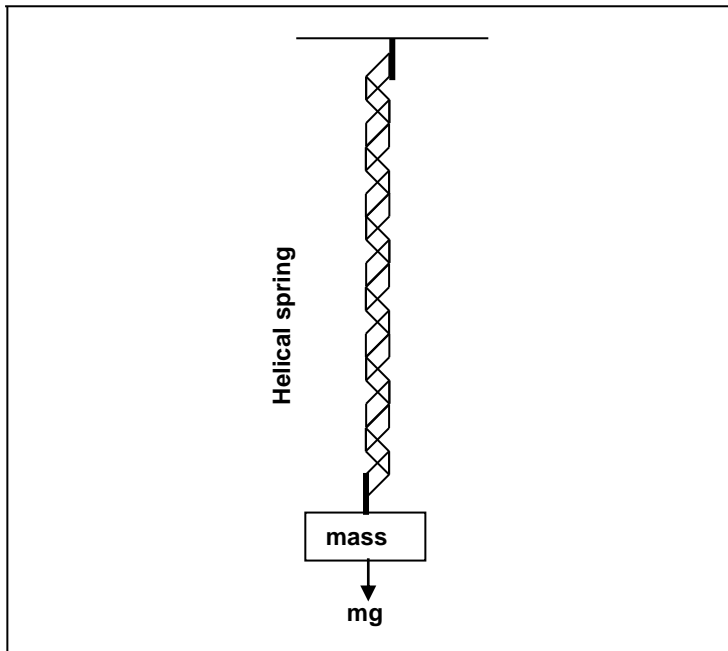
Fig. 5-6 Schematic representation of the Gulf gravimeter.

5.2.3.2 Unstable type of Gravimeters

In the design of this type of gravimeters, extra sensitivity is gained by making the system unstable about the null position. A principle, called astatization or labilization, is introduced to achieve this objective. In an astatized system the gravitational force is kept in an unstable equilibrium with the restoring (stabilizing) force. The instability feature is provided by an extra force which acts in the same direction as the gravitational force and in opposition to the restoring force. This extra force, called astatizing or labilizing force, is created once the suspended gravimeter mass is shifted from the null (equilibrium) position. The astatizing force acts as an agent that intensifies the effect of the gravity change with respect to the equilibrium value. This feature would greatly increase the measurement-sensitivity of the instrument.

One example of this unstable type of gravimeters is Thyssen gravimeter. As illustrated in Fig 5-7, the astatizing force is provided by an auxiliary mass (m). The main mass (M) which is suspended from one end of the gravimeter beam is balanced against the spring stabilizing force (**kx**).

The auxiliary weight is put exactly above the pivot which is balanced in an unstable equilibrium. A small change in **g** will cause the beam to tilt and the

auxiliary mass to move in the same direction, bringing about an additional couple which reinforces that of the changed gravitational force. This causes an additional increase in the spring length which is proportional to the change of gravity. The precision of an observation achieved with this gravimeter is about 0.25 mgal.
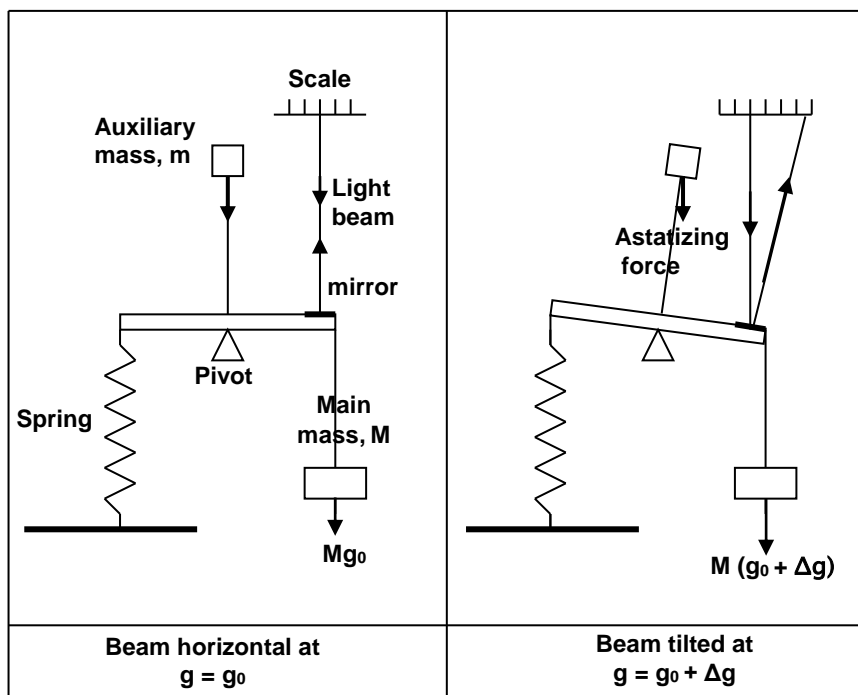
Fig. 5-7 Schematic representation of the Thyssen gravimeter.

LaCoste-Romberg Gravimeters

It consists of a hinged beam carrying a mass (M) which is supported by a spring. As shown in Fig 5-8, the angle between the spring and the beam (θ_1) changes with the change in gravity (Δg). This change will cause the moment of the spring on the beam to vary in the same sense as that of the moment created by the gravitational change. This kind of design would provide the required instability equilibrium (i.e. astatization effect) which magnifies the effect of gravity change. Measurement of the changes is made by applying the null-principle where an adjusting screw is turned to change the support position of the main spring.

Through electrical heating coils (thermostat device), the temperature of the system is maintained within 0.002 C and its measurement accuracy can be up to 0.01 mgal.

The LaCoste-Romberg gravimeter has an additional feature which is the use of the so called "zero length" spring. In the zero position of the gravimeter beam, the main restoring spring is designed in such a way that the beam weight is counteracted by an extra tension put into the spring when it is manufactured. This means that the beam, in its null position, produces zero extension in the spring. This kind of spring (called "zero length" spring) can be made by twisting and coiling a wire at the same time. Effectively the extension of the zero-length spring from equilibrium state caused by the beam weight in its null position is counteracted by the extra tension put into the spring when manufactured.
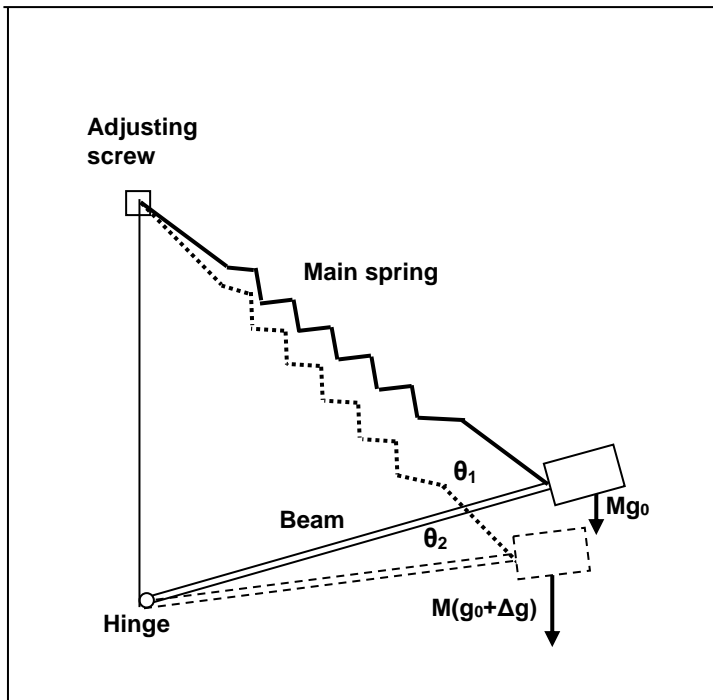
Fig. 5-8 Schematic representation of the LaCoste-Romberg gravimeter.

The advantage of the zero-length spring is that the beam deflection will be symmetrical about the equilibrium position. That is a positive reading and negative reading for the same magnitude of gravity change will be equal. Another advantage gained from the use of such springs is that the spring can be shorter than normal length for the same amount of sensitivity (Dobrin, 1960).

There are different models of LaCoste-Romberg gravimeters. Fig. (5-9) show two models (G and EG) of Romberg gravimeters.

Fig. 5-9 Show two models of LaCoste-Romberg gravimeters. Aliod G gravimeter (left side) and EG gravimeter (right side).

The modification changes of LaCoste and Rumberg gravimeters leads the mode of acquisition to a digital read-out and/or logging of the gravity measurement and no longer necessity to read through the eye-piece, the accuracy and repeatability of the instrument are much less subjective. Another modification changes the battery pack to a lithium-ion rechargeable that is located on the meter itself. The Gravition EG model specification are self-leveling, all meter functions are fully automated, most sensitive, data resolution 24-bit less than 0.0001 mgal bit size. In addition it is provide with a monochrome VGA LCD with backlight digital display, 32MB Flash RAM Memory (up to 100,000 stations) and integrated data logger.

Worden Gravimeter

The Worden gravimeter (introduced in 1948) consists of a small beam supported by a zero-length spring (Fig 5-9). The pointer is viewed through an eyepiece to see that it is back to the null position when the micrometer screw is turned. Differences in dial readings are converted into gravity units by use of the scaling factor of the instrument. Thermal compensation is affected by the differential expansion system which compensates temperature effect on the spring.

The design of the instrument is similar to that of the Lacoste-Romberg gravimeter. It is smaller (about 35cm high, 18cm in diameter and of weight less than 4kg and it has the capability of measuring large gravity change reaching more than 5200 mgal. Its accuracy reaches 0.01 mgal (Dobrin, 1960),
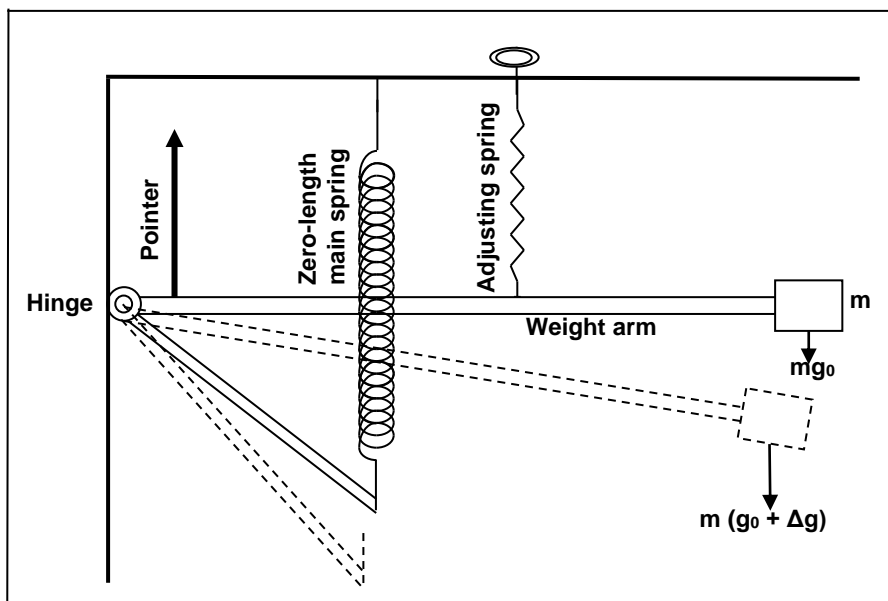
Fig 5-10 Schematic representation of the Worden gravimeter.

The Worden gravimeter became popular for its convenient size, weight and easy manipulation. It has a temperature compensation mechanism and of highly efficient thermal insulation. The instrument is entirely non-magnetic. It is read by the null-method and requires no clamping.

Scintrex gravimeter

It consists of a mass-and-spring assembly put in a vacuum chamber. Movement and null adjustment are made through electric transducer. The direct-current, feed-back voltage is proportional to gravity changes which are stored in the provided computer memory. Accuracy attained by this gravimeter is about 0.01 mgal (Robinson, 1988).

CG-5 Autograv Gravimeter

The new CG-5 Autograv system from Scintrex is one of the most versatile and advanced gravity systems for mineral exploration, oil and gas exploration and microgravity applications. The Autograv is a microprocessor-based automated gravity meter that has a measurement range of over 8000 mGals

without resetting and a reading resolution of 0.001 mGal. This enables the Autograv to be used for both detailed field investigations and large scale regional or geodetic surveys.

Accurate measurements are taken by simply pressing a key and under most conditions it takes under one minute to complete the reading. A series of readings of gravity measurements can be performed by setting the Autograv in the auto-repeat mode.

The individual readings are displayed directly in mGals. The data is stored in Flash memory and can be sent to a printer, modem, recorder or PC. The station positions are measured with the integrated GPS capability; the internal GPS and precise clock for X-Y positions and earth tide corrections and external GPS input for Z-position and altitude corrections and real time free air and Bouguer corrections.

Fig. 5-11 CG-5 Autograv gravimeter

The LaCoste-Romberg and the Worden gravimeters are examples of unstable gravimeters that use zero-length springs.

Vibrating-String gravimeter

This type of gravimeters (Robinson,1988) uses the concept of dependence of vibration-frequency (**f**) of a fiber string supporting a suspended mass (**M**) on gravity (**g**). The relation is expressed by the following formula:

$$f = [Mg / 4x^2m]^{1/2}$$

Where **m** is the mass per unit length of the string and **x** is the string length. Gravity changes are measured electronically. This type of gravimeters is still in the research state and they may become the future surveying-gravimeter.

5.3.   Instrument Calibration

Observations with a gravimeter are recorded in arbitrary scale divisions. To convert these divisions to milligals, it is necessary to calibrate the instrument that is to find a scale-division-to-milligal conversion factor. One method is to measure gravity at two points where the gravity difference between them is known, such as two base stations or top and bottom of a building with allowance for the building contribution. Another method is the use of a tilt table. In this method, gravity component (**g cosθ**) is varied by varying the table tilt, where θ is the angle of tilt.

To illustrate the method assume that two readings were taken at the two points A and B where the gravity at each of them is accurately known. For example, let the readings be 120.53 mgal corresponding to 359.60 s.d. at station (A) and 57.30 mgal corresponding to 233.14 s.d. at station (B). By dividing the difference 63.23 mgal by the difference 126.46 s.d. we get the conversion factor 0.50 mgal per scale division.

5.4.   Instrumental Drift

Gravimeters normally exhibit time-variant changes in their dial reading. The continual variation in the instrument reading observed over a defined time interval is caused mainly by the slow and continual creep of the gravimeter springs as they are not perfectly elastic bodies. The phenomenon of time-variant changes in the gravimeter reading, which are caused by mechanical and temperature effects, is known as instrumental drift.

It so happened that a gravimeter reading is simultaneously affected by another time-variant gravity changes. This is the tidal effect due to the sun and moon gravitational attraction. The tidal effects make the measured gravity fluctuate slightly with time introducing its own gravity component superimposed upon the other instrumental-drift component. The combined time variant-changes over a certain time interval are normally displayed in the form of a graph. The separation of the two effects is facilitated by the fact that the tidal component changes in a cyclic manner. The drift, on the other hand, changes fairly linearly especially when the observation is made over short time-intervals (Fig 5-10). The total tidal- and drift-effects is in the order of a fraction of a milligal. An alternative way to separate the tidal fluctuation component is by use of a special equation depending on sun and moon positions in relation to the observation point.

In a field gravity survey the instrumental drift is determined for each point in the survey area and corrected for accordingly.
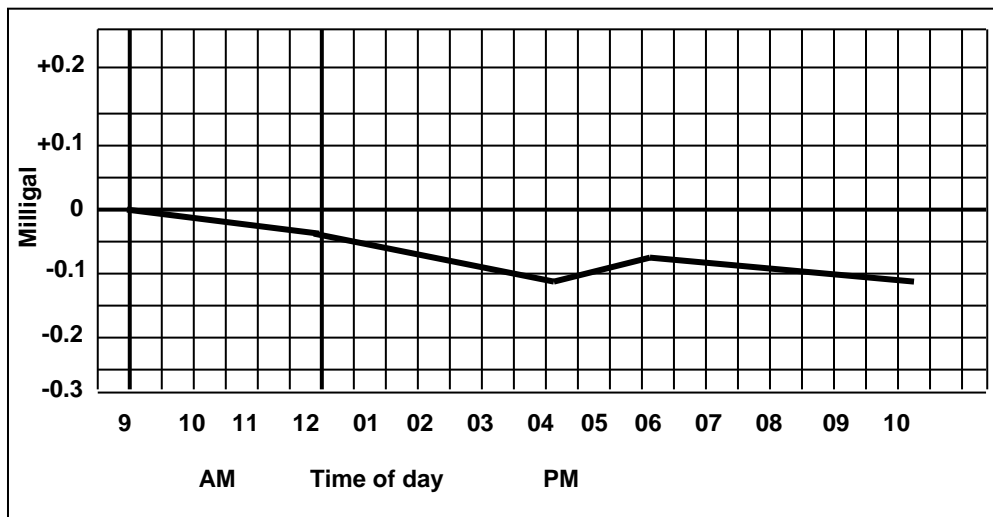
Fig. 5-10 Example of a drift curve

The instrumental drift can be determined only by repeated observations at the same site. Gravimeter drift may be of uniform variation where it is estimated to be in the order of about less than one milligal per week, or irregular and high, reaching one milligal per day. In normal surveying, a base station is reoccupied at least once every three hours during a work session. This is a necessary procedure for the establishment of a representative drift-characteristic curve for the employed gravimeter.

Chapter 6

GRAVITY FIELD SURVEYING

6.1. Land Gravity Surveying

Gravity surveying involves measuring the gravity values at defined locations (the survey station-points or stations) which are distributed throughout the assigned survey area. In addition, other measurements and pertinent data must be made available. These are the supporting data which principally include location coordinates (latitudes and elevations) and times of the readings. These data are necessary for computing the gravity anomaly in a later processing stage.

6.1.1 The Gravity Field Data

The Earth gravitational acceleration (i.e. the gravity, **g**), measured at any point on the Earth surface, is the vector sum of a number of gravity components. The gravimeter reading changes with position (xyz coordinates), and with time (t) to some extent. These changes, as it is explained in the chapters 3 and 4, are due to a group of factors which are of global and local origins.

In gravity field surveying, the gravity values are measured over a defined grid of points distributed over the survey area. The gathered gravimeter readings at the grid points (observation stations) form the basic raw data from which the gravity component caused by the subsurface geological anomaly is then isolated.

As it is with the case of seismic field surveying, gravity field data may be divided into two types. These are:

The gravity values furnished by the gravimeter measurements (the gravity readings).

The supporting data which cover all other data necessary for data reduction. Most important of these are position and time coordinates (xyz and t) in addition to the full picture of the surface terrain of the survey area.

A land gravity survey is normally conducted through two operation phases. These are: establishment of the base-station network and documenting the gravity readings at all of the station-points in the survey area. A location map with an adequate scale must be first made available (Fig. 6-1).
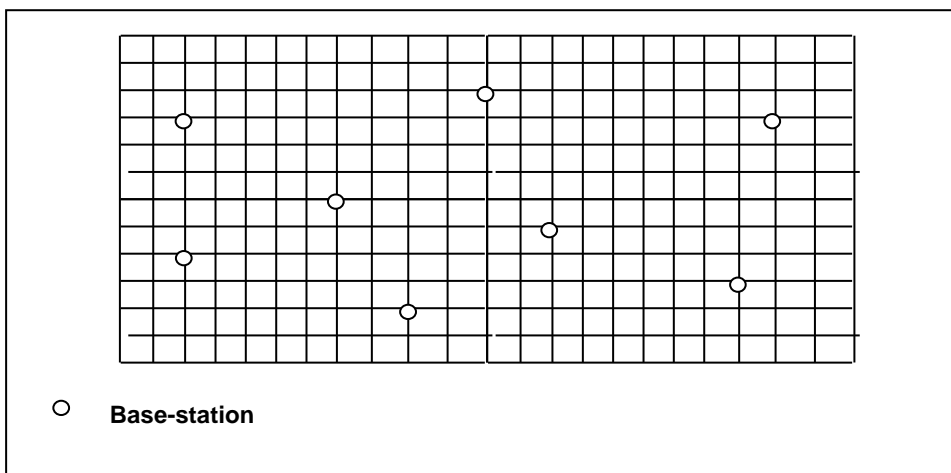
Fig. 6-1 Model of a grid-map of the field station locations

6.1.2 The Base-station network

A base-station is a point located within, or near, the survey area at which the gravitational acceleration is precisely known. The base station serves two purposes. First, the gravity value at the base station is used as a reference value for computing gravity at all of the survey-points. In addition to that, the tidal effect and the drift behavior of the measuring-gravimeter can be determined.

The main base station of the survey-area is established by gravimeter measurements adjusted to one of the world base stations of the International Gravity Standardization Net (IGSN71).

In a given survey-area, a network of base stations can be established by a special procedure called (looping-method). To avoid drift effect we require a technique whereby two stations are, in effect, read at the same time (Fig 6-2).

This is insured by applying the technique of the looping method which can be explained as follows.

Suppose we have five base stations (**A, B, C, D & E**) in a survey-area (Fig 6-3). Readings at these stations are made in the following order: (**A, B, A, B, C, B, C, D, C, D, E, D, E, A, E, A**).

Usually a closing error occurs within each of the created polygon. In each loop, the closing error is determined and the error-value at each base station is

re-adjusted by distributing the closing error over the observed gravity values. The mathematical procedure is explained in chapter 9.
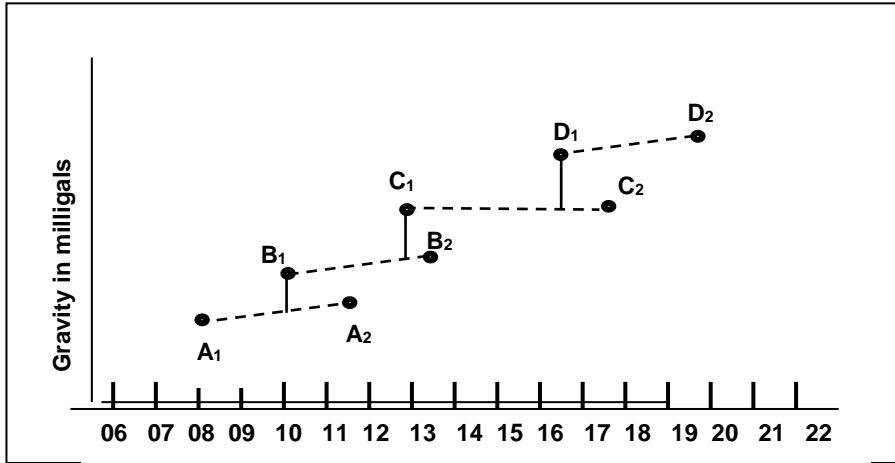
Fig. 6-2 Base station re-occupation technique for determining the short term tide-drift curves which are used to establish the base-station network.
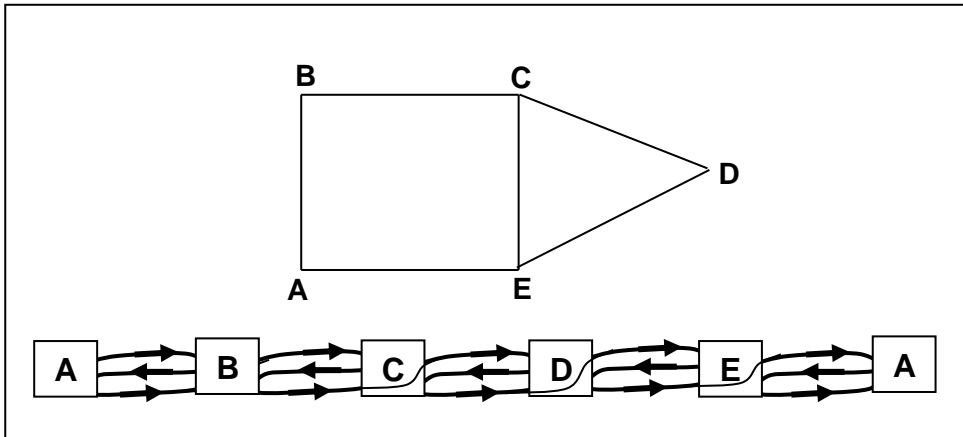
Fig. 6-3 Looping-method applied in the process of establishing a base-network made-up of five base stations (A, B, C, D, & E)

In a normal working day, a base station is reoccupied at least once every about three hours. Base station reoccupation is the way to determine gravimeter drift characteristics which shall be later used in the data reduction stage (Fig. 6-4).
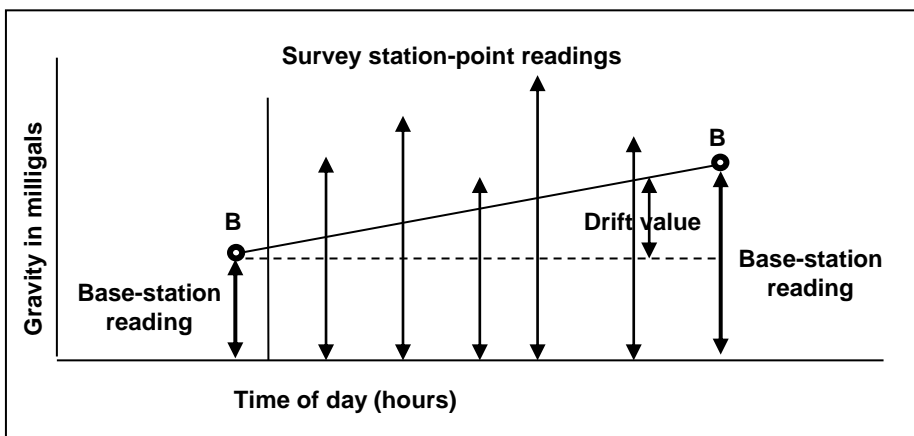
Fig. 6-4 Base station re-occupation during normal survey work

It is a good practice to determine the gravimeter drift characteristics before the start of the survey. This is done by reading the gravimeter at a certain site once, or few times, a day for several days. However, base-station reoccupation procedure must always be followed during the normal daily survey work.

6.1.3 The Survey Gravity Readings

The most important pre-requisite in any gravity survey project is an adequate location map. The survey design parameters (station locations and spacing) depend on the survey objectives. Station spacing depends on whether the survey is reconnaissance or detailed and whether it is regional or local. Station locations are normally defined by the corner-points of a square grid in a uniform grid map. The length of the side of the grid-cell is function of the size of the anticipated geological anomaly. In oil exploration it is in the order of 0.5-1.0 km, while in mineral exploration, the side-length is in the range of 10-50 m. This becomes in the order of 1-5 m. in microgravity surveys where the objective is to locate small-scale features such as subsurface cavities, buried archaeological objects or relatively shallow structures of engineering interests. Survey stations may be irregularly spaced when a sufficient number of points, of known coordinates, are available in the area.

The daily work is started by taking a reading at the nearest local base station. This is followed by reading the rest of the survey stations. The process is continued with reading of the base station at regular intervals of about 2-3 hours throughout the working day. Each day is started by reading the base station and concluded by reading that base station at the end of the day.

The gravity reading and the time at which it is taken are systematically tabulated in the field notebook. The xyz-coordinates are also noted alongside the gravity and time readings. An example of a field data-sheet is shown in Fig. 6-5.

Station number	Longitude	Latitude	Elevation	Time hours & minutes	Gravimeter reading	Remarks
Base-stn.						
Stn-1						
Stn-2						
Stn-3						
Stn-4						
Stn-5						
Base-stn.						
Stn-6						
Stn-7						
…….						

Fig. 6-5 An example of a field data-sheet for documenting gravimeter readings and other supporting data.

6.1.4 Station Locations and Elevations

Station locations and elevations may be determined from the location map which is showing the elevation as numeric data or as contour topographic map. Modern electronic satellite navigation systems can be applied for this purpose. To get an accuracy of 0.1 mgal in relative-gravity measurements, elevation difference from the datum level must be of an accuracy of within 30 cm. This is deduced from the fact that the gravity change is 0.3 mgal per meter change in height.

There are three basic ways to determine elevation. These are: the conventional optical (rod and telescope) method, the use of the aneroid altimeter and the use of topographic location maps.

6.2.   Marine Gravity Surveying

There are two ways to conduct a gravity survey at water-covered areas. These are done by using gravimeters placed at sea floor or on board of a ship. The sea-floor measurement is done using gravimeters sealed in special water-tight containers and operated by remote control systems. The on-board method, which is less accurate and faster to operate, suffers from problems caused by the ship movements.

6.2.1 Sea-Floor Measurements

This type of surveying is commonly conducted by use of the Lacoste-Romberg gravimeter, kept in a water-tight container. It is lowered into sea from a ship and operated through electric cables by remote-control system. This includes instrument leveling, clamping and unclamping of the instrument.

Most of sea-floor gravity surveying is conducted on continental shelves where water-depth is about 200 meters. The main difficulty this method faces is the effect of sea-waves, which can cause disturbance to the instrument especially in shallow water areas. In such environments measurement accuracy of about 0.2 mgal can be achieved in 10-15 minutes. The water depth of the observation point is measured by an echo-sounder.

6.2.2 Shipboard Measurements

The shipboard gravity measurements are done by gravimeters with special mountings that can provide the necessary protection for the gravimeter from being disturbed by the ship rolling and pitching.

As the boat moves along a survey-traverse, the on-board gravimeter system is made to output a continuous gravity record. This is achieved by an automatic beam-adjusting system which detects any movement of the gravimeter beam, and activates a mechanical device that restores the beam position. The gravity value is recorded from measuring the electric current required for the beam restoration.

Although it is relatively faster in covering a marine gravity survey, this method suffers from some problems introduced as a result of the non-static nature of the survey-ship. The on-board gravimeter responds to the resultant of all of the gravitational changes including those created by the motion of the ship. These are generated from three main sources:

 - Pitch and roll of the ship that can tilt the gravimeter.

- Vertical motion (rise and fall) of the ship.

- Ship travel-motion over the curved sea-surface path.

To overcome the pitch and roll effects, the gravimeter platform is kept in horizontal-level by free-swinging gimbals with additional gyroscopic stabilization system.

The imposed vertical-acceleration effect is treated in two ways. First, the gravimeter beam is designed in such a way as to be with a long-enough natural

period (longer than sea-wave period) and by a damping device fitted to the gravimeter-beam (Fig. 6-6).
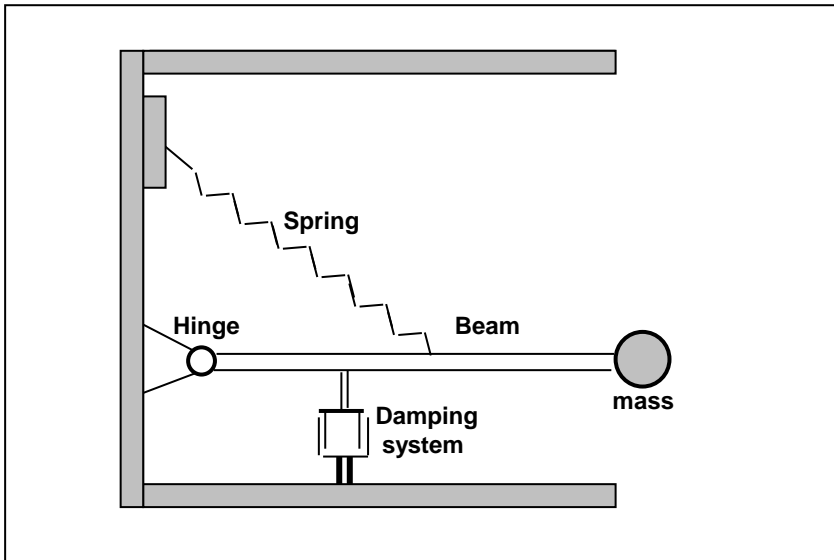
Fig. 6-6 Principle of beam-damping system fitted to shipboard gravimeter.

For the third type of effects, the acceleration contribution from the ship travel motion is function of the ship travel-velocity (speed and direction). This is corrected for in the processing stage. The gravity correction which compensates for ship-movement is called Eotvos Correction, after Baron Von Eotvos (1848-1919).

6.2.3 Eotvos Correction

Marine gravity measurement made by a gravimeter on board of a moving a ship is influenced by additional forces created as a result of the ship motion during the measuring process. Unlike land surveying, where the gravimeter is stationary during the measuring process, a shipboard gravimeter is moving with a certain cruising velocity (speed and direction) while it is measuring. In its motion, the ship (Fig. 6-7) moves over the sea surface along a curved path which forms a segment of a great circle of the Earth. Thus a gravimeter on board of a cruising ship would experience a centrifugal force (acceleration) due to its motion over a circular path. In addition to that, there is another factor that influences the gravimeter reading and that is the effect of the ship velocity on the centrifugal force (centrifugal acceleration) created by the Earth rotation about the

polar axis. As a result, the gravimeter will be measuring different values of gravity from that detected by a stationary gravimeter located at the observation point. The correction which is made to remove the effects due to ship motion from the shipboard-gravimeter reading is known as Eotvos correction.
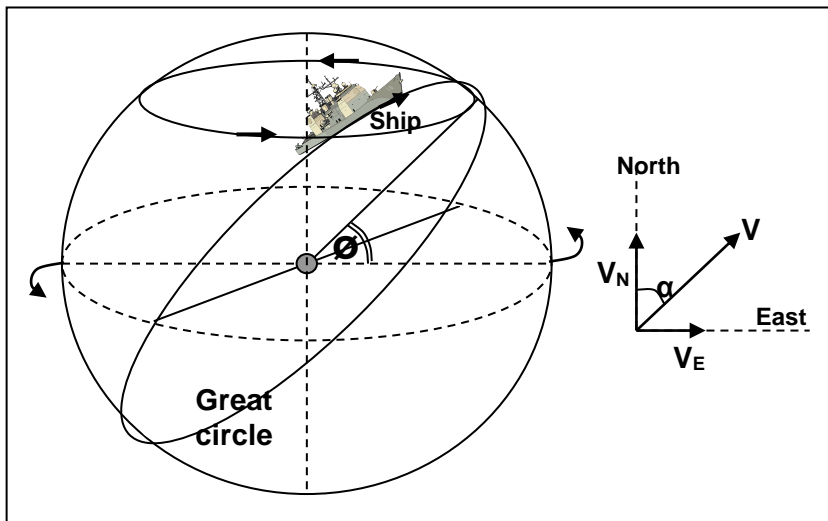
Fig. 6-7 Generation of an additional centrifugal acceleration due to the motion of the gravimeter-carrying ship over a segment of a great circle and at the same time rotating about the Earth polar axis .

In case where the measuring instrument is moving with a certain velocity while it is in the measuring process, it experiences centrifugal force due to this motion. This will incur a change on the gravity value if it were measured while it is at rest.

An eastward component of the ship velocity would add-up to the Earth rotation-velocity causing increase of the centrifugal acceleration which in turn causes the gravity reading to decrease. An opposite effect results from a westward velocity-component. The gravity reading must therefore be corrected for this effect. The correction is called Eotvos correction.

The Eotvos correction (**EC**) in milligals, due to the velocity of the ship carrying the gravimeter, is given by Telford, et al ,(1996):

$$EC = 4.040 \ V \cos\Phi \ \sin\alpha + 0.001211 \ V^2$$

Where **V** in km/hour is the ship velocity, **Φ** is the latitude of the measurement location, and **α** in degrees, represents the ship-path bearing which is measured from the geographical North.

The value of **EC** is positive (to be added to the measured gravity-value) when the ship is moving in westerly direction, i.e. when its velocity (**V**) has an East to West component, and it is negative when the ship is moving in easterly direction. The finally corrected value will be the value of gravity corresponding to that obtained for a stationary observation point at that location.

In summary, marine surveying may be carried out through measurements of gravity on sea floor or on sea surface. Each of these two methods has its own merits and problems. The sea-floor method needs gravimeters enclosed in water-tight casing and fitted with remote-control systems for their operation. This method is of high sensitivity but it is slow because of the lengthy transportation of the gravimeter between observation stations.

The other shipboard method is the more widely used technique where the gravimeter is mounted on board of a moving ship. In this case, a specially stabilizing instrument-base, must be provided to lessen the effect of ship due to rolling and pitching movements caused by the sea waves. Another and more important feature of this method is the gravity effect caused by the ship velocity of travel. Thus an eastward velocity-component would add-up to the Earth rotation-velocity causing increase of the centrifugal acceleration which in turn causes the gravity reading to decrease. An opposite effect results from a westward velocity-component. The measured gravity in this case must be subjected to correction called Eotvos correction.

6.3.   Airborne Gravity Surveying

As in the seaborne gravity surveying, airborne surveying suffers from the non-static nature of the measuring instrument. Error values in the airborne measurements are larger than those found in seaborne surveying due to more rapid change in aircraft altitude and other types of motion.

Experimentation with the use of helicopter began 1971. Reduced flight-speed in this case leads to improvements in the accuracy of both of Eotvos correction and navigation data. In calm weather and careful navigation, the accuracy in the range of few milligals can be obtained.

There are further two types of effects resulting from airborne gravity measurements. These are the aircraft height above land surface and the terrain gravity effects. Both of these factors lead to diminishing of the detected gravity

anomalies. Due to these problems, helicopter gravity surveying is used for reconnaissance surveying where the accuracy is in the range of few milligals. In such practices, the gravimeter is fitted with the appropriate devices that secure stability and reduce external acceleration changes.

6.4.   Microgravity Surveying

On the basis of the size of the objective exploration targets, a gravity surveying may be rated as large-, medium-, or small-scale survey projects. Large-scale gravity surveying projects aim at exploring features such as shape of the Earth, crustal-thickness variation, and isostatic compensation. The medium-scale surveying, on the other hand, includes studying geological structures such as igneous intrusions, sedimentary basins, hydrocarbon traps, and ore bodies.

In the later years, gravity surveys were designed to detect and delineate small scale structures of the type which serve engineering and archaeological purposes. In particular, fracture zones, subsurface cavities and buried ancient relics. Gravity surveying designed for this type of purpose is commonly referred to as microgravity surveying. The type of gravimeter used in microgravity surveys is one which is capable of detecting gravity changes as small as one microgal (= 0.001 milligal).

The main features of a microgravity survey are the closely-spaced observation points (1-5 meter) and the high measurement precision in detecting gravity anomalies which are in the order of 0.001-0.002 milligal.

Interpretation of microgravimetric data is based on relative gravity measurements and thus no need to have absolute gravity values for the interpretation process.

Chapter 7

GRAVITY DATA PROCESSING

Gravity values measured in the field are in fact representing the combined effect of the geological structure of the material below the observation point superimposed on which are gravitational effects from other sources. As we have explained previously (Chapters 3 and 4), these effects are space-variant and time-variant in nature. Thus, to isolate the gravity contribution of the subsurface geological anomalies, the objective of the exploration geophysicist, all effects other than those due to the geological changes, must be removed. This is achieved by subjecting the gathered field data to a series of predefined corrections which are collectively referred to as gravity data processing.

The process of removing all the non-geological effects from the raw observations is also known as data reduction, since they reduce the measured (raw) data to what would they be had the gravity been located on the geoid surface which is represented by the sea level. In effect, processing of the measured gravity data is removing all gravity contributions caused by material found above the sea level as well as the time-variant changes (Fig. 7-1).
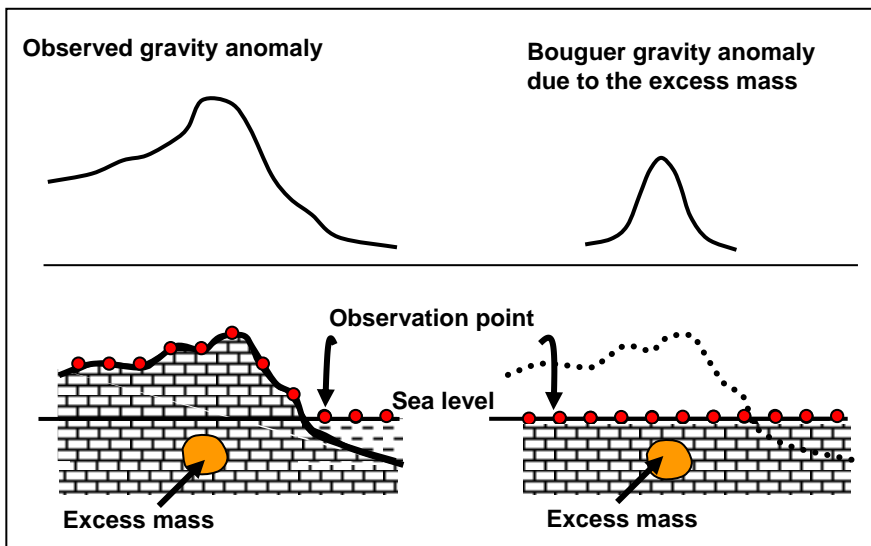
Fig. 7-1 Objective of the reduction processes of the observed gravity data is production of the Bouguer anomaly.

The processing steps which are normally carried out in processing of gravity raw data are as follows:

7.1. Instrument Calibration and Drift Correction

Gravimeter measurements are usually quoted by the instrument scale-divisions (sd.). Thus, the instrument reading must be converted into gravity units which are usually the milligal units. This is done by multiplication of the reading (in sd. units) by the instrument calibration factor which is normally determined at the start of the survey. The calibration factor is expressed in (milligal/sd) units.

During fieldwork the instrument is read at a certain base station regularly at 2 to 3 hour intervals. The gravimeter reading is plotted against time to obtain the instrumental drift characteristics curve. From this curve, the instrument reading can be determined at any time (between two consecutive points) by interpolation, assuming that drift change is linear. As we have already explained (Chapters 5 and 6), time-variant gravity changes include both of the instrumental and tidal effects and their combined effect is expressed by the so-constructed drift curve (Fig. 6-10).

Having constructed the drift curve, the gravimeter reading made at each gravity station of the survey area is corrected for the instrumental-drift of the gravimeter used in the survey.

7.2. Latitude Correction

There are two global related factors that cause the earth gravity to change with latitude. These are the Earth flattening and its rotation about its polar axis. This has led the Earth gravity to increase as the observation point moves from the equator towards either of the two poles. For this reason, the Earth gravity, measured at sea level, increases uniformly with the increase of latitude (Fig. 7.2).

Normally, the GRS67 formula in which $g_N(\Phi)$ (shown in Fig 3-7) would give the value of gravity (g_N) at sea level at any point having latitude (Φ) over the Earth surface. The value $g_N(\Phi)$ is considered to be the universal reference datum relative to which the final gravity anomaly is computed.

Latitude correction is achieved by subtracting the normal gravity (g_N), from the observed gravity value (g_0) to obtain (Δg_0) which is called the *observed gravity anomaly*. Thus:

$$\Delta g_0 = g_0 - g_N$$
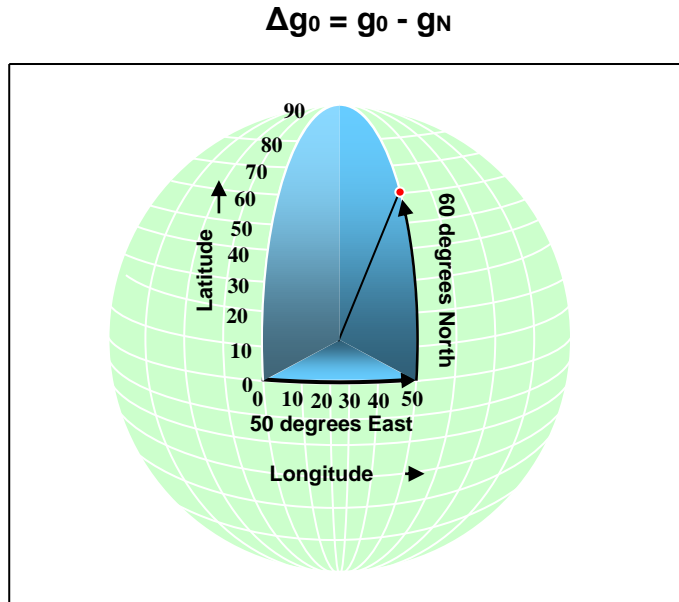
Fig. 7-2 The Earth latitudes and longitudes serve as location
coordinates for station points in gravity surveying.

It is important to note that if the gravity project contains mixed data in which a data-set was corrected using the 1930-Formula and another set corrected by GRS67 formula, unification of correction processes must be done. This is performed using the following correction formula (Kearey and Brooks, 1987, P151):

$$g_N(1967) - g_N(1930) = 13.6 \sin^2 \Phi - 17.2 \text{ mgal.}$$

7.2.1 Rate of Change of Normal Gravity

The g_N value at any observation point of latitude (Φ), can be obtained from the tables which are prepared from the GRS67 formula, or alternatively by computing the value based on another known value (reference point), using the formula for the rate of change of the normal gravity.

The rate of increase of the normal gravity with latitude $\Delta g_N/\Delta \Phi$ can be obtained from differentiating the $g_N(\Phi)$ equation. Within the accuracy of the gravimeter measurements we can neglect the terms in $\sin^4 \Phi$, as this will not affect the result too much, to give:

$$\Delta g_N / \Delta \Phi = 978.0327 * 0.005279 \sin2\Phi \text{ gal/radian}$$

or, $$\Delta g_N / \Delta \Phi = 5163 \sin2\Phi \text{ mgal/radian}$$

or, $$\Delta g_N / \Delta \Phi = 90.11 \sin2\Phi \text{ mgal/degree}$$

As these formulae indicate, the rate of change varies with the latitude. At latitude of 45 degrees, the rate of change reaches its maximum value of 90.11 mgal/degree, and it is zero at the poles and at the equator (Fig. 7-3).
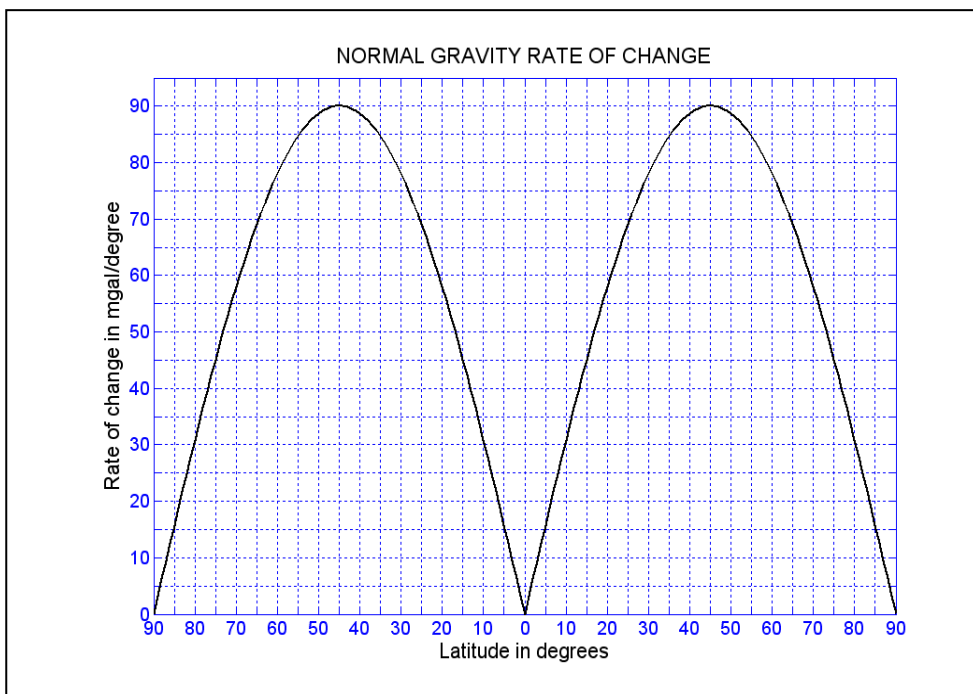
Fig. 7-3 Rate of change of the normal gravity value as function of latitude.

Since g_N decreases in the direction of the equator, the gravity difference between the observation point and the reference point must be added to that of the observation value if the observation point is located at a latitude nearer to the equator than that of the reference point.

Taking the Earth mean radius to be 6367.5 km which is the mean of the equatorial radius (6378.160 km) and the polar radius (6356.775 km), the Earth circumference becomes 40008 km and the distance corresponding to one degree becomes 111.13 km (40008/360). The rate of change can therefore be given as

gravity change in milligals per one meter of the distance measured in the N-S direction. That is:

$$\Delta g_N / \Delta s = 0.000811 \sin 2\Phi \text{ mgal/meter}$$

7.3.   Elevation Corrections

Change in elevation causes a corresponding change in gravity. Change in gravity that occurs as a result of change in elevation of the observation point is function of thickness and density of the material found between the observation point and the datum level, which is normally taken at mean sea level.

The correction may be divided into three parts; which are the free-air, Bouguer, and terrain corrections.

7.3.1 Free-air Correction (FAC)

This corrects for the change in gravity due to change in the height of the observation point. According to the universal law of gravity, gravity decreases as the distance from the Earth center increases. The change in gravity due to change in elevation is rated by 0.3086 mgal/meter (see chapter 4). Thus to reduce the change in gravity to sea level, a gravity value measured at elevation (**h**) meter must be done by increasing the observed gravity by **0.3086h** milligal (Fig 7-4). Correction of observed gravity to what it would be at sea level is called free-air correction, FAC.
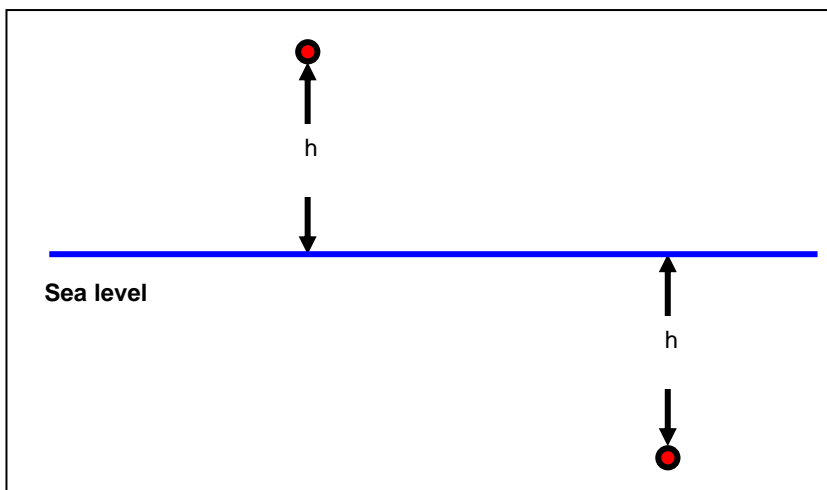
Fig. 7-4 Free-air correction (FAC)

After correction we obtain an anomaly value Δg_{FA} called free-air gravity anomaly expressed as:

$$\Delta g_{FA} = \Delta g_O + FAC$$

Hence

$$\Delta g_{FA} = g_O - g_N + 0.3086h$$

The correction is positive for observation points above sea level and negative for observations which are below it.

7.3.2 Bouguer Correction (BC)

The FAC accounts only for change in elevation and no account is made for the gravity change contributed by the rock-mass found between the sea level and the observation point. This contribution is computed on the assumption that an infinite horizontal rock slab of thickness equal to that of the material exists between the observation point and sea level (explained in chapter 4).

The correction (called Bouguer correction, BC) is given by:

$$BC = 2\pi G\rho h = 0.0419\rho h \text{ mgal,}$$

where (**h**) is elevation in meters and (**ρ**) density in gm/cc (Fig 7-5).
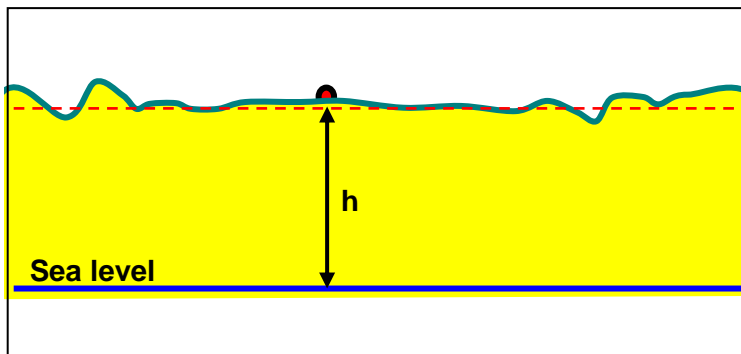
Fig. 7-5 Bouguer correction (BC)

It is to be noted here that the combined FAC and BC correction is forming one correction normally referred to as the combined elevation correction (**CEC**) which is defined by the combined formula:

$$\text{CEC} = (+0.3086 - 0.0419\rho)\,h.$$

The Bouguer correction for sea surface measurements (BC_{SS}) is equivalent to replacement of the water layer (water-depth **d** and density ρ_W) by rock layer (density ρ_R) giving for sea surface observations:

$$BC_{SS} = 2\pi G\,(\rho_R - \rho_W)d$$

The Bouguer correction (BC) must be subtracted from the observed gravity on land, whereas it must be added to the gravity values observed over sea surfaces since it is representing replacement of the water layer by the more dense rock material. Bouguer correction is therefore negative on land and positive over seas.

After applying the Bouguer correction, we obtain Bouguer gravity anomaly (Δg_B), in milligals, which is given by the expression:

$$\Delta g_B = \Delta g_{FA} - BC$$

Hence $\qquad\qquad \Delta g_B = g_O - g_N + 0.3086h - 0.0419\rho h$

In general, Bouguer gravity values are negative over most of the continental areas and positive over oceans. In and around coastal regions, Bouguer gravity values are near zero-level. This is a common worldwide observation.

7.3.3 Terrain Correction (TC)

The Bouguer correction is computed on the assumption that the rock material found between the observation point and the geoid surface is in the form of a horizontal infinite slab. Since, in actuality this is not the case, a correction is required to allow for the irregular topography of the earth surface around the observation point.

Elevated ground (such as hills) near an observation point creates a vertical component in gravity attraction reducing the gravity value at that point. Holes and valleys on the other hand represent lack of material in parts of the assumed horizontal rock-slab. In effect, these also create vertical components which would reduce the gravity value. Thus, in normal situations, terrain correction

(TC) which is always positive is introduced to compensate for the topographic irregularities existing around the observation point (Fig. 7-6).

The final Bouguer gravity anomaly which is including the terrain correction (**TC**) will take the form:

$$\Delta g_B = g_O - g_N + 0.3086h - 0.0419\rho h + TC$$
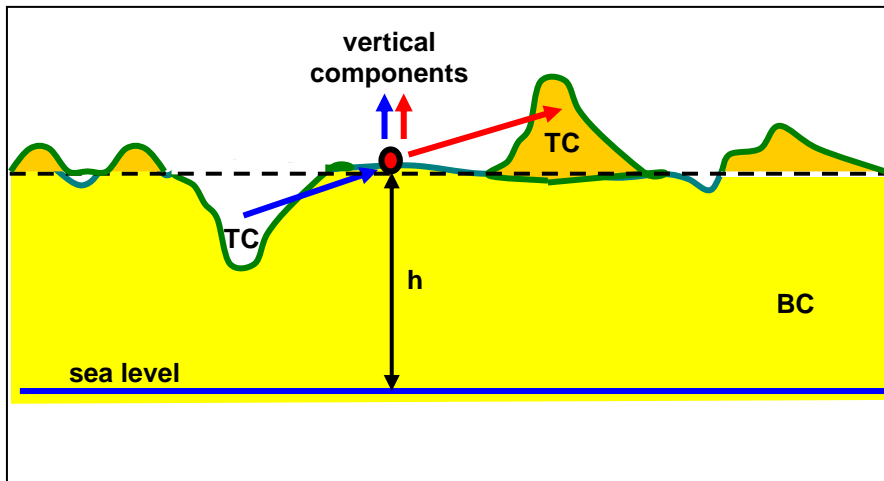
Fig. 7-6 Terrain correction (TC).

The classical method used in computing terrain correction is the use of the special chart (invented by S. Hammer in 1939) with an associated set of tables. Hammar chart consists of a set of concentric circles which are divided by radial lines forming compartments of varying areas.

Terrain gravity contributions of the compartments are computed based on the following computation approach:

Consider a solid cylindrical disc of thickness (**d**) and radius (**r**), (Fig. 7-7).

The gravity attraction of a solid disc (**g_D**) calculated at the center of its flat surface (see chapter 9 for derivation) is given by:

$$G_D = 2\pi \, G\rho[d + r - (d^2+r^2)^{1/2}]$$

where **r** is the disc radius, **d** is its height and **ρ** is its density.
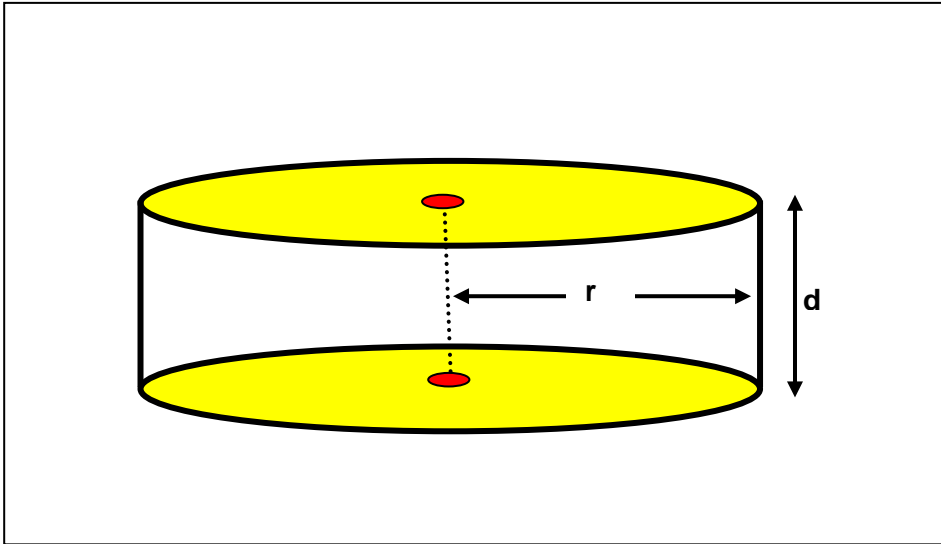
Fig. 7-7 Cylindrical disc used as basis for computing the terrain correction.

Now consider a ring-disc as being formed from subtraction of a solid cylindrical disc (radius r_1, say) from a larger disc (radius r_2) having a common axis with the smaller one (Fig. 7-8).
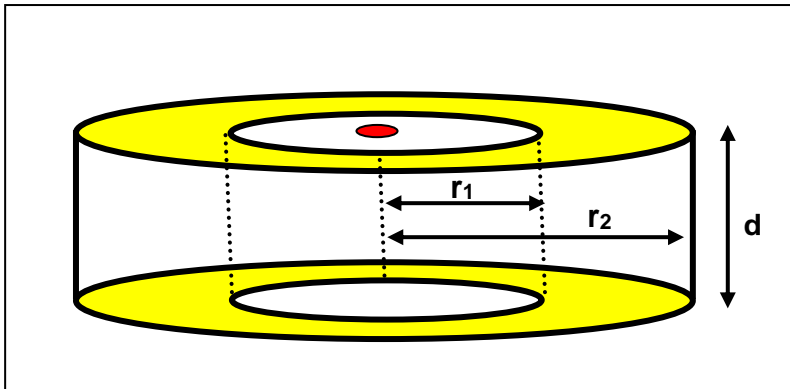
Fig. 7-8 Cylindrical ring-disc is formed from subtracting two solid cylinders of common axis

The gravity contribution (g_r) at the center of the flat surface of the ring-disc is obtained from subtracting the gravity effect of the small cylinder (radius r_1) from that of the larger cylinder (radius r_2), thus:

$$g_r = 2\pi G\rho[r_2-r_1 + (d^2+r_1^2)^{1/2} - (d^2+r_2^2)^{1/2}]$$

Now, if the ring is divided into a number (**N**) of equal segments (Fig 7-9), the gravity contribution (g_N) of each segment (compartment) is given by:

$$g_N = g_r / N$$
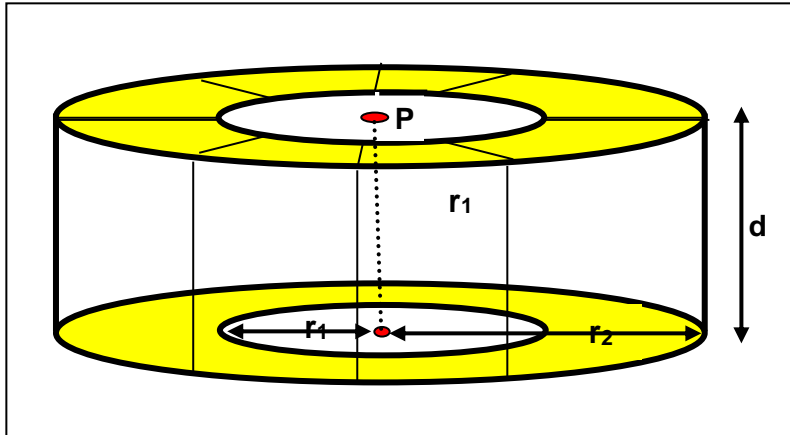
Fig. 7-9 Cylindrical ring-disc divided into eight equal sectors used to derive the formula for gravity effect of a sector of a ring disc at the central point (P).

Hammer tables (1939) give terrain correction values computed on the basis of circular flat-topped cylinders made up of material of density (ρ) equal to 2.0 gm/cc (Fig. 7-10).

zone	Radius (r_1) in meters	Radius (r_2) in meters	n
B	2.0	16.6	4
C	16.6	53.3	6
D	53.3	170.1	6
E	170.1	390.1	8
F	390.1	894.8	8
G	894.8	1529.4	12
H	1529.4	2614.4	12
I	2614.4	4468.8	12
J	4468.8	6652.2	16
K	6652.2	9902.5	16
L	9902.5	14740.9	16
M	14740.9	21943.3	16

n: number of segments in the zone, r_1 and r_2 in meters
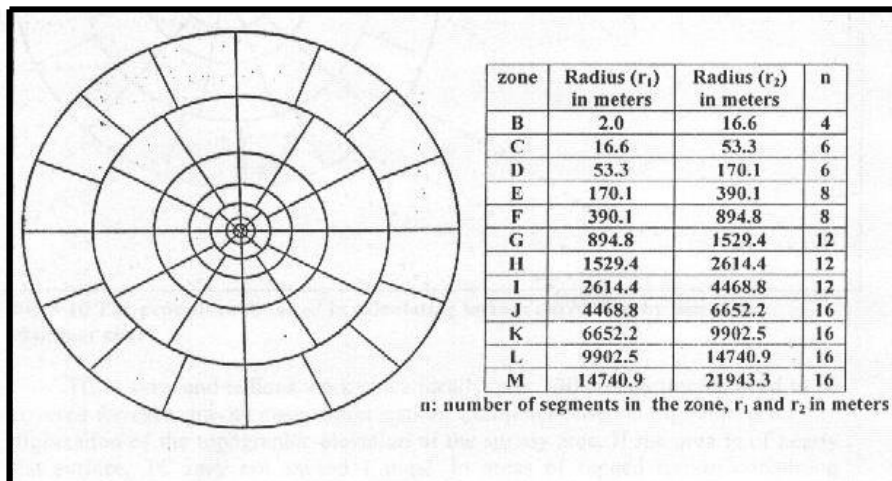
Fig. 7-10 Part of the Hammer chart. The complete chart consists of zones (B, C, D, …, M) varying in radius from 2m for zone-B to 22km for zone-M (Kearey and Brooks, 1987,pp 152-153)

One way to compute terrain corrections is by use of Hammer chart and equation for g_r; the one mentioned above. The computation procedure is done by placing the center of Hammer chart over the observation point on the topographic map of the area. The chart must be drawn at the same scale as the topographic map. The average elevation of the topography within a segment is estimated and the difference (call it **Δh**) in elevation of this average from that of the observation point is obtained. Now the terrain correction for that segment is found by substituting **Δh** for **d** in the expression for (g_r) and dividing the result by the number (**n**). The process is repeated for all other compartments in the chart then the contributions of all compartments are summed up to give the total terrain correction (**TC**) for that observation point. The density term (**ρ**) is substituted by the mean density of the material covered by all the compartments entering in the computation.

The more practical procedure than using Hammer chart and equation is by using Hammer chart and the associated tables (Dobrin, 1960, Fig. 11.9 and Table 11.1). The chart is first printed on transparent plastic sheet at the same scale as the topographic map of the survey area. The center of circles is placed over the observation point and the average elevation within a compartment is estimated from the contours seen through the chart-sheet. The difference in elevation (**Δh**) between the estimated average and the station elevation is determined. With this value the **TC** for that compartment can be read from the tables associated with the chart (Fig. 7-11).
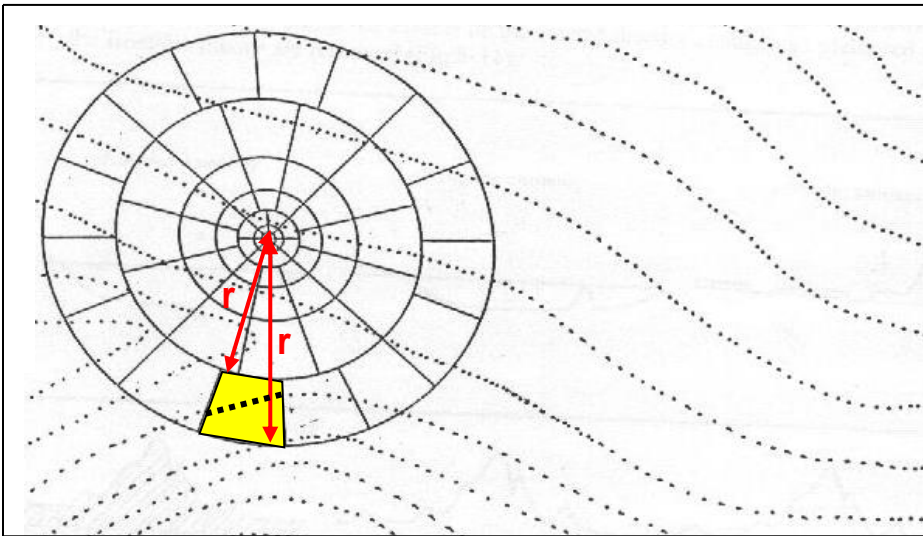
Fig. 7-11 The procedure followed in calculating terrain correction by use of the Hammer chart. Average elevation of the yellow compartment is estimated from the contours crossing it.

The terrain correction is slow and tedious work especially when it is done manually as has been done in the olden days. Computer based computations, as it is normally done nowadays, require digitization of the topographic elevation of the survey area.

In area where the topography is nearly flat, terrain correction may not exceed 1 mgal whereas in areas of rugged terrain containing mountains, steep cliffs and valleys, the correction may reach appreciable levels. In certain cases terrain corrections may be unnecessary especially when the computed values are less than the desired accuracy of the Bouguer gravity values. Computation decision is based on computation-tests which are conducted in certain parts of the area to find out whether **TC** values are small enough to be neglected or not.

7.4. Isostatic Correction

A Bouguer anomaly value is obtained with a group of correction steps which are in effect removing all effects of material existing above sea level and replacing the ocean water with material of average crustal density. In doing that we are assuming that there are no density variations below sea level except those due to the relatively shallow geological structures which the exploration geophysicists are looking for.

According to the isostatic theory there are, in certain parts of the Earth crust, indications of lateral density variations on large scale-extent which would cause corresponding changes in the Earth gravity. This is supported by the large and negative Bouguer anomaly normally observed over continental blocks and some mountainous areas.

Airy's isostatic model for the Earth's crust suggests that mountain ranges (such as the Alps and the Rocky Mountains) have roots bulging through the upper Mantle of the Earth. Such roots (being of lower density relative to its surrounding) would cause the Bouguer anomaly to decrease by an amount depending on the shape of the root and its density contrast. Thus according to the structural model suggested for the Earth crust existing below the survey area, gravity changes (due to these large-scale crustal features) can be determined and the Bouguer anomaly is corrected for. In so doing, the effects of the lateral density changes as predicted by the isostatic theory are removed (Fig. 7-12).

The isostatic anomaly (Δg_I) is thus defined to be the Bouguer anomaly (Δg_B) added to which is the isostatic correction (**IC**), that is:

$$\Delta g_I = \Delta g_B + IC$$
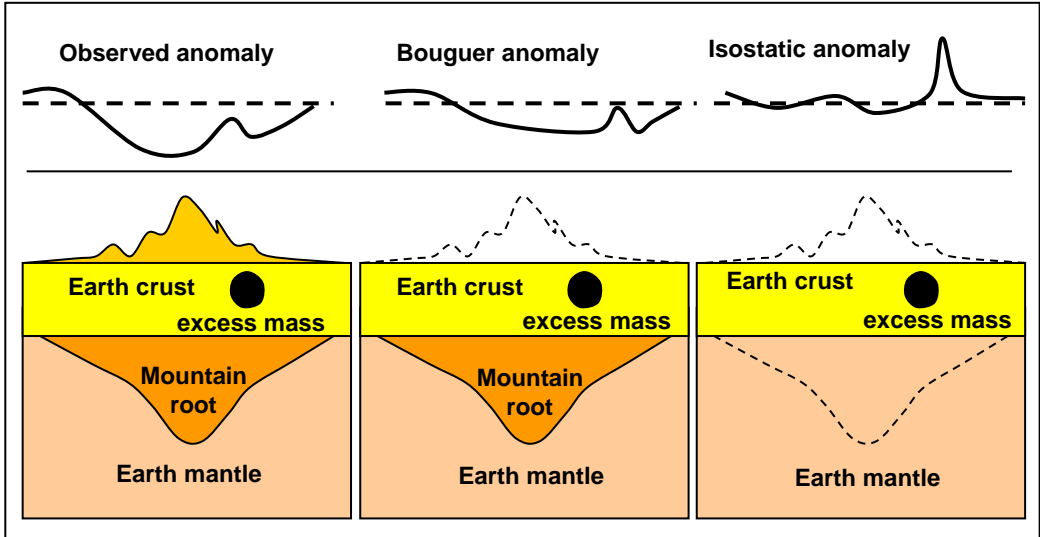
Fig. 7-12 Principle of isostatic correction.

Under-compensation and over-compensation of topographic features are reflected by positive and negative isostatic anomalies respectively. A topographic feature which is perfectly compensated is expected to give zero isostatic anomaly (more details are found in chapter 9).

The basic correction processes usually followed in normal gravity surveying can be summarized as shown in the following sketch (Fig. 7-12):

7.5.   Data Reduction of Marine Gravity Data

There are two ways to conduct a gravity survey at sea. The more practical and faster method is to measure gravity by a gravimeter mounted on a moving ship. The other alternative method is to carry out the measurements by a gravimeter resting on the sea-floor. As we have seen from the previous chapter (Chapter 6) each of these two methods has its own advantages and disadvantages. However in either case, the gravimeter readings must undergo certain reduction processes in order to derive the Bouguer anomaly in a form ready for the following interpretation work.

g_O is gravity value in milligals observed (measured) at a gravity station location

g_N is normal gravity value, computed from GRS67 Formula

$\Delta g_O = g_O - g_N$, Observed anomaly,

$\Delta g_F = g_O - g_N + 0.3086\, h$, Free-air anomaly,

$\Delta g_B = \Delta g_F - 0.0419\, \rho h + TC$, Bouguer anomaly,

$\Delta g_I = \Delta g_B + IC$, Isostatic anomaly,

FAC $= 0.3086\, h$, Free air correction

BC $= -0.0419\, \rho h$, Bouguer correction

TC $=$ Terrain correction

IC $=$ Isostatic correction
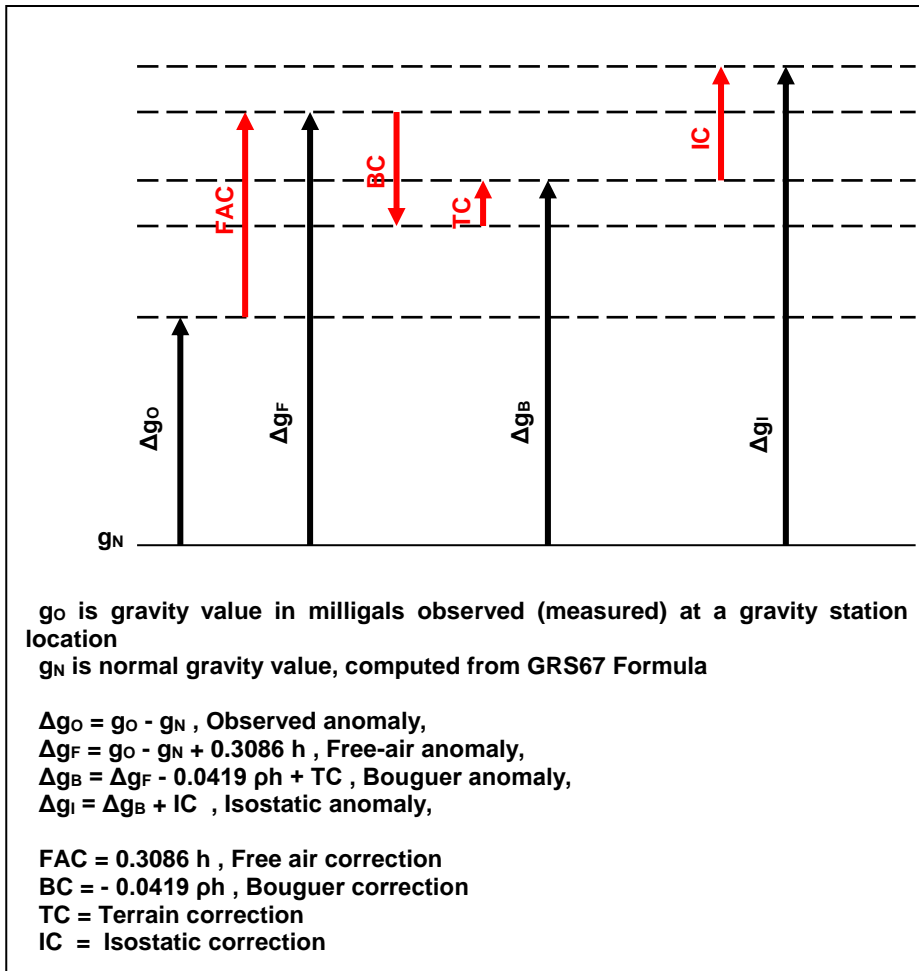
Fig. 7-12 The processing sequence normally followed in gravity data-reduction.

7.5.1 Reduction of Shipboard Gravity Data

For the case of gravity measurements made on board of a stationary ship, the Bouguer gravity anomaly (g_B) is computed in such a way as to compensate for the sea water-body existing below the ship. To start with, no free-air elevation correction is needed here since the measurements are located at sea level. However, the Bouguer gravity anomaly (Δg_B) is computed according to the following equation:

$$\Delta g_B \;=\; g_O - g_N + 0.0419\, d\, (\rho_R - \rho_W)$$

Where g_O and g_N are respectively the measured and normal gravity in milligals. Also ρ_R and ρ_W represent the density in gm/cc for rock and sea water respectively, and (d) in meters, is the sea-depth under the observation point.

This formula is derived on the basis of replacement of the sea water by rocks of average crustal density. In practice, the values 2.67 gm/cc and 1.03 gm/cc are used for ρ_R and ρ_W respectively.

In case gravimeter measurements are read during the ship motion, the Eotvos correction (**EC**) must be introduced in the correction formula. The correction is algebraically subtracted from the shipboard gravity measurement to give:

$$\Delta g_B \; = \; g_O - g_N + 0.0419 \, (\rho_R - \rho_W)d - EC$$

Eotvos correction can result in sizeable errors in this computation due to difficulty in controlling speed and direction of the ship movement. However, the accuracy of Bouguer anomaly of a shipboard gravity is expected to be within one to two milligals.

7.5.2 Reduction of Sea-Floor Gravity Data

For the sea-floor measurements, the observed gravity value (g_O) is corrected to get the corresponding Bouguer gravity anomaly (Δg_B) according to the following equation:

$$\Delta g_B \; = \; g_O - g_N + 0.0419 \, d(\rho_R + \rho_W) - 0.3086d$$

Where ρ_W and ρ_R are density of water (=1.03 gm/cc) and rocks (about 2.67 gm/cc) respectively, and d in meters is the water depth at the observation site. The quantities g_B, g_O and g_N are all in milligals.

Derivation of this formula (Fig. 7-13) is based on computing gravity change in moving the measurement point from the sea floor to the sea surface and replacement of the water layer of density (ρ_W) by rock material of density (ρ_R).

7.6.   Accuracy of Bouguer Gravity Data

The end product of the field gravity-measurement subjected to a set of data reduction processes, is the final Bouguer anomaly map. This map will show the variation in gravity caused by the subsurface geological structures which are showing lateral density variations. The amplitude of the Bouguer anomaly

depends not only on the value of the density contrast but also on shape and depth of the causing geological anomaly. Bouguer gravity maps are normally displayed in the form of gravity contours drawn with an adequate contour interval.
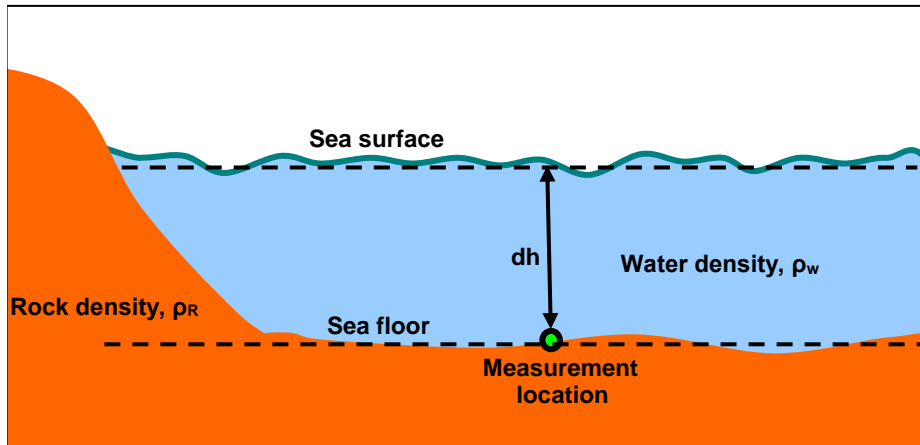
Fig. 7-13 Bouguer correction for the case of sea-floor gravity measurements

Bouguer anomaly maps serve as the basic data used in the interpretation phase to explore the subsurface geological structures such as anticlines, salt domes, ore-bodies, or even subsurface empty cavities. Being dependent on instrument measurements in the field data acquisition stage of the survey work and on approximations in the following processing stage, Bouguer anomaly value is expected to bear certain amount of error. In order to evaluate the accuracy of these data on which our interpretation reliability depends, it is important to identify the error sources and assess the extent of their effects.

(1) Error in Instrument Reading

Modern gravimeters which are carefully drift corrected can be read with accuracy close to 0.01 mgal. This forms a measurement sensitivity in reading changes in the Earth gravity reaching (10^{-8}) which is adequate for normal gravity surveys. In practice, the gravimeter gives the readings in scale-divisions which are converted into milligals using the instrument calibration factor expressed in milligals per scale division.

(2) Error in Location

According to the normal gravity formula (g_N), the rate of change of the Earth gravity (Δg_N) with respect to distance (**s**), measured in the N-S direction, is given by:

$$\Delta g_N / \Delta s = 0.811 \sin 2\Phi \ \text{mgal/km}$$

The maximum value of the change rate is at latitude of 45°, where it attains a value of 0.811 mgal/ km, or 0.0008 mgal/m.

From this result it can be concluded that an error in location of an observation point of one meter may introduce a corresponding error of 0.0008 milligals in the applied value of g_N. Such an error becomes even smaller in magnitude as the observation point moves towards the equator or towards the poles. It is therefore apparent that location coordinates can tolerate a relatively large error as far as latitude accuracy is concerned. Thus an error in location of say 100 meter in the N-S direction would introduce less than 0.1 mgal.

(3) Error in Elevation

The equation for the elevation correction includes two parameters, the contrast in density (ρ), and elevation (**h**). Thus considering $\rho = 2.0$ gm/cc, we have for the combined elevation correction (**CEC**):

$$\text{CEC} = 0.3086 \, h - 0.0419 * 2.0 * h = 0.2248 \, h$$

This formula shows that the error in elevation would cause a corresponding error in the computed Bouguer-anomaly value of about 0.2 mgal/meter. Hence to attain a Bouguer value to the accuracy of 0.1 mgal, elevation must be accurate to within 50 cm.

(4) Error in Terrain Correction

The errors introduced in computing the terrain corrections come from the rough estimation of the mean height of the topography and from the uncertainty in the value of the rock density used for the correction. In general, this varies from (0.05) to (0.30) mgals (Bott and Masson-Smith, 1957).

Chapter 8

THE GRAVITY ANOMALY

8.1.   Concept of the Gravity Anomaly

As far as gravity data is concerned, a geological anomaly is defined as any lateral change occurring in the subsurface geology of the area. This can happen as a result of either change in density of a horizontal layer or change in the horizontality of a constant-density layer (Fig. 8-1). In either case, such a geological anomaly would create the corresponding disturbance in the gravity field, known as the gravity anomaly. It is called regional gravity anomaly when it describes large-scale geological changes and residual anomaly when the changes are of localized nature.
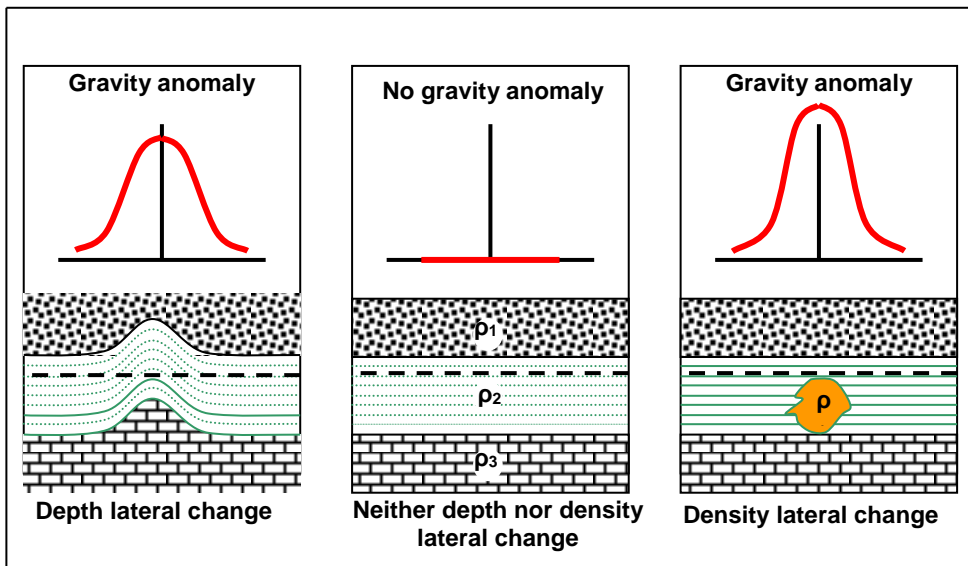
Fig. 8-1 A gravity anomaly is created by a local geological anomaly with lateral changes in depth or in density or with both.

A gravity anomaly at an observation point is formally defined as the deviation of the gravity value (corrected to the Earth ellipsoid) from the theoretical value computed at that point. The type of anomaly depends on the corrections made in the data reduction. The free-air anomaly is obtained if only the free-air correction has been applied to the observed data. The Bouguer anomaly is, on the other hand, obtained when both of free-air and Bouguer corrections have been applied.

A Bouguer anomaly (non-zero gravity value) indicates lateral density changes. If the density of the rock material below sea level varies only with depth (i. e. no lateral variations), no Bouguer anomaly is created, that is the anomaly is of zero value. Local density contrast (surplus or deficit) of the material below sea level would give non-zero Bouguer anomaly.

8.2.   Computation of Gravity Anomalies

Study of gravity anomalies associated with anomalous masses of simple geometrical shapes is useful to gravity interpreters. Information on the theoretical function of the gravity anomaly of certain geological models is very useful since it gives indications on depth, shape, and density distribution of the anomalous mass.

In the field measurements, gravimeters measure Δg which is the vertical component of the gravitational acceleration due to an anomalous subsurface mass. The vector quantity (Δg) is function of its depth, geometrical dimensions and density contrast (ρ) which is the difference in specific gravity between the material of the body and that of the surrounding medium.

Here-below, mathematical formula of the vertical component (Δg) for the most common simple geometrical models are theoretically computed. Derivation is based on Newton's Law of gravitation ($F=G\ m_1\ m_2\ /r^2$) and Newton's second law of motion which relates the acceleration vector (Δg) to the attracting mass of the model.

The models dealt with here are presented under the following categories:

- Spherical shapes
- Cylindrical shapes
- Sheets and Slabs
- Rectangular parallelepipeds
- Bodies of irregular shapes

8.3.   Spherical Shapes

8.3.1 Point Mass

The vertical component of gravity effect Δg of a point mass (Δm) buried at depth (z) which is at distance (r) from an observation point (P) located on the surface, is given by (Fig. 8-2):

$$\Delta g = G \, \Delta m \, \cos\theta \, / \, r^2$$

or, since
$$r = (x^2 + z^2)^{1/2}$$

$$\Delta g = G \, \Delta m \, z \, / \, (x^2 + z^2)^{3/2}$$
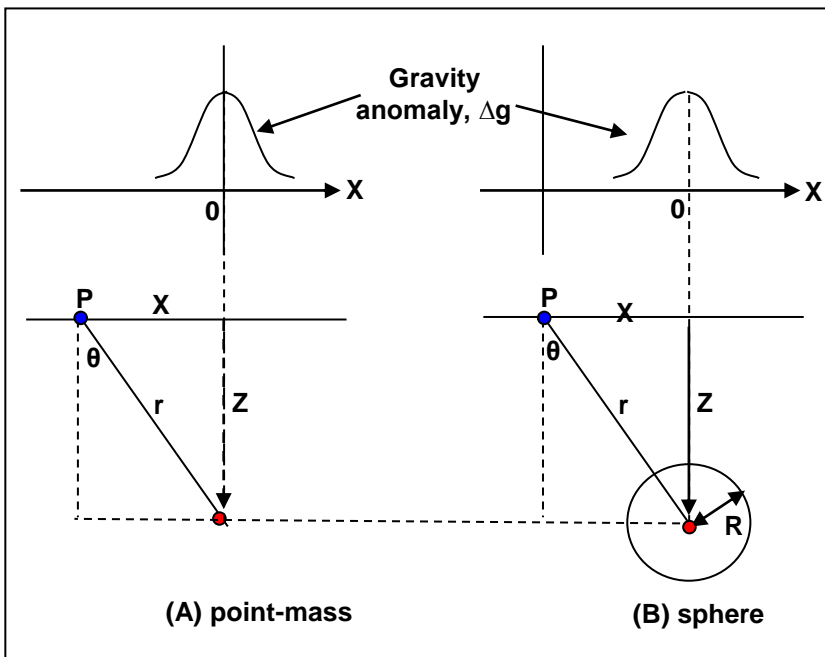
Fig. 8-2 The gravity anomaly due to a point-mass (A) and due to a sphere (B) at depth z.

8.3.2 Spherical Shell

Consider a spherical shell (hollow sphere) of radius (R), density contrast (ρ), and thickness (t). The gravitational attraction at a point located at distance

(**r**) from its center is derived by considering an elementary ring (width **δs = Rδθ**) cut from the sphere at right angles to the distance (**r**), as shown in Fig. 8-3.
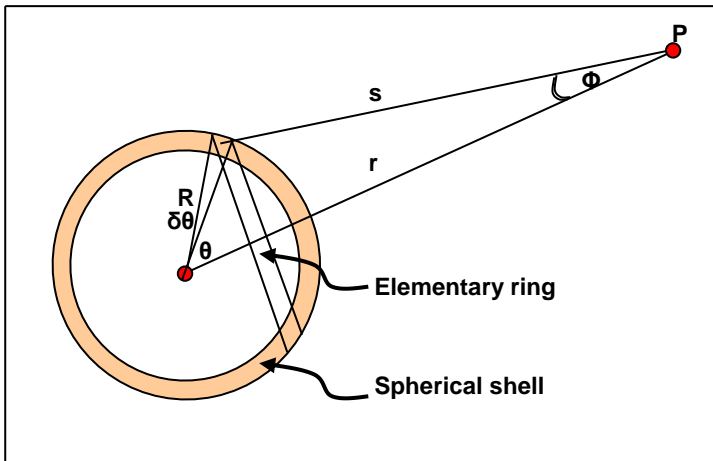
Fig. 8-3 An elementary ring cut from a spherical shell.

Choosing the ring to be perpendicular to the line joining the observation point (**P**) with the center of the spherical shell, insures that each point (infinitesimal element) of the ring is at the same distance (**s**) from the point (**P**). Thus, at (**P**), the gravity component **[Δg]ring** (which is acting along the distance (**r**) towards the shell center) due to the elementary ring is given by:

$$[Δg]_{ring} = (G.\ Rδθ.\ t.\ 2πR sinθ.ρ\ /\ s^2\ )\ cosΦ$$

By making the substitutions**:**

$$cosθ = (R^2 + r^2 - s^2)\ /\ 2Rr,$$

$$cosΦ = (s^2 + r^2 - R^2)\ /\ 2sr,$$

$$sinθ\ dθ = s\ ds\ /\ Rr\ ,$$

and integrating with respect to the variable (**s**) from (**s=r-R**) to (**s=R+r**), we get the gravity effect at the external point (**P**) for the whole shell. That is:

$$[Δg]_{sh} = 4πGρtR^2/r^2$$

or

$$[Δg]_{sh} = Gm_{sh}/r^2$$

where **m$_{sh}$** is the mass of the complete spherical shell.

This result has shown that a spherical shell has the same gravity effect of a point mass having the mass of the spherical shell located at its center. It can be also shown that the gravity effect at a point located inside the shell is zero regardless of the point-distance from the shell center. This can be proved by carrying the integration from **s=R-r** to **s=R+r**,

8.3.3 Solid Sphere

By considering a solid (full) sphere to be consisting of infinite number of elementary thin shells, the gravity effect of the sphere at an external point (**P**) at distance (**r**) from its center is obtained from integrating the gravity effects of all of the infinite number of shells considered to be making up the sphere (Fig 8-4). Since the distance (**r**) is the same for all shells, the gravity effect (**Δg**) of the solid sphere at (**P**) is obtained by multiplying the summation of the shell masses (mass of the sphere, **m**) by **G/r²**. That is:

$$\Delta g = Gm/r^2$$

This significant result tells that, as in the case of a spherical shell, the gravity effect of a solid sphere, at an external point located at distance (**r**) from its center, is the same as that due to a point-mass having the mass of the sphere and located at the sphere center. In other words, the gravity effect of a sphere at an external point (located outside the sphere) is the same as though the whole mass of the sphere is concentrated at the sphere center.

Now, if the observation point (**P**) is located inside the sphere (**r<R**), the gravity effect at **P** of a homogeneous sphere of density (**ρ**) will be given by:

$$[\Delta g]_{sphere} = G \ (4\pi \ / \ 3) \ r^3 \ \rho \ / \ r^2$$

$$[\Delta g]_{sphere} = G \ (4\pi \ / \ 3) \ \rho r$$

In this case (observation point is inside the sphere) the gravity effect, which is the vector acceleration (**Δg**) in the direction of the sphere center, is proportional to distance (**r**) and not to (**1/r²**). The part of the sphere between radius (**r**) and radius (**R**) can be considered to be made up of infinite numbers of shells which have zero gravity effect at point (**P**) as shown above. This means that **Δg** is of zero value at the center of a homogeneous solid sphere.
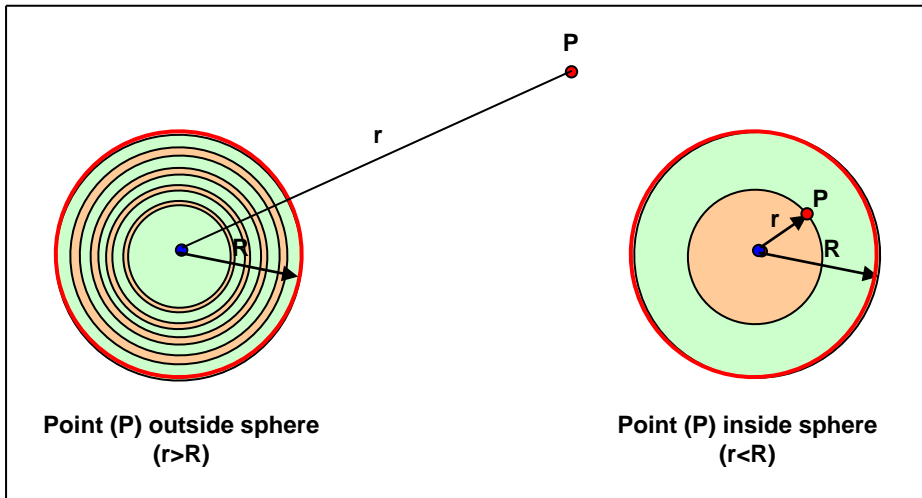
Fig- 8-4 Principles of computing gravity effect of a solid sphere at a point (P) outside or inside the sphere

Gravity Anomaly of a Buried Sphere

In gravity surveying, the measuring instruments are designed to measure only the vertical component of gravity effects of anomalous bodies that are buried at certain depths below ground surface. Customarily, surveying is conducted by measuring of the gravity effect over linear traverses. In other words, the gravity variation is established as a function of horizontal distance on the ground surface.

The gravity anomaly (vertical component of gravity, **Δg**) of a buried sphere of mass (**m**), radius (**R**), and depth of its center-point (**z**) can be expressed as function of distance (**x**) as follows (Fig. 8-5):

$$\Delta g = (G\, m\, /\, r^2)\, .\, \cos\theta$$

$$\Delta g = 4\pi G\rho R^3 z\, /\, 3\, (x^2 + z^2)^{3/2}$$

and,

$$\Delta g = \Delta g_{max}\, (\, 1 + x^2\, /\, z^2\,)^{-3/2}$$

where,

$$\Delta g_{max} = \Delta g, \quad at\ x = 0$$

That is,

$$\Delta g_{max} = \ 4\pi G\rho R^3/3z^2 = 0.02794\ R^3\rho/z^2 \quad (\textbf{R}\ \text{and}\ \textbf{z}\ \text{in meters})$$
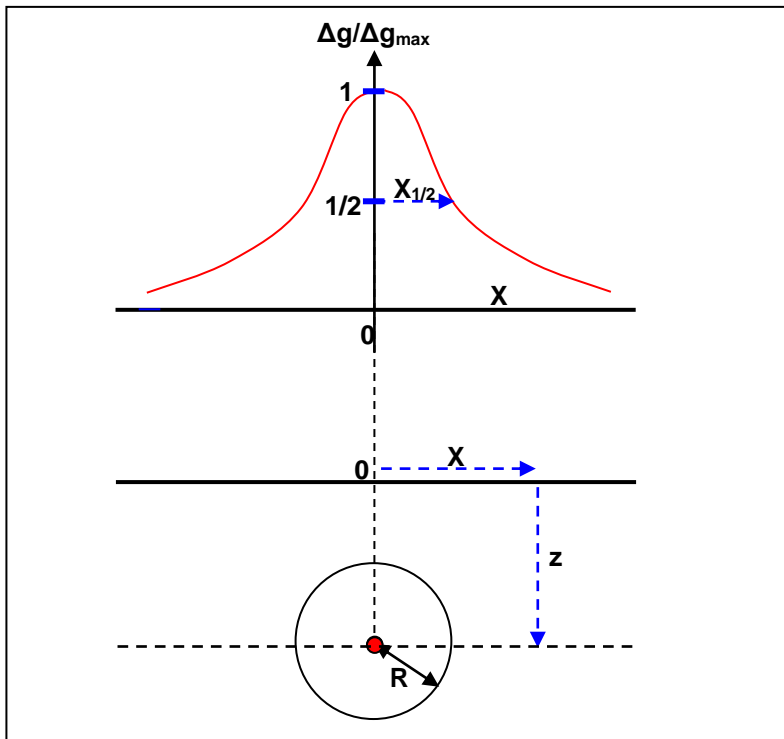
Fig. 8-5 The gravity anomaly due to a solid sphere.

As an example for application, a sphere with the radius of 500 m and density contrast of 0.4 gm/cc having its center at 2km-depth will have a maximum value of gravity directly above its center, **[Δg]$_{max}$** = 0.349 mgals.

It is apparent from these formulae that **[Δg]$_{max}$** will reduce by a factor of 1/4 when the depth of the sphere is doubled, and increase by a factor of 8 when the radius is doubled. Another significant note is that the anomaly curve (**Δg**) is symmetrical about the origin, and that the maximum amplitude of the anomaly (**Δg$_{max}$**) varies inversely with the square of depth of the center. It is also important to note that it is not possible to determine (**ρ**) and (**R**) separately from a given gravity profile, since all concentric spheres having the same products (**R^{3}ρ**) would produce the same gravity profile.

The Half-Width Concept

It is useful to note here that these formulae can be used to determine the depth of the sphere center (**z**) as well as its mass contrast (**m**). This can be achieved by measuring the x-distance (call it **x$_{1/2}$**) for the point on the anomaly

where the anomaly value (call it $\Delta g_{1/2}$) is half the maximum value Δg_{max} (Fig 8-5). By equating the ratio ($\Delta g_{1/2}/\Delta g_{max}$) to (1/2), the depth of the sphere center (z) is calculated as follows:

$$\Delta g_{1/2} / \Delta g_{max} = 1/2$$

And from substituting $\Delta g_{1/2} = Gmz / (x^2_{1/2} + z^2)^{3/2}$ and $\Delta g_{max} = Gm / z^2$,

we get:

$$1 + (x_{1/2}/z)^2 = 4^{1/3}$$

Hence,

$$z = x_{1/2} / (4^{1/3} - 1)^{1/2}$$

$$z = 1.3\ x_{1/2}$$

This formula (called half-width formula) is used by interpreters in depth determination of buried anomalous masses approximating to spherical shapes. Also, it can be applied in computing the contrast mass (m) from substituting $z = 1.3\ x_{1/2}$ in the formula $\Delta g_{max} = G\ m/z^2$.

8.4. Cylindrical Shapes

8.4.1 Horizontal Line Mass

Referring to Fig. 8-6, consider a horizontal line mass ($y_1 - y_2$) buried at depth of (z) and at a distance (r) from an observation point (P). The xyz-coordinate system is chosen such that its origin is at the observation point (P) and the y-axis is parallel to the line mass.

Using the formula for the point mass, the vertical component of gravity (Δg) of an elementary segment (Δy) of mass (Δm) located at distance (s) from the observation point (P) is given by:

$$\Delta g = (G.\Delta m.cos\theta) / s^2$$

$$\Delta g = G.\mu\Delta y.z\ (y^2 + r^2)^{-3/2}$$

where μ is mass per unit length of the line-mass and ($r^2 = x^2 + z^2$)
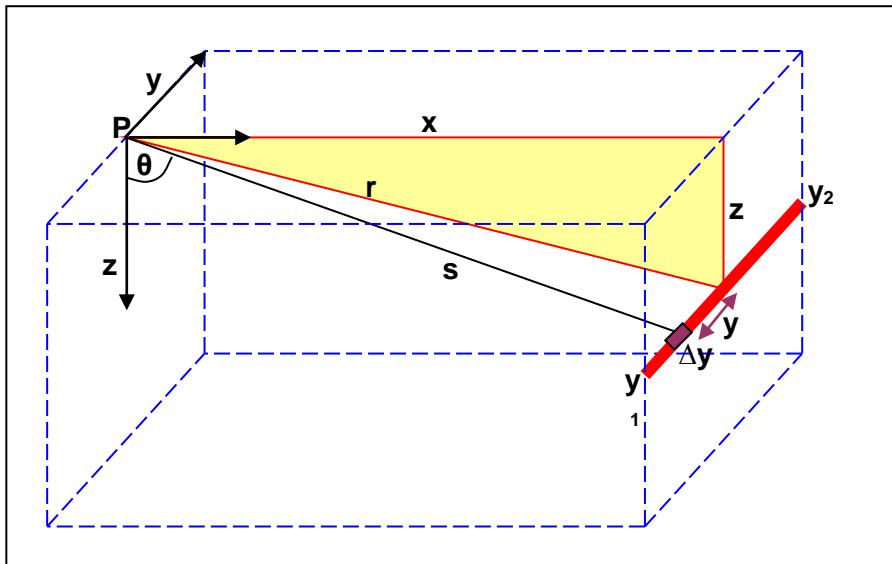
Fig. 8-6 Principle of computing gravity for a horizontal line-mass

By integration with respect to (**y**) from (**y₁**) to (**y₂**) and putting $Y_1 = (r/y_1)^2$, $Y_2 = (r/y_2)^2$:

$$\Delta g = (G\mu z / r^2) [(Y_2 + 1)^{-1/2} - (Y_1 + 1)^{-1/2}]$$

For infinite length of the line-mass, (**y₁**) and (**y₂**) are extended to **-∞** and **+∞** respectively, we obtain:

$$\Delta g = 2G\mu z / r^2$$

or,

$$\Delta g = 2G\mu \, z / (x^2 + z^2)$$

8.4.2 Horizontal Cylinder

Like the case of the sphere, a thin homogeneous cylinder can be approximated by a uniform line mass having the mass of the cylinder concentrated in its axial line. Applying this concept to an infinite horizontal cylindrical rod (Fig. 8-7) of the radius (**d**) and density (**ρ**), lying at depth (**z**). The gravity anomaly (**Δg**) can be expressed as a profile along a line that extends in the direction of the x-axis which is taken as perpendicular to that of the cylinder's axis. Substituting **πd²ρ** for **μ**: in the line mass formula gives:

$$\Delta g = 2\pi G\rho d^2 z / r^2$$

or:

$$\Delta g = 2\pi G\rho d^2 z / (x^2 + z^2)$$
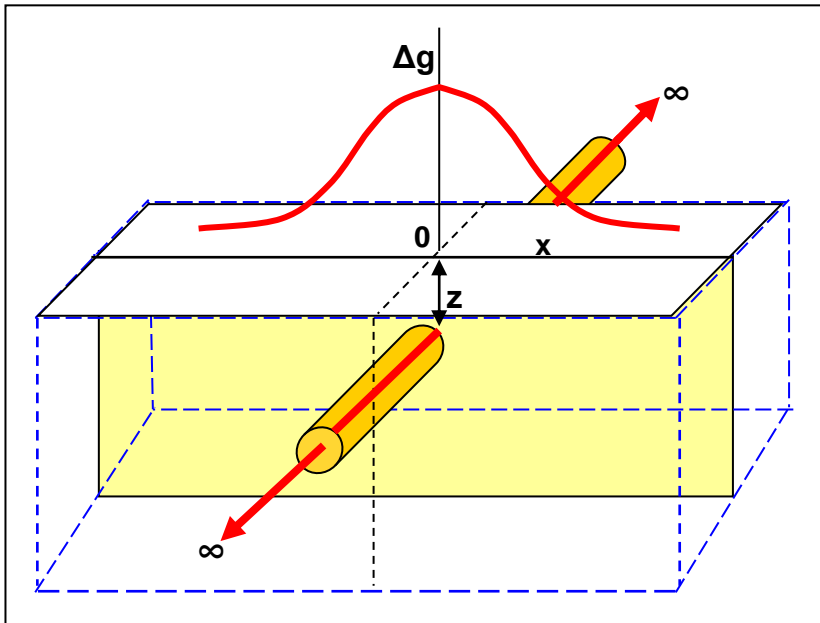
Fig. 8-7 Horizontal cylinder is approximated by a thin long cylindrical rod.

As in the case of sphere, the maximum value of the anomaly (Δg_{max}) is found at the point vertically above the rod's center. That is:

$$\Delta g_{max} = 2\pi G\rho d^2 / z$$

and,

$$\Delta g = \Delta g_{max} (1 + x^2 / z^2)$$

It is noted that the anomaly formula for the rod is the same as that due to the line mass except for the change of μ to $\pi d^2\rho$.

Comparing this anomaly with that of the sphere, it is noted that the anomaly due to a buried rod having same density, same radius and buried at the same depth of a sphere, is less sharp than that created by the sphere (Fig. 8-8).
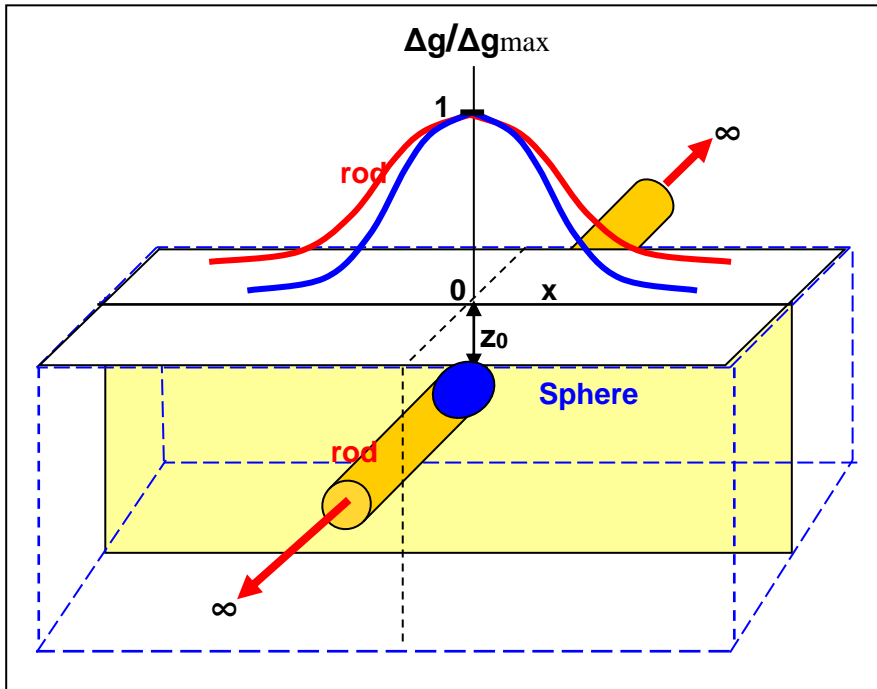
Fig. 8-8 Anomaly due to an infinite cylindrical rod is less sharp than that of a
sphere of same radius and buried at the same depth.

This is because the variable (x) appears with lower power in the
denominator of the rod's formula.

It is useful to note that the amplitude of the gravity anomaly due to the
infinite rod Δg_{max} decreases as the first power of depth (z), and that its value is
larger than that due to the sphere of same specifications and buried at the same
depth. This is logical since the infinitely long rod contains much more mass than
that of a sphere of the same radius and same density. The ratio of the gravity
amplitude due to the rod to that due to sphere is given by:

$$[\Delta g_{max}]_{rod} = 2\pi G\rho d^2 / z$$

$$[\Delta g_{max}]_{sphere} = 4\pi G\rho d^3 / 3 z^2$$

$$[\Delta g_{max}]_{rod} / [\Delta g_{max}]_{sphere} = 1.5z/d$$

This comparison has shown that the ration has a minimum value of (1.5)
which increases with depth of burial (z) for a given radius.

8.4.3 Vertical Line Mass

Referring to Fig. 8-9, consider a vertical line mass with its ends buried at depths (z_1) and (z_2) and located at a distance (x) from an observation point (P). The xyz-coordinate system is chosen such that its origin is at the observation point (P) and the z-axis is parallel to the line mass.
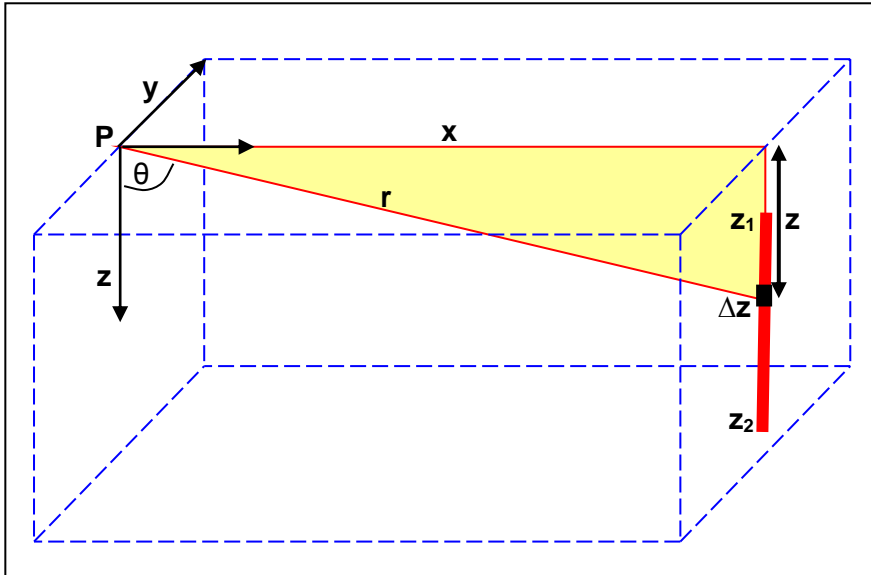
Fig. 8-9 Principle of computing gravity for a vertical line-mass

Using the formula for the point mass, the vertical component of gravity (Δg) of an elementary segment (Δz) of mass (Δm) from the vertical line mass is given by:

$$\Delta g = (G\ \Delta m\ \cos\theta) / r^2$$

$$\Delta g = G\mu\Delta z.z / (x^2 + z^2)^{3/2}$$

where (μ) is mass per unit length of the line-mass and $r^2 = x^2 + z^2$.

By integration with respect to (z) from (z_1) to (z_2):

$$\Delta g = G\mu\ [(x^2 + z_1^2)^{-1/2} - (x^2 + z_2^2)^{-1/2}]$$

For an outcropping line-mass ($z_1 = 0$) and of finite length ($z_2 = L$):

$$\Delta g = G\mu \left[x^{-1} - (x^2 + L^2)^{-1/2}\right]$$

When in this case the line-mass is of infinite length ($L = \infty$):

$$\Delta g = G\mu/x$$

8.4.4 Vertical Cylinder

The anomaly of a vertical cylinder at a point away from its axis cannot be represented in a simple formula. However, the gravity effect at a point on the axis of the vertical cylinder, which is the gravity maximum value, can be computed. The approach followed in derivation is based on integrating gravity effects of a series of elementary discs.

Consider an elementary cylindrical ring of radius (r), width (Δr), thickness (Δz), and mass (Δm) as shown in Fig 8-10.

The vertical component of gravity (Δg) at a point (P) on the axis of the elementary ring is given by:

$$[\Delta g]_{ring} = G\,\Delta m\,\cos\theta\,/\,s^2$$

$$[\Delta g]_{ring} = G\,\Delta m\,\cos\theta\,/\,(r^2 + z^2)$$

$$[\Delta g]_{ring} = G\,(2\pi r.\Delta r.\Delta z.\rho)\,z\,/\,(r^2 + z^2)^{3/2}$$

This is the basic formula from which we may derive the gravity effects (at axial points) of cylindrical discs and cylinders of finite dimensions. From this formula, the following special cases can be reached at:

(i) Hollow Disc

By integrating of the formula for the elementary ring with respect to r from R_1 to R_2, will give the gravity effect (Δg) of a hollow disc defined by the radii R_1 and R_2 :

$$\Delta g = 2\pi G\rho.z.\Delta z \left[(R_1^2 + z^2)^{-1/2} - (R_2^2 + z^2)^{-1/2}\right]$$

(ii) Full Disc

For full disc of thickness (Δz), put $R_1=0$ and $R2=R$ in this formula to obtain:

$$\Delta g = 2\pi G\rho.\Delta z \left[1 - z / (R^2 + z^2)^{1/2}\right]$$
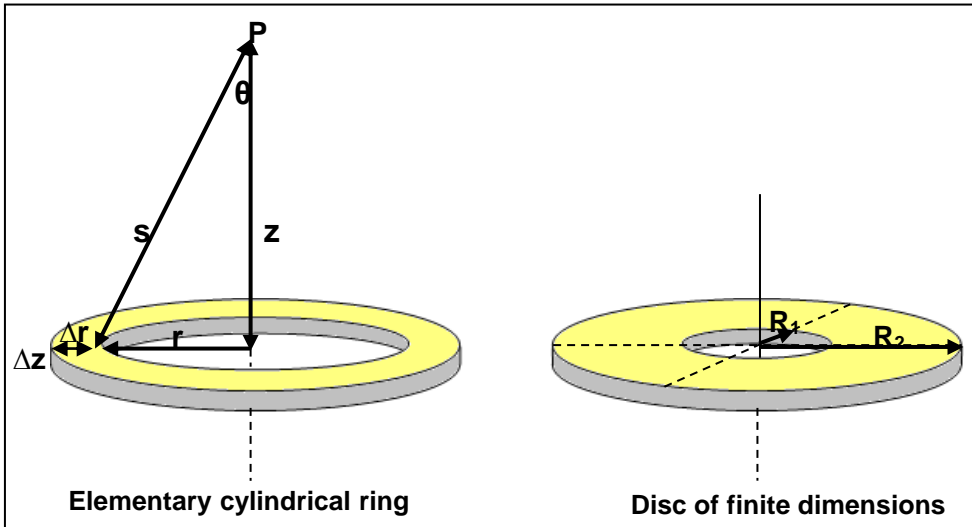
Fig. 8-10 Computation of gravity at a point (P) on the axis of an elementary cylindrical ring and on a hollow disc of finite dimensions.

(iii) Horizontal Slab

For infinite radius ($R = \infty$), we get:

$$\Delta g = 2\pi G\rho.\Delta z$$

This formula expresses the gravity effect of an infinite horizontal slab of thickness (Δz), It is apparent that (Δg) is independent of the slab depth (z), but dependant only on its thickness (Δz) and density contrast (ρ).

This formula is used in Bouguer correction as we have seen in chapter 7.

(iv) Hollow Cylinder

By integrating Δg for the hollow disc with respect to z from z_1 to z_2 we get the formula for the vertical component of the gravity effect at a point on the axial line of a hollow cylinder (Fig 8-11).

$$\Delta g = 2\pi G\rho[(z_2^2 + R_1^2)^{1/2} - (z_2^2 + R_2^2)^{1/2} - (z_1^2 + R_1^2)^{1/2} + (z_1^2 + R_2^2)^{1/2}]$$
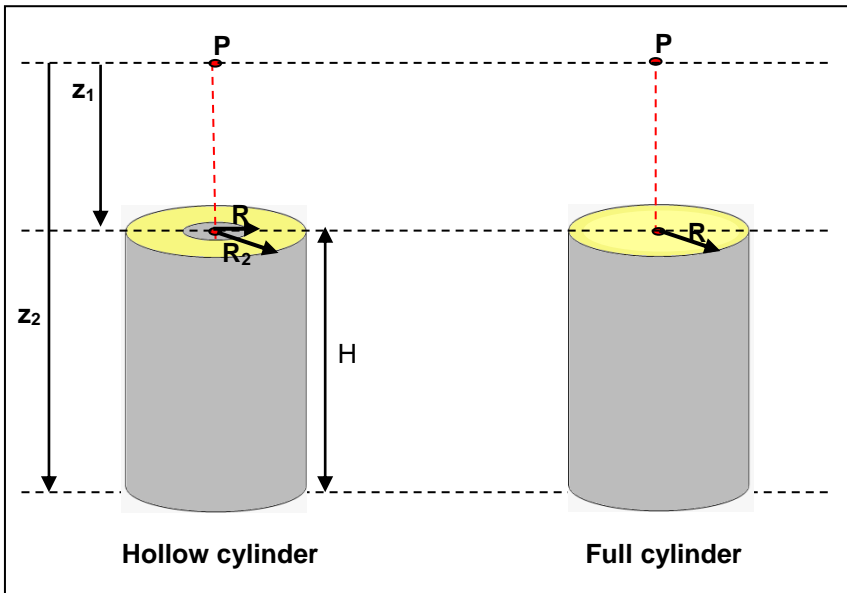
Fig. 8-11 Computation of gravity at a point (P) on the axis of a vertical hollow and full cylinders.

(v) Outcropping Hollow Cylinder

Put $z_1 = 0$ and $z_2 = H$,

$$\Delta g = 2\pi G\rho \ [R_2 - R_1 + (R_1^2 + H^2)^{1/2} - (R_2^2 + H^2)^{1/2}]$$

The formula for a cylindrical sector defined by the radii R_1 and R_2 (Fig. 8-12) having a central angle (θ) in radians is obtained by multiplying the Δg formula for the outcropping hollow cylinder by the factor $\theta/2\pi$:

$$\Delta g = G\rho\theta \ [R_2 - R_1 + (R_1^2 + H^2)^{1/2} - (R_2^2 + H^2)^{1/2}]$$

Which is the formula used for computing the terrain correction.

(vi) Full Cylinder

The formula for a full cylinder (Fig 9-10) of the radius (R), height (H) and buried at depth (Z) is obtained by putting $R_1=0$, $R_2=R$, $z_1 = Z$, and $z_2 = Z+H$ in the Δg formula for the hollow cylinder. Thus the gravity effect of a full cylinder of radius (R), height (H), and buried at depth (Z) is:
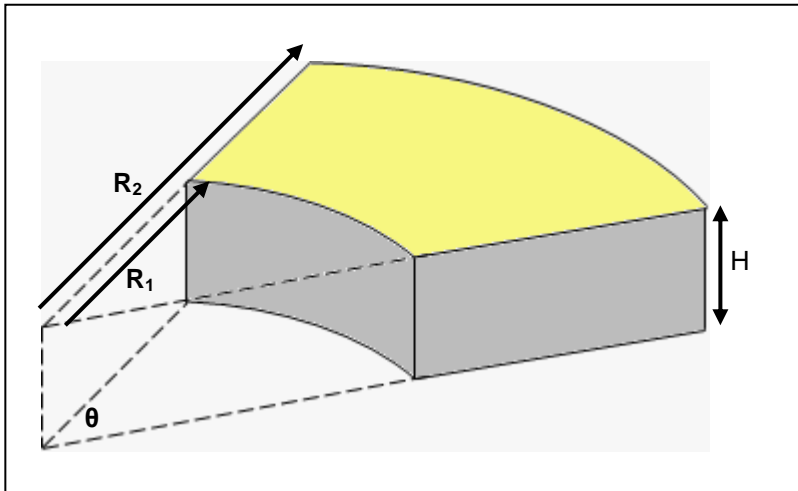
Fig. 8-12 cylindrical sector having inner radius R_1, outer radius R_2, height H, and angle θ.

$$\Delta g = 2\pi G\rho[\ H + (R^2 + Z^2)^{1/2} - \{\ R^2 + (H + Z)^2\}^{1/2}\ ]$$

and for an outcropping solid cylinder (**Z=0**), we get:

$$\Delta g = 2\pi G\rho[\ H + R - (H^2 + R^2)^{1/2}\ ]$$

Gravity Profile of a Vertical Cylinder

So far all formulae for gravity effect of a vertical cylinder express the gravity value at the point which is located directly above the cylinder center i.e. at the cylinder vertical axis. For the gravity variation of a buried cylinder at points shifted by x distance from cylinder axis, there is no simple formula to express it. However, an approximate formula for the gravity contribution can be derived assuming the cylinder mass (Fig. 8-13) to be compressed to its axial line as shown in paragraph (9.4.3) above.

Based on the approximation made by representing a slim cylinder by a line mass concentrated at its center, the following formula for the gravity effect (**Δg**) is derived:

$$\Delta g = \pi G R^2 \rho\ [(x^2 + z_1^2)^{-1/2} - (x^2 + z_2^2)^{-1/2}]$$
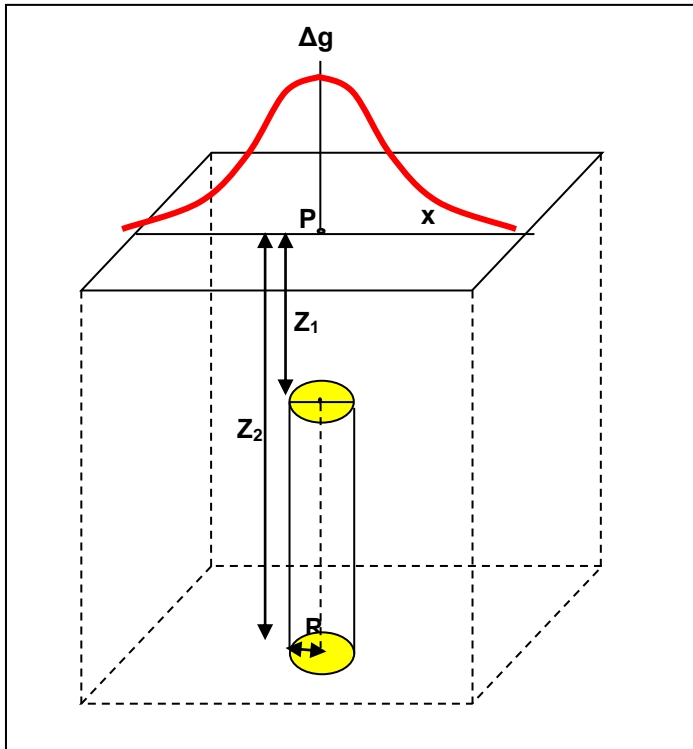
Fig. 8-13 Gravity profile of a buried vertical cylinder, approximated by a cylindrical thin rod (mass line).

For outcropping thin rod ($z_1 = 0$), this formula reduces to:

$$\Delta g = \pi G R^2 \rho \left[x^{-1} - (x^2 + H^2)^{-1/2} \right]$$

It should be noted here that the approximation accuracy is improved the smaller the radius of the cylindrical rod.

Another way to compute the gravitational attraction of a buried vertical cylinder at a point off its axis is suggested by another approximate formula (Dobrin 1960, P. 176). For derivation, first, we compute the gravity effect of a cylindrical shell $[\Delta g]_{SH}$ at a point on its axis which is equal to the difference of the coaxial cylinders, Δg_o for the outer cylinder and Δg_i for the inner cylinder. That is:

$$[\Delta g]_{SH} = \Delta g_o - \Delta g_i$$

Referring to Fig 8-14, the gravity attraction of the small cylinder (radius **d**) at a point (**P**), which is at distance (**x**) from its center, is obtained as follows:

The ratio of the gravity effect **[Δg]$_{SM}$**, due to the small cylinder to that of the shell **[Δg]$_{SH}$** is equal to their respective cross-sectional areas. That is:

$$[Δg]_{SM} = [Δg]_{SH} \cdot d^2 / [(x+d)^2 - (x-d)^2]$$
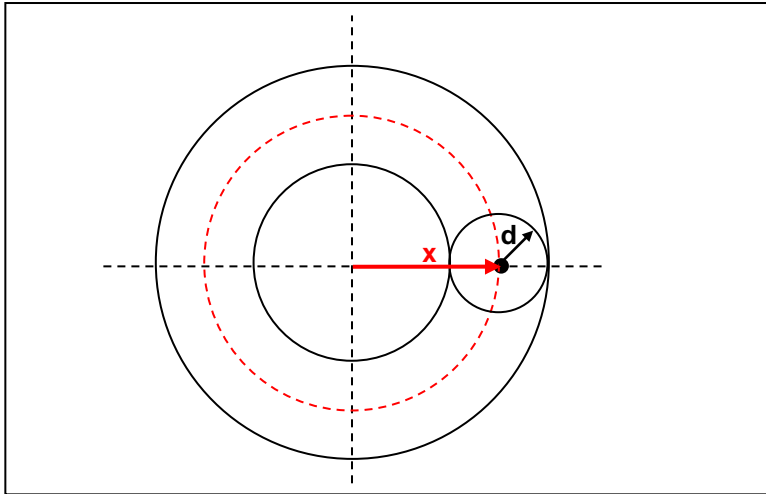
Fig. 8-14 Principle of computing gravity profile of a buried vertical cylinder using coaxial cylinders approach (after Dobrin, 1960)

8.5.   Sheets and Slabs

In computing gravity expressions for sheets and slabs we are considering that the anomalous bodies are two-dimensional. This implies that the third dimension (taken to be along the y-axis) extends from minus infinity to plus infinity. Computation results obtained for such infinitely long models can be applied to long bodies of finite lengths. This approximation is justified because distant parts of the model incur insignificant contribution to the gravity value at the observation point.

8.5.1 Horizontal Sheet

As it is shown in paragraph 8.4.1, the vertical component of gravity (**Δg**) at a point (**P**) of a horizontal line-mass of an infinite length and located at depth (**z**) is given by:

$$Δg = 2Gμz / (x^2 + z^2)$$

Let this line mass be in the form of an elementary strip of width (Δx) which is infinite in the y-direction (extending from $-\infty$ to $+\infty$) as shown in (Fig 8. 15). With this form, the Δg formula, putting $\mu = \sigma \Delta x$, can be re- written as:

$$\Delta g= 2G\sigma\Delta x.z / (x^2 + z^2)$$

where (σ) is the mass per unit area of the elementary strip.
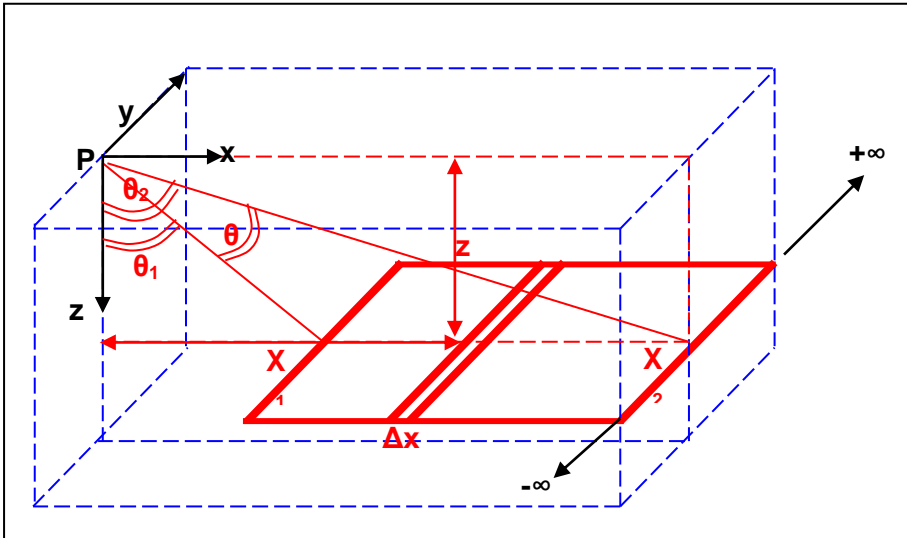
Fig. 8-15 Principle of computing gravity for a horizontal sheet from an elementary strip of infinite length in the y-direction and of width (Δx)

By integrating over the finite width (x_1-x_2), the gravity effect (vertical component at the observation point **P**) of the horizontal sheet extending from x_1 to x_2 which is subtending the angle θ (= θ_2 - θ_1) reduces to the following form:

$$\Delta g= 2G\sigma \, (tan^{-1} \, x_2/z - tan^{-1} \, x_1/z)$$

or,

$$\Delta g = 2G\sigma \, (\theta_2 - \theta_1) = 2G\sigma\theta$$

For such a sheet which is extending from $x = x_1$ to $x = \infty$, the formula will be:

$$\Delta g= 2G\sigma \, (\pi / 2 - tan^{-1} \, x_1 / z)$$

or,

$$\Delta g= 2G\sigma \, tan^{-1} \, z / x_1$$

By substituting π for θ in $\Delta g = 2G\sigma\theta$ we get the gravity value for an infinite sheet which is extending from $x = -\infty$ to $x = +\infty$, that is ($\Delta g = 2\pi G\sigma$).

8.5.2 Horizontal Thin Slabs

Sheet models can be used to approximate thin horizontal slabs with an error of less than 2% when its depth is greater than twice its thickness (Telford, et al, 1996, P40). With so thin slabs the formulae derived above can be used to express the gravity effect for slabs of thickness (Δz) and density (ρ) which is expressed in mass per unit volume. Thus, with the substitution of $\mu = \rho \, \Delta z \, \Delta x$ in the elementary line mass, or $\sigma = \rho \, \Delta z$ in the elementary strip, the Δg formula for an elementary line mass in a form of a rectangular rod of cross sectional area ($\Delta z \, \Delta x$) can be re- written as:

$$\Delta g = 2G \, \rho \, \Delta z \, \Delta x \, z / (x^2 + z^2)$$
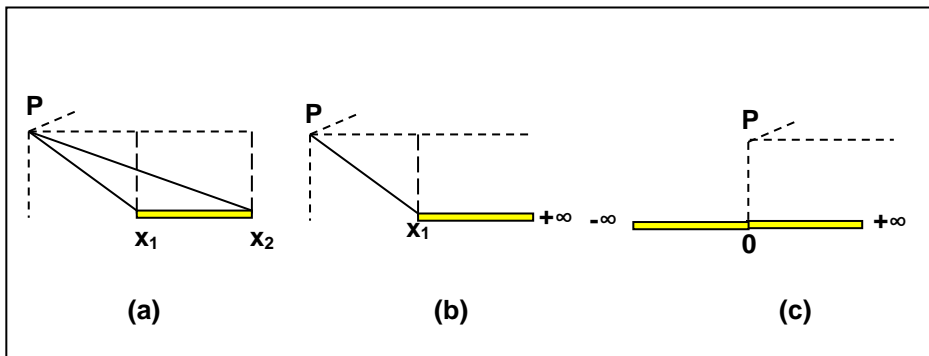
Fig. 8-16 Three models of horizontal thin slabs

The three models of thin horizontal slabs corresponding to the sheet models presented above are (Fig. 8-16):

(a) $\Delta g = 2G\rho \, \Delta z \, (\tan^{-1} x_2/z - \tan^{-1} x_1/z)$ for a slab extending from $x=x_1$ to $x=x_2$

(b) $\Delta g = 2G\rho \, \Delta z \, (\pi/2 - \tan^{-1} x_1/z)$ for a slab extending from $x=x_1$ to $x=\infty$

(c) $\Delta g = 2\pi G\rho \, \Delta z$ for a slab extending from $x = -\infty$ to $x = +\infty$

8.5.3 Horizontal Thick Slab

Let us start with the formula for the elementary rectangular rod which is infinite in length and lying horizontally at a given burial depth. Referring to (Fig. 8-17), the rod which is of cross sectional area ($\Delta z \, \Delta x$) is lying at depth (z) and extending in the y-direction from ($-\infty$) to ($+\infty$). With the origin of coordinates

chosen to be at the observation point (P), the gravity effect (vertical component) due to this rod can be readily computed.

The gravity effect due to the elementary rectangular rod (dealt with in paragraph 8.5.2) is given by:

$$\Delta g = 2G \rho \, \Delta x \, \Delta z \, z / (x^2 + z^2)$$

For an infinitesimally thin rod, where Δx and Δz are allowed to approach zero, the formula can be re-written as:

$$\Delta g = 2G\rho z (x^2 + z^2)^{-1} \, dx \, dz$$

Now, the gravity effect (Δg) due to a horizontal slab of finite thickness can be computed by mathematical integration of this expression over the variables x and z.

One of the models which is of useful application in interpretation work is the semi-infinite horizontal slab of a finite thickness. The gravity effect of this model is obtained by integrating the formula $\Delta g = 2G\rho z (x^2 + z^2)^{-1} \, dx \, dz$ over x from $x = x_1$ to ($x = \infty$) and over z from $z = z_1$ to $z = z_2$. By carrying out this definite integral we get the Δg formula for the horizontal slab of thickness ($z_2 - z_1$), shown in (Fig 8-18), with its vertical face at distance (x_1) from the observation point (P) we get:

$$\Delta g = 2G\rho \left[\pi(z_2 - z_1)/2 + z_2 \Phi_2 - z_1 \Phi_1 + x_1 \ln(r_2/r_1) \right]$$

By varying the distance (x_1), that is using the variable x the gravity effect (Δg) can be expressed as function of x :

$$\Delta g = 2G\rho \left[\pi(z_2 - z_1)/2 + z_2 \Phi_2 - z_1 \Phi_1 + x \ln(r_2/r_1) \right]$$

Where
$$r_1 = (x^2 + z_1^2)^{1/2} \, , \; r_2 = (x^2 + z_2^2)^{1/2} \, , \; \Phi_1 = \tan^{-1}(x/z_1) \text{ and}$$
$$\Phi_2 = \tan^{-1}(x/z_2)$$

The gravity profile of the semi-infinite slab, drawn in Fig. 8-18, shows that the value of Δg is increasing with x. In fact it attains its maximum value $\Delta g = 2\pi G\rho \, (z_2 - z_1)$ at ($x = +\infty$) and tends to zero as x approaches $-\infty$. At $x = 0$, $\Delta g = \pi G\rho \, (z_2 - z_1)$. When the slab is infinite in all directions, the gravity effect becomes constant at the value of $\Delta g = 2\pi G\rho \, (z_2 - z_1)$ and independent of x. This is recognized to be the formula used in Bouguer correction.
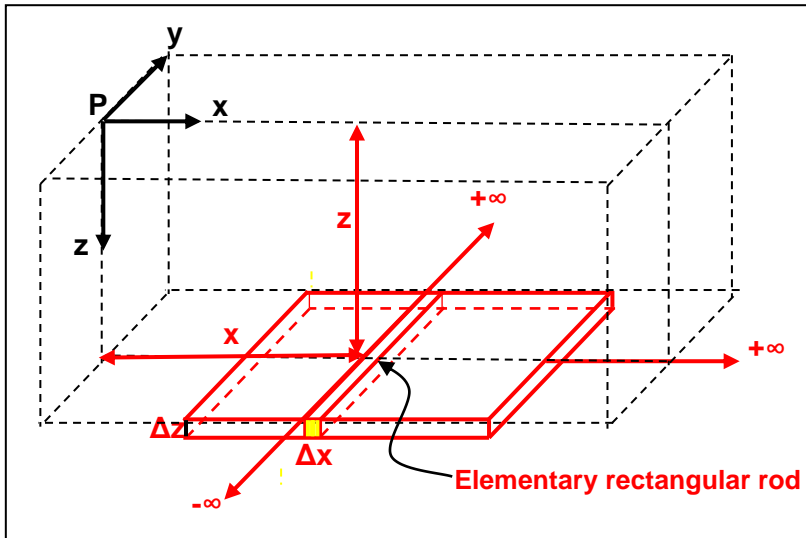
Fig. 8-17 Principle of computing gravity for a horizontal slab from an elementary rectangular rod of infinite length in the y-direction and of cross sectional area $\Delta x\, \Delta z$
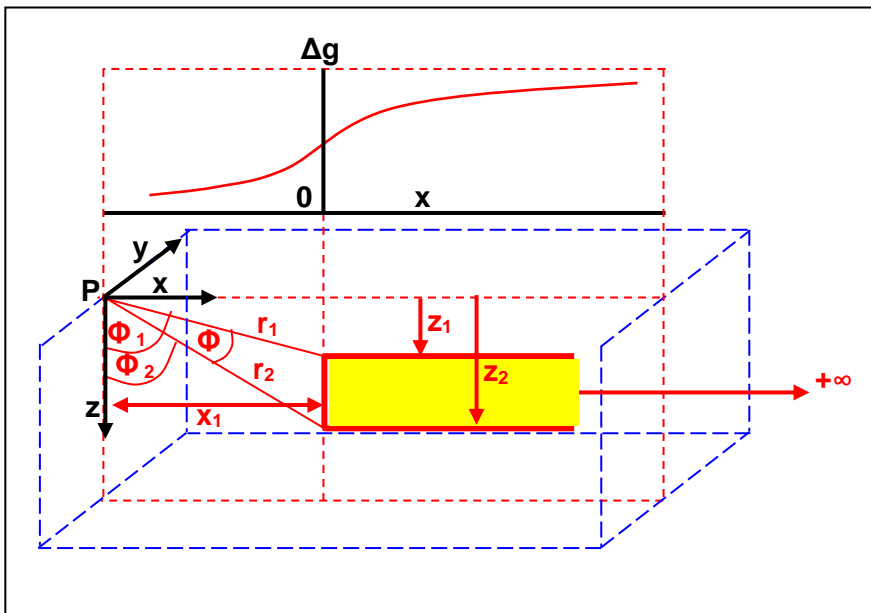
Fig. 8-18 A semi-infinite horizontal slab of thickness $(z_2 - z_1)$ having its vertical face at x_1-distance from the observation point, P.

Another type of bodies which are of practical applications is the semi-infinite slab with sloping edge-face. This type of bodies is particularly useful in computing gravity anomalies of two-dimensional bodies having polygonal cross sections. The formula is rather complicated and can be found in some other publications (see for example Telford, et al, 1996, p.46)

8.6.   Rectangular Parallelepiped

The gravity effect of a body in the shape of a rectangular parallelepiped can be computed by summing up the gravity contributions of all of the mass elements making up the bulk of the body.

Consider an elementary volume mass ($\boldsymbol{\rho \Delta x\ \Delta y\ \Delta z}$) taken within a buried body having the shape of a parallelepiped (Fig 8-19). By making the origin of the rectangular coordinate system to be coincident with the observation point (**P**) the vertical component of the gravity at this point due to the elementary volume mass located at distant (**r**) from (**P**) is given by:

$$\Delta g = G\ (\rho \Delta x\ \Delta y\ \Delta z)\ \cos\Phi\ /\ r^2$$

or,

$$\Delta g = G\ (\rho \Delta x\ \Delta y\ \Delta z)\ z\ /\ (x^2 + y^2 + z^2)^{3/2}$$
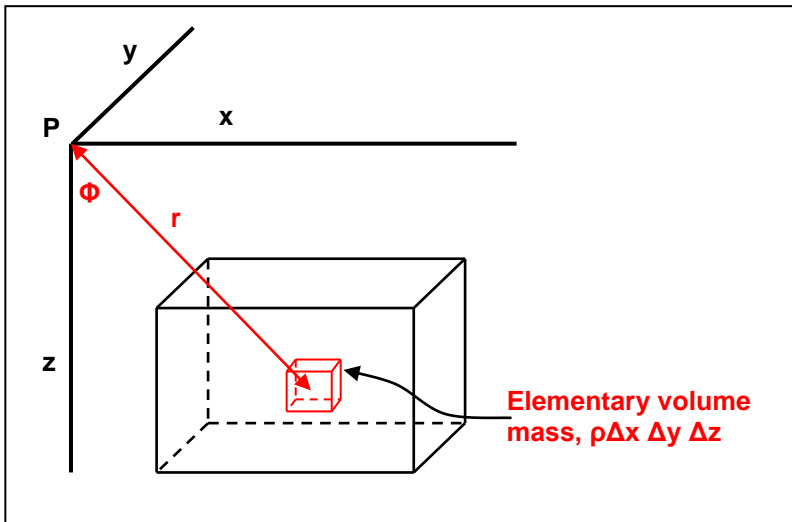
Fig 8-19 A rectangular parallelepiped with the elementary volume mass

The gravity effect (Δg) for the parallelepiped at the point (**P**) is then obtained by successive definite integration over the dimensions of the parallelepiped, thus:

$$\Delta\mathbf{g} = \mathbf{G}\boldsymbol{\rho} \iiint \frac{zdxdydz}{(x^2 + y^2 + z^2)^{3/2}}$$

For an irregular three dimensional mass, the computation may be carried out based on numerical integration using the following summation formula:

$$\Delta\mathbf{g} = G \rho \, \Sigma \, \Sigma \, \Sigma \, (\Delta x . \Delta y . \Delta z) \, z / (x^2 + y^2 + z^2)^{3/2}$$

8.7. Bodies of Irregular Shapes

The models considered so far (spheres, cylinders, sheets, slabs and parallelepipeds) can serve for computing gravity effects of certain geological bodies which can be approximated by such simple geometrical shapes. In addition to that, the derived formulae of such models can serve in computing effects for models of irregular shapes. This can be done through combination of several regularly shaped models. If, for example a geological body can be approximated by a gather of few spherical bodies, then the effect of this model is calculated by summing the effects of the chosen spheres computed separately. Another common example is a model consisting of a set of coaxial cylinders of different radii (Fig. 8-20).
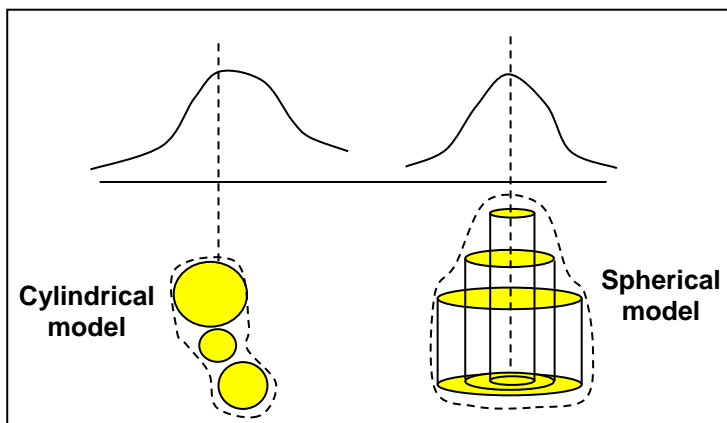
Fig. 8-20 An irregular body can be approximated by a combination of models of regular shapes such as spherical and cylindrical models

There are two types of irregularly shaped models for which gravity effects can be computed. These are: two-dimensional (2D) and three-dimensional (3D) models.

8.7.1 Two-Dimensional Models

A two-dimensional (2D) body is defined to be an infinitely long body with a cross sectional area which is of a constant geometrical form throughout its entire length. The cross section may be of a regular simple geometrical form or of an arbitrary, non-regular form. As it was presented above (sections 8.4.2 and 8.5.2), the gravity profile, for models in the form of thin cylindrical or rectangular rods is computed along a line which is perpendicular to the strike direction of the body.

One of the 2D models, which is of a practical use in interpretation, is a buried infinite horizontal body of polygonal cross section (Fig. 8-21).

Computation of gravity effect of such a 2D-model is based on considering the body to be formed of horizontal thin rods which are infinitely-long. The net gravity effect is obtained by integrating the effects of the individual elementary rods. The derived expression can be included in a computer program to solve for specific cases. The input needed to run the program is the xyz-coordinates of the polygon vertices and its density contrast.
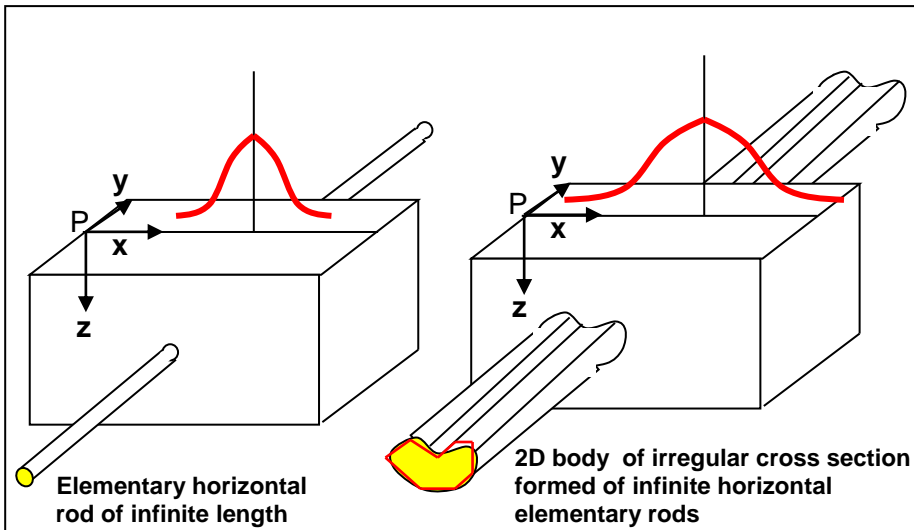
Fig. 8-21 Gravity anomaly of a buried horizontal 2D-body (of infinite length) of polygonal cross-section, which is formed from a pack of elementary horizontal rods of infinite lengths

It is quoted in the geophysical literature (Telford, et al, 1996, p.39) that computed gravity effect based on infinitely long models is considered representative (with tolerable error) when the length of the body in the strike direction is about 20 times its geometrical dimensions including its width and depth.

Use of Templates

A technique was developed (Hubbert, 1948) for graphical computation of gravity effect of a 2D-body having an irregular cross section. This is accomplished by using a specially designed template which is made up of two systems of straight lines. The first system is made up of lines radiating from the origin point and forming equal angles (**ΔΦ**) with each other. The other system consists of equally-spaced horizontal lines with spacing of (**Δz**). In this way, the resulting template will be consisting of trapezoidal cells, each of which will have the same gravity effect at the origin point of the template (Fig. 8-22).
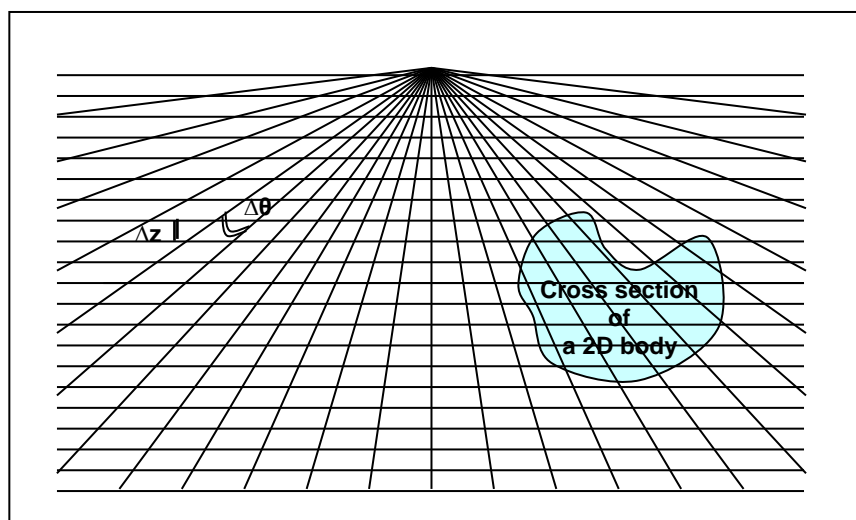
Fig. 8-22 Template for Computing gravity anomaly of a 2D-body of arbitrary cross-section.

The theoretical basis for the construction of this template is explained as follows:

For sake of computation, a 2D body having an arbitrary cross sectional area is considered as being formed of elementary rectangular rods closely packed together. Thus, the gravity profile of such a body can be obtained from summing up the contributions of the constituent elementary rods. As it is explained in section 8.4.2, the vertical component of gravity Δg due to a thin rectangular rod of infinite length, which is extending in the y-direction, is expressed by:

$$\Delta g = 2G\,\rho\,\Delta x\,\Delta z\,z\,/\,(x^2 + z^2)$$

where the product $\Delta x.\Delta z$ represents the cross sectional area of the elementary rod.

The gravity effect of a 2D body which is considered to be composed of a pack of these rods is obtained from summing up the individual effects of the elementary rods. That is:

$$\Delta g = 2G\,\rho\,\Sigma\,\Sigma\,(\Delta x \Delta z)\,z\,/\,(x^2 + z^2)$$

$$\Delta g = 2G\,\rho\,\Sigma\,\Sigma\,\Delta z\,\tan^{-1}(x/z)$$

$$\Delta g = 2G\,\rho\,\Sigma\,\Sigma\,\Delta z\,\Delta\theta$$

where $\Delta\theta$ represents the angle subtending the rod-width (Δx) in the **x**-direction.

In application, the template-origin is placed at the surface point where the gravity is to be calculated, then from the number (**N**) of the trapezoidal cells included in the cross-sectional area of the 2D-body the gravity value (Δg), in milligals, is found from the following formula (Telford, et al, 1996, p.45):

$$\Delta g = 7.1\,\rho\,N\,\Delta\theta\,\Delta z\,.10^{-5}\ mgal$$

where Δz in meters.

8.7.2 Three-Dimensional Models

For the sake of computing gravity effect, an anomalous three dimensional (3D) model can be assumed to be made up of a pile of horizontal polygonal plates. Derivation of the gravity expression for the 3D body is based on integrating the effects of the individual plates forming the model and the computation is normally done by a computer program. The input in this case is the xyz-coordinates of the vertices of each plate comprising the model together with the density contrast.

The gravity effect of a three dimensional body having an arbitrary shape may be calculated by dividing the body into a series of horizontal slices (plates) and approximating each slice by a polygon (Fig 8-23). The gravity anomaly due to a polygonal plate at a given observation point can be expressed by certain mathematical relations. Such expressions are normally complicated, but can be solved by computer programs to compute the gravity effect of a buried horizontal plate of polygonal face and of a constant thickness. The input to the program is the geometrical parameters of each plate which include the xyz-coordinates of the plate vertices, its thickness, and density contrast. The gravity effect of the whole body is then found by summing up the contributions of the individual polygonal-plates.

In practice, the procedure consists of a series of steps. First, the model is divided into horizontal slices by means of contours at a defined contour interval. Then each contour closure is replaced by the best fitting polygon. Lastly, the coordinates of each polygon-corner and other model parameters are input to the computer which is programmed to calculate the gravity anomaly of the defined model. The mathematical expressions for models of irregularly shaped 2D and 3D bodies can be found in (Robinson, 1988, p 297-299).
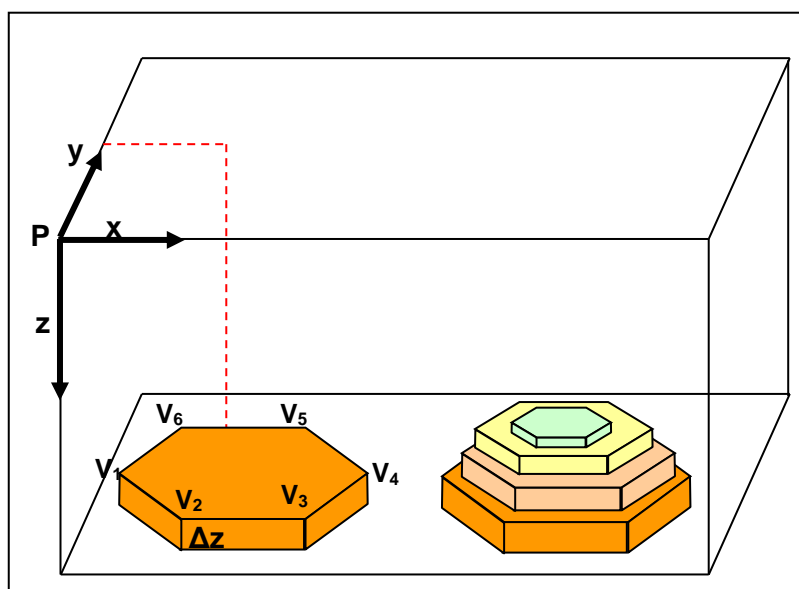
Fig. 8-23 A polygonal plate of constant thickness (Δz) is defined by the xyz-coordinates of its vertices (v_1, v_2, v_3, …) and a three dimensional model is approximated by a series of horizontal polygonal plates.

Chapter 9

INTERPRETATION OF GRAVITY ANOMALIES

9.1. Scope and Objective

The basic principle underlying gravity data interpretation is the fact that any subsurface change in density (i.e. density contrast) would have a corresponding signature or imprint on the Earth gravity field. In fact, it is an inverse problem where the interpreter aims at translating (interpreting) gravity data, normally expressed by Bouguer gravity maps or gravity profiles, into the corresponding geological structures (Fig. 9-1).
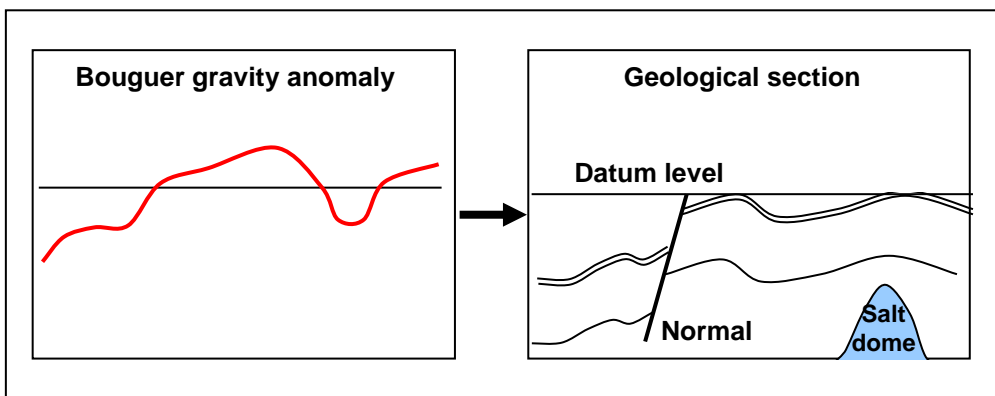
Fig. 9-1 The objective of the gravity interpretation process is the translation of the Bouguer gravity anomaly into the corresponding geological section.

The interpreter should bear in mind that a measured gravity value is in fact the resultant (vector sum) of the attraction forces from all subsurface and over surface gravity effects. The Bouguer gravity image, resulting from processing of the raw data, represents gravity variation caused only by the sub sea level geological anomalies. The value of the Bouguer anomaly, which may be positive or negative, is function of a number of factors. These are mainly the size, shape, and depth as well as the value of the density contrast of the anomalous body in respect to the surrounding medium.

To facilitate the interpretation process, the interpreter normally uses further data analyses applied on the Bouguer anomalies in order to obtain more direct evidence on the causing geological anomalies. Separation of the regional trend, computing gradients, and modeling (using trial density and trial shapes and depths) are all ways and means to determine the geological structure causing the gravity anomaly.

9.2. Role of Rock Density

As we have seen in previous chapters, the gravitational attraction force of a certain body is function of the total mass of that body. For a defined body shape, the created gravity force (or acceleration) is directly proportional to the mass distribution (i.e. density) within the body. Thus, density plays a principal role in all the phases of the gravity surveying activities. Bouguer and terrain corrections for instance depend on density of the rocks of the survey area.

Most important of all is that a gravity anomaly is caused by a density contrast between the body and its surrounding material. The algebraic sign of the gravity anomaly may be negative or positive depending on whether the anomalous body has a density-deficiency or density-surplus in respect to the host medium (Fig. 9-2).
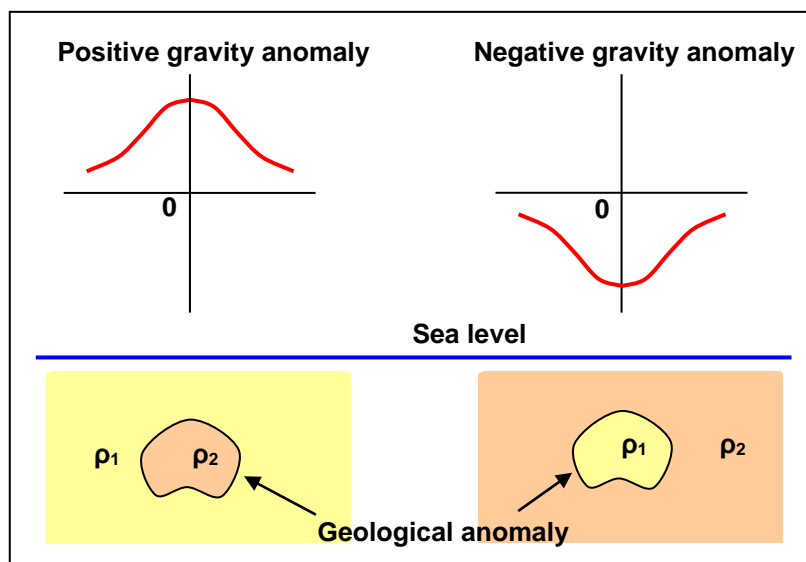
Fig. 9-2 The sign of the gravity anomaly depends on density contrast ($\rho_2 - \rho_1$) of the anomalous mass (geological anomaly), where ($\rho_2 > \rho_1$). The positive sign for density surplus and the negative sign for density deficiency

The interpreter must always remember that it is not the absolute value of density that produces a gravity anomaly. What matters in this regard is the contrast in density between the anomalous mass and its surrounding material. The greater the contrast is the more pronounced the caused anomaly will be.

Naturally, geological conditions control density distribution in the subsurface geological formations. Rock bulk-density depends on a number of factors, most important of which are lithology, porosity, mineral composition, and fluid content. It is commonly observed that the density of a sedimentary rock increases with geological age and with depth of burial, due to increase of compaction. As for igneous rocks, density increases with the increase from acidic (e.g. granite) to basic and ultra basic rocks (as in gabbro and syanite).

9.2.1 Densitiy Variations

Like any other physical properties of rock media, density varies according to rock type and the prevailing geological conditions under which the rock specimen is existing. As regards rock type, the igneous rocks are generally of higher densities than sedimentary rocks. Based on laboratory measurements of samples from on-surface outcropping rocks and from subsurface rocks (core samples), bulk densities for various types of rocks are made available. The mean density values for the commonly known rock types are given in the following table (Dobrin, 1960, p.251).

Rock Type	Average Density
Sandstone	2.32
Shale	2.42
Limestone	2.54
Acidic Igneous	2.61
Dolomite	2.70
Metamorphic	2.74
Basic Igneous	2.79

It is apparent that the density values cover a wide range of values and that there is overlap between densities of various rock types. This property which is common in rocks forms the main source of uncertainty in rock identification.

An important factor affecting density of a rock formation is the depth of burial of the formation. Since compaction increase with the increase of depth, it is expected that rock density increase with depth. Nettleton (1934) published the result of a study based on combination of gravity data and theoretical analysis.

The result expressed in the form of a curve expresses the type of relationship between density and depth of formations from the Gulf Coast area (Fig. 9-3).
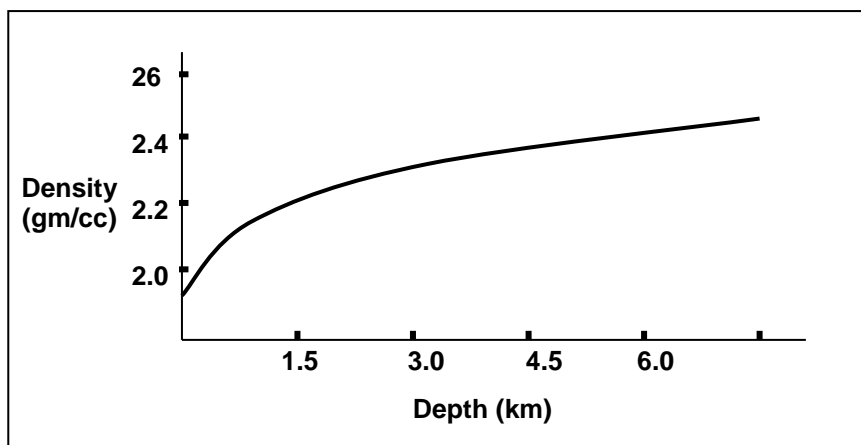
Fig. 9-3 Density of Gulf Coast sediments as a function of depth (Nettleton, 1934, roughly re-drawn)

9.2.2 Ranges of Rock Densities

As it is stressed, the gravity anomaly results from density differences existing between the various subsurface rock formations. In fact, the success of the interpretation process depends largely upon the accuracy of the available knowledge of the subsurface density variations. It is therefore very useful for the interpreter to have at hand some statistics about the bulk density of rocks and minerals in nature. Ranges of density values for common rock types and minerals are given in the following tables (Telford et al, 1996, p.16).

(A) Wet Sedimentary rocks

Rock type	Density range (gm/cc)	Average (gm/cc)
Soil	1.20 - 2.40	1.92
Clay	1.63 - 2.60	2.21
Gravel	1.70 - 2.40	2.00
Sandstone	1.61 - 2.76	2.35
Shale	1.77 - 3.20	2.40
Limestone	1.93 - 2.90	2.55
Dolomite	2.28 - 2.90	2.70

(B) Igneous rocks

Rock type	Density range (gm/cc)	Average (gm/cc)
Rhyolite	2.35 - 2.70	2.52
Andesite	2.40 - 2.80	2.61
Granite	2.50 - 2.81	2.64
Granodiorite	2.67 - 2.79	2.73
Porphyry	2.60 - 2.89	2.74
Quartz diorite	2.62 - 2.96	2.79
Diorite	2.72 - 2.99	2.85
Lavas	2.80 - 3.00	2.90
Diabase	2.50 - 3.20	2.91
Basalt	2.70 - 3.30	2.99
Gabbro	2.70 - 3.50	3.03
Peridotite	2.78 - 3.37	3.15
Acid igneous	2.30 - 3.11	2.61
Basic igneous	2.09 - 3.17	2.79

(C) Metamorphic rocks

Rock type	Density range (gm/cc)	Average (gm/cc)
Quartzite	2.50 - 2.70	2.60
Schists	2.39 - 2.90	2.64
Greywacke	2.60 - 2.70	2.65
Marble	2.60 - 2.90	2.75
Serpentine	2.40 - 3.10	2.78
Slate	2.70 - 2.90	2.79
Gneiss	2.59 - 3.00	2.80
Amphibolite	2.90 - 3.04	2.96
Eclogite	3.20 - 3.54	3.37

(D) Metallic minerals

Oxides, carbonates

Rock type	Density range (gm/cc)	Average (gm/cc)
Bauxite	2.30 - 2.55	2.45
Limonite	3.50 - 4.00	3.78
Siderite	3.70 - 3.90	3.83
Manganite	4.20 - 4.40	4.32
Chromite	4.30 - 4.60	4.36
Ilmenite	4.30 - 5.00	4.67
Magnetite	4.90 - 5.20	5.12
Hematite	4.90 - 5.30	5.18
Cuprite	5.70 - 6.15	5.92

Sulfides, arsenides

Rock type	Density range (gm/cc)	Average (gm/cc)
Malachite	3.90 - 4.03	4.00
Chalcopyrite	4.10 - 4.30	4.20
Pyrrhotite	4.50 - 4.80	4.65
Molybdenite	4.40 - 4.80	4.70
Pyrite	4.90 - 5.20	5.00
Chalcocite	5.50 - 5.80	5.65
Cobaltite	5.80 - 6.30	6.10
Arsenopyrite	5.90 - 6.20	6.10
Galena	7.40 - 7.60	7.50

(E) Non-Metallic minerals

Rock type	Density range (gm/cc)	Average (gm/cc)
Petroleum	0.60 - 0.90	-
Ice	0.88 - 0.92	-
Sea water	1.01 - 1.05	-
Lignite	1.10 - 1.25	1.19
Soft coal	1.20 - 1.50	1.32
Anthracite	1.34 - 1.80	1.50
Chalk	1.53 - 2.60	2.01
Graphite	1.90 - 2.30	2.15
Rock salt	2.10 - 2.60	2.22
Gypsum	2.20 - 2.60	2.35
Kaolinite	2.20 - 2.63	2.53
Orthoclase	2.50 - 2.60	-
Quartz	2.50 - 2.70	2.65
Calcite	2.60 - 2.70	-
Anhydrite	2.29 - 3.00	2.93
Biotite	2.70 - 3.20	2.92
Magnisite	2.90 - 3.12	3.03
Fluorite	3.01 - 3.25	3.14
Barite	4.30 - 4.70	4.47

As it is seen from these tables, the density values of the rock types are falling within the small range of 2-3 gm/cc. It is also apparent that densities of igneous rocks are generally tending to be higher than those of the sedimentary rocks and densities of the metallic minerals are higher than those of the non-metallic compounds.

9.2.3 Density Determination Methods

It is commonly known that the density of a certain rock type can be quite variable. For this reason, an average density value may be obtained from many repeated measurements. Another important point is the need for density measurement for a rock specimen existing in its natural environment. Direct and indirect methods are available for use in density determination. For the gravity surveying work it is preferable to determine density of rocks in-situ since the obtained values in this case give the more true representation of the gravity causing bodies. Several techniques can be applied to determine rock bulk density. These are:

(i) By Direct method

By this method, a sample is weighed in air and then in water and from the difference the bulk density can be computed. If it is porous, then the specimen is saturated with water beforehand and the obtained density value, in this case, represents near realistic values of rocks existing under the water table.

(ii) By Underground Measurement

Two gravity readings are taken; one is taken at the surface of a rock slab and the other reading is taken directly below the slab. This is possible if there is a mineshaft or a cave opening that allows measuring gravity at the two faces of the slab.

Referring to Fig. 9-4, let AB be an opening of depth (h) and g_A and g_B be the gravity values (in milligals) measured at points (A) and (B) respectively.
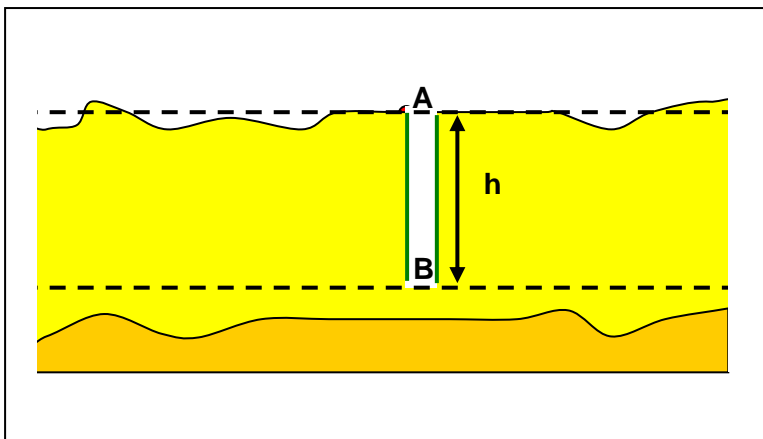
Fig. 9-4 Principle of the method of density determination from under-ground measurements

The difference (g_B - g_A) is related to the rock slab of thickness (**h**, in meters) and density (ρ, in gm/cc) by:

$$g_A + 0.3086\ h - 0.0419\ \rho\ h + T_A = g_B + 0.0419\ \rho\ h + T_B$$

giving,

$$g_B - g_A = (0.3086 - 0.0838\rho)\ h + \Delta T$$

hence,

$$\rho = 3.68 - 11.93(g_B - g_A - \Delta T) / h$$

where (ΔT) is the difference in terrain correction (T_A-T_B) which is needed to be taken into consideration if cavities exist in the neighborhood of the shaft opening.

(iii) From Borehole Measurements

Rock density can be measured in boreholes using a gamma-ray logger which consists of a source of gamma-rays at one end of the logging tool and a detector (usually a Geiger counter) at the other end. The intensity of the back-scattered radiation from the rocks penetrated by the well is approximately proportional to the electron concentration in the rocks which is proportional to the wall rock density. A curve (density-log) is usually drawn showing the density variation with depth. It should be noted here that, because of the penetration limitation, density information given by this method expresses density variation of a rather limited penetrated zone which is of less than half a meter in extent.

Another way of density determination from borehole measurements is by use of borehole gravity meters (BHGM) method. The technique involves lowering a special type of gravimeter through a borehole and measuring gravity at different depths giving an estimate of the average density of the material between any two measurement points inside the borehole.

The relation between density (ρ) and gravity difference ($g_B - g_A$) at two points **B** and **A** is expressed by the equation ($\rho = 3.68-11.93(g_B - g_A - \Delta T)/h$) which has been derived in the previous paragraph.

The difference between gravity readings g_A and g_B at two different points (A) and (B), which are (h) distance apart, would give the apparent density of the material between the two points. Thus, dropping the Terrain-correction term (ΔT) which is not necessary in borehole measurements we get:

$$\rho = 3.68-11.93\ (g_A \text{ and } g_B) / h$$

This shows that the density is determined from the vertical gradient of gravity measurements made by the borehole gravimeter.

(iv) Nettleton's Method

The well-known geophysicist L. L. Nettleton introduced a method for density determination using gravity measurements (Nettleton, 1939).This method involves measuring gravity along a line across an isolated prominent topographical feature such as a small hill or valley. The raw gravity readings are subjected to Bouguer and terrain corrections using a series of different trial densities. The resulting gravity profiles are then drawn for each trial density value. The real density value, representing that of the surveyed topographic feature (a hill for example), is that one which yields a Bouguer profile which is of least resemblance to the outlines of that feature (Fig. 9-5).

If an applied density value (ρ_1) is smaller than the actual value (ρ_0) of the surveyed topographical feature, we get a computed Bouguer gravity value (Δg_{B1}) higher than the optimum Bouguer value (Δg_{B0}). On the other hand, when the applied density is greater than the actual density, the Bouguer values will be lower than the optimum value.

The deviation of the computed Bouguer value from the optimum is dependent on elevation. This means that the computed Bouguer profile will be of a shape which resembles that of the surveyed topographic feature when the applied trial density is smaller than the optimum density. However when the applied density is greater than the optimum, the obtained Bouguer profile will also resemble the shape of the topographic feature but inverted form. This can be seen as follows:

Let the optimum density for the topographic feature be (ρ_0) and the applied trial density (ρ_1) is less than (ρ_0) by ($\Delta\rho$) then we have for the computed Bouguer anomaly:

$$\Delta g_B = g_O - g_N + 0.3086h - 0.0419 (\rho_0 - \Delta\rho) h$$

$$\Delta g_{B1} = \Delta g_{B0} + 0.0419 \Delta\rho h$$

This shows that the deviation ($\Delta g_{B1} - \Delta g_{B0}$) is in direct proportionality with the elevation (**h**) giving in this case, where $\Delta g_{B1} > \Delta g_{B0}$, is the resemblance of the Bouguer profile with the outlines of the topographic feature.

For the case ($\rho_1 > \rho_0$) we get $\Delta g_{B1} = \Delta g_{B0} - 0.0419$) $\Delta\rho h$ which means that $\Delta g_{B1} < \Delta g_{B0}$. Since the deviation ($\Delta g_{B1} - \Delta g_{B0}$) is dependent on the elevation (**h**) we get the inverted form of the Bouguer profile in this case.
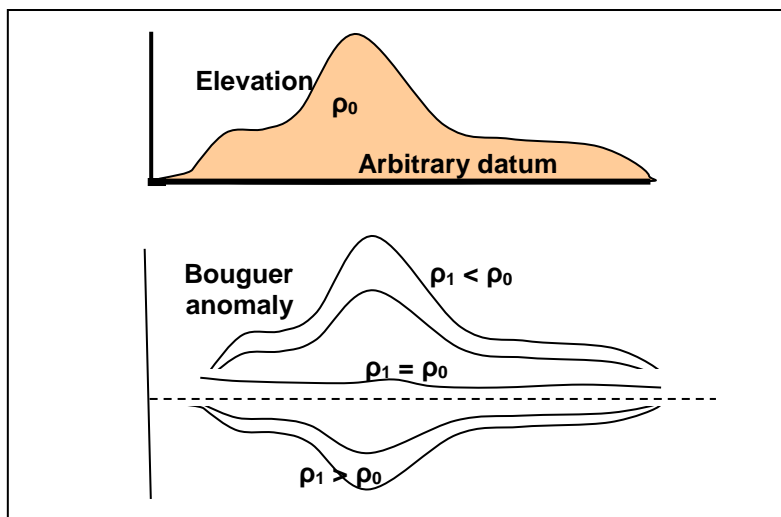
Fig. 9-5 Schematic representation of the Nettleton's method for density determination

The advantage of this method is that it gives an average value for the density of material existing above the seal level with no need for extra tools and measurements requirements as boreholes. The disadvantage is that the prominent feature may not be representative sample for the rest of the survey area, or the feature may be due to an isolated density-anomaly such as an igneous intrusion or anomalous salt body. Ideally measurements should be made over a homogeneous erosion feature which is not formed due to near-surface density anomaly.

(v) From P-wave Velocity

This method is based on the empirical relationship existing between rock density and the P-wave interval-velocity obtained from seismic data. Based on a number of researches such as Nafe and Drake (1963), and Gardner et al (1974), a number of empirical relationships between P-wave velocity and density have been established. Plot of the empirical relationship connecting P-wave velocity to rock bulk density is shown in Fig. 9-6.

This method is suitable for density determination for deep strata that are inaccessible by directly measuring instruments. The accuracy of the density determined by this method is estimated to be in the order of ± 0.1 gm/cc (Kearey and Brooks, 1987, p.157).
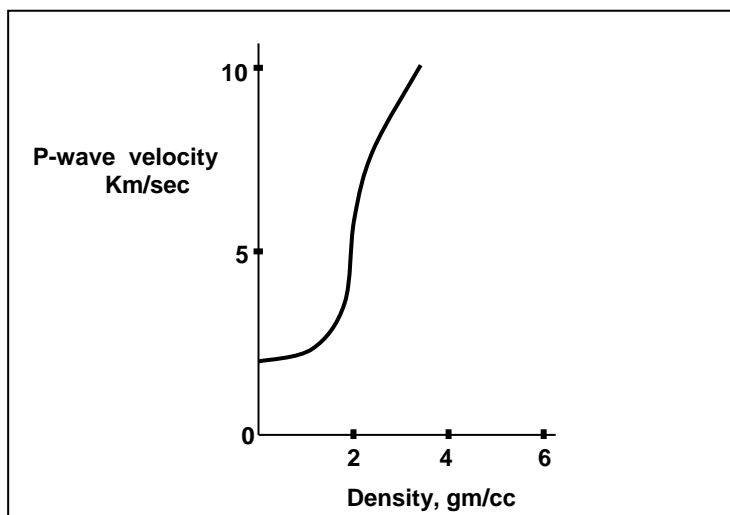
Fig. 9-6 Plot of the empirical function connecting P-wave velocity
to bulk density of rocks (Redrawn from Nafe and Drake, 1963).

9.3.   Ambiguity in Gravity Interpretation

Interpretation of gravity data (and other potential field data such as magnetic and electrical anomalies) suffers from the ambiguity phenomenon. A given buried anomalous mass gives a unique gravity anomaly. On the other hand, a given gravity anomaly can be created by an infinite number of possible density distribution models. Thus, for instance, a number of concentric spheres of the same mass but of different densities and volumes, or of different masses located at different depths, can produce the same anomaly (Fig. 9-7).

9.4.   The Direct and Inverse Problems

There are two alternative approaches followed in geophysical interpretations. These are commonly known among geophysicists by the term; direct (or forward) problem and the inverse-problem.

The direct problem approach involves computing the geophysical response (the gravity anomaly, in this case), given the parameters (geometrical shape, size, depth, and density distribution) of the causing anomalous body. The inverse problem approach, on the other hand, involves determination of the body parameters from the given gravity anomaly (Fig. 9-8).
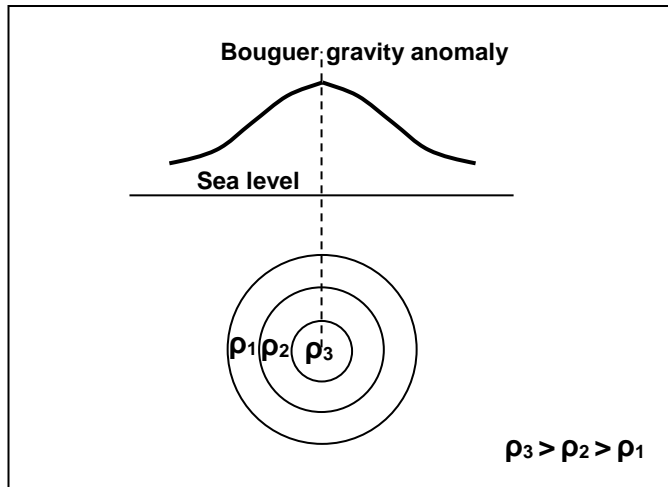
Fig. 9-7 Interpretation ambiguity, one gravity anomaly can be produced by concentric spheres of the same mass and different densities and different volumes.

As it is stated above, the ambiguity in gravity interpretation implies that an anomalous body which produces a gravity anomaly is not unique. This means that the inverse problem approach used in interpretation cannot, by itself, lead to a single solution. In other words, with the inverse problem method it is not possible to deduce the causing anomalous body with certainty. However, with additional data, that is with additional constraints, this method becomes a practical and successful tool in interpretation.
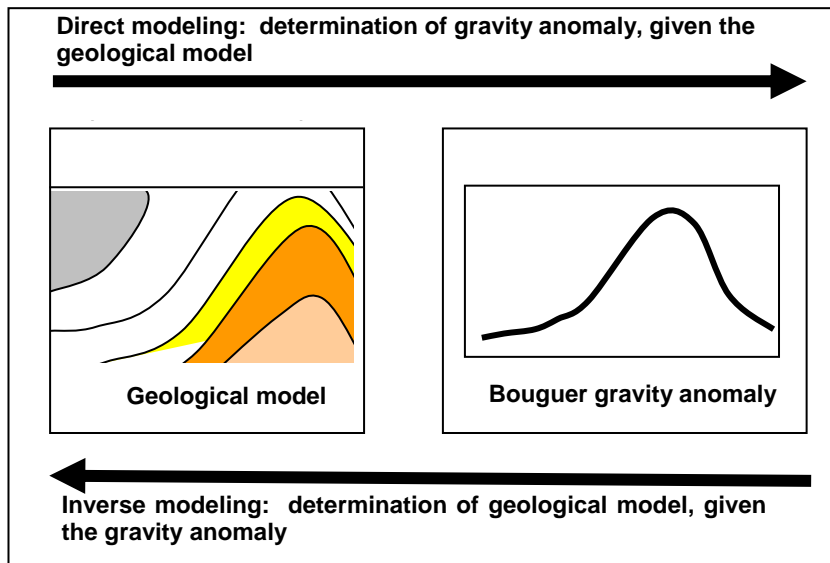
Fig. 9-8 Concept of the direct- and inverse-problems. Deduction of model from gravity effect and vice versa.

9.5.   Regional and Residual Gravity

The gravity field expressed by a Bouguer map is the sum of gravity effects resulting from density changes (geological anomalies) existing in the subsurface medium of the surveyed area. These changes, expressed by the gravity anomalies, are produced from lateral changes in density. The amplitude of the anomaly is function of both the density difference (density contrast) and the depth of the responsible geological structure. In fact, the anomaly amplitude gets larger with the increase of density contrast and with the decrease of the depth of the anomalous body. For a given anomalous mass, the amplitude of the gravity anomaly, its smoothness and width are governed by depth of the mass. As the depth increases, the resulting gravity anomaly gets wider, weaker, and smoother. This is schematically illustrated in Fig. 9-9.

Bouguer gravity anomalies

Sea level

z_1

z_2

z_3

ρ_h

ρ_b

ρ_b

ρ_b

Anomalous bodies at different depths, z
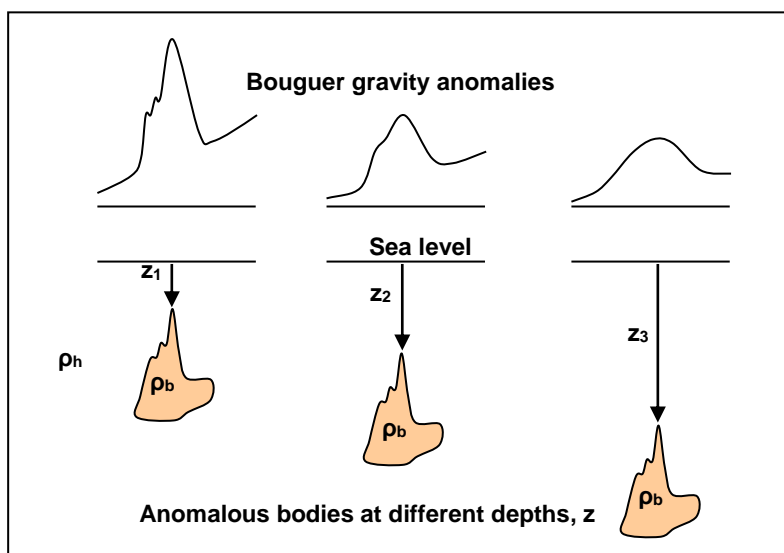
Fig. 9-9 Depth effect on the Bouguer gravity-anomaly of a body of density (ρ_b) buried in host rocks of density (ρ_h) where $\rho_b > \rho_h$.

A Bouguer anomaly-map normally shows gravity variations that consist of two components. These are:

(i) Long wavelength (low wave number) variation, reflecting deep geological anomalies which are of large and of regional extent. This component which shows the general trend of variation is called the *regional gravity*.

(ii) Short wavelength (high wave number) variation reflects relatively shallow geological anomalies which are of restricted or local nature. Because, this component is normally obtained by removing the trend-component (the

regional) from the Bouguer map, it is normally referred to as the *residual gravity* or just the *residuals*.

It should be remarked here that geophysicists sometimes use other terms like low frequency and high-frequency components for the slow (long wavelength) and fast (short wavelength) variations respectively.

9.6.   Anomaly Separation Schemes

The first step in interpreting Bouguer gravity data is the isolation of the residual anomalies by removing the regional anomaly from the original Bouguer anomaly map (or profile). Separation of residual anomalies (sometimes called *residualizing* process) can be achieved by one of several types of approach, which can be grouped into two main types. These are graphical and analytical types of approach.

9.6.1 The Graphical Approach

A Bouguer gravity variation may be expressed in the form of a profile (one-dimensional function, f(x)) or in the form of a contour map (two-dimensional function, f(x, y)). In the case of a profile, the smoothing process can be carried out manually by drawing a linear or curvilinear curve that follows the general trend of the anomaly variation. The drawn line is considered to be representing the regional gravity which is then subtracted from the observed Bouguer gravity values at each observation point. The result of this process is getting the residual gravity variation along that profile (Fig. 9-10).
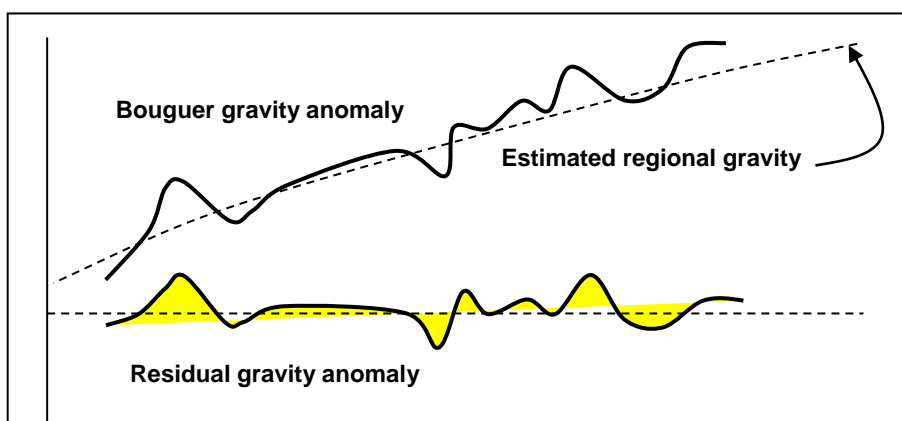
Fig. 9-10 Determination and separation of the residual anomaly by the graphical method (case of a gravity profile).

For a Bouguer gravity map, a similar procedure is followed. In this case, the gravity contours are smoothed by drawing lines expressing the general trends of the contour lines (Fig. 9-11).

Another way of separation which can be applied in case of a Bouguer gravity map is by constructing a set of gravity profiles from the given map. Each profile is then smoothed as explained above to determine the regional trend which is subtracted from the observed gravity to give the residual anomaly variation along the profile. By posting the values from the processed profiles onto the map, the final regional and residual maps can then be obtained.
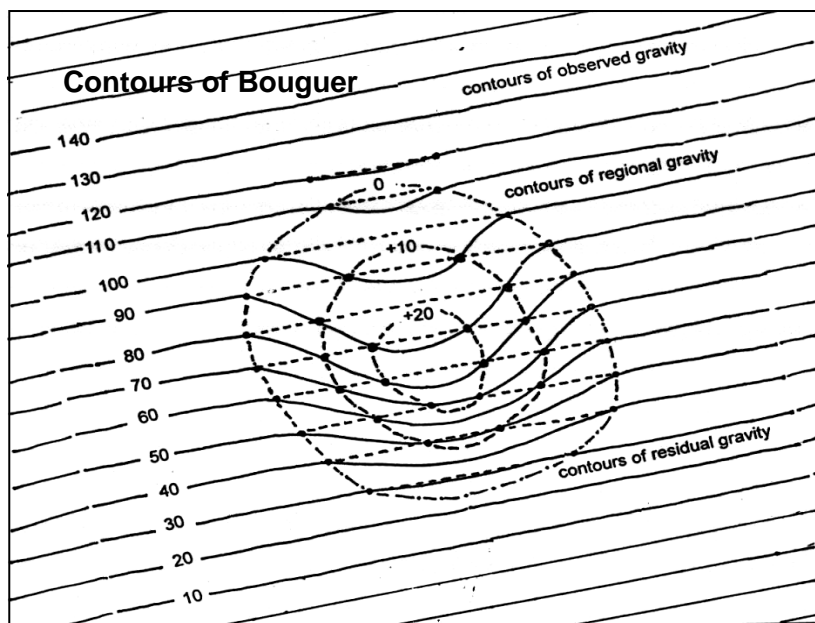
Fig. 9-11 Determination by the graphical method of residual gravity by subtracting the regional gravity contours from the Bouguer contours (case of a gravity contour map).

The regional trend curve can be drawn in such a way that all the computed residual anomalies are of positive values. In analytical methods, the average value of the residual anomalies is usually set at zero. This will result in both positive and negative residuals giving a residual gravity map in which each anomaly is surrounded by neighboring anomalies of opposite algebraic sign.

Whether it is a profile or a contour map, the graphical smoothing technique is basically dependent on personal judgment. For this reason, the computed regional and residual variations may differ from one interpreter to another. The extent of difference depends on the degree of complexity of the given Bouguer gravity data and on the interpreter individual skill.

9.6.2 The Analytical Approach

Analytical methods for separation involve numerical operations applied on the Bouguer gravity map. This process requires the basic data to be known at points organized in a uniform grid pattern. For this reason, the Bouguer gravity values which are irregularly spaced are re-organized in such a way that the gravity values become known on a square grid of points. This process, which is a necessary pre-requisite for all analytical methods, is called gridding or digitizing of the gravity data.

Several analytical methods exist for the separation process. These are: data averaging, polynomial fitting, upward continuation, second derivatives and wavelength filtering.

(i) Data Averaging

Griffin Method:

The simplest averaging technique is that suggested by Griffin in 1949. The method serves as a direct way to compute residual gravity from a given Bouguer gravity map. It involves averaging of the gravity values of a set of points on the gravity map which are located at equal distances from the point at which the residual is to be computed. The residual gravity value at a point (as point **P** in Fig. 9-12) is equal to the observed Bouguer value (g_P) at that point minus the computed average of the gravity values at a set of points which are equally spaced about the circumference of a circle of a suitable radius. The process is repeated for all observation points in the survey area.

Running-Average Method:

Other methods based on the same principle (data averaging) may be implemented to determine the regional gravity. One common way to achieve this is by use of the running-average technique. The process carried out over a given Bouguer profile will bring about a smoothing effect to that profile. This process involves taking the average of a number of values taken at a set of points (called the running set) in the neighborhood of a central point at which the average is to be computed.

To illustrate the technique, let us consider computing the running average for a Bouguer gravity profile from which gravity values can be read at a sequence of observation points (g_1, g_2, g_3, g_4, g_5, g_6, g_7, g_8, …). Using a 5-point

running set, the value of the central point (g_3) of the first running-set (g_1, g_2, g_3, g_4, g_5) is then replaced by the computed average of these five values. In the second step, the running set is shifted forward by one point (that is for the points g_2, g_3, g_4, g_5, g_6). The central value (g_4) is likewise replaced by the average of the new running set. The shifting and averaging process is continued over all the points in the profile from start-point right through to the end-point producing a smoothed gravity profile.
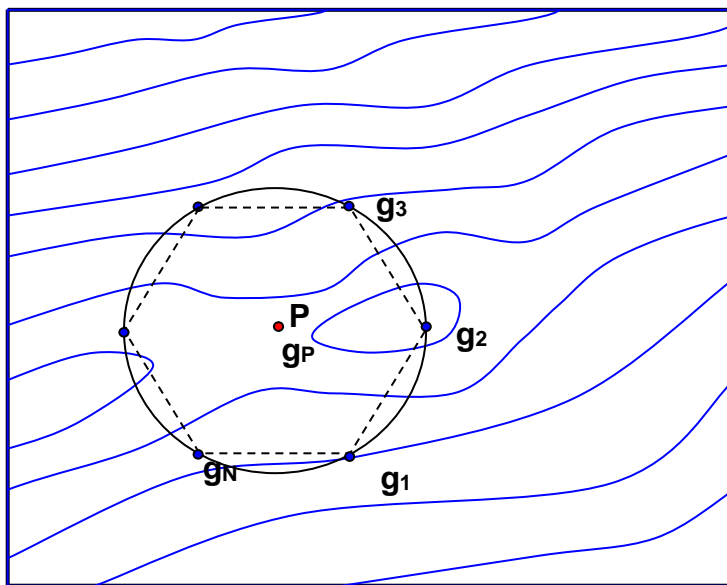
Fig. 9-12 Computing residual gravity by Griffin method. The value g_P of residual gravity at a point (P) is calculated by subtracting the mean of Bouguer values, (g_1 + g_2+ g_3 +… + g_N) / N, from the Bouguer value at that point. Then, Residual gravity at point (P) is equal to g_P - (g_{1} + g_{2} + g_{3} + g_{4} + g_{5} + g_{6} + g_{7} + g_{8}) / 8.

It should be noted here that if instead of five points, fifteen points are used for the running-set, we get more severe smoothing effect. The number of points used in the running-set is decided upon after making several tests. Of course, the larger the number of points taken in the average, the smoother the profile becomes (Fig. 9-13). In all cases, the smoothing effect is incomplete at both ends of profile due to decrease of the number of points in the running set at the two ends of the profile.

The running average (called also moving average) would result in a smoothed regional anomaly which is then subtracted from the Bouguer gravity to obtain the residual (local) gravity anomaly.

The running average technique can be applied in the same way on a Bouguer anomaly map, where the values are known over uniformly spaced grid points. In

this case, the gravity value of each observation point in that map is replaced by the average of all points in a square area whose center coincides with that point. As in the profile case, the smoothing effect will be incomplete over the margins of the survey area.

The Weighted Averages

In the simple Griffin method, the average is computed for values of points which are at equal distances from a central point, and thus in this case a simple arithmetic average is adequate. However when the gravity-values entering in the adopted running-set belong to points of varying distances from the central point of the set, weighted averaging becomes necessary. Since the contribution of a point in the applied running-set is inversely proportional to its spacing-distance from the central point, its value must be multiplied by an appropriate weighting factor before being used in the average computation. The weighted average (g_w) is calculated by summing the value-by-weight products ($g_i\,w_i$) and dividing by the sum of the weights (w_i). That is:

$$g_w = (g_1\,w_1 + g_2\,w_2 + g_3\,w_3 + \ldots + g_N\,w_N) / (w_1 + w_2 + w_3 + \ldots + w_N)$$

or:

$$g_w = (\Sigma\ g_i.w_i) / \Sigma\ w_i$$

Customarily, the weighting factors (w_i) of the points in the running set are inversely proportional to the point-spacing from the central point. One can readily see that the simple average (g_s) is a special case of the weighted average and can be obtained by making all weight values be equal $w_1 = w_2 = \ldots = w_N$, giving for **N**-points:

$$g_s = (g_1 + g_2 + g_3 + \ldots + g_N) / N$$

or:

$$g_w = (\Sigma\ g_i) / N$$

The running set may be one-dimensional array (as in case of a profile) or two-dimensional array as in case of gravity data given at a uniform grid map. To clarify the concept of applying running average method on a given gravity map where the gravity values are expressed in the form of a two-dimensional array, consider the data set shown in Fig 9-14. The grid spacing in this example is assumed to be 3m in the x-direction and 4m in the y-direction. By choosing a 9-point (3 by 3 - array) for the running set and using the inverse-proportionality principle, the weighting factors become 1/3, 1/4, 1/5 for the spacing of 3m, 4m, and 5m respectively.
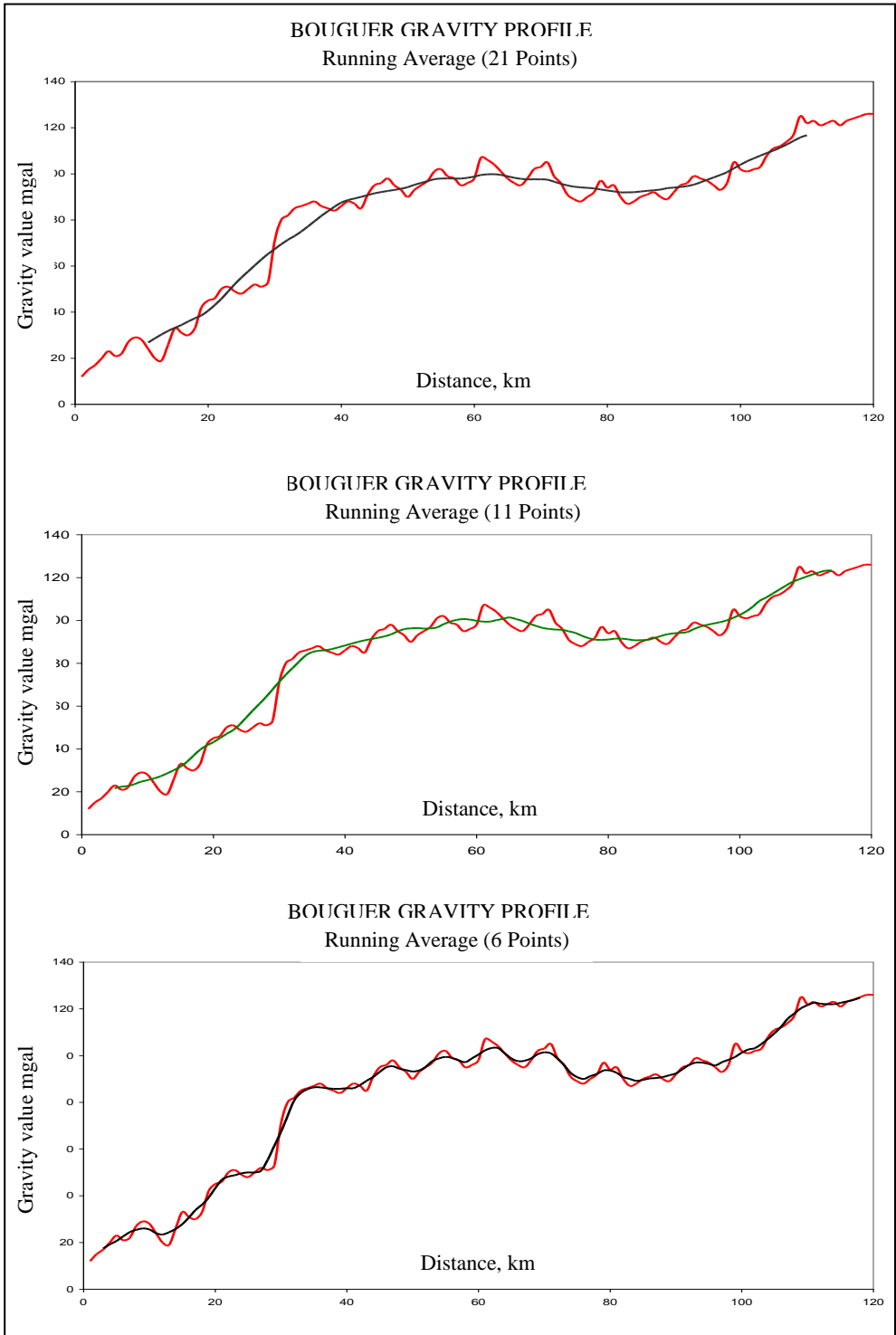
Fig. 9-13 Determination of regional gravity profile by running-average method. The
regional trend-line (black curve) is superimposed on the original Bouguer profile (red curve)

The weighted average of the 9-point running-set at the central point (**P**) is given by g_P, where:

$$g_P = (g_1.1/5 + g_2.1/4 + g_3.1/5 + g_4.1/3 + g_5.1 + g_6.1/3 + g_7.1/5 + g_8.1/4 + g_9.1/5) / (89/30)$$
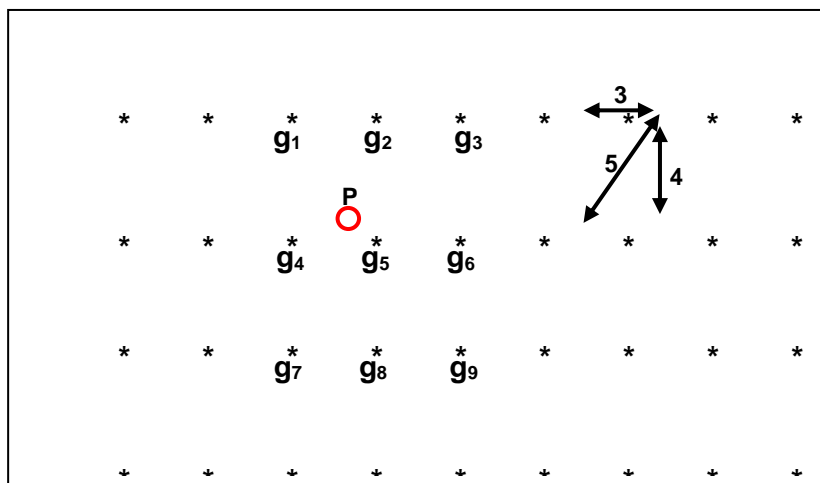
Fig. 9-14 Use of weighted averages to smooth Bouguer gravity data-set is given in the form of a uniform grid of points on a gravity map.

The particular choice of weights taken in this example, gives more importance to gravity variations near the central points. However, if it is required that greater importance is to be given to gravity values at distant points (which is not the normal case) a direct proportionality is used in the design of the weight-factors. Thus, instead of the values (1/3, ¼ and 1/5) which have been used in the above example, the weight-factors (3, 4 and 5) may be used. Choice of the running average parameters (number of weight factors in the running set and weight values) is decided upon by the interpreter according to his own judgment.

(ii) Polynomial Fitting

In this method, the Bouguer gravity profile (or map) is expressed by a low-order polynomial such as the following:

$$g(x) = C_0 + C_1x + C_2x^2 + C_3x^3 + + C_4x^4 + C_5x^5 + \dots \quad \text{(for a profile)}$$
$$g(x,y) = C_0 + C_1x + C_2y + C_3xy + + C_4x^2 + C_5y^2 + \dots \quad \text{(for a map)}$$

The coefficients (C_0, C_1, C_2, C_3, …) are determined by a least-squares analysis. This will express the regional gravity which is subtracted from the Bouguer values to obtain the residual. This procedure (polynomial fitting) may be repeated several times to 1D-variation (gravity profile) or to 2D-variation (gravity map) using different polynomial degrees. The final choice depends on the degree of smoothing required by the interpreter (Fig. 9-15).

(iii) Upward Continuation

Mathematical theories have shown that a potential field, such as gravity and magnetic fields, can be determined over an arbitrary surface if it is known over an another surface below or above it (Peters, 1949). In other words, a Bouguer gravity map can be mathematically projected upward or downward relative to an adopted datum plane. This process, which is based on mathematical analyses, is called upward continuation when the field is transformed into a plane above the survey datum plane, and downward continuation when the transformation is to a plane below that datum plane which is closer to the causing geological anomaly.

The important feature of this method is the fact that upward projection of the gravity field introduces a smoothing effect to the observed Bouguer anomaly map. With the increase of height of the projection, the gravity variations due to shallow and local sources (residual gravity) diminish, while at the same time, the regional anomalies become the more dominant.

The upward continuation transformation can be carried out using a formula based on Stokes theorem but computation can be carried out numerically using the following formula (Robinson, 1988, P. 307):

$$g_P = (g_1 f_1 + g_2 f_2 + \ldots + g_N f_N) / N$$

or,

$$g_P = (\Sigma\, g_i \cdot f_i) / N$$

where,

g_P : Upward continuation transformed gravity at point (**P**)

g_i : Bouguer gravity value of the basic data, (**i = 1, 2, 3, …, N**).

N : Total number of Bouguer values included in the computation of g_P.

f_i : Weighting factor ($= h_i . A_P / 2\pi\, r_i^3$)

h_i : Height of point (**P**) above the Bouguer anomaly plane.

A_P : Area over which the utilized Bouguer gravity values are distributed

r_i : Distance of the point (**P**) from the gravity value (g_i)

BOUGUER ANOMALY PROFILE
with polynomial trend line

$y = -1E-07x^5 + 5E-05x^4 - 0.0057x^3 + 0.2572x^2 - 2.2876x + 23.597$

BOUGUER ANOMALY PROFILE
with polynomial trend line

$y = 0.0002x^3 - 0.0453x^2 + 3.5262x$

BOUGUER ANOMALY PROFILE
with polynomial trend line

$y = -0.009x^2 + 1.8597x + 14.145$
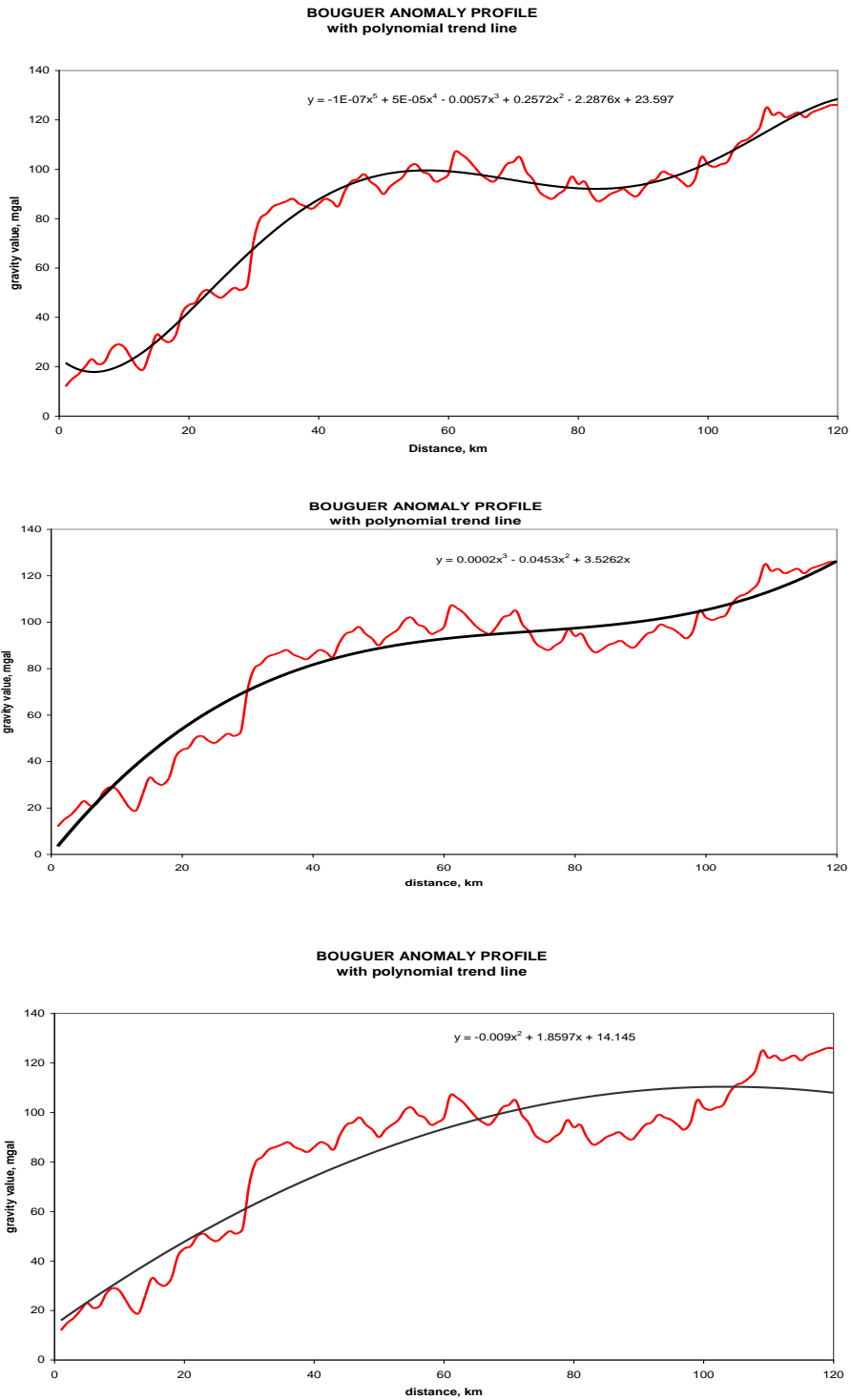
Fig. 9-15 Use of polynomial fitting method to smooth Bouguer gravity profile. The regional trend line (black curve) is superimposed on the original Bouguer profile (red curve).

These parameters are shown in Fig. 9-16. The area (A_P in this example) is made up of 5-by-5 cells with Bouguer gravity values (g_1 , g_2 , g_3 , ... , g_{25}).
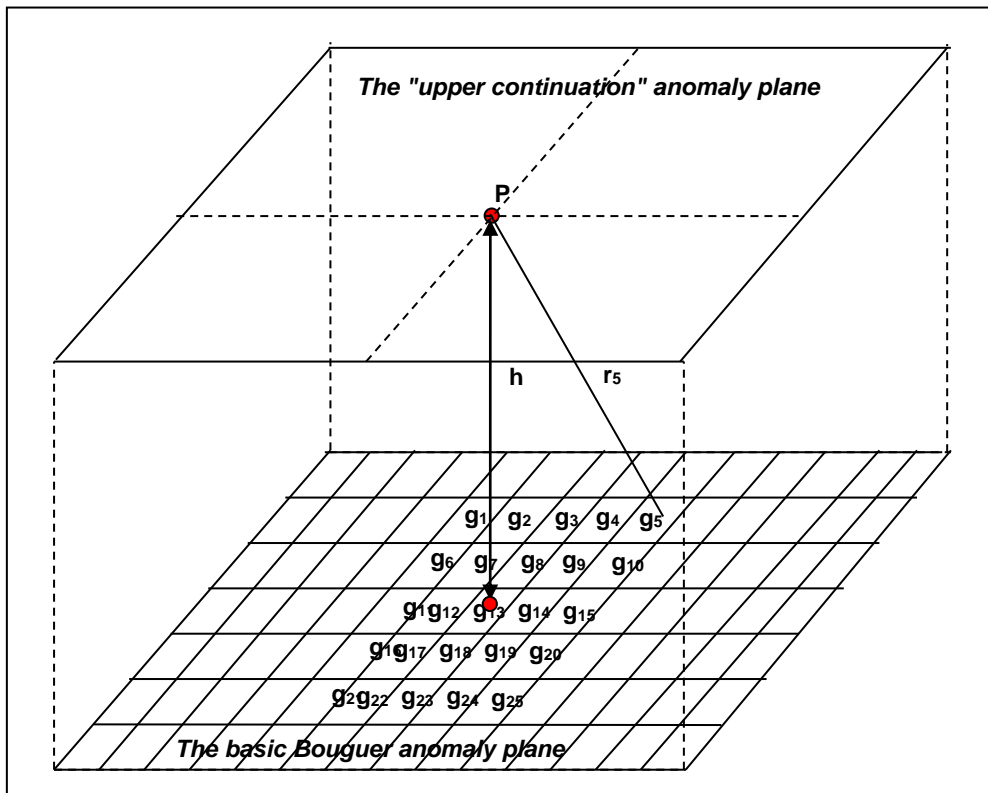
Fig. 9-16 Definitions of the parameters used in the numerical computation of the upward continuation formula.

It is to be noted here that the weighting factors (f_i) decrease with the increase of (r), the distance of point (P) from each of the original Bouguer values. Practically only a limited number of points (g_1, g_2, ... , g_N) are included in the computation of one transformed value, since the weighting factors (f_i) become too small, and hence insignificant, for too-distant points on the Bouguer map.

(iv) Second Vertical Derivative (SVD)

The first vertical derivative (or the vertical gradient) of the gravity field, **g** is mathematically expressed by **g`** (= **dg/dz**) and hence, the second vertical derivative is given by **g``** (= **d₂g/dz²**). The quantity **g`** expresses the rate of change of the gravity anomaly with elevation. If it is computed at each

observation point and contoured, a vertical gradient map will be obtained. If we further derive the **g``**- map from the **g`-** map, we will obtain the second vertical derivative map. Since this map (also called curvature map) expresses the degree of sharpness of anomaly surface at each observation point, the regional anomaly will be effectively removed leaving the enhanced residual anomaly which is associated with shallow geological structures.

The basic theory of the method and its application techniques are presented by Elkins (1951). In practice, the Bouguer gravity map can be transformed into a second derivative map through a number of computational methods.

According to Dobrin (1962, P. 245-248), the second vertical derivative of gravity at an observation point (**P**) is the slope at the origin of a curve constructed by plotting the average of the gravity values (taken at points around concentric circles centered at **P**) against the square of the circle's radius. The graphical procedure described by Dobrin involves construction of a special chart (shown in Fig. 9-17) used together with a formula for computing the second derivative anomaly.
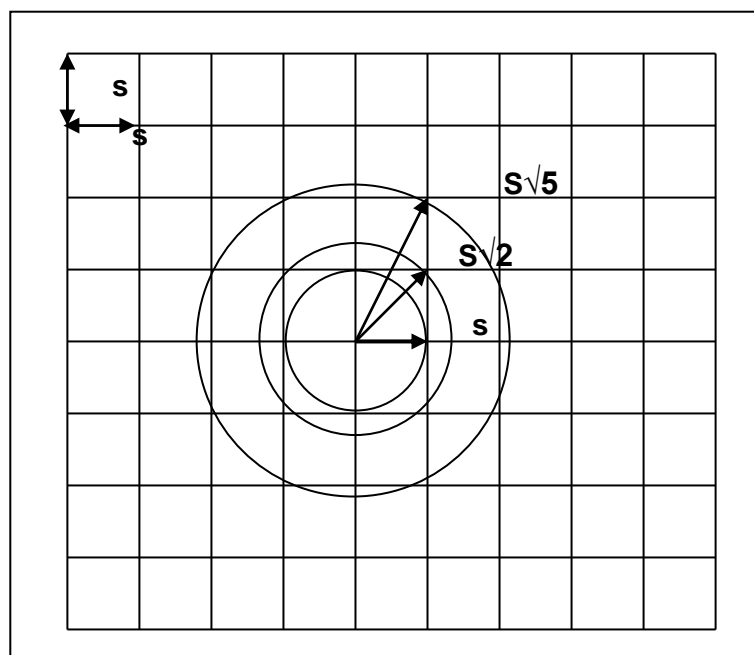
Fig. 9-17 Use of the circle-and-grid chart in computing the averages over circles of different radii, as applied in the graphical method of computing the SVD of a gravity map.

It should be pointed out here that instead of the graphical method, a more accurate method can be achieved through using a numerical coefficient

technique. Thus it is also possible to determine a set of weighting coefficients that can be used in an equation similar to that used in the upward continuation method to compute gradients (first derivatives) and curvatures (second derivatives) from a Bouguer gravity map.

The numerical computation method is based on the fact that the gravity field satisfies Laplace`s equation $\nabla^2 g = 0$, which allows computing the second vertical derivative from the horizontal derivatives. Thus:

$$\nabla^2 g = \partial^2 g / \partial x^2 + \partial^2 g / \partial y^2 + \partial^2 g / \partial z^2 = 0$$

That is:

$$\partial^2 g / \partial z^2 = -(\partial^2 g / \partial x^2 + \partial^2 g / \partial y^2)$$

When axes of coordinates are chosen such that contour lines become in the direction of one of the map-axes, we get a one-dimensional form of variation. Thus when x-axis is chosen to be perpendicular to contours, contour trend becomes parallel to the y-axis ($\partial^2 g / \partial y^2 = 0$) and the relation takes the form:

$$\partial^2 g / \partial z^2 = -(\partial^2 g / \partial x^2)$$

This equation allows to compute the SVD ($\partial^2 g / \partial z^2$) from the horizontal second derivative ($\partial^2 g / \partial x^2$) which can be readily computed from the Bouguer gravity map. To clarify the principle, let us see how to derive ($\partial^2 g / \partial x^2$) at a given point, based on an available gravity anomaly (Fig 9-18).The first derivative ($\Delta g/\Delta x$) and second derivative ($\Delta(\Delta g/\Delta x)/\Delta x$) of the gravity profile (Fig 10-18a) are given by:

$$[\Delta g / \Delta x]_1 = (g_2 - g_1) / \Delta x \text{ --------- at point } P_1$$

$$[\Delta g / \Delta x]_2 = (g_3 - g_2) / \Delta x \text{ --------- at point } P_2$$

hence,

$$(\partial^2 g / \partial x^2) = \Delta(\Delta g / \Delta x) / \Delta x = (2g_2 - g_1 - g_3) / (\Delta x)^2 \text{ ---- at point } P$$

In the case of a gravity map (Fig 10-18b), the SVD can be computed using the same principle followed in the profile case.

$$(\partial^2 g / \partial x^2) = [2g_2 - g_1 - g_3]_x / (\Delta x)^2 \text{ ---- at point } P, \text{ in the } x\text{-direction}$$
$$(\partial^2 g / \partial y^2) = [2g_2 - g_1 - g_3]_y / (\Delta y)^2 \text{ ---- at point } P, \text{ in the } y\text{-direction}$$

giving,

$$(\partial^2 g / \partial z^2) = - [(\partial^2 g/\partial x^2) + (\partial^2 g / \partial y^2)] = \Sigma[g_i - 4g_2]/(\Delta s)^2$$

where,

$$\Delta s = \Delta x = \Delta y$$
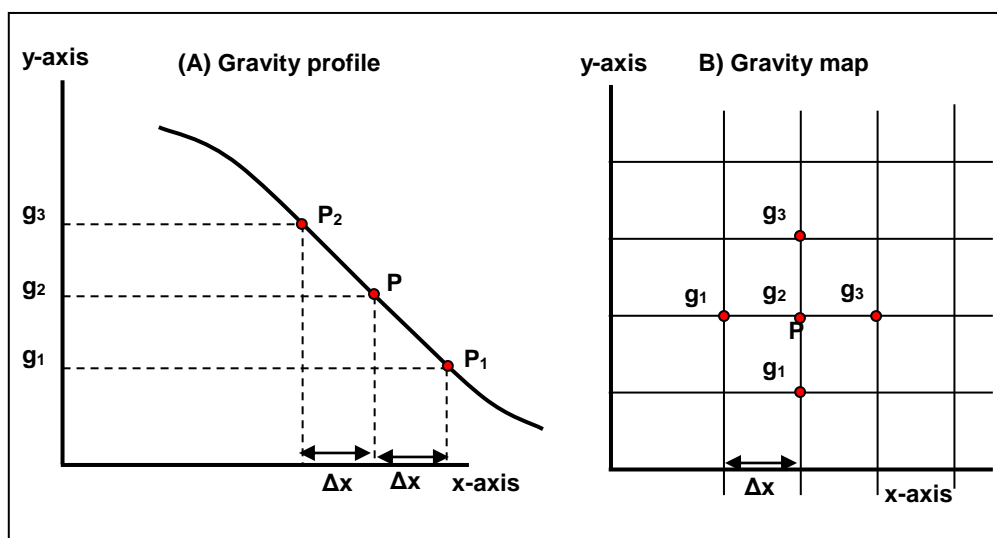
Fig. 9-18 A graphical method used in computing the second derivative of Bouguer gravity in two cases: (a) gravity profile and (b) gravity map

The resolving power of the SVD method in bringing out the local and shallow-type of subsurface structures is greater than that brought about by normal graphical techniques. As it is shown in Fig. 9-19, the residual gravity map (Fig. 9-19, map-C) computed by the SVD method shows more details of the gravity anomaly changes than the anomaly map (Fig. 9-19, map-B) computed by conventional graphic techniques. Both of these maps were assumed to have been derived from the same Bouguer gravity map (Fig. 9-19, map-A).

(v) Wavelength Filtering

As in normal frequency filtering, wavelength filtering is based on Fourier Spectral-analysis theory. According to this theory, a function **f(x)**, such as a gravity profile, can be analyzed into a number of cyclic curves (sinusoids) where each of them has its own wavelength (λ), amplitude (**a**), and phase shift (**p**) which is defined by geophysicists to be the offset of the nearest peak from the start-point of the profile (Fig. 9-20).
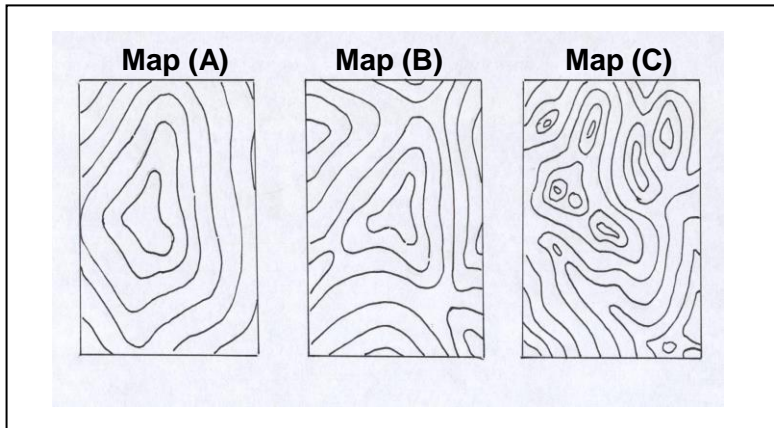
Fig. 9-19 Schematic representation of a hypothetical Bouguer gravity, map (a) , residual gravity computed by a graphical method, map (b) , and residual gravity computed by second derivative method, map (c).
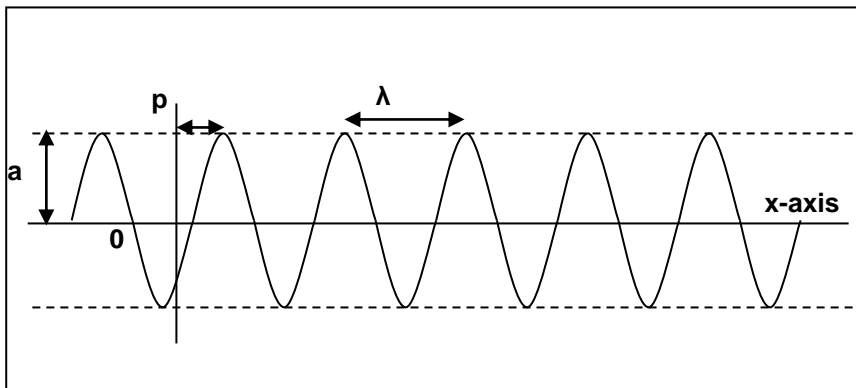
Fig. 9-20 Parameters of a sinusoidal function, $f(x) = a \sin 2\pi(x-p)/\lambda$

By special mathematical integral (Fourier Transform), the given Bouguer gravity function can be transformed into the corresponding wave number domain. In fact, the Bouguer gravity variation, whether it is a profile **g(x)**, or a map **g(x,y)**, can be transformed into the corresponding Fourier spectrum which shows the distribution of gravity value as function of wavelength (or wave-number).

Wavelength filtering is a two-stage process. First the Bouguer data is Fourier transformed into the spectrum domain. In the second stage, a certain wavelength range is deleted (filtered out) from the spectrum image to obtain (by inverse transform) the filtered gravity picture.

By deleting long-wavelength components of the spectrum, we obtain local (residual) anomaly profile (or map). Similarly, the regional anomaly picture is obtained by deleting short-wavelengths. Since the separation effect is not always perfect, several trial parameters of the designed filter are done and, the appropriate result can then be chosen according to the judgment of the interpreter.

9.7. Interpretation Techniques

The end result of a gravity survey (data acquisition and processing) is the Bouguer anomaly which is generally presented as a profile, g(x) or as a contour map g(x,y). As we have previously mentioned, the Bouguer gravity anomaly is created when a lateral change in the density (density contrast) occurs in the sub sea level plane. Since a gravity anomaly represents local (residual) variations superposed on a more extensive (regional) variation, then the separation of these two types of effects is first done, leaving the residual anomaly which is subjected to further analysis techniques for resolving the causing geological-anomaly. The gravity-to-geology transformation processes (i.e. gravity data interpretation) aim mainly at the determination of geometrical shape, location, depth, and mass of the causing anomalous mass. These are the main objectives of the interpretation process.

Gravity data Interpreters normally use two types of interpretation techniques. These are the direct and indirect approaches of interpretation. As explained previously (Fig 10-8), the direct (or forward) approach involves calculating the geophysical response (gravity effect in this case) of a given geological model. The indirect (inversion) approach involves calculating the model parameters (shape, depth, mass, etc.) of a subsurface geological structure that has created the gravity anomaly. Based on these two concepts, interpretation of gravity data may use one or both of the following techniques: Trial-and-Error model analysis approach and Inversion model analysis approach.

9-7-1 Trial-and-Error model analysis

This method involves testing several different models by trial and error until the model which gives a gravity anomaly that best fits the observed anomaly. Here the anomalous body is simulated and its gravity effect is theoretically calculated and compared with that obtained from the actual gravity survey. The model parameters (shape, size, depth and density contrast) are altered several times until the computed gravity anomaly matches the observed anomaly which

is obtained from the survey. The proposed models are usually of simple geometrical shapes which can be of 2D or 3D types. Bodies such as spheres, cylinders, right rectangular prisms, slabs, elongated models of polygonal or circular cross sections are mostly adopted in these computations.

In brief, the trial-and-error model analysis method consists of four steps:

- Definition of the parameters (shape, size, depth and density contrast) of the model

- Computation of the gravity anomaly of the adopted model.

- Comparison of the computed anomaly with the observed anomaly.

- Changing of model parameters to minimize differences between computed and observed anomalies aiming at getting best anomaly matching.

This four-step procedure is iterative, repeated with different model parameters several times until best fit between the observed and the computed anomalies is obtained. Special computer programs are normally used to perform the iteration automatically. Thus, model parameters (including body shape, subsurface location and density contrast) are all allowed to vary within defined limits. The program will automatically alter the parameter values (within the pre-stated limits) producing successively improved resemblance between observed and computed anomalies.

As an example for the application of this method let us assume that the observed gravity profile is represented by the continuous curve shown in Fig. 9-21.

As a first trial, an interpreter may suggest a spherical body (model M_1) buried at depth (Z_1) below sea level. If this model gave a computed profile which indicates that the model should be deeper, then a second deeper model (M_2) at depth (Z_2) is tested. If the computed profile indicated too-deep body then, the model parameters are appropriately changed in the subsequent trials until the computed profile for the model (such as M at depth Z), that fits best the observed anomaly profile, is obtained. In this simple example only one model parameter (burial depth) was tested. In more complicated cases, other parameters (such as geometrical shape and density distribution) may need altering before a final acceptable model is achieved.

It is very important to remember here that this process suffers from ambiguity since a given gravity anomaly could be produced by an infinite number of possible structural models. However, in the process of interpretation using model analysis, the additional geological information will reduce the ambiguity effect.
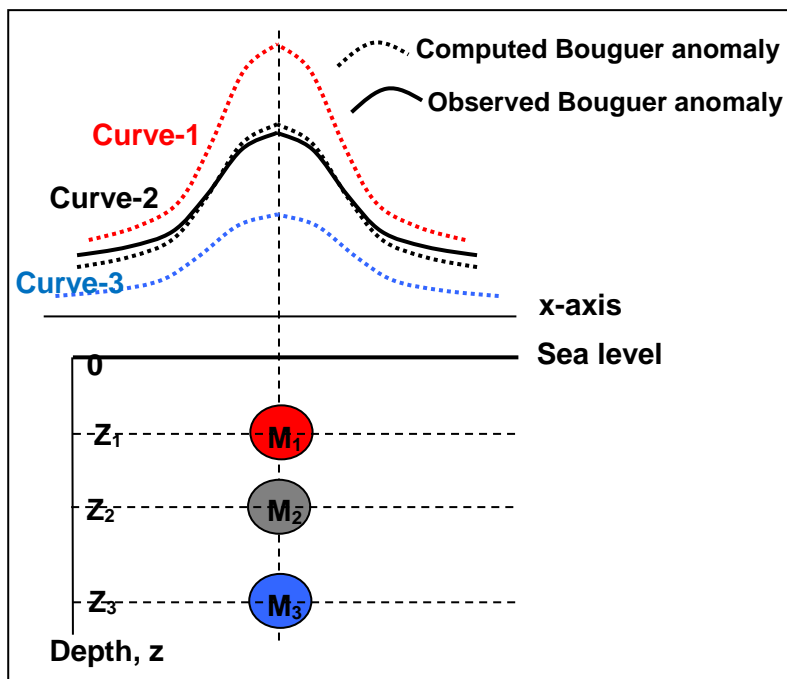
Fig. 9-21 Trial-and-error method applied in gravity interpretation. The model (M_2) at depth (z_2) gave a gravity profile (dotted curve) which is of best match with the observed Bouguer anomaly (continuous curve).

In simple model analysis, the most common simple geometrical shapes used are spheres, cylinders, right rectangular prisms, slabs and sheets. On the other hand, a compound model is made up of a number of bodies having arbitrary shapes. Normally the model (reached at by trial-and-error method) is considered as the final acceptable solution when it gives an anomaly that fits best the observed anomaly.

Sometimes a model of simple geometrical form may furnish the adequate interpretation solution. In other cases where the anomalies are complicated, detailed data of the structural model need to be taken in consideration. In such complicated models, it is more practical to use a compound model that consists of several bodies of arbitrary shapes and densities. Commonly, the adopted models are either compound 2D models made up of several elongated bodies or compound 3D models made up of horizontal polygonal plates. Thus, with additional knowledge (as for example from seismic data and from other geological information) 2D bodies of defined polygonal cross sections, or 3D models made up of a pile of polygonal plates, are used in building up of the proposed compound models (Fig. 9-22). As it is mentioned above, the extent of

success in the interpretation process depends on the amount of additional geological information to be incorporated in the proposed model.
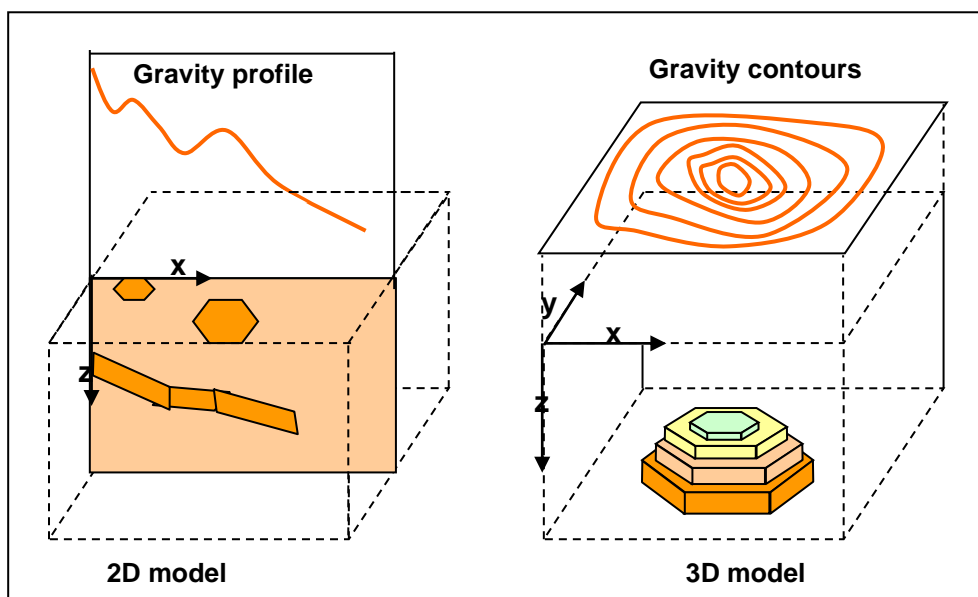
Fig. 9-22 Trial-and-error method of interpretation of gravity anomalies using compound 2D and 3D structural models.

Definitions and derivations of the gravity anomaly (vertical component of the gravitational acceleration) of the most common geological models are presented in chapter 8.

9-7-2 Inversion Model Analysis

The inversion technique is a procedure in which the model parameters are computed from the given observed gravity anomaly. This approach is normally referred to as "inversion" because computation is in the reverse direction to the process of nature where the buried mass creates the gravity anomaly.

The gravity anomaly, expressed as a mathematical function $g(x)$, or $g(x,y)$, carries useful information about the causing anomalous body. The parameters of a gravity profile $g(x)$, normally used to extract such information, are:

- Anomaly maximum amplitude (g_{max})
- Anomaly width (x_w)
- Anomaly horizontal gradient (first derivative, $g`$)

- Anomaly second horizontal derivative (g``)

Using measurements of the parameters (g_{max}, , g`, g`` and x_w) of the gravity anomaly, the inversion method can help to determine the model parameters (like depth or mass) of the anomalous body.

9-7-2-1 Depth Determination

The relation of depth of a body to the amplitude of its gravity profile comes from the fact that gravity value varies with the inverse square of the distance between the source and observation point. Thus, as the body depth increases, its anomaly amplitude decreases and vice versa.

Pioneering work by Bott and Smith (1958, 1959) led to mathematical formulae connecting depth of the body to the parameters of its gravity anomaly (maximum values of amplitude, gradient and second derivative). The depth which is given by these formulae is the maximum depth at which the top of the anomalous body is located. This is also called (the limiting depth) of the anomalous body. The principle is applicable on anomalous bodies whose density contrast with respect to the host material is either entirely positive or entirely negative; a restriction which is normally satisfied in almost all cases met with in the exploration work.

The following depth determination methods are in common use:

(i) Anomaly Width Method

One way of using the anomaly width is the half-width parameter ($x_{1/2}$) which is defined to be the horizontal distance found between the maximum-point of the anomaly and the point at which the gravity is half of its maximum value (Fig. 9-23).

As an example let us consider the anomaly of a point-mass. The gravity profile, **g(x)**, is given by:

$$g(x) = G\, mz\, /\, (\, x^2 + z^2\,)^{3/2}$$
$$g_{max} = G\, m\, /\, z^2$$

Thus at the point where $g(x_{1/2})\, /\, g_{max} = 1/2$, we get the relation:

$$z = (x_{1/2})\, /\, (4^{1/3} - 1)^{1/2} = 1.305\ x_{1/2}$$
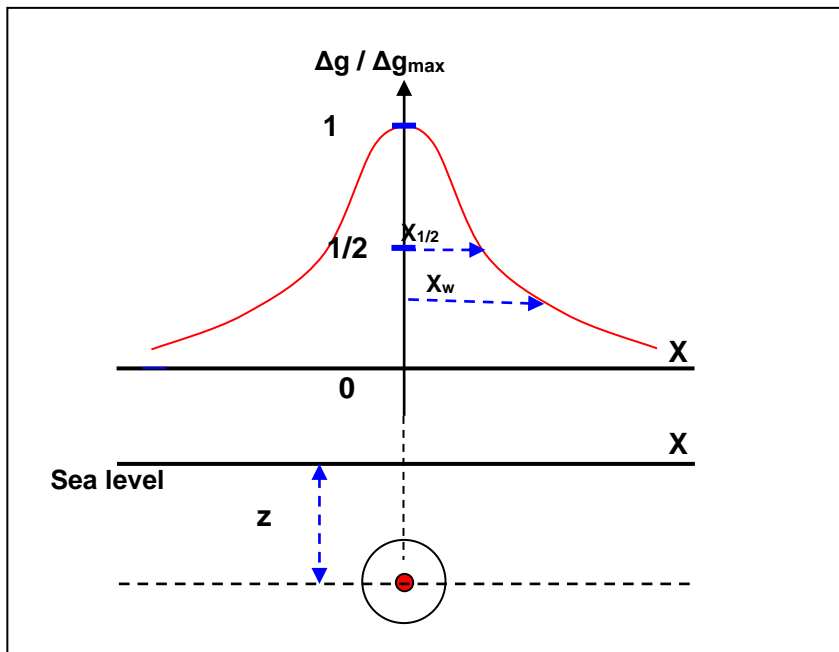
Fig. 9-23 Anomaly parameters used in inversion analysis used in depth estimation.
Δg : Gravity anomaly, Δg_{max} : anomaly maximum value,

In case of a spherical body (which has the same form of anomaly as the point mass), the depth **z** from surface to the top of the spherical body (i.e. limiting depth) is always less than depth to its center. That is:

$$z \leq 1.305 \ x_{1/2}$$

For an anomaly $g(x) = 2G \ \mu \ z \ / \ (\ x^2 + z^2 \ )$ caused by an infinite horizontal line mass, a similar procedure would give the depth (**z**) to be equal to the half-width ($x_{1/2}$). That is:

$$z = x_{1/2}$$

Again when the 2D body is not an idealized line mass, **z** would represent the limiting value of the depth to the top of the 2D body. Hence:

$$z \leq x_{1/2}$$

It should be noted here that by assuming a simple relation between an anomaly arbitrary width (x_w), defined in Fig 10-23, and depth (z) the corresponding value for the $g(x_w)/g_{max}$ ratio can be calculated. Thus for example, by taking $x_w = z$ for the case of a point-mass anomaly, we get :

$$g(x_w) \ / \ g_{max} = z^3 \ / \ (2z^2)^{3/2} = 0.354$$

Thus at the point where $g(x_w)/g_{max} = 0.354$, the depth (z) is equal to the anomaly width (x_w) measured at that point.

(ii) Anomaly Gradient Method

By definition, the gradient (dg/dx) of a function $g(x)$ expresses the rate of change of the function $g(x)$ with respect to the horizontal distance (x). This parameter (also called horizontal gradient, $g`$) of gravity anomaly bears a mathematical relation to depth of the causing anomalous body. By considering the line-mass and point-mass to be representing shapes of a 2D- and spherical 3D-models respectively, it is possible to derive estimates of their limiting depths from the expressions that relate the maximum amplitude of the anomaly (g_{max}) to the maximum value of its gradient ($g`_{max}$).

Taking the case of an infinite horizontal line mass, the gravity anomaly $g(x)$, its gradient $g`(x)$ and second horizontal derivative $g``(x)$ are given by:

$$g(x) = 2G \ \mu \ z \ / \ (\ x^2 + z^2 \ )$$

$$`(x) = -4G \ \mu \ zx \ / \ (\ x^2 + z^2 \ )^2$$

$$g``(x) = -4G \ \mu \ z \ (z^2 - 3x^2) \ / \ (\ x^2 + z^2 \ )^3$$

where the first and second horizontal derivatives $g`(x)$ and $g``(x)$ express the rate of change of anomaly $g(x)$ and gradient $g`(x)$ with respect to horizontal distance (x).

Solving $g`` = 0$ for $x$, we get $z^2 - 3x^2 = 0$, giving $z = \pm x.\sqrt{3}$ which means that the second horizontal derivative ($g``$) is equal to zero at the two points ($x = +z/\sqrt{3}$) and ($x = -z/\sqrt{3}$) and it has a negative sign between these two points and positive sign outside them. This implies that at the two points ($x = \pm z/\sqrt{3}$) the gradient $g`(x)$ attains the maximum value of:

$$g`_{max} = 3\sqrt{3}G \ \mu \ / \ 4z^2$$

and from the anomaly maximum value ($g_{max} = G\ m/z^2$), we can form the ratio:

$$g_{max}\ /\ g`_{max} = 8z/3\sqrt{3} = z\ /\ 0.65.$$

Thus for a 2D body, the limiting depth $[z]_{2D}$ can be computed from the ratio of maximum value of its anomaly (g_{max}) to the maximum value of its gradient ($g`_{max}$). That is:

$$[z]_{2D} \leq 0.65\ g_{max}\ /\ g`_{max}$$

Similar mathematical analysis for the 3D body (approximated by a sphere), gives the following corresponding formula:

$$[z]_{3D} \leq 0.86\ g_{max}\ /\ g`_{max}$$

and for a semi-infinite horizontal sheet, the gravity anomaly (g) and its gradient ($g`$) are given by:

$$g = 2G\rho t\ (\pi\ /\ 2 + \tan^{-1}(x/z)),\quad g_{max} = 2\pi G\rho t$$

$$g` = 2G\rho tz\ /\ (x^2 + z^2),\qquad g`_{max} = 2G\rho t/z$$

From these relations the limiting depth (z) of the sheet is therefore given by:

$$z \leq (1/\pi)\ g_{max}\ /\ g`_{max}$$

Again, by assuming a simple relation (for example, $x_w=z$) between an anomaly arbitrary width (x_w) and depth (z) the ratio $g(x)/g`(x)$ can be used to calculate the limiting depth, thus:

$$[z]_{LINE\ MASS} \leq 1.0\ [g\ /\ g`\ ]$$

$$[z]_{SPHERE} \leq 1.5\ [g\ /\ g`\ ]$$

$$[z]_{SHEET} \leq (2/3\pi)\ [g\ /\ g`\ ]$$

It is worth noting that on comparing the gradient value $g`_{max}$ ( $= G\ \mu.3\sqrt{3}/4\ z^2$) with $g_{max}$ ( $= 2G\ \mu\ /z$), we find that the gradient of the anomaly falls off with depth more rapidly than the anomaly itself by one degree of power. This implies that the gradient ($g`_{max}$) is more sensitive in indicating depth changes than the anomaly (g_{max}) and $g``$ (x) has the effect of getting rid of the constant gradient

(i.e. constant-dip regional) anomaly, since in this case (where **g`** = constant) its derivative is equal to zero.

9-7-2-2 Layer Thickness Determination

By making use of the formula for the infinite horizontal slab, it is possible to calculate a rough estimate of the thickness (**t**) from its gravity anomaly (**g = 2πGρt**):

$$t = g \,/\, 2\pi G\rho$$

Since, in practical application **g** is computed for a defined model which is of restricted and not infinitely extensive model, the calculated thickness is always under estimated.

9-7-2-3 Basin-Shape Determination

In general, a sedimentary basin is characterized by its inward dipping contacts whereas a granite intrusion, for example, has its edges dipping outward. The Bouguer gravity profiles of these types of structures show inflection points where the horizontal second derivative is of maximum value.

The position of inflection points on the gravity profile can be used as an indication guide for discriminating the type of structure of the anomalous body. The inflection points on the gravity anomaly are found near the uppermost part of the anomaly in case of a sedimentary basin and near the lowermost part of the anomaly in the case of a granitic body. Identification of these points becomes easier and clearer on the second horizontal derivative (g``(x)) where the points are located at the maximum values of the g``-profile (Kearey & Brooks, 1987, P. 162).

9-7-2-4 Mass Determination

As in the case of depth determination, the inversion approach can furnish information about the total mass of the anomalous body. Since the gravity anomaly is function of the density contrast (and not of the actual body-density), the mass of the anomalous body, computed from its gravity anomaly, will represent mass contrast rather than actual mass. The mass contrast (normally referred to as excess mass, M_e) is defined to be the difference in mass between the body's actual mass (M_a) of density (ρ_a) and the mass of the host medium of density (ρ_h) filling the same volume occupied by the body. Since, by definition

M_a/ρ_a is equal to $M_e/(\rho_a - \rho_h)$ which is equal to the volume of the anomalous body, the actual mass M_a is computed from the relation:

$$M_a = M_e \cdot \rho_a / (\rho_a - \rho_h)$$

Derivation of the formula used to compute the excess mass (and then the actual mass) from the gravity anomaly is based on Gauss's flux theorem. The flux of a vector field (F) through an elementary area (dS) is defined to be the normal component of the field ($F \cos\theta$) multiplied by the traversed area (dS), and the total flux (Φ) through the whole of a defined area (S) is given by the surface integral:

$$\Phi = \int F \cos\theta \, dS$$

Gauss's flux (or divergence) theorem states that the total flux of a vector field (Φ) through a closed surface is proportional to the total strength of the enclosed field source (Fig 9-24). This relation holds regardless of the surface shape, size, and position of the enclosed field source.
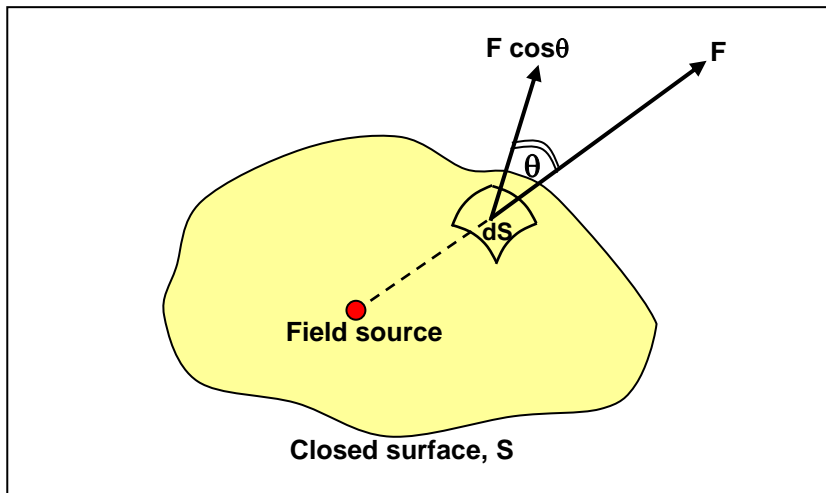
Fig. 9-24 Definition of the flux of a vector field (F) generated by a field source located inside a closed surface (S), Fcosθ is normal to surface.

According to Gauss's theorem, the normal component of the gravity field (g_M) due to an anomalous body of mass (M) located inside a sphere of radius (R) and surface area ($4\pi R^2$), is given by:

$$\int g_M \cdot dS = - (G \, M/R^2) \cdot 4\pi R^2 = - 4\pi G \, M$$

The minus sign indicates that $\mathbf{g_M}$ is in opposite direction to the outward pointing normal. The enclosing spherical surface is taken to be of a radius ($\mathbf{R}$) which is large enough to the extent that allows using the gravity formula for the point-mass model.

To find an estimate of excess mass ($\mathbf{M_e}$) of a 3D-body causing a gravity anomaly $\mathbf{g(x,y)}$, let the body be enclosed by a hemisphere for which the plane ($\mathbf{z=0}$) forms the flat part of its surface. For this model, the value of the surface integral for the hemisphere is half that of the whole sphere, and hence the surface integral of the plane surface (xy-plane) will be given in Fig. 9-25:

$$\int g(x,y) \, dx \, dy = -\, 2\pi G \, M$$

Hence the excess mass ($\mathbf{M_e}$) is given by:

$$M_e = (1 \, / \, 2\pi G) \int g(x,y) \, dx \, dy$$
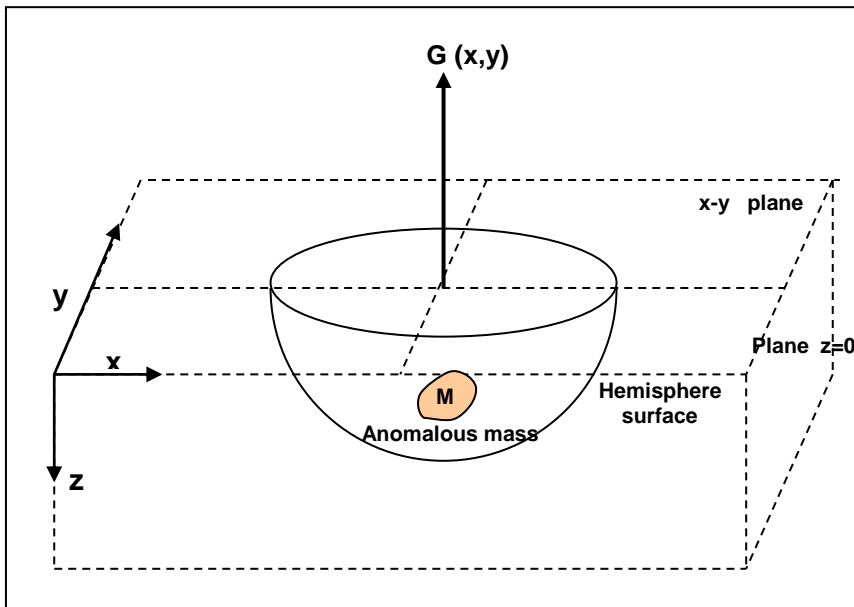
Fig. 9-25 Computation concept of excess mass from gravity anomaly, using Gauss's theorem.

In practice, the integration is replaced by summation over the survey area which is the xy-plane. This involves dividing the area into square cells of area $\mathbf{\Delta S}$ (= $\mathbf{\Delta x \, \Delta y}$) each, and measuring anomaly value ($\mathbf{g_M}$) for each of these squares. The excess mass ($\mathbf{M_e}$) is then computed from the following summation formula:

$$M_e = (1/2\pi G) \; \Sigma \; g_M \; \Delta x \; \Delta y$$

The excess mass (M_e) in metric tons, obtained from the numerical summation, where the residual gravity (g_S) is in milligals and distances (Δx and Δy) are in meters, is given by Telford et al (1990, p 48):

$$M_e = 26.3 \; \Sigma \; g_M \; \Delta x \; \Delta y$$

The actual mass (M_a) is then found from the relation:

$$M_a = M_e \cdot \rho_a / (\rho_a - \rho_h)$$

Since the summation is taken over a finite area, which is not infinite as required by the theorem, the calculated mass is always underestimated.

In applying this formula, the residual anomaly (g_M) must be free from any regional trends or other noises. The advantage of the method is that it is applicable regardless of the shape and position of the enclosed model.

In certain cases where the buried anomalous masses are of simple geometrical shape, there are faster ways of estimating excess masses. These are based on measurements of the maximum value of the gravity anomaly. For a spherical body of excess mass (M_e) at depth (z), for instance, the maximum value of anomaly (g_{max}) is equal to GM_e/z^2 and hence the excess mass (M_e) is given by:

$$M_e = z^2 \; g_{max} / G$$

Where the depth (z) is determined from $g_{max}/g^`_{max}$ ratio as shown above.

For a given density contrast ($\rho_a - \rho_e$), the radius (R) and size of the sphere can be obtained from:

$$M_e = 4\pi R^3 (\rho_a - \rho_e) / 3$$

Chapter 10

CRUSTAL STUDIES AND ISOSTASY

10.1. The Structural Model of the Earth

Earthquake seismology was the principal source of information that led to the discovery of the Earth internal structure. From reflection and refraction seismic waves generated by earthquakes, it is inferred that the Earth is made up of three main zones. These are a central spherical body (the Core) surrounded by a thick solid mantle covered by the surface relatively thin crust (Fig. 10-1).
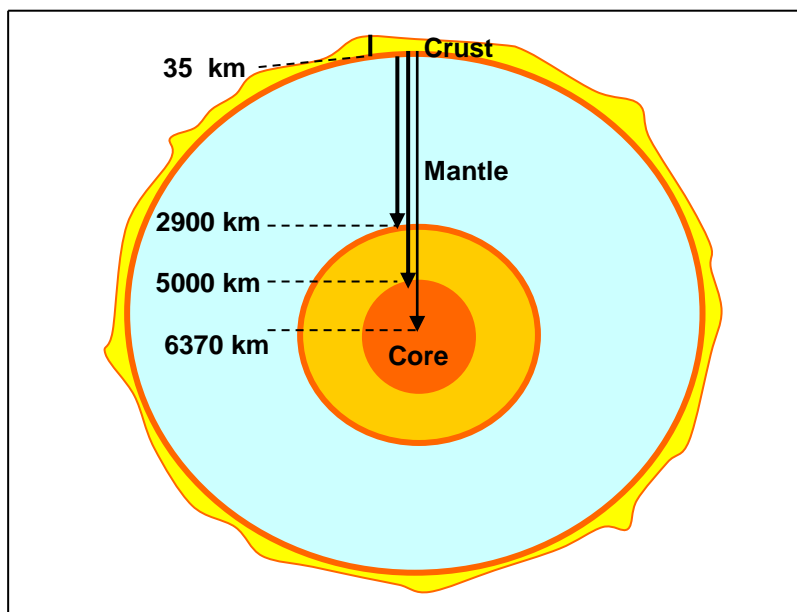
Fig. 10-1 Structural model of the planet earth

The Core is found to be made up of a solid nucleus (the Inner Core) surrounded by a liquid zone called the Outer Core. These zones are separated by discontinuity surfaces. The surface separating the Core from the Mantle is called

Gutentberg Discontinuity and that separating the Mantle from the Crust is called *Mohorovicic*, or just *Moho Discontinuity*.

The Earth zones are characterized by their own physical properties. In particular the mean values of density and seismic propagation velocity have been determined for each zone. Statistics of the densities and velocities are given in the following table.

DISCONTINUITY	EARTH ZONE
	CRUST **Mean thickness 35 km** **Density = 2.7 – 2.9 gm/cc**
(Mohorovicic, 1909)	**MANTLE** **Thickness = 2900 km** **Density = 3.3 – 5.7 gm/cc** **V_P = 8.0 – 13.6 km/sec**
(Gutenberg, 1914) **Depth = 2900 km**	**OUTER CORE** **Thickness = 2100 km** **Density = 10.0 gm/cc** **V_P = 10.3 km/sec**
(Lehman, 1936) **Depth = 5000 km**	**INNER CORE** **Density = 15.0 gm/cc ,** **V_P = 11.2 km/sec**
	EARTH CENTRE **At Depth = 6372 km**

Summary of density and seismic velocity characteristics of the Earth different zones

10.2. The Structural Model of the Crust

From seismological and other geophysical studies, it became apparent that the Earth Crust under continents is of thickness (30-60) km. made up of felsic (SiAl) rocks of density 2.6 - 2.8 gm/cc and mafic (SiMa) rocks of density 2.8-3.0 gm/cc. At the base of the crust there is the Mohorovicic (Moho) discontinuity which separates the crustal rocks from the underlying homogeneous ultra basic (ultramafic) denser rocks of the Mantle whose density exceeds 3.3 gm/cc. The crust beneath the oceans is of thickness 5-10 km and consists mainly of mafic rocks of the SiMa type. The SiAl is believed to be missing under the oceans.

Another important feature of the crustal zone is that it is thicker under the elevated continental land blocks and thinner under oceans. Seismological data (supported by gravity data) indicated that the crustal thickness near coastal areas is about 30 km increasing to about 60 km under mountain ranges (mountain roots) and decreasing to about 5 km below ocean floors (Fig. 10-2).

Anatomy of the Earth Crust

1. Surface rock cover (Sedimentary, Igneous & Metamorphic)
2. SIAL (acidic rocks of granitic type composed of 65% Si + 35% Al, density (2.6-
3. SIMA (basic rocks of basaltic type composed of 50% Si + 50% Al, density (2.8-
4. MANTLE (density (3.3 gm/cc)
5. Mountain Range
6. Continental Platform
7. Continental Shelf
8. Continental Slope
9. Ocean Floor (typically 5 km
10. Oceanic Deep (5-8 km deep)
11. Basement (typically 15 km
12. Conrad discontinuity
13. Moho discontinuity (about 35km below continental platforms and 10 km under ocean
14. Mountain root (Over 60-60 km deep)

Fig. 10-2 Schematic representation of the anatomy of the Earth crust

10.3. Role of Gravity Data in Crustal Studies

In 1735, an expedition headed by Pierre Bouguer was setup by the French Academy of Science to collect information for studying the shape of the Earth. In his studies of the Andes mountain range in Peru, Bouguer noted that the measured gravitational attraction is smaller than that expected from those mountains. More than a century later, Pratt in 1855, working in a plain south of

the Himalayas, found that the observed plumb line deflection angle (5.23 seconds) is less than one-third the theoretical value (15.885 seconds).

Both of Bouguer and Pratt observations have led Airy in 1855 (shortly after Pratt's observation) to the inference that mountain ranges have roots. The mountain material filling the depression of the Moho discontinuity caused by the sinking crustal block represents the mountain root. This ice-berg like model assumes that a mountain (including its root) is composed of relatively low-density material of Sialic type extending down in the denser medium of the Upper Mantle. Seismological information showed that the depth of the Moho under the Alps in South Germany, for instance, increases from 30 km to about 50-60 km in the Central Alps (G. Dohr, 1975, p176).

In correspondence to lateral variations of thickness and density of the Crust, Bouguer gravity is expected to change over the Earth surface. In actuality, Bouguer anomalies are commonly found to be of large and negative values over thick (mountainous) crust, near zero-value over coastal regions, and large and positive over thin (sub oceanic) crust (Fig. 10-3).
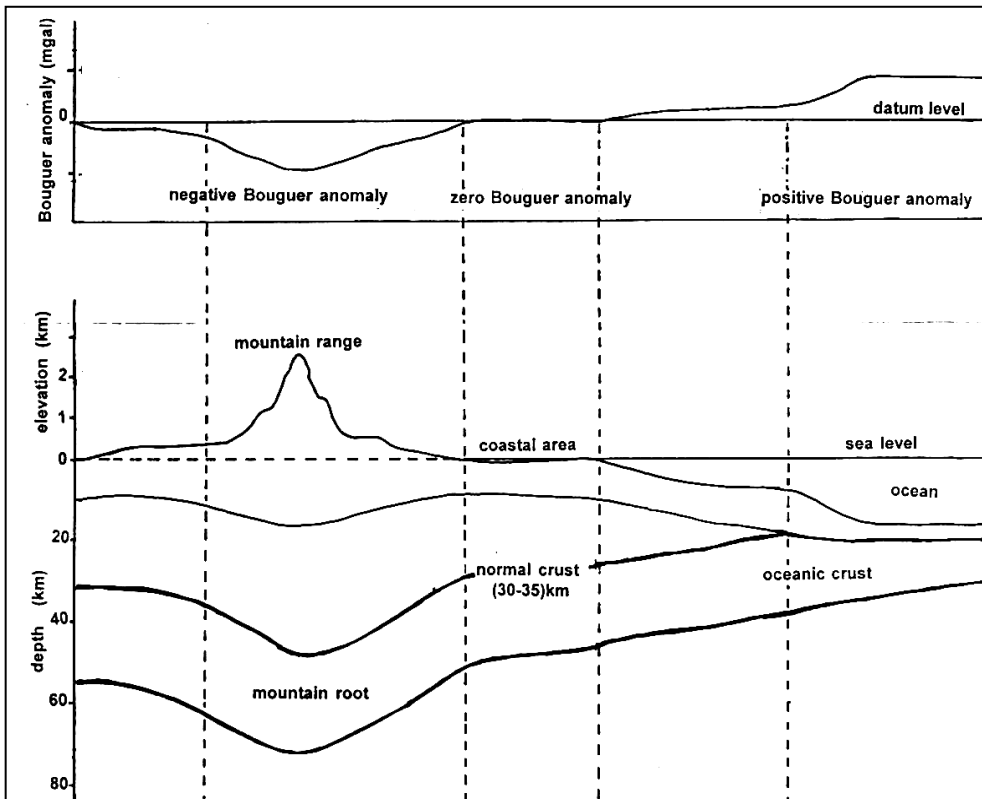
Fig. 10-3 Large-scale variations of Bouguer anomaly due to Earth major structural changes.

The zero value of the Bouguer anomaly found at coastal areas represents gravity effect of a crust having uniform thickness and density. In general terms, deviations from the zero value are due to density changes in the crustal material below the geoid surface. Decrease of the Bouguer anomaly, which is observed in practice, is related to density deficit under elevated areas, whereas the increase is due to density surplus under oceanic crust.

Thus the Bouguer gravity computed at an observation point located over an elevated continental area becomes lower than that found over normal coastal areas where Bouguer anomaly is zero. Similarly, the Bouguer value over an oceanic region where the crust is thin (having greater share of high-density mantle material) becomes larger than the normal coastal crust. This kind of behavior is explained by the fact that, in computation, no allowance is made to the existence of mountain roots and of sub oceanic antiroots. The root model furnished an adequate interpretation for the negative Bouguer gravity anomaly commonly found over elevated continental blocks.

In practice, Bouguer gravity over the normal Earth crust is found to be in the range of -20 to +20 mgal, averaging to about zero over coastal areas. However, over elevated areas where the crustal thickness reaches 60 km, the Bouguer value decreases to less than -200 mgal, whereas over oceans, where the solid part of the crust reaches a thickness of about 5 km, the corresponding value becomes greater than +200 mgal.

10.4. Concept of Isostasy

The term isostasy was introduced by C.E. Dotton in 1889 to describe the phenomenon which expresses the state of hydrostatic balance of the Earth Crust which is resting on the Mantle. According to the isostasy concept, the structural model of the Crust consists of continental blocks "floating" on effectively liquid Mantle-medium and the balancing states of these blocks are governed by block thicknesses and density distribution within them.

For a system of crustal blocks at hydrostatic equilibrium, the exerted cumulative pressure at a point within the mantle is function of the density by height product of the rock column extending from that point to the top of the block. A datum-plane (normally taken at the deepest level of the crustal base where the pressure is constant (isopiestic plane) is called compensation level and its depth below sea level is called depth of compensation (Fig. 10-4).

The equilibrium state (referred to as isostatic equilibrium) is achieved when the crustal blocks are in hydrostatic balance with each other and each block is perfectly compensated by the denser material of the Mantle.
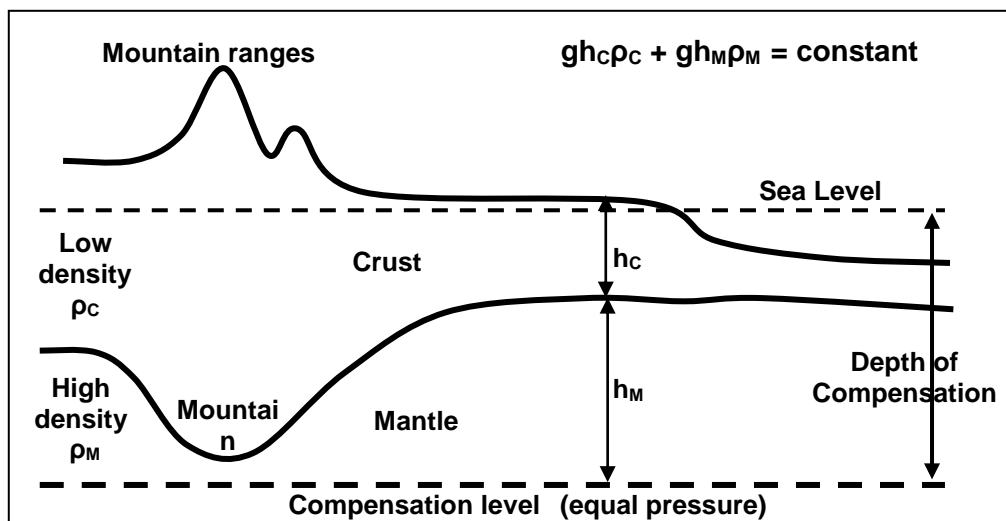
Fig. 10-4 Definition of depth of compensation concept associated with the Earth Crust under hydrostatic equilibrium. At the level of depth of compensation the cumulative pressure ($\sum gh\rho$) is constant .

Deviation from the free float equilibrium conditions occurs when the crustal parts have some elastic strength causing partial support to these parts and consequently leading to incomplete hydrostatic equilibrium. Thus, with the presence of material having elastic strength, topography can be partially supported by the near-by crustal parts leading to the state of incomplete compensation. Conversely, those parts of the crust where compensation is not perfectly achieved (i.e. incomplete isostatic equilibrium) exhibit a state of material under stress conditions.Perfect hydrostatic balance (i.e. full compensation) occurs at those parts of the crust where they effectively have no elastic strength.

10.5. Isostasy-Density Relationship

Since isostasy is based on the condition of hydrostatic balance of crustal blocks, it is therefore mainly governed by the density factor. Strictly speaking, the rise or fall of a certain crustal block under an isostatic effect is dependent upon the density contrast between the moving block and that of the surrounding Mantle medium. In other words, the isostasy phenomenon is governed by mass surplus (high-density) and mass deficiency (low-density) of the Earth crustal blocks resting on the Mantle. Thus, according to the buoyancy principles, the higher the density (ρ) of a crustal block the deeper it will sink into the Mantle (Fig. 10-5).
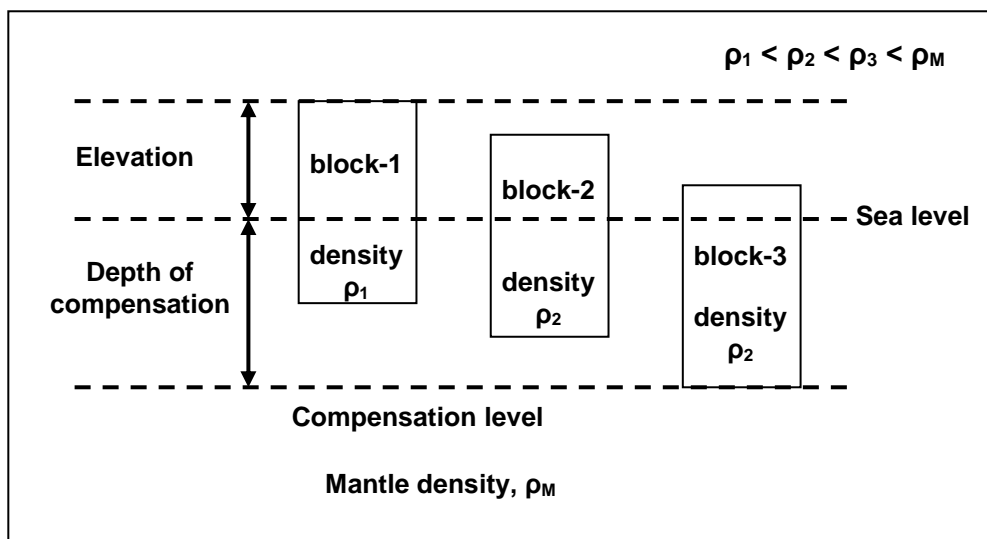
Fig. 10-5 Isostatic sinking movement of crustal blocks as function of density contrast with respect to the Mantle.

The direct relationship between isostatic balancing-state of the different crustal blocks and rock-density distribution within these blocks forms the basis for making the gravitational measurements as the appropriate tool for isostasy investigation.

There are two proposed models concerning density distribution within the isostatically balanced masses of the Earth Crust. These are the Pratt-model (blocks of different densities) and Airy-model (blocks of equal densities). It is worth noting here that gravity data have supported the isostasy phenomenon but cannot differentiate between the two proposed models. Geological and seismological information supports Airy's model more than Pratt's.

10.6. Hypotheses of Isostacy

In the year 1855, two hypotheses for the isostatic models were suggested by two British scientists; the geodesist J. H. Pratt (1809 - 1871) and the astronomer G. B. Airy (1809 - 1892). Both of these hypotheses are based on the "free-float" model where large-scale crustal blocks are assumed to be resting on the lower heavier medium (the earth Mantle). The crustal masses are at hydrostatic balance where the weight of these masses is balanced by the force (created due to the

displaced material below) which is tending to elevate them. The extent of a block-sinking is function of both of the density and thickness of the block.

Basically, the two hypotheses are built upon the floating-block model where by the Earth lithosphere (crustal material) is at a gravitational equilibrium with the heavier rock medium below (asthenosphere). The difference fundamental difference between the two hypotheses is in the density distribution of the moving blocks.

The two hypotheses are briefly described here below:

10.5.1 Pratt's Hypothesis

J. H. Pratt, in 1859, postulated that the upper part of the Earth crust is lighter than that of the supporting lower medium. The proposed model consists of a crust of variable elevation but having constant thickness below sea-level. In other words, depth of compensation is taken to be coincident with a base-level which is common to all of the crustal blocks. At this level (the compensation level), the hydrostatic pressure exerted by the mountain system as well as ocean trenches will be the same. The rock density of the different blocks varies in such a way as to keep hydrostatic pressure constant at the compensation level regardless of the surface elevation (Fig 10-6).

In the oceanic areas, this theory demands higher density of sub-sea rocks to compensate for the lower density of water in those parts of the crust. The mountains, on the other hand, are compensated by density deficiency. This implies that the rock density (ρ) of the whole mountainous block (from surface down to the compensation level) is in inverse proportionality to its surface elevation (**E**). For two blocks of densities (ρ_1 and ρ_2) which are hydrostatically balanced, we can write:

$$\rho_1 (E_1 + D) = \rho_2 (E_2 + D)$$

that is:

$$\rho_1 / \rho_2 = (E_2 + D) / (E_1 + D)$$

This formula says that the outcropping part of a crustal block is inversely proportional to its density. In other words, the higher the elevation (**E**) of the block the lower density (ρ) of its constituent material will be.
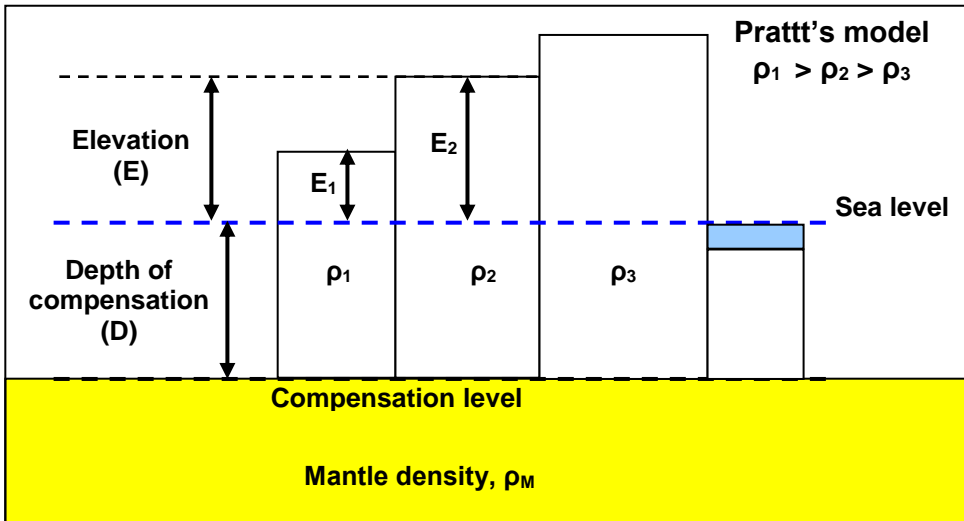
Fig. 10-6 Isostatic equilibrium model according to Pratt's hypothesis

10.5.2 Airy's Hypothesis

From a triangulation survey in India, J. H. Pratt observed in 1855 that the Himalaya Mountains have deflected the plumb line by an angle of 5 seconds instead of 15 seconds as theoretical calculations demanded. Less than two months later, G. B. Airy put a hypothesis to explain Pratt's observation. He suggested the existence of the mountain-root which is formed of material having the same density as that of the outcropping part of the mountain which is floating on a "liquid" substratum of greater density.

Airy's hypothesis states that the Earth crust is a rigid shell floating on the liquid-like Mantle material which is of greater density. Thus, under high mountains, the base of the crust is pushed into the Upper Mantle deeper than that of non-elevated plane-land such as coastal areas (Fig. 10-7).

Depth of compensation is taken to be at the depth of the deepest part in the crust. At this level (the compensation level), the hydrostatic pressure exerted by the mountain system and ocean trenches is constant. Crustal blocks which are under hydrostatic equilibrium, as this hypothesis demands, will give rise to "roots" under mountains and "anti-roots" under oceanic deeps. The amplitude of the mountain root is directly proportional to the mountain elevation. Referring to (Fig. 11-7), we can write (approximating the root-depth by the depth of compensation, D):

$$\rho_C (E + D) = D \rho_M$$

$$D = \rho_C\, E / (\rho_M - \rho_C)$$
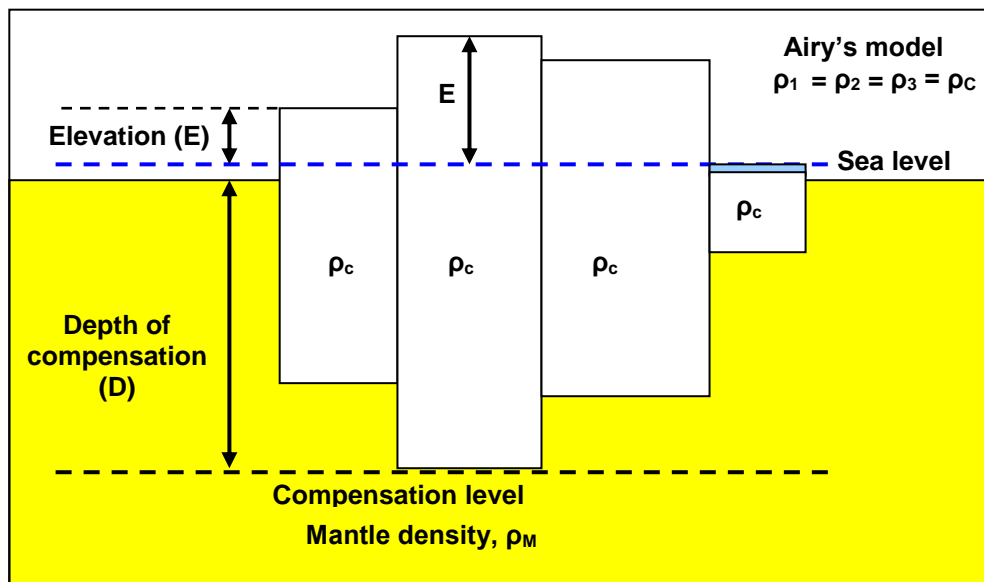
Fig. 10-7 Isostatic equilibrium-model according to Airy's hypothesis

In worldwide calculations, a density of $\rho_C = 2.8$ is used as an average value for the whole Crust and $\rho_M = 3.27$ for the material below the Moho discontinuity (Gutenberg, 1959, p. 50). From the substitution of these values in this equation, it becomes apparent that the depth of a mountain root is about six times greater than the mountain elevation.

It is apparent that Airy's model differs from that of Pratt in the assumption that in Airy's model the rock density of the crustal block is constant while the depth of compensation level below the surface of the crustal block varies in such a way as to bring about the necessary hydrostatic equilibrium.

10.7. Modifications to the Isostatic Models

Both of the two hypotheses have been subjected to modifications. J. H. Hayford (1868-1925) has done modification to Pratt's hypothesis and W. A. Heiskanen (1895-1971) has introduced modifications to Airy's hypothesis. Heiskanen modification of the Airy hypothesis allows some of the balance to be accommodated laterally by the surrounding medium in addition to the vertical buoyancy-created forces.

In the gravitational anomaly studies, an isostatic anomaly depends on the type of the crustal model (Airy's or Pratt's) adopted in the reduction computations.

The problem of how much of isostasy in a given region is a consequence of depth variation (Airy's model) and how much of it is due to density variation (Pratt's model). This subject is extensively discussed by many geophysicists (Gutenberg, 1959, p46-59).

Two main modifications to the original models were introduced for getting more realistic results. These are:

(i) Pratt-Hayford Isostatic System

Hayford (1910) modified the Pratt model by assuming that the depth of compensation to be taken as being measured from the Earth's physical surface and not from the sea level. This implies that the compensation level is not constant but varies with measurement location (Gutenberg, 1959, p49).

(ii) Airy-Heiskanen Isostatic System

Heiskanen (1936) suggested using a crustal model that consists of a number of layers having thickness and density values inferred from other independent sources (as from seismic data). Heiskanen modification to Airy's model allows density to vary compensating 2/3 of the topography with roots. The crustal blocks, due to their finite strength, are not perfectly free floating bodies. The icebergs like mountains have roots which start at sea-level and extend deeply into the Upper Mantle.

Vening Meinesz (1887-1966) suggested that some of the balance is accommodated laterally by the surrounding region rather than being balanced in the vertical direction only. The "radius of regionality" is of the order of 200 km. (Sheriff, 1973, p117).

10.8. The Isostatic Correction

As mentioned, the Earth Crust is, in general, thicker under elevated regions, getting thinner towards coastal areas and under oceans. The lateral variation in thickness and density of the crustal material is one of the prevailing physical characteristics of the crust. The isostatic models for the crust provided evidence

for the large-scale variations in thickness and density like mountain roots and sub oceanic anti-roots as presented above. These changes are supported by the computed Bouguer regional gravity, which is found to be of large and negative values over thick (mountainous) crust, near-zero over coastal regions, and large and positive over thin sub oceanic crust (see Fig 11-3). The explanation for these variations of the Bouguer anomaly is that, in the corrections, no allowance is made for the changes demanded by the isostatic model of the Crust. Thus, to remove the gravity contribution of the isostatic changes, the Bouguer gravity needs to be further corrected for the effect of the isostatic model.

The isostatic correction is defined to be the gravitational effect of lateral density and thickness variations of the major crustal blocks. The computation method depends on the adopted type of the isostatic model; Pratt's, Airy's, or that modified by Heiskanen and Meinesz. In calculating the isostatic correction, the Earth surface surrounding the observation point is divided into zones (as in terrain correction) and the total isostatic correction is obtained by adding up the contributions of the individual zones. To facilitate calculation, tables and maps were compiled to be used for the corrections.

10.9. The Isostatic Anomaly

The isostatic anomaly expresses the gravity value at sea level in which gravity contribution, from all of the material found between observation point and the sea-level, is removed. In addition to that is removing the effect of the isostatic density-model as mountain roots and sub-ocean anti-roots.

Thus the isostatic anomaly is obtained by adding the isostatic correction (**IC**) to the Bouguer anomaly ($\Delta\mathbf{g_B}$). The formal definition of the isostatic anomaly ($\Delta\mathbf{g_I}$) would therefore take the following form:

$$\Delta g_I = \Delta g_B + IC$$

hence,

$$\Delta g_I = g_O + FAC - BC + TC - g_N + IC$$

Where $\mathbf{g_O}$ is the measured gravity, $\mathbf{g_N}$ the Normal gravity, **FAC, BC and TC** are the free-air, Bouguer and Terrain corrections respectively.

10.10. State of Isostatic Compensation

The state of isostatic compensation of the various parts of the earth crust can be inferred from gravity anomalies. Because the root material has lower density than the adjacent Mantle rocks, the gravity effect due to the root body is negative and hence the isostatic correction (**IC**) will be positive. As given above, the isostatic anomaly (Δg_I) is defined as the Bouguer anomaly corrected for the low-density root zone. That is:

$$\Delta g_I = \Delta g_B + IC$$

$$\Delta g_I = \Delta g_{FA} - BC + IC$$

Where Δg_{FA} is the Free-Air anomaly, Δg_B Bouguer anomaly, and **BC** is Bouguer correction.

In general, Bouguer anomalies are negative over elevated parts of the Crust and positive over oceanic areas. These observations confirm that continental topographies and ocean basins are compensated by the deep parts which are of negative and positive density contrasts respectively.

The isostatic anomaly may be negative, zero, or positive, depending on the value of the isostatic correction relative to the computed Bouguer anomaly. These cases can be interpreted as follows (Fig 10-8):
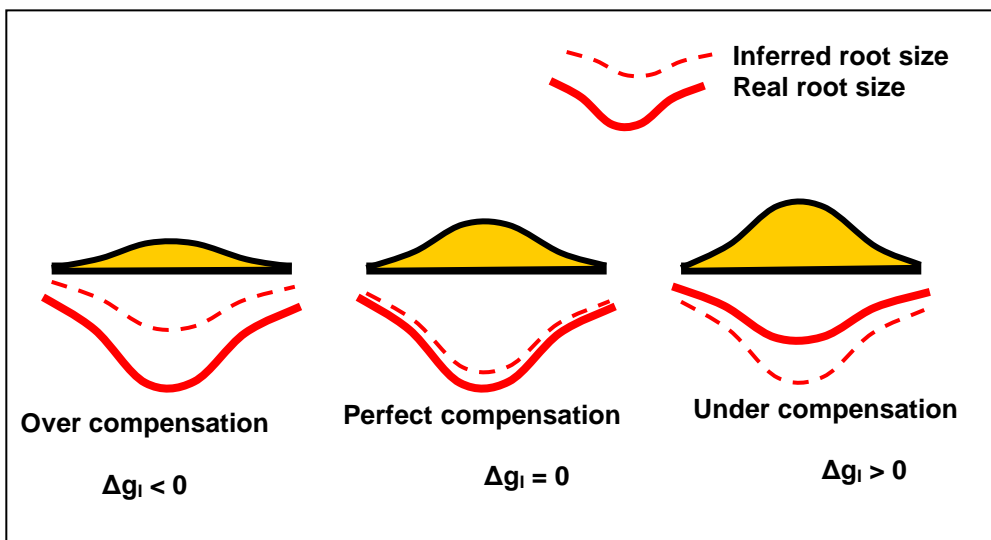
Fig. 10-8 The three types of compensation state

(i) Negative Isostatic Anomaly (case of over compensation)

A negative isostatic anomaly indicates a case of over compensation. This occurs when a land-high is reduced (as by erosion) faster than density-deficiency is readjusted to bring about the necessary condition for regaining the isostatic equilibrium. In this case, the isostatic anomaly suggests a root body which is smaller than the real root size, so, Δg_B, reflecting real root size, is negative and numerically larger than the computed isostatic correction (IC) . Thus, adding the positive anomaly of the smaller-than-real root to the large and negative Bouguer anomaly leaves a negative isostatic anomaly ($\Delta g_I < 0$).

When this is the case, the topographic feature is expected to be rising to regain isostatic balance.

(ii) Zero Isostatic Anomaly (case of perfect compesation)

Zero isostatic anomaly expresses that a topographic feature, such as a mountain range, is in hydrostatic equilibrium with its root zone. In this case, the Bouguer anomaly (Δg_B) and the isostatic correction (IC) are equal in magnitude but opposite in algebraic sign giving zero-value for the isostatic anomaly ($\Delta g_I = 0$).   perfect isostatic compensation.

(iii) Positive Isostatic Anomaly (case of under compensation)

With the case of under compensation state, an elevated topographic feature suggests a root-body which is larger than the real root size. In this case, the Bouguer anomaly (Δg_B) caused by the real root-body, which is smaller than the predicted size, is negative and numerically smaller than the computed isostatic correction (IC).By adding the larger isostatic correction (IC) to the smaller negative Bouguer anomaly () we obtain a positive isostatic anomaly ($\Delta g_I > 0$).

The case of under compensation occurs when an elevated topographic feature is supported wholly or partially by an external force (as the rigidity of the crust) rather than being supported only by the buoyancy effect created by the density-deficiency of the root-zone. If, for any reason, the external force ceased to be effective then that feature is expected to be involved in the sinking process.

It is apparent from the above discussion that determination of the isostatic anomaly depends on the type of assumption (Pratt's- or Airy's-model) adopted for the computation. isostatic anomaly investigations gave stronger support to Airy's hypothesis as they gave results that are supported by seismological

information as regards the crustal structure. In general, the isostatic anomalies are found to be of large negative values reaching -200 mgal along some ocean deeps as in East and West Indies. On the other hand, they are as large as +100 mgal on under-compensated areas as for example, on Cyprus (Dobrin, 1960, p196). In general, the continents are in near-equilibrium giving near-zero isostatic anomalies.

The isostatic anomaly is not usually needed when the interest is focused on small and local anomalies. This is because isostatic anomalies give information on large-scale continental and oceanic features of the earth crust. Thus, it is not needed in geophysical exploration activities oriented to detailed relatively shallow geological structures.

10.11. Deviations from Isostatic Equilibrium

A crustal block is in isostatic equilibrium when it can freely move in a vertical direction under the effect of the Earth gravitational force. The block is considered to be deviating from isostatic equilibrium when it is uplifted or down-pulled by any cause other than the gravitational force. For perfect isostasy we must have a rigid block freely floating over liquid medium. This is not the case in reality since crustal blocks are not perfectly separated masses and the mantle material is not an ideal liquid medium. Deviations from the ideal isostatic equilibrium have been cited in certain parts of the earth crust. Examples of such isostatic deviations are presented here below (paragraph 11.13).

Isostatic gravity anomalies can provide indications on the nature of deviation from the ideal isostatic equilibrium. Thus large-scale elevated regions of the crust which have actual roots (anomalous crustal sagging creating perfect isostatic equilibrium) lead to negative Bouguer anomaly and zero-value isostatic anomaly. Cases where the elevated areas have no roots will give zero Bouguer anomaly and positive isostatic anomaly. If, however, the root is still there after the overburden deposits (elevated topographies) have been removed, both of the Bouguer and isostatic anomalies become negative.

10.12. Testing for Isostatic Equilibrium

To test for the isostatic equilibrium, consider a block of topographic elevation (E) and density (ρ_C), which is having a root of thickness (R). For Airy-type of compensation, we can write:

$$\Delta g_I = \Delta g_{FA} - BC + IC$$

Since,

$$\Delta g_I = \Delta g_B + IC \text{ and } \Delta g_B = \Delta g_{FA} - BC.$$

The root is normally broad compared with its thickness and thus can be considered as a slab as far as computation of its gravity contribution (**IC**). Using this approximation we can write (as in computation of Bouguer correction (**BC**) presented in 8.3.2):

$$IC = 2\pi G (\rho_M - \rho_C) R$$

$$BC = 2\pi G \rho_C E$$

But, from Airy's isostatic model, isostatic equilibrium (see paragraph 10.5.2) the root thickness (**R**) is given by:

$$R = \rho_C E / (\rho_M - \rho_C)$$

hence,

$$\Delta g_I = \Delta g_{FA}$$

The final conclusion is that the isostatic anomaly (Δg_I) of an Airy-type isostatic model (in perfect isostatic equilibrium) is equal to the free-air anomaly (Δg_{FA}). This result furnishes a simple method for testing the state of isostatic equilibrium.

10.13. Isostatic Rebound Phenomenon

Geological processes which are going on throughout the geological history bring about material redistribution in the earth crust. These processes cause upsetting of the isostatic equilibrium among the different parts of the crust. Loaded zones of the crust start to sink and the unloaded zones to rise. This readjustment process leads to a restoration process of the original isostatic equilibrium.

Recovery of isostatic equilibrium after removal of the load is known *as isostatic rebound*. It is controlled by the size and density distribution of the concerned crustal block and the viscosity of the asthenosphere in which the block is sinking. The rate of isostatic rebound movement can therefore provide some assessment of the viscosity of the Upper mantle.

10.14. Examples of Isostatic Deviation

10.13.1 Gulf of Bothnia

The area of the Gulf of Bothnia is a typical example of the rebound phenomenon. During the last Pleistocene ice age, the North European area was under ice load. On melting of the ice, the region was relieved of its load and, in order to restore isostatic balance, began to rise ever since. At the northern shores of the Gulf of Bothnia, the present rate of uplift is 1 cm per year (Fig. 10-9).
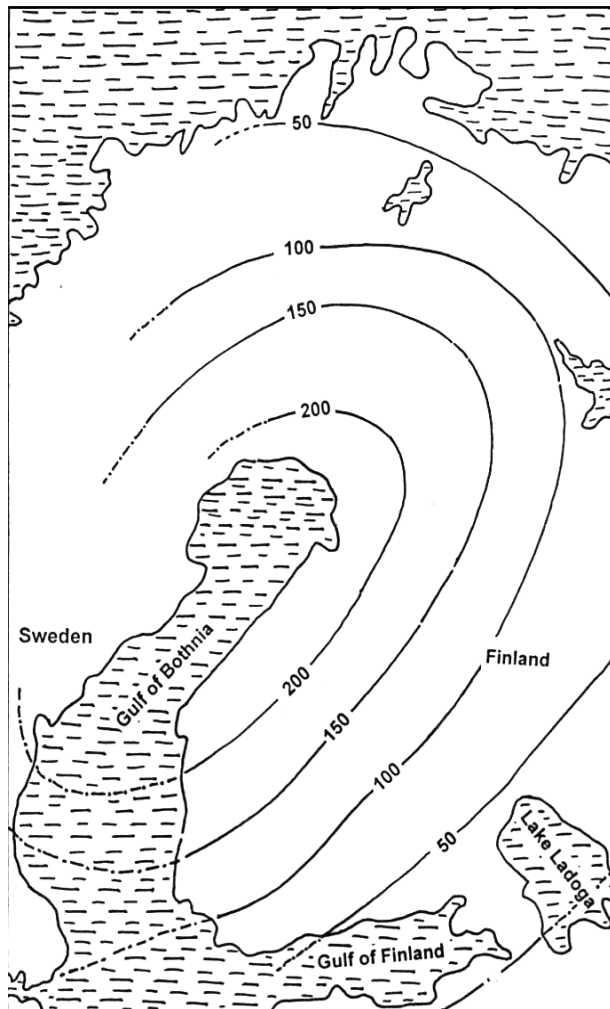
Fig. 10-9 Post glacial uplift of the Gulf of Bothnia region. The contours represent uplift in meters from 6800 B.C. to present time. (Redrawn from Holmes, 1975, p59)

The isostatic anomaly over this area is found to be of negative value reaching about -50 mgal at its centre. As it is explained above, this represents the case of overcompensation which implies that the present size of the root is larger than it is inferred from the elevation of the surface topography. The subsidence caused by the ice-load was accompanied by lateral movement of the sub-crustal material and the ice removal seems to have occurred too fast to an extent whereby the readjustment process was not keeping pace with the ice removal rate.

10.13.2 Rift Valleys

Rift valleys or grabens are tectonic features formed as result of a faulting process creating a long strip of a subsided block bounded by normal faults. The Great Rift Valley of East Africa, the Rhine Graben, the Mid-Atlantic Ridge Rift are typical examples of such large-scale tectonic structures. These are thought to be formed as a result of regional uplift associated with tension and rifting, a process similar to that taking place with uplifted formations pushed by a growing salt dome. The end result is a graben in which the inner sinking block is forming a "root-like" mass-deficiency structure. This model furnishes adequate interpretation for the negative isostatic anomalies normally found over these rift valleys.

The African Rift Valley extends from the Zambezi northwards passing through the Red Sea and the Dead Sea depressions. Across certain parts of this Rift Valley it is found that the isostatic anomaly is of large negative values over the central zone and small positive values over the surrounding rims. This indicates that a density-deficient "root structure" must exist underneath the Rift Valley at those locations (Fig. 10-10).
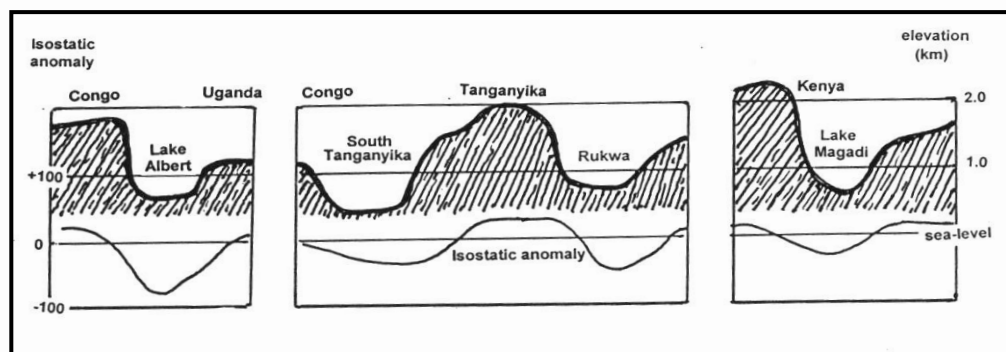
Fig. 10-10 Profiles across four of the African rift valleys with the corresponding gravity isostatic anomalies determined by E. C. Bullard (1936). Redrawn from Fig. 773 in Holmes, 1975. p. 1062.

10.13.3 The Red Sea

Due to ocean floor spreading and crustal separation phenomenon, Arabia is moving away from Africa forming an intervening gap which is the Red Sea structural depression. The Red Sea is considered to be an extension to the African Rift Valley since it is a graben-form depression bounded by normal faults. However it differs from the African Rift in that it shows positive gravity anomaly over its central part. From seismic data it was inferred that the Sialic layer is missing in the zone bellow the Red Sea and it is replaced by intrusive basic rocks which are of a higher density. Thus the presence of such high-density rocks near the surface instead of the lighter Sialic rocks explains the positive isostatic anomaly over the trough of the Red Sea (Fig. 10-11).
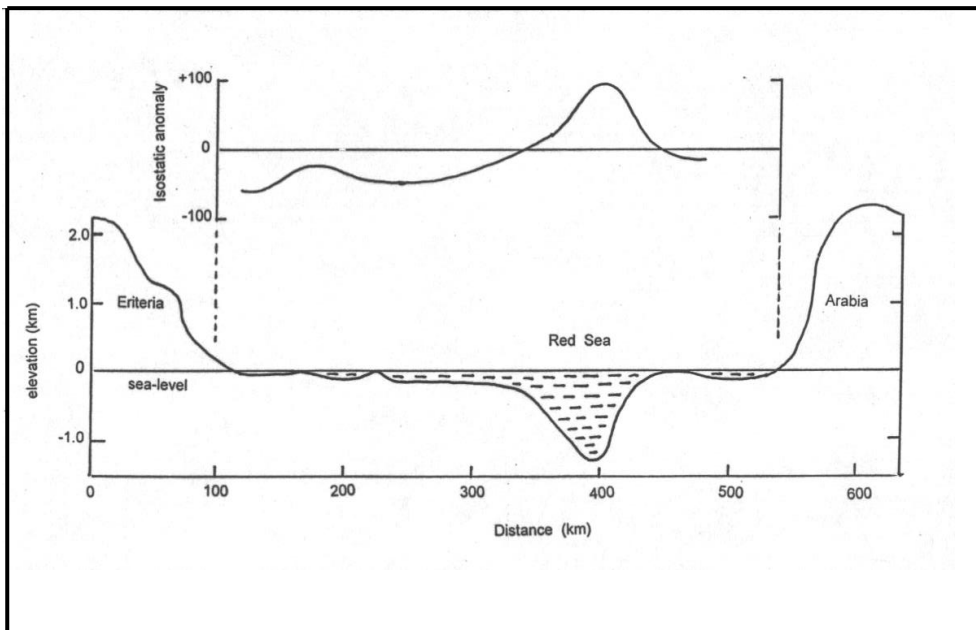
Fig. 10-11 Profile across the Red Sea (near its southern end) with the corresponding gravity isostatic anomaly determined by R. W. Girdler (1958), redrawn from Fig. 787 in Holmes, 1975. p. 1080.

10.13.4 Ocean Deeps and Island Arcs

Large negative isostatic anomalies (less than –200 mgal) are found over a belt that parallels approximately the ocean deeps near the East Indies, Philippines Islands and Aleutian Islands. On both sides of the belts of the large negative anomalies, positive isostatic anomalies are usually observed, especially

on the side facing towards the continents. The amplitudes of these positive anomalies are usually smaller than those of the negative anomaly belts.

10.13.5 Cyprus and Hawaii Islands

Large positive isostatic anomalies are observed over some restricted zones of the earth crust. Examples of such zones are Cyprus (exceeding +150 mgal), portions of Hawaii (exceeding +100 mgal) and Armenia (exceeding +100 mgal). These represent cases of under compensation. This means that these structures have no roots which are evidently supported by the rigidity of the crust rather than being supported by the buoyancy effect.

Chapter 11

GRAVITY EXPLORATION RECENT DEVELOPMENTS

Throughout the 20th century, the classical geophysical exploration methods, including the gravity method, were extensively applied in the search for mineral and hydrocarbon deposits. Geophysical research has led to great progress in instrument technology as well as in the other basic exploration elements. Satellite radar-based positioning technique, computer hardware, and software systems and all other modern supporting technologies (based principally on modern digital electronics) have collectively contributed to the development of the gravity method.

The main developments that occurred in the gravity exploration method were in the airborne gravity, borehole gravity, and in geodetic studies. It is useful to know that satellite-borne instruments cannot measure acceleration while the satellite is in free fall. Satellite-based gravity information can be indirectly inferred from the satellite altitude and its orbit shape.

Here-below, we shall give brief presentation on the basic fundamentals of the airborne gravity and borehole gravity since these have their principal application in the field of petroleum and mineral deposits.

11.1. Airborne Gravity

Airborne gravity measurements (or aerogravity, as it is referred to sometimes) are concerned with measuring the acceleration due to the Earth's force of gravitational attraction by instruments carried by a moving airplane or helicopter. In essence, the aerogravity observation includes measurements of the acceleration vector, location, velocity vector, and altitude of the aircraft.

The main difficulties met with in airborne gravity surveys are introduced by the too large and rapid changes in the measured gravity values caused by the aircraft complex motion. During flight, this may experience a side-way, head-way, and latitude changes. These effects are similar to those found in ship-borne

gravimetry, but with much slower changes. Compensation of these changes is usually done in the processing stage.

Processing of the observational data involves compensation for aircraft vertical motion, gravimeter platform velocity changes, Eotvos effect, free-air, and latitude corrections. Residual random noise can be removed by applying a low-pass filter. The processed data are usually downward continued to the ground surface or to the sea level for interpolation and/or comparison with conventionally recorded gravity data (Dobrin and Savit, 1988, p 556).

11.1.1 Aerogravity Basic Principles

In the stationary type of environment as in the case of land gravity measurements, the measured gravity would be the effective acceleration vector sensed at that position. In the airborne gravity, the sensed gravity is a combination of the Earth gravitational acceleration component, in the direction of the measuring gravimeter-axis, and all acceleration components created from the aircraft motion. In the geophysical literature, these two types of acceleration are usually termed the gravitational and the kinematic accelerations respectively. Due to the aircraft complex motion, two problems need to be solved. These are the gravimeter stabilization and isolation of the gravitational acceleration from that created by the kinematic motion.

Schwartz and Li, (1997) and Wei, (1999) classified airborne gravimetry in general into three types. These are:

- Scalar gravimetry
- Vector gravimetry
- Gravity gradiometry

(i) Scalar gravimetry

In scalar gravimetry, only the magnitude of the gravity vector is determined. One way to accomplished this is with the use of the so-called Strapdown Inertial Navigation System (SINS). This approach, called the Strapdown INS Scalar Gravimetry (SISG) System, is concerned with measuring only the vertical component of the gravity vector.

Another approach is based on the use of a triad of three orthogonal accelerometers from which the gravity magnitude is determined by subtracting the acceleration vector due to the aircraft motion from the measured acceleration

vector. This system is normally referred to as the Rotation Invariant Scalar Gravimetry (RISG) system.

(ii) Vector gravimetry

This type of gravimetry is concerned with determination of the full gravity vector. This is accomplished by using inertial platform system, with which each of the three components; one vertical and two horizontal components (Jekeli and Kwon, 1999).

(iii) Gravity gradiometry

An arrangement of two gravimeters aligned on a common vertical axis can give the vertical gradient of the gravitational field at the measurement location. In airborne gravity gradiometry, the first derivative of the acceleration vertical component (= the second derivative of the gravity potential) is measured. Gravity-gradient measurement is normally evaluated in Eotvos units, where one Eotvos is equal to 10^{-6} mgal/cm.

Gradiometry measuring instruments in common use (like the Falcon gravity gradiometer) proved to be of higher accuracy and resolution compared with the scalar and vector gravimetry, gradiometers. In an actual airborne gravity survey, the flight was conducted along a grid of orthogonal flight-tracks spaced at about 2-5 km apart at an altitude of about (200-500) m above the mean terrain level (Jekeli, 1993).

A comprehensive overview of gravity gradiometry is found in Bell et al, (1997).

11.1.2 Aerogravity Main Objectives

Airborne gravity surveying aims at two main objectives. These are the geodetic and geologic exploration studies of the Earth surface, based on the airborne gravity measurements.

(i) Geodesy (local geod exploration)

The geoid (defined to be the equipotential surface of the gravity field) can be represented by the mean sea level. Airborne gravity data have proved to give highly accurate information on the local geodetic changes.

(i) Geology (regional geologic exploration)

In geophysical studies, airborne gravity is extensively applied in mapping geological changes especially on the large-scale (regional) changes. The gravity maps obtained from aerogravity surveys are compared and tied up with existing conventional gravity data and interpreted to determine subsurface geological structures. Structural and stratigraphic anomalies, with mineral and hydrocarbon contents, can be explored by this fast, accurate, and cost effective technique.

11.1.3 Historical Development of Aerogravity

The first reported test of airborne gravity measurements was conducted in the mid-1950s (Lundberg, 1957), where a system based on gravity gradiometry was applied. Due to lack of the accurate navigation system and insufficient technical control available then to avoid gravity interferences, the airborne gravity, as an exploration tool, did not develop until the 1980s, when the Differential Global Positioning System (GPS) was introduced. Since then, the technique has experienced continuous improvements in both measurement-accuracy and spatial resolution.

The major problems met with in the early experiments of airborne gravity surveying were the aircraft navigation control, and lack of a gravimeter capable of accurate measurements of acceleration changes in a dynamic environment. However it is found that better accuracy is obtainable when using large aircraft smoothly flying at high altitudes.

The tests carried out in the early 1960s were based on gravimeters installed in fixed-wing aircrafts. In those experiments, the gravimeters used were modified sea-gravimeters (developed by LaCoste and Romberg for ship-borne gravity measurments) that use gimbal suspension to handle horizontal acceleration changes. The first successful gravity measurement from a helicopter was performed in 1965. In the following year, a more accurate helicopter-borne test (of about 3 milligal) has been successfully performed. This test has led to the development of a complete helicopter-borne gravity measuring system (HGMS). The main advantages of a helicopter over a fixed-wing aircraft are lower altitude and slower flight which are increase the spatial resolution.

The break-through in the development of the aerogravity as an effective exploration tool came at the end of the 1980s when the DGPS technology was introduced. This highly advanced navigation system helped in accurate measurement location and in developing gravimeter stabilization systems to overcome those turbulences affecting the gravity measurements during flight. One of the first large-scale airborne gravity surveys, with the application of these developments, was conducted over Greenland in 1991 and 1992 by joint cooperation between U.S Naval Research Laboratory and the Danish National Survey. Other examples of such surveys were the airborne gravity surveys of Switzerland in 1992 and over the West Antarctic ice sheet in (1991-1997). After these pioneering works many airborne gravity surveys were conducted with reported accuracies of 1.5-2.0 milligal at 5-6 km spatial resolution. Examples of these surveys are done over Malaysia (2002-2003), Mongolia (2004-2005), Ethiopia (2006-2007), and Taiwan (2007). The information cited above is based on the more detailed account presented by Alberts (2009, p7).

11.1.4 Advantages and Limitations of Airborne Gravimetry

The main advantages of airborne gravity exploration are the following:

(i) Fast exploration tool, as it is possible to cover thousands of line kilometers in few weeks survey-time. It is, therefore, suited for reconnaissance (regional coverage) surveying rather than for detailed local investigations.

(ii) Capable of surveying inaccessible areas and territories which are hard to survey with the conventional measuring tools, such as rugged mountains and iceberg covered areas.

(iii) Providing uniform coverage of the gravity field measurements, where the reading locations are independent of the terrain nature of the survey area.

(iv) Cost-effective exploration-technique in surveying large areas, due to being fast, efficient, and using fully automated field procedure.

Corresponding to these advantages, airborne gravimeter surveys suffer from a number of limitations. The principal limitation of the method is its need for highly sophisticated equipment carried by a fixed-wing airplane or a helicopter. This feature made the use of the technique restricted to a few number of specialized exploration companies. The second important limitation is its relatively low spatial-resolution that makes the technique more suited for large-scale (regional) surveying rather than for detailed (local) geophysical investigations.

11.1.5 Accuracy and Spatial Resolution of Airborne Gravimetry

In the geophysical literature, it is stated that acceleration changes due to aircraft flight disturbances may reach as much as 0.1G (= 100 000 mgal). An airborne gravimeter is required to measure gravity to better than one milligal. In this noisy environment, a sufficiently accurate value for the vertical acceleration is extracted by the appropriate measures taken in the design of the measuring system.

In the early 1980s, measurement accuracy attained in airborne gravity was estimated to be of 5 milligals (Brozena, 1984). With the more modern airborne gravimetry systems, an accuracy of 1-2 milligals, at a 2-km spatial resolution has been attained (Alberts, 2009). Airborne gravity measurements are of accuracy and spatial resolution which are insufficient for detailed mineral exploration. This limitation is believed to stay unresolved hindrance for being applied as a detailed mineral exploration tool (van Kann, 2004).

The attainable resolution depends upon flight speed, survey-line grid, elevation, sampling period, and type of the applied filter. Airborne gravity surveys seem to be controversial; some geophysicists believe that for regional-type surveys, airborne gravity can yield usable results. Others have reported that inconsistent results were obtained when airborne and ground surveys were compared after allowance was made for elevation differences. The magnitude of this error was greater than the internal precision of most airborne gravity systems (Dobrin and Savit, 1988, p 557).

11.1.6 Processing of the Aerogravity Data

In essence, processing of the aerogravity measurement data is to remove all non-gravitational acceleration components from the total gravimeter measurement acceleration. Due to the complex aircraft motion, the computation of the non-gravitational components becomes much more complicated than that involved in the case of the traditional ground gravity surveying data. Especially designed software systems are applied in the data processing.

The Main Corrections

The main corrections done for the gravimeter reading involve subtraction of acceleration components due to aircraft motion, Eotvos correction, tilt correction due to non-level position of the measuring system, and the normal gravity. For the free-air gravity, a term, which is a function of the elevation and geoid

undulation, is added. Finally, the Bouguer anomaly is computed based on the available density model.

Over the survey time, a number of airborne base readings are normally made to construct the gravimeter drift function which is used for the drift correction. A land-based gravimeter, tied to absolute gravity stations, is used to establish the reference gravity values. Certain measures are applied to determine the calibration factor of the measuring accelerometers.

Data Filtering

Airborne gravity measurements are made in very dynamic operation conditions in which high-frequency, large-energy levels are introduced in the readings. Typically, noise-to-signal ratios of 1000 or more can be observed (Schwartz and Li, 1997). In such an environment, resolving of the gravity signal forms a serious problem in aerogravity surveying. To extract the useful gravity signal from such a high-noise record, a low-pass filter is usually applied.

Low-pass filtering forms an important feature of the airborne gravity processing. The main purpose of the filtering is to remove the high frequency gravity noise which is usually present in the gravity measured record, obscuring the gravity anomaly signal. Low-pass filtering forms an important feature of the airborne gravity processing. The main purpose of the filtering is to remove the high frequency gravity noise which is usually present in the gravity measured record, obscuring the gravity anomaly signal.

Modern gravity-data interpretation work is mostly using inverse and forward modeling techniques (Jacobi and Smilde, 2009)

Airborne Gravity versus Land Gravity

Comparison of the airborne gravity data with the traditional land-surface gravity data can give an evaluation measure to aerogravity as a geophysical exploration tool. In general, it is found that a small constant offset-shift is existing between the airborne gravity map and the corresponding ground gravity map. For comparison purposes, this offset is removed by a bulk-shift of the airborne data.

There are two ways to tie airborne- and ground- gravity maps. The simple way is to add the average of the gravity differences found at the grid points to the airborne gravity map, and the other way is to upward continue of the ground

gravity data to the aircraft mean flying level. By subtraction, the mean difference between the two types of survey can be calculated.

To assess the accuracy of airborne gravity surveying, a comparative study is made on an area for which airborne gravity and ground gravity data are available (Elieff, 2003). In this study, a comparison was made between the airborne gravity data with the upward continued ground data, giving a standard deviation of 0.62 mgal (for the differences between air gravity and ground readings) at flight level, in addition to a constant offset-shift of 1.4 mgal between the air- and ground-data.

At present, airborne gravity surveying is claimed to achieve accuracies of about 0.5 mgal with spatial resolution of 2-4 km, and is compared favorably with most ground gravity data sets. The following figure (published by Fugro on its web site) shows the correspondence between the results of traditional ground gravimetry (A), the airborne conventional gravimetry (B), and the airborne gravity gradiometry (C).

Ground Gravimetry
500m to 5km Stations
Difficult Access

Airborne Gravimeter
4km Line Spacing
~ 7km Filter

FALCON AGG
1km Line Spacing
150m Resolution

A
Ground Gravimetry
500 m to 5 km stations

B
Airborne Gravimeter
4 km Line spacing

C
Airborne Gravity
Gradiometry
1 km Line spacing
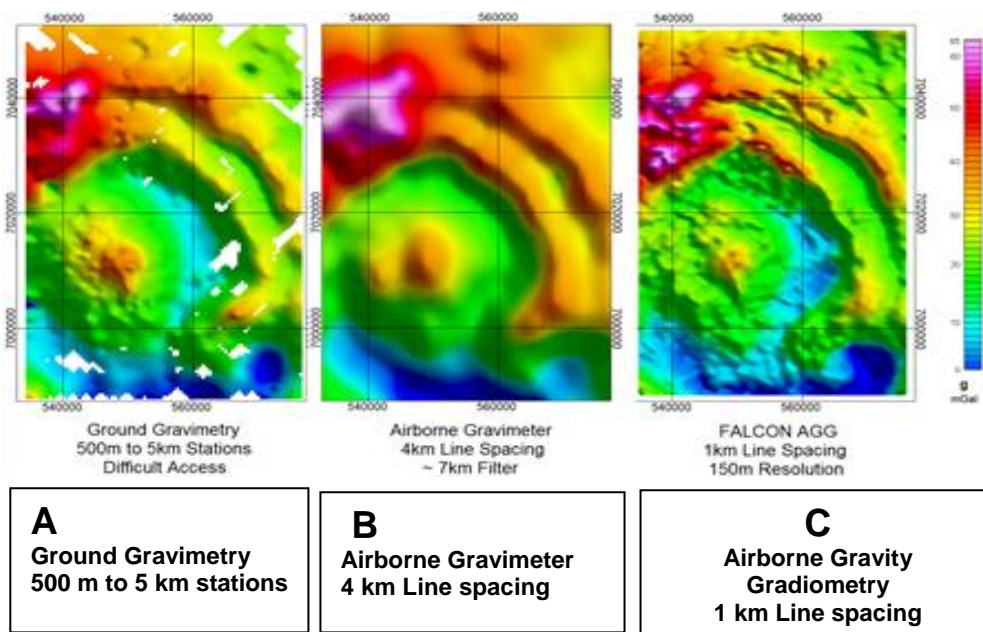
It is clear from this example that the airborne gravity map is in remarkable coincidence with the ground-gravity map. The almost perfectly matching results of the airborne gravity map, compared with that obtained from the standard ground gravity surveying, strongly support the reliability and compatibility of the modern aerogravity. Further, the gradiometry map shows, as expected,

improved resolution-power compared with the airborne and conventional ground gravity measurements.

11.2. Borehole Gravity

Borehole gravity is concerned with measuring the gravity variation down a drilled hole. The measurement instrument is a specially designed gravity logging sonde (the borehole gravity meter, BHGM) which can measure the gravity variation with depth. The BHGM technology, considered to be part of the micro-gravity exploration, was developed by the well known LaCoste & Romberg Inc. into an efficient and reliable geophysical exploration tool capable of detecting changes in density and porosity of geological formations in addition to reservoir monitoring and mapping of structural anomalies such as salt domes and reef deposits.

As early as 1950s, scientific papers were published in the geophysical literature dealing with the borehole gravity in detail, as for example, (Smith, 1950) and (LaFehr, 1983).

11.2.1 Principles of Borehole Gravity

The geophysical principles of this method are based on the direct relationship connecting the gravity changes with the density contrast. The measured change in density is a function of the vertical gradient of gravity. Thus, a density measurement requires measuring gravity at two different depths. Since the expected changes in gravity are very small, the borehole gravity sensor is required to be very sensitive measuring instruments. Accuracy of the produced density values depends on the accuracy of the corresponding gravity and depth readings.

11.2.2 Operational Considerations

The measuring meter is effectively, a very sensitive spring balance which measures changes in gravitational force acting on the mass attached to its spring. Since the sensing mass is constant, the changes are expressing the gravity (acceleration) changes.

Logging operation is similar to the procedure followed in well velocity surveying. The measurement tool is stopped at the planned depth levels at which BHGM readings are taken. The borehole must not be deviating from the vertical

by more than that defined for the measuring system, and the meter, which is well thermostat-controlled, needs to be leveled at each measurement station.

The vertical resolution obtained depends on the discrete depth intervals adopted for the measurements.

11.2.3 Advantages and Disadvantages of Borehole Gravity

The borehole gravity logging is a passive exploration tool, in the sense that it does not require any artificial energy source. Further, the produced gravity log can be directly interpreted in terms of density variation with depth. This logging tool has the merit of being unaffected by the borehole conditions, such as poor cementing, washout, and fluid invasion. The logging process can be carried out in case, as well as in open holes.

With an available gamma-ray log, porosity and nature of pore fluid (gas or liquid), in addition to density variations can be determined.

11.2.4 Scope of Applications

There are two main fields of application of the BHGM logging work. These are the close-up sensing of formation rock density (down-hole density logging) and the remote-sensing of neighboring geological structures. Borehole gravity logs can give useful information on density and porosity variation as well as detection of types of bore fluids and hence contribute to reservoir evaluation studies. Coupled with gamma-ray logging data the technique can give important information on the anomalous geological structures found in the vicinity of the logged section. In this context, structures of sufficiently high density contrast, like salt domes and reef deposits, can be detected by BHGM.

Chapter 12

CASE HISTORY OF GRAVITY SURVEYS

In this chapter, we shall present two actual surveys carried out by the authors. The first one was carried out by Dr. Hamid N. Al-Sadi in the County of Devonshire, England (Al-Sadi, 1967) and other survey was carried out jointly by Zuhair. D. Al-Shaikh and Ezzadin N. Baban in Iraqi territories (Z.D. Al-Shaikh and E.N. Baban, 1991).

(A) GRAVITY SURVEY IN ENGLAND BY AL-SADI, 1967

12.1. Location of the Survey Area

The survey area (8 x 12 mile^2) is located in the extreme North-Western corner of Devonshire in England (Fig. 12-1). The latitude 51° 05' N and the longitude 3° 55' W form the southern and eastern boundaries of the area respectively. The ground elevation lies in the range 900-1000 feet above sea level. There is a gradual decrease in elevation level in the western and South Western direction.

Fig. 12-1 Location map of the survey (North Devon, England)

The survey was carried out in the summer of 1965 using a Warden gravimeter. There was no need for conducting a topographic survey for the survey-area since a large number of station points (bench marks and spot heights of known elevation) exist at an adequate coverage-density throughout the area.

12.2. Geological Structure of the Survey Area

All of the outcropping rocks are of Devonian age, with the oldest rock of the sequence is found on the north coast of the area. The Lower Devonian consists of coarse arenaceous rocks with shaly or slaty beds. The Middle Devonian consists of slates within which there are two 30-foot bands of limestone. The Upper Devonian is dominantly made up of slates and sandstones that include the outcropping Pickwell Down Sandstone member which was mainly investigated in this case-study.

The succession of the Devonian rocks forms parallel tracts striking at bearing of about 285° with an average dip of 35° due south. The axial planes of folds are parallel to that of the synclinorium of which North Devon is part-of. The fold axes are generally pitching 15° - 30° due west.

12.3. The Field-Work

12.3.1 Measurement Instrument

A Worden gravimeter was used in the survey. The instrument is housed in an evacuated chamber (thermo flask) with a built-in temperature-compensating device. Instrument reading is made by observing an illuminated index-fiber through a built-in microscope which is provided with a hair-line eyepiece for viewing the scale changes.

12.3.2 Instrument Calibration

The gravimeter, used in this survey, has been previously calibrated by the instrument makers. The determined calibration factor was (0.4240) mgals/scale division. The instrument was re-calibrated before the start of the survey by taking readings at two points at which the gravity value is accurately known. From dividing the difference in gravity value by the difference in the corresponding dial-readings, the scale factor is obtained. The scale factor 0.4240 mgal/s.d was confirmed by this experiment and thus was adopted in the reduction of readings of this survey.

12.3.3 Instrument Drift

As a first step of the survey, the curve of the drift characteristics of the gravimeter is constructed. As it was explained, the instrumental drift is due mainly to three causes. These are the slow plastic deformation, thermal expansion in the instrument components due to the Earth tidal effect. To determine the drift characteristics, the gravimeter was set up at a location and read at frequent intervals for several hours. The mean drift rate was determined from the established drift-curve and found to be within the range of 0.03-0.04 mgal/hour. These figures serve as guide for giving an idea about the degree of stability of the instrument used in the survey. However, the drift has been accurately computed alongside the survey readings and allowed for gravity value determination be done in the data reduction stage. The established drift curve has shown that the drift is linear over 2-3 hours time-span. This information was made use of in conducting the survey as explained below.

12.3.4 Instrument Set-Up

The slightly concaved tray, on which the gravimeter rests, is placed on the spot where a reading is to be taken. The bull's eye spirit level found at the center of the tray indicates the leveling state of the tray which is firmly placed on the ground. The gravimeter is then placed on the tray and accurately leveled at each station reading.

12.3.5 Instrument Reading

To read the gravimeter, after being properly set-up over its base-tray, the light of the scale dial is switched on and the beam is brought to the null-position using the torsion screw of the instrument. Before taking the reading, the instrument levels are checked and the index beam is viewed again to make sure that it is still in the null position. The reading is then taken to a precision of 0.1 scale-division by reading the verniere scale of the gravimeter after restoration of the illuminated index-fiber to the null position..

12.4. The Base-Station Network

The second step in conducting the gravity survey, after calibration and drift determination of the gravimeter, is the establishment of the base-station network. A base station is defined to be that point which is accurately located within the survey-area, at which the gravity value is precisely known. The base-station serves two purposes; first it is used as a reference point for computing gravity value at other

station-points from reading gravity differences. The second purpose is the determination of drift changes which take place during the survey-work. This is done by taking repeated gravity-readings at the base station at different time-intervals.

12.4.1 Base-Station Network Establishment

In this survey area, eight well-spaced base-stations (B1, B2, …, B8) were established (Fig. 12-2).
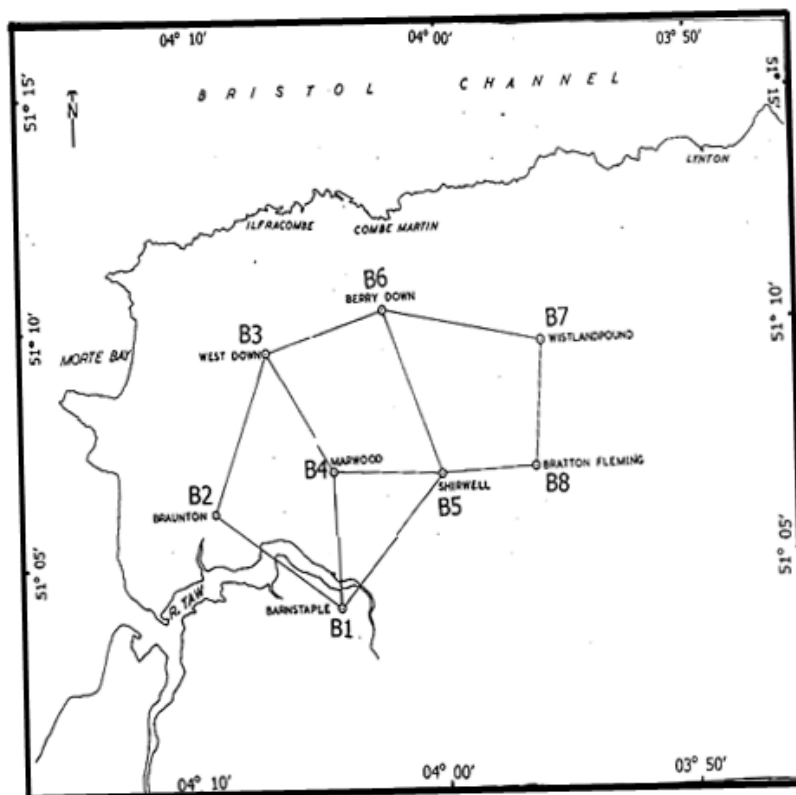
Fig. 12-2 Location map of the base-station network used in the survey. The connecting lines represent the routes along which the base-stations were tied up.

The main base station (B1) at which the absolute gravity value is already known (= 981192.35 mgal) is located near Barnstaple town, whose coordinates are 51° 04' 12" N for its latitude and 04° 04' 24"W for its longitude.

Starting with the reference base station (B1), the second base station (B2) and the rest of the eight base stations are established by taking readings in the following sequence:

B1 ⟶ B2 ⟶ B1 ⟶ B2 ⟶ B3 ⟶ B2 ⟶ B3 ⟶ B4 ⟶

The actual readings (taken on the 26th of June, 1965) are shown in the following table:

Drift curves	Base-station	Gravimeter reading (s.d.)	Time of reading (hour:
Gravity reading			
	B1	544.2	18 : 21
			19: 10
	B2	566.9	
			19 : 28
	B1	544.0	19 : 55
	B2	566.6	

From the drift curve (shown in the first column of this table), the drift value is determined and the true gravity difference between B1 and B2 is found and then after being converted into milligals (using the conversion factor 0.424 mgal/s.d) the gravity value of B2 is determined. Now B2 can be used as a new reference base station in computing another base station such as B3. This procedure is repeated to establish the rest of the base stations (B4, B5, B6, B7, and B8).

12.4.2 Closing-Error Distribution

In this survey, the base stations (B1, B2, B3, B4, B5, B6, B7, & B8) were connected by four loops (compartments). The four closing errors in these loops were determined and found to be -0.11, +0.62, -0.48 and -0.63 scale-division. These

closing errors are distributed among the eight base stations. A simple method of closing-error distribution (explained here-below) is done by assigning an error-variable for each polygon-side and then solving simultaneous equations. The procedure can be explained as follows:

In this survey, we have four compartments (A, B, C, & D). For each free side a variable was assigned. The variable (a) was assigned for the free sides of the first polygon (A), b for the second polygon (B) and so on. For the common sides, assign differences, (a-b) for the side which is common between polygons A & B, (b-c) for the side which is common between polygons B & C, and so on as shown in (Fig. 12-3).
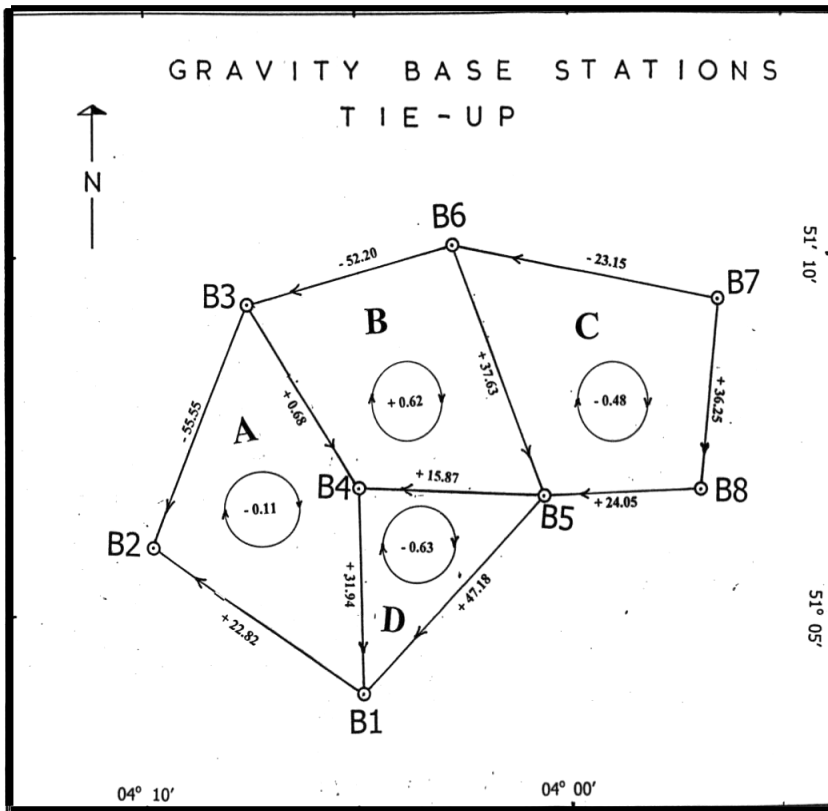
Fig. 12-3 Base-station network (forming four compartments) with the computed closing-error values (a, b, c, d). Arrow direction indicates relative increase in gravity value between base stations.

An equation of each polygon is obtained from equating its closing error to the algebraic sum of the variables of its sides. The following four simultaneous equations are then obtained:

$$4a - b - d = -0.11$$

$$4b - a - c - d = + 0.62$$
$$4c - b = - 0.48$$
$$3d - a - b = - 0.63$$

Solution of this set of equations gives:

$$a = - 0.0657$$
$$b = + 0.0592$$
$$c = - 0.1052$$
$$d = - 0.2122$$

The correction in milligals per each side is thus determined by using the conversion factor (0.424 mgal/s.d.), and reversing the algebraic sign of each of the correction values. Fixing the main base-station (B1) at its given value (981192.35 mgal), the adjusted values of the other seven base-stations are finally determined. The whole process is summarized in the following table:

Polygon side	Original difference (s.d)	Correction (s.d)	Corrected difference (s.d)	Corrected difference (mgal)	Corrected Base-Station gravity (mgal)
B1-B2	+22.82	+0.066	+22.89	+9.71	B1= 981192.35
B2-B3	-55.55	+0.066	-55.48	-23.52	B2= 981202.06
B3-B4	+0.68	+0.125	+0.81	+0.34	B3= 981178.54
B4-B1	+31.94	-0.147	+31.79	+13.48	B4= 981178.88
B3-B6	-52.20	-0.059	-52.26	-22.16	B5= 981172.27
B6-B5	+37.63	-0.164	+37.47	+15.89	B6= 981156.38
B5-B4	+15.87	-0.271	+15.60	+6.61	B7= 981146.61
B5-B1	+47.18	+0.212	+47.39	+20.09	B8= 981162.03
B6-B7	-23.15	+0.105	-23.05	-9.77	
B7-B8	+36.25	+0.105	+36.36	+15.42	
B8-B5	+24.05	+0.105	+24.16	+10.24	

The last column of the above table contains the adjusted gravity values of the base stations used in this survey. The main base station B1 (having gravity value of 981192.35 milligal) was made as reference point to which the other gravity values (B2, B3,…,B8) were corrected. As shown in the above table, the corrected differences read over each of the lines connecting the base-stations were used in the correction process.. This process (called base-station tie-up) furnished eight base stations that are well distributed throughout the area.

To further clarify the correction process let us explain the procedure followed in calculating the closing error in the first compartment (compartment-A) formed by the loop (B1 B2 B3 B4). This is done as follows:

Let the difference between station B1 and station B2 be diff.1, between B2 and B3 to be diff.2, between B3 and B4 to be diff.3, between B4 and B1 to be diff.4. The closing error is then found by summing diff.1 + diff.2 + diff.3 + diff.4 algebraically. In the same way, the closing errors in the rest of the compartments are found and converted into gravity units using the conversion factor (0.424 mgal/s.d).

The closing errors in the four compartments were found to be -0.047, +0.263, -0.204, and -0.267 mgals, giving a mean absolute closing error of 0.195 mgal, and standard deviation of ±0.174 mgals. These residual errors were distributed over the gravity values of the base stations. Fixing the main (reference) base station (B1) at the value of 981192.35 mgal, the adjusted values of the other seven bases became as follows:

Base-Station	Location name	Latitude (N)	Longitude (W)	Adjusted gravity (mgal)
B1	Barnstaple	51° 04' 12"	04° 04' 24"	981 192.35
B2	Braunton	51° 06' 10"	04° 09' 25"	981 202.06
B3	West Down	51° 09' 34"	04° 07' 24"	981 178.53
B4	Marwood	51° 07' 05"	04° 04' 39"	981 178.87
B5	Shirwell	51° 07' 04"	04° 00' 16"	981 172.25
B6	Berry Down	51° 10' 29"	04° 02' 37"	981 156.37
B7	Wistlandpound	51° 09' 50"	03° 56' 19"	981 146.60
B8	Bratton Fleming	51° 07' 11"	03° 56' 35"	981 162.01

12.5. Station Reading

Once the base-station network is established, a systematic field procedure is followed to execute gravity measurements at all station-points in the survey area. The daily work is normally started and ended by taking a reading at a reference base-station. Both of the gravity reading and its reading-time are documented. This process (reading and documenting the gravimeter reading and the time of the reading) is repeated at each of the survey station-point. Readings at the base station are repeated at about two-hour intervals throughout the working day.

Station-points of this survey are not uniformly distributed in the survey area. There was no need to establish a uniform station-grid, since an adequate number of station-points of known x, y, z -coordinates was available over the whole area. The

following table shows a sample data-sheet in which the data set was read and documented on the 23rd of June, 1965.

Station seq. no	Longitude (W)	Latitude (N)	Elevation (Feet)	Time (h-min)	Reading (s.d)	Drift (s.d)	Gravity Reading (drift-corrected)	
							(s.d.)	(mgal)
B4	04° 04' 39"	51° 07' 05"	384.5	14 - 22	503.4	0.0	503.4	178.87
7	04° 02' 11"	51° 08' 54"	826.6	14 - 57	448.4	0.0	448.4	155.55
8	04° 01' 23"	51° 08' 53"	852.0	15 - 12	444.5	0.0	444.5	153.90
9	04° 01' 46"	51° 08' 52"	849.7	15 - 26	444.4	0.0	444.4	153.85
10	04° 01' 30"	51° 08' 51"	804.0	15 - 40	449.5	0.0	449.5	156.02
11	04° 01' 28"	51° 08' 41"	810.0	15 - 54	448.8	0.0	448.8	155.72
12	04° 01' 26"	51° 08' 35"	821.5	16 - 04	446.7	0.0	446.7	154.83
13	04° 01' 14"	51° 08' 26"	756.4	16 - 14	452.7	0.0	452.7	157.37
B4	04° 04' 39"	51° 07' 05"	384.5	16 - 37	503.4	0.0	503.4	178.87
14	04° 01' 07"	51° 08' 09"	723.2	17 - 14	453.9	0.0	453.9	157.88
15	04° 01' 07"	51° 08' 01"	717.0	17 - 31	453.5	0.0	453.5	157.71
16	04° 01' 03"	51° 07' 52"	663.0	17 - 40	460.0	-0.1	459.9	160.43
17	04° 00' 57"	51° 07' 40"	577.5	17 - 55	471.8	-0.1	471.7	165.43
B4	04° 04' 39"	51° 07' 05"	384.5	18 - 27	503.5	-0.1	503.4	178.87

The first column in this table contains the sequence number, and the following three columns contain the x y z coordinates of the station points. Columns 5 and 6 are assigned for time and gravimeter-readings respectively. The rest of the columns contain the data-reduction results, where the last column shows the final drift-corrected gravity value in milligals. Conversion to milligals is achieved through multiplication by the scaling factor (0.4240 mgal/s.d).

12.6. Reduction of Field-Data

Data reduction (Data processing) of field data involves a sequence of corrections applied to reduce the field-data to the final Bouguer gravity values. To achieve this objective, the following corrections were applied:

(i) Drift Application and Reading Conversion

The instrumental drift is determined from the repeated readings made at the concerned base-station over time-spans which, in this survey, were about two hours. Readings, after being corrected for drift, were then converted into milligals using the instrument calibration factor which was 0.424 milligals/scale division.

(ii) Latitude Correction

This correction removes the gravity change (systematic increase in equator-to-poles direction) due to flattening and rotation of the Earth. In this survey, the correction is done by measuring the latitude of each observation point to the nearest second and the corresponding theoretical gravity value (as given by the International Formula) was read, and then subtracted from the observed gravity for each station of the survey. It is be noted that the whole survey area is located between latitudes 51° 05` 44`` N and 51° 12` 32`` N.

(iii) Combined Elevation Correction

This includes the combined effect for the Free-Air and Bouguer corrections. The formula for the combined elevation correction (CEC) is given by:

CEC = 0.09406 - 0.01276 * density   milligal/foot

In this survey, the density value used for the Bouguer correction was 2.7 gm/cc. With this value, the combined correction was found to be of 0.05961 milligals per foot of station elevation.

(iv) Terrain Correction

Both hills above a station-level and valleys below have positive terrain-corrections on the gravity value at that station. The correction per each station was calculated by a computer program (Bott, 1959). The input data consists of location-coordinates, elevations of station-points, mean density and relief information of the area. The input data for the correction included areas that extend beyond limits of the survey area in order to insure adequate correction for those stations located on the outer fringes. Thus, the survey area was subdivided into (1km x 1km) squares forming a total of 768 squares). In addition, a surrounding 8 km-wide strip was included in the computation and was subdivided into (4km x 4km) squares (total of 72) and a second strip immediately beyond this of about the same width was also divided into 8km x 8km squares. The average elevation of the topography in each square (1x1, 4x4, and 8x8 dimensions) was manually estimated. The value (2.70 gm/cc) was used for the mean rock density.

By carrying these corrections, the gravimeter reading at each station in the survey area was reduced to give the final Bouguer gravity anomaly in milligals. These values are then posted on the base map of the area and finally presented as a contour map (Fig. 12-4) ready for the next phase of the project which is the interpretation process.
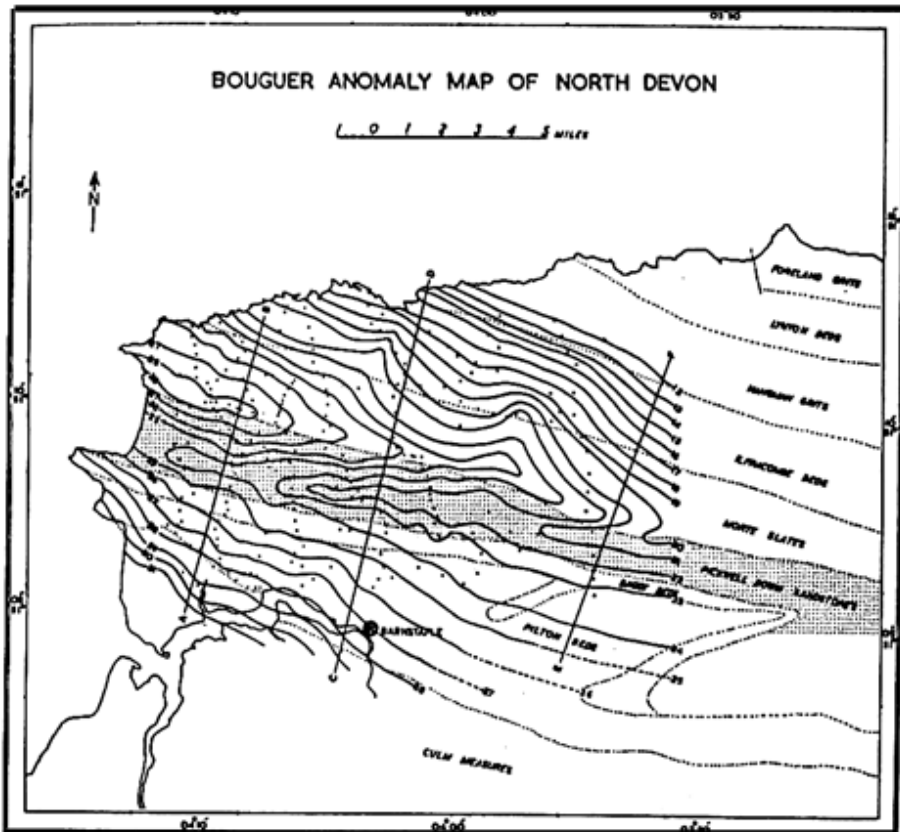
Fig. 12-4 Bouguer anomaly map of North Devon-England, drawn at one-milligal
contour intervals (Al-Sadi, 1967).

12.7. Interpretation

Interpretation of the final Bouguer gravity map forms the ultimate aim of any
gravity survey project. In short, this phase of the survey gives the geological
structural model which is nearest to the realistic picture of the subsurface geology of
the area. The input data to the interpretation process is the Bouguer anomaly map
(shown in Fig 12-4) which was drawn at one-milligal intervals.

There are two types of approach for interpretation. These are qualitative and
quantitative approaches. After a descriptive approach and trying to associate the
main apparent changes with the available geological knowledge of the area, a more
deterministic approach is followed. This includes computations of the regional and
residual gravity then gravity-to-geology translation using model-analysis technique.

(i) Qualitative Approach

A visual inspection of this map revealed that the anomalies show a fairly constant strike, which follows the trend of the Devonian outcrop very closely. In addition, there exists a central region of anomaly disturbance. In general, the gravity values are noted to be falling in a northerly direction. The Bouguer contour map (Fig 12-4) reveals a remarkable resemblance between the gravity picture and that of the known geological structure of the area. In particular there is a close coincidence between the central gravity-low and the outcrop of one of the Upper-Devonian sedimentary members (the Pickwell Down Sandstone).

(ii) Quantitative Approach

Based on the general contour appearance and on the known geological structure of the area, the gravity map was considered as being reflecting a two-dimensional geological model consisting of parallel rock-layers dipping in a southerly direction. For this reason, interpretation was based on drawing gravity-profiles perpendicular to strike of the geological layers. To simplify the quantitative interpretation, regional and residual anomalies are determined for the derived profiles rather than for the whole contour map.

The Regional Gravity Anomaly

Due to the simplicity of the Bouguer gravity map, a manual method was used in establishing the regional anomaly. Based on the analysis of ten profiles taken at right angles to the general trend, it was found that the mean regional gradient is 1.2 ± 0.20 mgals per mile. With this gradient the regional gravity is generally decreasing in a northerly direction which was found to be in close agreement with the assumption of thickening of the Carboniferous sediments which is separated from the outcropping Devonian rocks by an assumed thrust zone. For a density contrast of -0.15 gm/cc, these sediments must reach a thickness of about 3 miles at the northern coast of Devon to account for the 30-milligal gravity change over the area.

The Residual Gravity Anomaly

The separated residual-anomaly profiles were subjected to model analysis. These analyses have shown that they are caused by the dipping belt of sandstone (the Pickwell Down Sandstone) and that the dip angle of the formation decreases with depth. At a depth of about two miles, the formation becomes nearly horizontal. Alternatively, it may terminate against an assumed thrust plane underlying the whole Devonian beds. A typical profile is shown in Fig. 12-5.
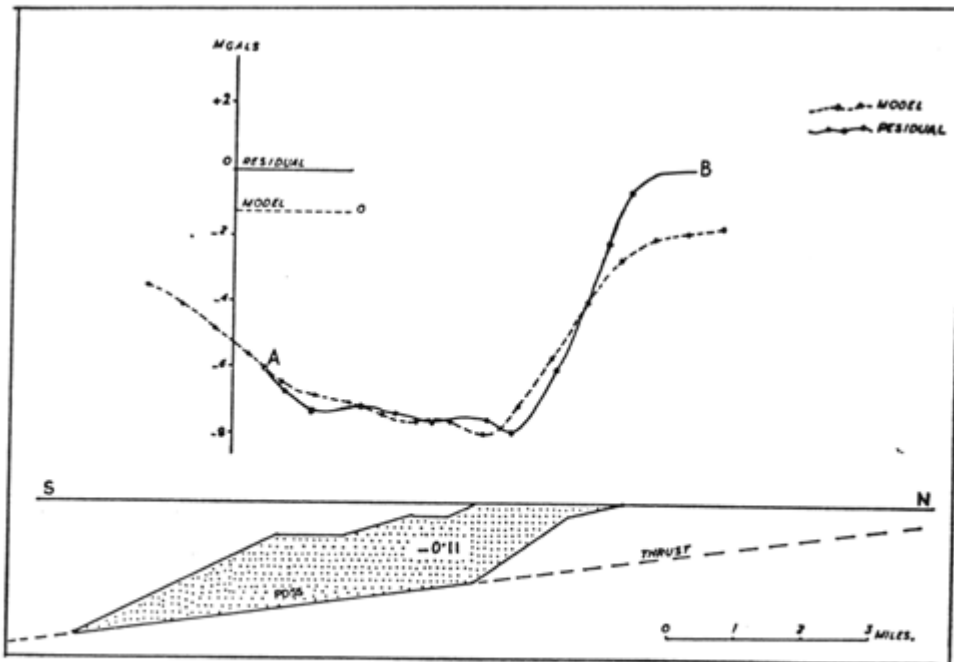
Fig. 12-5 Gravity profile (A-B) compared with the calculated anomaly for a theoretical model based on the thrust hypothesis model analysis.

POSSIBLE TRIASSIC FOLDING BELOW ABU RASSAIN, THE WESTERN DESERT, IRAQ

12.8. INTRODUCTION

The area of study is situated in the west of Iraq, a few kilometers to the west of the town of Hatra (Fig.12.6). It is a flat lying country except for sporadic hills such as Kurat Tayarat.The area as a whole has a regional inclination towards the east and northeast.

The surface geology is made up of Middle Miocene Lower Fars Formation (cycles of clay, marl, limestone and gypsum) followed by the Upper Miocene Upper Fars (sandstone, siltstone and clays). The well Khleisia-1(Kh-1) (35^0 20' northing, $41^0$44' easting) gives the thickness of the L. Fars to be 550m while that of the U.Fars 200m. The deeper geological information is obtained from Kh-1 which penetrates the succession to the Ordovician at a depth of3731.7m. Two other deep wells are also used, namely Tel Hajar-I to the north (36^0 06' northing $41^0$39' easting), which penetrates to the Upper Triassic, and Ana-2 to the south (34° 22' northing, $41^0$28' easting), which penetrates to the Lower Jurassic. Correlating the various successions between these wells shows that the Silurian is missing at Kh-1 due to uplift and erosion during the late Ordovician and early Devonian. The succession from the Upper Carboniferous to the Middle Triassic is also missing due probably to the Hercynian orogeny. Kh-1 and Ana-2 show, furthermore, that the succession from the Middle Jurassic up to the Upper Cretaceous is missing because of the uplifting during the Kimmerian orogeny. The Alpine movement has also caused the removal of the Palaeocene to the Middle Eocene in the area.

 Tectonically, the area lies within the Hatra Uplift which belongs to the near platform flank of the foredeep (Ditmar,1971). It has been subjected to successive uplifting during different periods of its geological evolution. On the surface, only few local anticlines exist among which Tayarat anticline is prominent in the southwest of the area. It forms elongated hills stretching in a NE-SW direction for some 20 kms.

Previously, the area was covered by gravity survey (Sayyab *et. al.,* 1968) and by aeromagnetic survey in 1978. Mohammed (1981) has studied a detailed seismic reflection survey over the area and produced a topographical map of the basement and an isopach map of the Lower Paleozoic rocks.
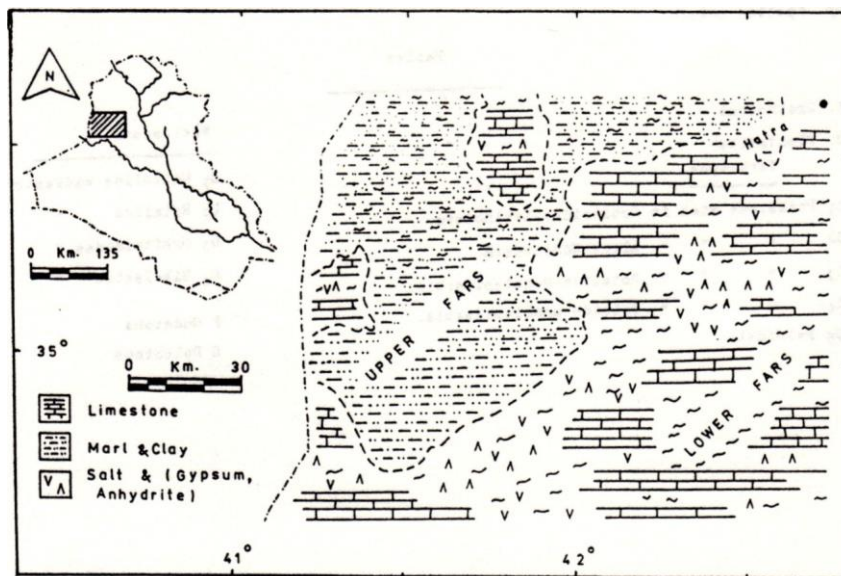
Fig. 12.6 Location and Geological maps of the area.

In the following analysis, gravity features of local nature observed on the gravity map will be concentrated upon.

12.9. PROCEDURE

The Bouguer anomaly map was prepared by Iraqi Petroleum Company (IPC) with 1:200000 scale and a contour interval of one milligal is used (Fig. 2). It is dominated by a large oval positive anomaly occurring in the middle of the area. It has a sharp northern gradient with the well Kh-1lying in the middle of it. The southern and eastern gradients are gentler. Its westerly extensions believed to run to considerable distance into the Syrian territory Superimposed on this main anomaly are sharp anomalies of various shapes and dimensions. One important anomaly of these is the elongated one which extends from the town of Hatra to the southwest for a considerable distance. Other local disturbances can also be seen.

To separate out local anomalies from the regional ones, smoothing procedure is used. The smoothing procedure is carried out by profiles. Two sets of profiles east-west and north-south) are taken on the map of Fig. 2. Smoothing regional field is assumed for each profile. The intersection points serve as control over the regional field taken. Using this procedure the smooth regional map of Fig. 3 is produced. It shows the oval gravity "high" in the middle having a sharp gradient (reaching 0.6 rngal/km) toward the north. It has a maximum amplitude of 20 mgal and a half-

width of 47 km. Subtracting the regional field of Fig. 3 from the observed field of Fig. 2, the residual map is produced, Fig. 4.

12.10. INTERPRETATION

Fig. 4 shows a number of local anomalies of which the anomaly (I), referred to here as Abu Rassain anomaly, is the most prominent. It is a positive, elongated anomaly lying within the Khleisia graben (Ditmar, 1971). It stretches for more than 60 km in a NE-SW direction. It has maximum amplitude of 3 mgal and an average" half-width of 11 km. Ditmar's evidence for the graben is apparently the linear irregularities of the contours (Fig. 12-7) which stretch from Hatra southwestwards. However, no deep origin (e.g. within basement) for this linearity is observed on the seismic reflection records (Mohammed, 1981).
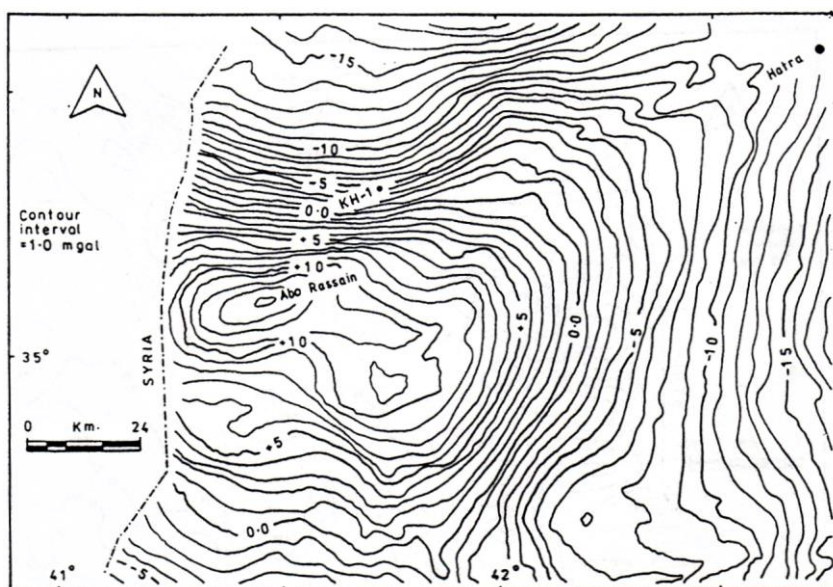
Fig. 12-7 Bouguer anomaly map of the area.

To the northeast of Abu Rassain anomaly occurs another large, three-dimensional one (III) referred to here as Abu Jurd anomaly. It is positive with maximum amplitude of 2.4mgal and an average half-width of 13 km. Other local anomalies such as anomaly (IV) in the south and anomaly II near the town of Hatra are also apparent. Only Abu Rassian and Abu Jurd anomalies are, however, considered here for further interpretation.
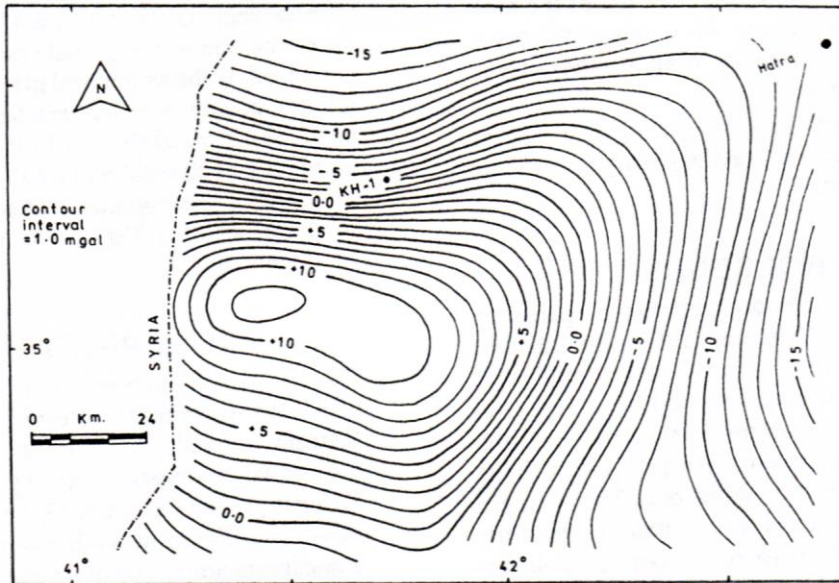
Fig. 12-8 Regional anomaly map of the area.

To locate the source of these anomalies, a density contrast within the succession of the wells referred to above is Kh-1 well which shows that an unconformity surface exists on top of the Upper Triassic, so that the succession involving rocks from the Middle Jurassic up to the Middle Cretaceous is missing. It is possible that even the Lower Jurassic may be missing below the positive anomalies as the well Kh-1 occurs only on the side of the anomaly and not at its culmination (see Fig. 12-7). No information is available regarding direct and detailed density measurements of the rocks involved in the western desert. However, Ditmar (1971) gave the average density of the systems of the geological column in the western desert as follows:

System	Average density (gm.cm^{-3})
Middle & Lower Miocene	2.64
Palaeogene - Middle Cretaceous	2.46
Lower Cretaceous	2.61
Jurassic-Upper Triassic	2.71
Middle Triassic-Cambrian	2.62

If this table is considered for a density boundary, it can be seen that such a boundary occurs between the Jurassic and the Cretaceous. A value of the density contrast of 0.18 gm.cm^{-3} seems to exist between the Jurassic and the lower succession on one side and the upper succession on the other. This contrast is similar to that used by Mohammed (1981) to interpret the local anomalies in the

southwestern desert and is near enough the value used by Abass *et. al.,* (1982) who used 0.2 gm.cm^{-3} to interpret anomalies in the Hit-Shthatha area, the western desert. Furthermore, referring to Fig.12-7 and noting the position of Kh-1 which shows only a small thickness of L. Jurassic, it is believed that these rocks may further be removed on top of the structure below the anomaly maximum. Therefore, a contrast of 0.18 gm.cm^{-3} is considered representative for the difference between the Triassic (Kurra Chine Formation) and the later succession.
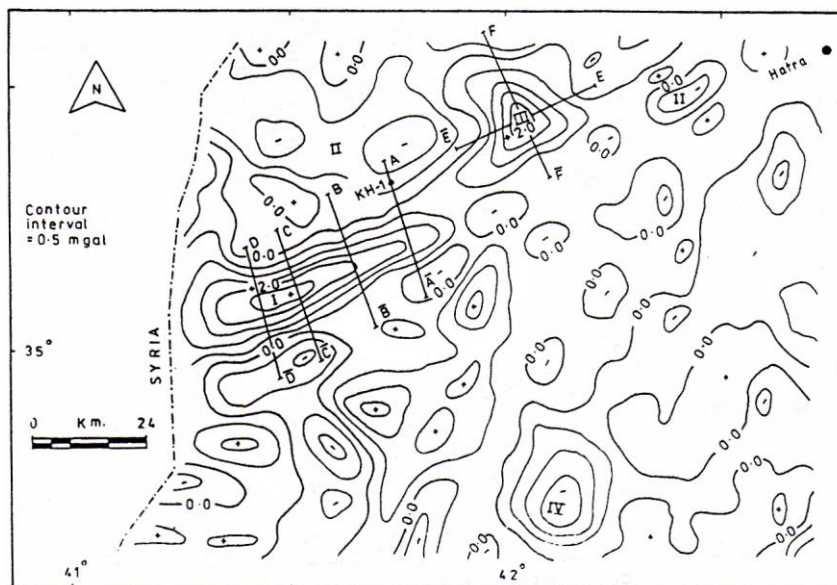
Fig. 12-9 Residual anomaly map of the area

A. Abu Rassain anomaly

Figs. 12-9, 12-10 and 12-11 show the Bouguer anomaly profiles. Slightly inclined regional gradient towards the northwest is chosen. Obviously, this inclination is not taken in account by the smoothing procedure of the observed contours. This slight "extra" regional effect is subtracted from the observed curve to yield a simple "high" over the uplift. The best cross-section of the uplift was found by trial and error using a computer program to compute the theoretical values of gravity of two-dimensional models

The suggested model is an elongated uplift whose topmost rocks are made up of Upper Triassic. The uplift is not symmetrical with the northern limb having greater inclination. It is possible that the northern limb is faulted hence becoming steeper. The top surface of the model along the profiles AA, *BB,* CC and DD occurs at

depths 580,550, 420 and 440 m successively. These figures are calculated using a density contrast of 0.18 gm.cm^{-3} as referred to earlier. An error of -0.01 gm.cm^{-3} in the contrast will result in an error in depth of -50m. Fig.7 shows a subsurface contour map on top of the upper Triassic as deduced from the above considerations.
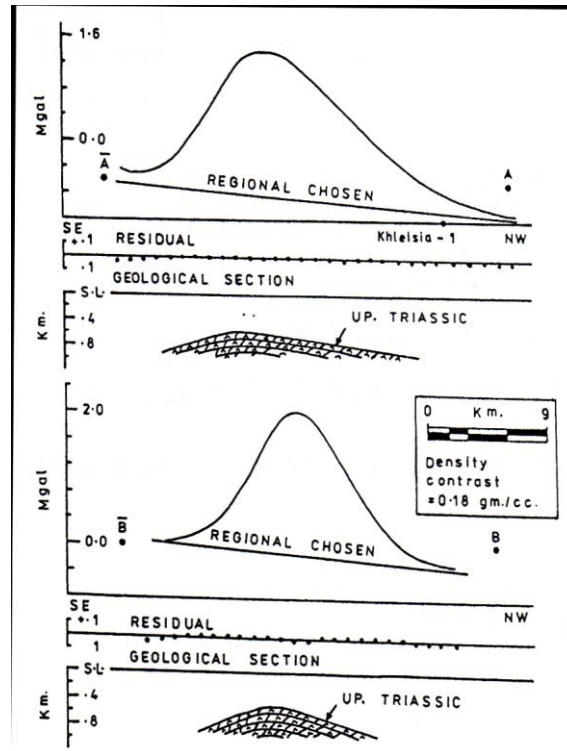
Fig. 12.10 Modeling of the Abu Rassain anomaly

B. Abu Jurd Anomaly

It is a three-dimensional positive anomaly, lies to the northeast of well Kh.-1 (Fig. 4). It has maximum amplitude of 2.4 mgal. It is believed that, according to the same reasoning, its origin lies in the uplifting of the unconformity above the Triassic rocks. To obtain the geological structure causing the anomaly two profiles (FF, EE) running normal to each other are considered (Fig. 12-9). A similar procedure as that used for Abu Rassain anomaly which is followed by the computer program is used for calculating the gravitation effect of a three-dimensional model (Fig. 12-13). The suggested solution is nearly-circular uplift of the Upper Triassic which is slightly a symmetrical with its top occurring at a depth of 530m. A subsurface structure contour map of the uplift is shown in Fig. 12-14.
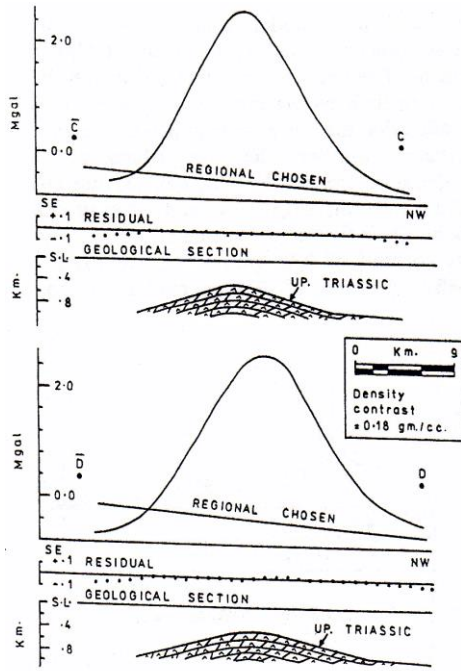
Fig. 12-11 Modelling of the Abu Rassain
anomaly
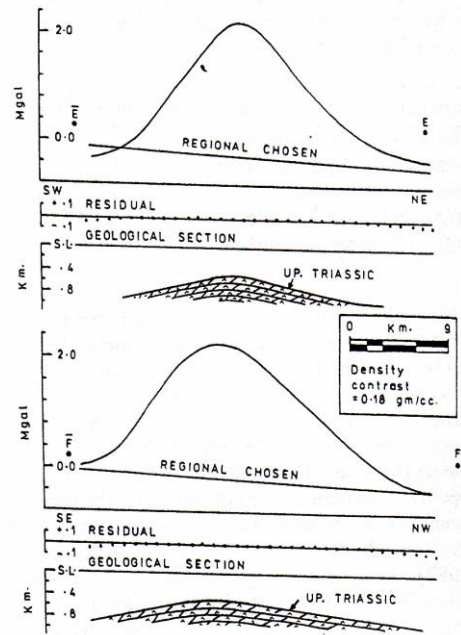
Fig. 12-12 Modelling of the Abu Jurd
anomaly
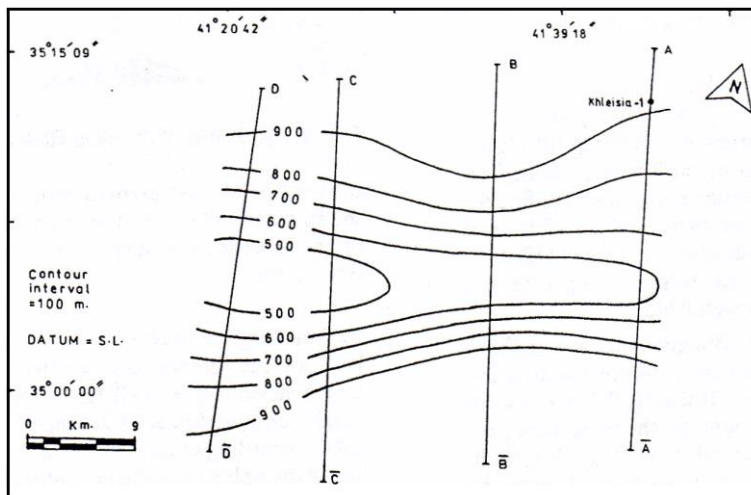
Fig. 12-13 Structural contour map on top of the Up. Traissic
(Abu Rassain anomaly).
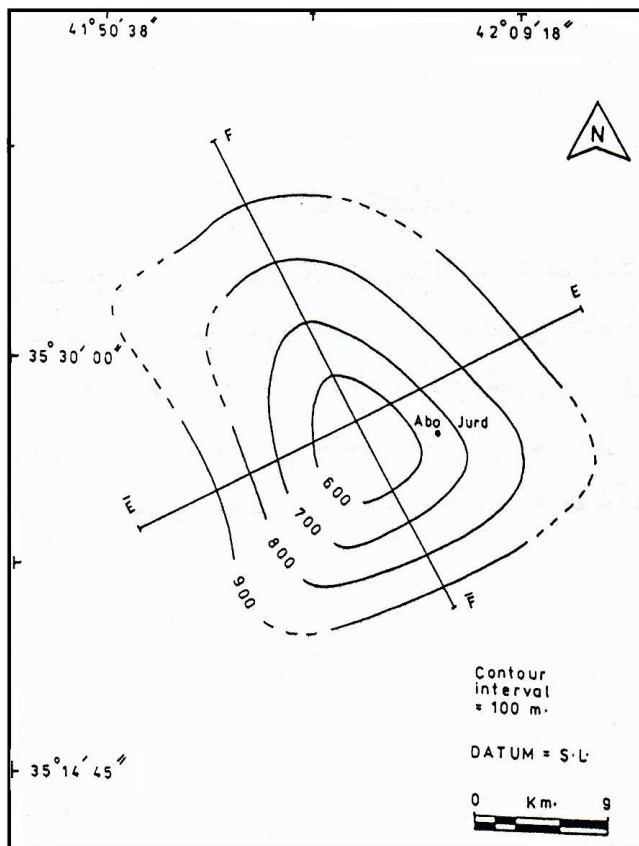
Fig. 12-14 Structural contour map on top of the Up. Traissic
(Abu Jurd anomaly).

REFERENCES

Abbas, M.J. AI.Khatib, H. H.,1982, Complex geophysical interpretation of Hit -
Abu Jir- Shthatha area, NIMCO Library, Unpublished.

Alberts, B., 2009, Regional gravity field modeling using airborne gravimetry
data. Publications on Geodesy 70, Netherlands Geodetic Commision, p. 1-
79.

Al-Sadi, H. N., 1967, A gravity investigation of the Pickwell Down Sandstone,
North Devon. Geological Magazine, vol 104, no. 1, 63-72.

Al-Shaikh Z.D. and Baban E.N, 1991, Possible Triassic folding below Abu
Rassain, The Western Desert, Iraq, J.Sci.Nat. 1(1A), 28-34.

Baban, E. N., 1983; Analysis of the geophysical data available on Abu Rassain
Area. M.Sc. Thesis, Univ, of Mosul, Unpublished.

Bell, R. E. Anderson, R., and Pratson, L., 1997, Gravity gradiometry resurfaces.
The Leading Edge, 16, p. 55-60.

Bott, M. P. H., 1959, The use of electronic digital computers for the evaluation
of gravimetric terrain corrections, Geophys. Prosp., v. 7, 45-54.

Bott, M.H.P., Day, A.A., and Masson-Smith, D., 1958, The geological
interpretation of gravity and magnetic surveys in Devon and Cornwall.
Philosophical Transactions of the Royal Society of London, vol. 251, no.
992, 161-191.

Bott, M. H. P. and Smith, R. A. 1958, The estimation of the limiting depth of
gravitating bodies. Geoph. Prosp. Vol-VI, no. 1, 1-10.

Brozena, J. M., 1984, A preliminary analysis of the NRL airborne gravimetry
system. Geophysics, vol. 49, p. 1060-1069.

Ditmar, V., 1971; Geological conditions and hydrocarbons prospects of the
Republic of Iraq, OEC Library, Baghdad, unpublished.

Dobrin, M. B. 1960. Introduction to Geophysical prospecting, 2nd ed. New York:
McGraw-Hill.

Dobrin, M. B. and Savit, C. H., 1988, Introduction to Geophysical Prospecting. McGraw-Hill, New York, USA, 867p.

Dohr, G. 1975, Applied Geophysics, Pitman, London

Elieff, S., 2003, Project report of an airborne gravity evaluation survey, Timmins, Ontario: Report produced for the Timmins Economic Development Corporation, Canada.

Gardner, G. H., Gardner, L. W., and Gregory, A. R. 1974, Formation velocity and density-the diagnostic basics for stratigraphic traps, Geophysics, 39, 770-780

Girdler, R. W. 1958, The formation of new oceanic crust. Q. Jl. Geol. Soc., Lond., 114, 79-105.

Gutenburg, B. 1959, Physics of the Earth's Interior. Academic Press, New York, 240p.

Hammer, S. 1939, Terrain corrections for gravimeter stations. Geophysics, vol. 4, 184-94.

Holmes, A. 1975, Principles of Physical Geology. Nelson Publ.. London, 1288p.

Hubbert, M. K., 1948, A line integral method of computing gravimetric effects of two-dimensional masses. Geophysics 13, 215-25.

Hwang, C., Yu-Shen, H., Hsuan-Chang, S., Ming, Y., Kwo-Hwa, C. Rene, F., and Olesen, A. V., 2007, Geodetic and geophysical results from a Taiwan airborne gravity survey: Data reduction and accuracy assessment, Journal of Geophysical Research, vol. 112, p. 1-14.

Jacobi, W. and Smilde, P. L., 2009, Gravity Interpretation. Springer-Verlag, Berlin Heidelberg, 395p.

Jekeli, C., 1993, A reviewof gravity gradiometer survey system data analysis. Geophysics, 58, p. 508-514.

Jekeli, C. and Kwon, J. H., 1999, Results of airborne vector (3D) gravimetry. Geophysical Research Letters, 26, p. 3533-3536.

Kahn, M. A. 1983. Satellite contributions to geophysical exploration at sea. In Handbook of Geophysical Exploration at Sea, R. A. Geyer, ed., pp. 3-68. CRC Press.

Kearey, P. and Brooks, M., 1987, An Introduction to Geophysical Exploration. Blackwell Scientific Publications, Oxford.

La Fehr, T. R. 1980, History of geophysical exploration: Gravity method. Geophysics 45, 1634-9.

LaFehr, T. R., 1983, Rock density from borehole gravity surveys, Geophysics, vol. 48, p. 341-356.

Lee, J. B., 2001, Falcon gravity gradiometer technology. Exploration Geophysics, vol. 32, p. 247–250.

Lundberg, H., 1957, Airborne *gravity* surveys . Canadian Mining and Metallurgical Bulletin, Aug., p. 465–473.

Mohammed, A. M., 1981, Geophysical study to establish basement configuration in the western desert. M.Sc. Thesis, Univ. of Mosul., Unpublished.

Nafe, J. E. and Drake, C. L. 1963, Physical properties of marine sediments, The Sea, Interscience, New York, 794-815.

Nettleton, L. L. 1934, Fluid mechanics of salt domes. Bull. Am. Assoc. Petr. Geol. 18, 1175-1204.

Nettleton, L. L. 1939, Determination of density for reduction of gravimeter observations. Geophysics, 4, 176-183,.

Nettleton, L. L. 1976, Gravity and Magnetics in Oil Prospecting. New York: McGraw-Hill.

Peters, L. J. 1949, The direct approach to magnetic interpretation and its practical application. Geophysics, 14, 290-319.

Robinson, E. S. and Coruh, C. 1988, Basic Exploration Geophysics. Wiley, New York, 576p.

Sayyab A. & Valek, R., 1968, Pattern and general properties of the gravity field of Iraq, 23rd Int. Geol. Congo Czechoslavakia, 5:129-42

Schwartz, K. P. and Li, Z., 1997, An introduction to airborne gravimetry and its boundary value problems. In: Santo, F. and Rummel, R., (ed) geodetic boundary value problems in view of the one centimeter geoid volume 65 of lecture notes in earth sciences, p. 312-358, Springer-Verlag, New York.

Sheriff, R. E., 2002, Encyclopedic Dictionary of Applied Geophysics, SEG, USA.

Sheriff, R. E. 1973, Encyclopedic Dictionary of Exploration Geophysics, Society of Exploration Geophysicists (SEG), Tulsa, Oklahoma, USA.

Smith, N. J., 1950, The case of gravity data from boreholes, Geophysics, , vol. 15, No. 4.

Smith, R. A. 1959, Some depth formulae for local gravity and magnetic anomalies. Geophys. Prosp. 7, 55-63.

Telford, W. M., Geldart, L. P. and Sheriff, R. E.., 1996, Applied Geophysics 2nd ed., Cambridge, England Cambridge University Press.

Van Kann, F., 2004, Requirements and general principles of airborne gravity gradiometers for mineral exploration. In: Lane RJL, (ed.), Airborne Gravity 2004 – Abstracts from the ASEG-PESA Airborne Gravity 2004 Workshop, volume 2004/18 of Geoscience Australia Record, p. 1–5.

Wie, M., 1999, From airborne gravimetry to airborne geoid mapping – Report of SSG 3.164. In: Forsberg, R., (ed) determination of the gravity field of LAG section III, p. 25-32. Danish National Survey, Copenhagen.

Other Useful References

(i) Books

Dehlinger, P., 1978, Marine Gravity. Elsevier, Amsterdam.

Dobrin, M. B., 1976, Introduction to Geophysical Prospecting, 3rd. edition, New York, McGraw Hill.

Dohr, G. 1975, Applied Geophysics, Pitman, London

Garland, G. D., 1965, The Earth's Shape and Gravity. Pergamon, Oxford.

Grant, F. S., and West, G. F. 1965. Interpretation Theory in Applied Geophysics. New York: McGraw-Hill.

Gutenburg, B. 1959, Physics of the Earth's Interior. Academic Press, New York, 240p.

Kearey, P. and Brooks, M., 1987, An Introduction to Geophysical Exploration. Blackwell Scientific Publications, Oxford.

Nettleton, L. L. 1971. Elementary Gravity and Magnatics for Geologists and Seismologists. Tulsa: Society of Exploration Geophysics.

Nettleton. L. L., 1976, Gravity and Magnetics in Oil Prospecting. New York, McGraw-Hill.

Parasnis, D. S. 1997, Principles of Applied Geophysics. Chapman & Hall, London.

Robinson, E. S. and Coruh, C. 1988, Basic Exploration Geophysics. Wiley, New York, 576p.

Sharma, P., 1976, Geophysical Methods in Geology. Elsevier, Amsterdam.

Telford, W. M., Geldart, L. P. and Sheriff, R. E.., 1996, Applied Geophysics 2nd ed., Cambridge, England Cambridge University Press.

(ii) Published Papers

Ager, C. A., and Liard, L. O., 1982, Vertical gradient surveys: Field results and interpretation in British Colombia. Geophysics, vol. 47, p. 919-925.

Airy, G. B.: Phil. Trans. Roy. Soc. London, Vol. 145, pp. 101-104, 1855.

Arzi, A. A. 1975. Microgravity for engineering applications. Geophys. Prosp. 23, 408-25.

Bible, J. L. 1964. Gravity for the geologist. World Oil, Oct. and Nov. issues.

Bhattacharyya, B. K. 1978. Computer modeling in gravity and magnetic interpretation. Geophysics 43, 912-29.

Bott, M. H. P., 1973, Inverse methods in the interpretation of magnetic and gravity anomalies. In: Alder, B., Fernbach, S. & Bolt, B. A. (eds.), Methods in Computational Physics, 13, 133-62.

Butler. D. K. 1984. Microgravimetric and gravity gradient techniques for detection of subsurface cavities. Geophysics 49, 1084-96.

Dean. W. C. 1958. Frequency analysis for gravity and magnetic interpretation. Geophysics 23, 97-127.

Elkins, T. A. 1951. The second derivative method of gravity interpretation. Geophysics 16, 29-50.

Ervin, C. P. 1977. Theory of the Bouguer anomaly. Geophysics 42, 1468.

Falklewicz, Z. J. 1976. Gravity vertical gradient measurements for the detection of small geologic and anthropogenic forms. Geophysics 41, 1016-30.

Geldart, L. P., Gill, D. E., and Sharma, B. 1966. Gravity anomalies of two-dimensional faults. Geophysics 31, 372-97.

Griffin, W. R., 1949, Residual Gravity in Theory and Practice, Geophysics, Vol. 14, pp. 39-56.

Gupta, V. K., and Ramani, N. 1982. Optimum second vertical derivatives in geological mapping and mineral exploration. Geophysics 47, 1706-15.

Hammer, S. 1983. Airborne gravity is here. Geophysics 48, 213-23.

Hussain, A., Walach, G., and Weber, F. 1981. Underground gravity survey in alpine regions. Geophys. Prosp. 29, 407-25.

Kanasewich, E. R., and Agarwal, R. G., 1970 Analysis of Combined gravity and magnetic fields in wave number domain. J. Geophys. Res., vol. 75, P. 5702-5712.

La Coste, L. J. B. 1967, Measurement of gravity at sea and in the air, Reviews of Geophysics, v. 5, pp. 477-526.

La Coste, L. J. B., Ford, J., Bowles, R., and Archer, K., 1982, Gravity measurements in an airplane using state of the art navigation and altimetry. Geophysics, vol. 47, P. 832-837.

La Fehr, T. R. 1983. Rock density from borehole gravity surveys. Geophysics 48, 341-56.

Paterson, N. R., and Reeves. C. V. 1985. Applications of gravity and magnetic surveys: The state of the art in 1985. Geophysics 50, 2558-94.

Pratt, J. H.: Phil. Trans. Roy. Soc. London, Vol. 149, pp. 747-763, 1859.

Schmoker, J. W. 1978. Accuracy of borehole gravity data. Geophysics 43, 538-42.

Skeels, D. C. 1947. Ambiguity in gravity interpretation. Geophysics 12, 43-56.

Stanley, J. M. 1977. Simplified gravity interpretation by gradients-the geological contact. Geophysics 42, 1230-5.

INDEX

Chapter-1

Chapter-2

Chapter-3

Chapter-7

Chapter-8

Chapter-9

Chapter-10

Chapter-11

Chapter-12

مقدمـة الـى
طريقـة الاستكشاف الجـذبي

حامد نصار السعدي

خبير جيوفيزيائي سابق في شركة الاستكشافات النفطية — العراق

عزالدين نجم الدين بابان

أستاذ الجيوفيزياء — قسم الجيولوجي — جامعة السليمانية

سـەرەتایەك بـۆ

ڕێگـەی دۆزینـەوەی ڕاکێشان

حامد نصار السعدي

شارەزای کۆن لە بواری جیوفیزیك لە کۆمپانیای دۆزینەوەی نەوت — عیراق

عزالدین نجم الدین بابان

پڕۆفیسۆر لە بواری جیۆفیزیك — بەشی جیۆلۆجی — زانکۆی سلێمانی